Diffusing wave spectroscopy applied to material analysis and process control

Thesis

DIFFUSING WAVE SPECTROSCOPY APPLIED TO MATERIAL ANALYSIS AND PROCESS CONTROL

Christopher James Lloyd

Submitted as a PhD Thesis to the Open University

April 1997

Sponsoring Establishment

CAMR

Porton Down

Wiltshire

SP4 OJG

Collaborating Establishment

RSRE Malvern

St Andrews Rd

Malvern

Worcester

WR14 3PS

Contents

List of Contents

Figures

Tables

Acknowledgements

I would like to extend my thanks to the numerous people who have aided me in this work and in particular to: Dr R.G. B. Carr who acted as director of studies for this work, Dr E. A. Perkins who acted as second supervisor and aided this project with general guidance on light scattering theory and application, Dr J. Rarity (DRA Malvern) who acted as my external supervisor, Dr M. Scawen and Dr D. Horne for acting as my internal and external examiners, Professor D. J. Clarke who was kind enough to proof read the document for grammatical errors and advised on the thesis layout.

A significant amount of knowledge, outside my field of expertise, was utilised in this work and I would also like to those who helped with particular problems notably: Dr A. Tinsley-Bown who suggested methods of applying no-stick surface coatings, Dr H. Aojula (of Peptide Products) who supplied the required materials and advised on their use *gratis*, Mr M. Hutchins who gave a significant amount of his time modifying photon multiplier amplifier circuits to allow higher speed operation, Dr. D Svendesen (Sensor Dynamics) who supplied efficient polynomial curve fitting algorithms used within the software, Dr J Lawson (Tioxide plc) who gave many practical suggestions and methods in the generation of stable suspensions and the effects of Non-Newtonian viscosities and the physical properties of TiO_2, Robert Buhler of Aston University who carried out Flow Cytometry of the Tioveil pigment samples.

A DTI Link Grant under the Nanotechnology initiative funded this work.

Declaration

I declare that the this work has not previously been submitted in whole or in part, to any other University or awarding body. All the work described in this PhD with the exceptions acknowledged, is a result of my own unaided research.

Published Prior to Submission

The following publications and talks have been given relating to, or based on, the results presented in this document:

Lloyd C. J., Perkins E. A., Atkinson T., Carr R. J. G., 1993, Diffusing wave spectroscopy, Proc. Biomedical Optics Europe, Budapest. SPIE, Vol. 2082, pages 279-287

Lloyd C. J.,1993, Diffusing wave spectroscopy, invited presentation, Rank Prize Funds Mini Symposium on Optical Localisation and Slow Waves, Grasmere, September,

Lloyd C. J., Carr R. J. G., 1995, Diffusing wave spectroscopy, invited presentation, Ann. Chem. Conf., Heriot Watt University, April

Lloyd C. J., Perkins E.A., Carr R. J. G., 1997, Dynamic light scattering and its application in concentrated dispersions, Advances in Fibre Sensors, Editors Culshaw B. and Dakin J., Artech Books, pages 109-127

The chemical conference lead to reports in the press notably

Goddard A., Freshness test gets to the thick of it, New Scientist page 6, May 1995

Abstract

Diffusing Wave Spectroscopy (DWS) was studied as a method of laboratory analysis of sub-micron particles, and developed as a prospective in-line, industrial, process control sensor, capable of near real-time feedback. No sample pre-treatment was required and measurement was via a non-invasive, flexible, dip in probe.

DWS relies on the concept of the diffusive migration of light, as opposed to the ballistic scatter model used in conventional dynamic light scattering. The specific requirements of the optoelectronic hardware, data analysis methods and light scattering model were studied experimentally and, where practical, theoretically resulting in a novel technique of analysis of particle suspensions and emulsions of volume fractions between 0.01 and 0.4. Operation at high concentrations made the technique oblivious to dust and contamination. A pure homodyne (autodyne) experimental arrangement described was resilient to environmental disturbances, unlike many other systems which utilise optical fibres or heterodyne operation.

Pilot and subsequent prototype development led to a highly accurate method of size ranking, suitable for analysis of a wide range of suspensions and emulsions. The technique was shown to operate on real industrial samples with statistical variance as low as 0.3% with minimal software processing.

Whilst the application studied was the analysis of TiO_2 suspensions, a diverse range of materials including polystyrene beads, cell pastes and industrial cutting fluid emulsions were tested. Results suggest that, whilst all sizing should be comparative to suitable standards, concentration effects may be minimised and even completely modelled-out in many applications. Adhesion to the optical probe was initially a significant problem but was minimised after the evaluation and use of suitable non stick coating materials. Unexpected behaviour in the correlation in the region of short decay times led to consideration of the effects of rotational diffusion coefficient. The inherent instability of high density suspensions instigated high speed analysis techniques capable of monitoring suspensions that were undergoing rapid change as well as suggesting novel methods for the evaluation of the state of sample dispersion.

Abbreviations

APD	Avalanche Photodiode
AR	Anti-Reflection
CPU	Central Processor Unit
DLS	Dynamic Light Scattering
DWS	Diffusive Wave Spectroscopy
FODA	Fibre Optic Dynamic Anenometry
FODLS	Fibre Optic Dynamic Light Scattering
FOQELS	Fibre Optic Quasi-Elastic Light Scattering
FT	Fourier Transform
GRIN	Graded Index
GUI	Graphical User Interface
HeNe	Helium Neon Laser
NA	Numerical Aperture
PCS	Photon Correlation Spectroscopy
PMT	Photon Multiplier Tube
PN	Postive-Negative (Diode Junction)
PSD	Particle Size Distribution
Div	Divergence
Grad	Gradient
lim	Allowable error in number of channels in sample time module
LP	Hybrid transverse electromagnetic mode
ME	Maximum Experimental duration in the measurement module
MMD	Minimum Measurement Duration
MSE	Maximum Experimental duration in the Sample time module
mlim	the allowable error in the number of channels in the measurement module
ND	Number of Durations
NQ	Number to Quit number (software)
NT	Number of Times
TEM	Transverse Electromagnetic Mode
RAM	Random Access Memory
RAMdisk	An artificial fast hard disk implemented in RAM allowing fast read/write.
RC	The selected correlator channel that f_b should lie on
S/N	The signal to noise ratio
UV, UVB	Ultraviolet Radiation
Var	Variance of
v.f.	Volume Fraction
RF	Radio Frequency
%intercept	Ratio of difference in intercept values between the 1st and 2nd order polynomial fit
%curvature	Ratio of difference in gradient values between the 1st and 2nd order polynomial fit

Symbols

a	dimensionless size parameter
A	amplitude field
A*	complex conjugate of A
A_d	Airy disk point spread function
b	dynode factor
B	constants
B	normalised birefringence
c	speed of light, subscript 0 in *vacuo*
C	concentration
C_v	specific heat-constant volume
C_p	specific heat constant pressure
C_{sca}	scattering cross section
D	diffusion coefficient
D_0	free diffusion coefficient
D_C	collective diffusion coefficient
D_R	rotational diffusion coefficient
D_S	self diffusion coefficient
D_T	translational diffusion coefficient
E_{ab}	the total error in the fit to the ab plane
E_b	preset (initial) experimental duration used
E_S	error due to random scatter
E_F	error due to the incorrect fit
f,f'()	functions of ()
f_b	fraction of the baseline that will be used for short-time linear fit
F	arbitrary function
$\underline{F}$	mean value of F
$\underline{F}_{axy}$	mean value of the measured parameter used to evaluate F_M
F_{ab}	parameters of a fit in the ab plane
F_A	actual value of F
F_M	measured value of F
F_T	theoretical value of F
g	gravitational attraction
g	cavity parameter
g_s	correlation of scattering field
g^1	amplitude correlation
g^2	Intensity correlation
G^1	normalised amplitude correlation
G^2	normalised intensity correlation
h	Planck's constant
I	intensity,
I_C	intensity due to fluctuations of entropy (central line)
I_D	intensity due to fluctuations of pressure (doublet line)
I_H	intensity - horizontally polarised,
I_O	incident intensity
Is	scattered intensity
I_V	intensity - vertical polarised
k	Boltzmanns constant
K	wave vector,
K'	difference in wave vectors
l	photon scattering path
l_*	photon transport path
L	sample thickness
m	transverse mode order
m	mass
n	refractive index
n	APD noise parameter
N	the number of photons
N	number of dynodes
N_A	Avagardos number
N_e	number of electrons
N_v	number of particles/unit volume
p	transverse mode order
p	momentum
P()	probability of ()

q	longitudinal mode order	t_c	solute-particle collision period
Q	efficiency factor	T	temperature
R	radius	T_B	turbidity
R_2	major aspect ratio	u	emitter detect spacing
R_b	blur circle radius	V	voltage
s	speed (scalar)	x	co-ordinate
S	displacement	x	blur circle factor
t	time	y	co-ordinate
t_b	solvent- solute interaction time	Y	intercept value
α	correlator accumulator value	θ	angle
β	Stokes Einstein friction coefficient	ρ	density
$\beta_{x,y}$	birefringence in x or y plane	ρ_S	density of suspension
χ	instrument factor	ρ_P	density of particle
ε	permitivity	τ	time - correlation delay
ϕ	volume fraction	τ_0	$1/\Gamma$
γ	ballistic to diffusion constant	τ_S	a time constant
χ	instrument factor	ω	frequency
η	viscosity	Δ	refractive index ratio
η_E	effective electrostatic viscosity	Γ	Line-width for DLS analysis
η_{eff}	effective viscosity	Γ	gradient of Log (α) versus $\tau^{0.5}$
η_H	effective hydrodynamic viscosity	Γ_0	Γ for translation if $R \neq R_2$
η_{HS}	effective hard Sphere viscosity	Γ_2	Γ for rotation if $R \neq R_2$
η_L	effective cross-linking viscosity	Ω	runs test
λ	wavelength		

CHAPTER 1

Introduction

1.1 Scope of the Project

Emulsions and dispersions are used in a wide range of applications throughout industry and the particle size is often of critical importance in terms of the final product characteristics. Its variation not only affects the optical characteristics, of particular importance in pigments, but also the rheology and stability of the dispersion. In the analysis of pigments light scattering would appear the optimum analysis method. However, all conventional light scattering methods operate only on dilute samples. The requirement for dilution not only limits in-line process control but also, in many instances, makes the techniques of limited value, as dilution significantly affects the properties of an emulsion or suspension.

This project aimed to evaluate and optimise the technique of Diffusing Wave Spectroscopy (DWS) to allow direct in-line analysis of concentrated dispersions, particularly within the pigment industry.

The work by Pine *et al.* (1988) on multiple scattering led to a diffusion approximation for the transport of light in dense scattering media. The technique of DWS, which allowed direct analysis of multiply scattered light, was successfully used in the analysis of dairy products (Horne 1989). Work by Lloyd (1991) suggested that a modification of the DWS analysis gave a function that was linear with the particle size, whilst concentration effects were minimal. Collaboration was undertaken with an optical sensor instrumentation company (SensorDynamics) and a major producer of titanium dioxide pigments (Tioxide). The project used the pigment as an optimum model scattering particle and the industry as a probable major application.

The project aimed to assess DWS as an in-line monitor for quality control of pigment manufacture. This required the study of the dependence of the DWS signal to a range of variables, which included concentration and analysis methods. Significant developments in methods of both experiment control and data analysis were required to allow relative size information to be obtained from highly unstable samples.

1.2 The Scattering of Light by Particles

1.2-1 Historical Note

Whilst techniques such as dynamic light scattering required the advent of both the laser and integrated circuit to operate successfully, the study of light and its interaction has a considerable history. One of the first observations of light scattering was possibly made by da Vinci (*circa.* 1500). When considering the blue colour of the sky, he suggested "*the atmosphere assumes this azure hue by reason of the particles of moisture which catch the rays of the sun*". Newton continued this reasoning suggesting that the colour was due to simple reflection in water droplets. In 1860 Govi, and nine years later, Tyndall studied not only the colour but also the polarisation properties of light scattered by small particles. This led Rayleigh to model light scattering as a dipole moment, induced by an electromagnetic wave in 1871. Planck's study of Rayleigh's later work, notably the ultraviolet catastrophe of the blackbody radiation law, led to quantum theory. This in turn gave rise to the concept of the photon as a particle, the photoelectric effect, hence the photon multiplier tube and the laser, all integral phenomena to a modern dynamic light scattering experiment. Light scattering was limited to low concentrations of suspended particles and special cases, until the concept of localisation was studied (Anderson 1958). The theory, although devised to explain semiconductor properties, was extended to optical radiation (de Wolf 1971). This led to the pioneering work of the concept of the diffusing photon and thus a model of light scattering at high concentrations (Pine *et al.* 1988).

1.2-2 Rayleigh Scattering

Rayleigh modelled light as an electromagnetic wave and scattering as a consequence of an induced dipole, which oscillated in the same direction as the field of the wave. The secondary emission of the dipole gives rise to a scattering pattern. For a small ($10R<\lambda$) non-absorbing sphere, illuminated with polarised light, this is given by:

$$I = [(16 \pi^4 R^6)/ (r^2 \lambda^4)] \; [(n_1 - 1)(n_2 + 2)]^2 \sin^2 \theta \qquad \text{Equation 1}$$

Where θ is the angle measured from the scattering direction to the dipole, r the distance from the dipole, n_1 the particle refractive index, n_2 the refractive index of the continuous phase, R the particle size, and λ the wavelength.

The total energy scattered, integrating over all θ, known as the scattering cross-section is thus:

$$C_{sca} = [\ 128\ \pi^5\ R^6\ ) / (\ 3\ \lambda^4\ )]\ [\ (\ n_1 - 1\ )(\ n_2 + 2\ )\ ]^2 \qquad \text{Equation 2}$$

This may be termed an efficiency factor by dividing by the cross-section illuminated:

$$Q = [(8\pi^4\ R^4\ )/\ (3\ \lambda^4)]\ \ [(n_1-1)(n_2+2)]^2 = [(8\ a^4\ )/\ 3]\ \ [(n_1-1)(n_2+2)]^2 \qquad \text{Equation 3}$$

Where a is the dimensionless size parameter $a = (2\ \pi\ R)/\ \lambda$.

The Rayleigh scattering approximation relies on the fields within a scattering particle being uniform, since the particle is small compared with the wavelength of light. This limits accurate analysis to particles with $10R\ [1+(n_1-n_2)] < \lambda$, however, calculations are often acceptable up to $R\ (1+n_1-n_2)<\lambda$.

The Rayleigh-Gans model, where the particle is treated in sections each of which is a separate scattering centre, increases the size range but not the refractive index difference that can be modelled (Kerker 1969). This limitation suggests only the general case solution, given by Mie theory, can be considered accurate for TiO_2 pigment suspensions.

1.2-3 Scattering by a Sphere, The General Case

Titanium dioxide has a refractive index of between 2.4 and 2.7, dependent on its crystal structure, as it is stable in two forms. Pigments used in this project were milled from a few microns to around 300nm, which made the material unsuitable to model accurately by either Rayleigh or Rayleigh-Gans scattering. The general case of scattering by a sphere requires the use of Mie theory, the full solution of Maxwell's equations for electromagnetic waves scattered by spheres. These show highly complex oscillations in Q, with refractive index, as well as significant variation with size in the lobed scattering patterns. A significant amount of work has been carried out on approximations of Mie theory but until the advent of economic computing, full solutions were tedious and time consuming. The increasing speed and capacity of personal computers has recently made application of the full model available to all workers.

In concentrated particle systems a significant amount of work has been done using Monte-Carlo models, where each photon is traced round many scattering events (Zaccanti 1991).

When diffuse scattering occurs the random nature of the wave vectors removes all angular dependence (θ). As the project has aimed only at measurement and analysis of diffuse scattering, no Mie calculations have been carried out and the theory will not be discussed further.

1.3 Analysis of Size by Static Light Scattering

1.3-1 Principles of Operation

The strong dependence of scattering on the cross-section of the particle (in the regime Equation 2 applies) makes the quantity of light scattered an accurate measure of particle size, provided the concentration and refractive indices are known. However, the strong weighting towards larger particles can make the analysis of polydisperse systems more complex and leads to significant problems with dust contamination.

1.3-2 Transmission Measurements -Turbidity

Turbidity, T_B, is defined as the extinction of light per unit sample thickness, due to scattering and absorption (Kerker 1969), which may be expressed as:

$$\text{Transmission} = I_t / I_0 = \exp (-N_V C l) = \exp (-T_B L) \qquad \text{Equation 4}$$

Where N_v is the number of particles per unit volume, L the optical path length, I_o the incident intensity, I_t the transmitted intensity and C the particle concentration. The loss of light by the primary beam, per unit volume of the sample is then given by:

$$T_B = N_v C \qquad \text{Equation 5}$$

The weight average molecular weight of small suspended particles can then be found from:

$$(T_B / C) = 3 / (4\rho_2) (Q / R) \qquad \text{Equation 6}$$

Where ρ_2 is the density of the suspended particles.

1-3-3 Limitations of Single Angle Static Light Scattering

Static Light Scattering (SLS) requires a high level of cleanliness. The measurement is based on measurement of the scattered intensity thus high quality stable light sources, detectors and sample cells are required. For single angle measurements, the particle refractive index and concentration require to be accurately known[1]. This limits the use in many applications where flocculation or processing causes a change in the number of particles present. Possibly, the major limitation is that only very dilute (single scattering) samples can be analysed.

The complex scattering of large particles ($R >> \lambda$) may be used to size directly. Plotting scattered intensity as a function of angle allows the mean size to be calculated and the distribution deconvoluted. This requires significant mathematical processing and precise angular alignment of the arrangement, Section 1.2-3.

1 Section 4.4-2 details a method of SLS analysis based on scans at multiple wavelengths, as opposed to angles. In this case the concentration dependence is lost.

1.4 Dynamic Light Scattering in Dilute Suspensions

1.4-1 Scattering by Liquids

This section details the development of Dynamic Light Scattering (DLS), which allowed a measurement that is independent of the scattered intensity. This method gave significantly higher accuracy, sensitivity and stability than SLS. DLS can be traced to Brillouin's study of standing sound waves in a homogenous body in 1922. In 1934, Gross not only noted these doublets as predicted but also a central line. Landau and Placzek explained this, as light scattered by unorganised thermal motions or fluctuations of temperature (entropy) at constant pressure. The result was given as: $I_c / (2 I_D) = (c_p - c_v) / c_v$ Equation 7

Where c_v is the specific heat capacity at constant volume, c_p the value at constant pressure and $I_{C,D}$ the intensity of the central and doublet lines respectively.

1.4-2 Scattering by Suspensions

The measurement of a collection of separate scattering particles within a liquid was not considered feasible until after it was shown that two light sources could be considered coherent (Forrester *et al.* 1955, Hanbury Brown and Twiss 1956). The work also showed that measuring two sources reduced the measured frequency, a phenomena known as beating, allowing a practical method of the measurement of the dynamics of particles in suspension (Forrester 1961). Whilst it was possible for the coherence criteria to be met using mercury lamps, the advent of the first laser (Javan *et al.* 1961), allowed practical measurement systems. Early work utilised signal analysers to measure the scattered line-width which was noisy and required heterodyne operation to remove the signal from the noisy low frequency regime.

1.4-3 Photon Correlation Spectroscopy

Jakeman (1973) has discussed how measurement of a photon pulse train contains similar information to that of the analogue signal. Analysis is well suited to parallel electronic digital circuits, which are used to calculate the autocorrelation function of the signal. The resulting exponential decay of the correlation is a measure of the speed the laser is de-phased hence the rate of the particles motion, which may be due to diffusion. The diffusion coefficient is then related to particle size, Section 2.3-2. The technique has been reviewed extensively (Cummins and Swinney 1970, Chu 1970, Ford Jr. 1970, Pusey and Vaughan 1975, Pecora 1985).

1.4-4 Brownian Motion

The frequency range over which the PCS signal is analysed has a dramatic effect on the dynamic information present in the signal. The solvent particles will have a momentum due solely to their temperature; H_2O molecules travel the order of 1km/s at 20^0C. This energy is transferred to a suspended particle via collision giving rise to an instantaneous ballistic speed given by:

$$\text{Speed} = [(k T m_1^2) / m_2]^{0.5} \qquad \text{Equation 8}$$

Where k is Boltzmanns constant, m_1 is the solvent particle's mass, m_2 the solute particles mass and T is temperature. However, the collision frequency between the suspended particle and the continuous phase molecules is given as (Ford 1972):

$$t_c = m_2 / (6 \pi \eta R) \quad \text{or} \quad (2 R^2 \rho) / (9 \eta) \qquad \text{Equation 9}$$

Where m_2 is the particles mass, R the solute particle's radius, η viscosity of the continuous phase and ρ is the density of the continuous phase. For a micron particle, suspended in water at 20°C, t_c is of the order of 1GHz such that the particle movement can be considered ballistic only over distances of a few nanometers.

1.4-5 Diffusion

The distances monitored by PCS are set by the requirement to dephase the incident light, typically in the range 488-633nm. Over these distances the scattering particle has undergone many collisions allowing its motion to be considered diffusive.

Brownian motion is via momentum transfer, thus a particles speed is mass dependent as above. However, the large number of collisions makes the particles instantaneous speed irrelevant to its diffusion, which is governed by how frequently the particle changes direction, thus its cross sectional area. The decay time τ_0 of the correlation (or linewidth $\Gamma=1/\tau_0$) may then be related directly to the diffusion coefficient:

$$\tau_0 = 1/ (D K^2) \qquad \text{Equation 10}$$

Where D is the diffusion coefficient and K the scattering vector defined as $(4\pi n \sin \theta)/\lambda$. Where n is refractive index, λ the wavelength of the incident light and θ is the scattering angle. The measure is based on particle diameter, as opposed to mass as previously, Equation (9).

1.4-6 Correlation

Thus it is necessary to measure τ_o, which underlies the random signal due to scattering. As alluded to previously, correlation is a method of measuring of the similarity between two signals, where the phase of the signal is ignored:

$$G_{f,g}(\tau) = \int f(t)\, f'(t+\tau)\, dt \qquad \text{Equation 11}$$

Where G is equivalent to the value of the product of the functions f and f' at positions t and $t+\tau$.

The integral ensures the product is a measure only of the similarity of the two signals, independent of position. If f and f' are the same function, then G is known as autocorrelation and measures the similarity of the signal with itself at various time offsets, irrespective of the time of the start of the analysis. For a function of zero mean, at $\tau = 0$ $G = 1$. The signal is perfectly in phase, decreasing with τ, to 0 at $\tau = \infty$, signifying no correlation, Figure 1. In PCS, we obtain a measure of the intensity autocorrelation function, which decays exponentially in the case of weak scattering by diffusing particles. This must be related to the autocorrelation of the field amplitude, $g^1(\tau)$, to allow particle size analysis, Section 3.2-1.

1.4-7 Particle Size

PCS is thus an absolute measure of the intensity weighted, average diffusion coefficient. In most applications the user requires a particle size, which may be calculated using the Stokes-Einstein relationship. This takes account of the frictional forces the particle experiences and thus allows determination of the spherical equivalent, hydrodynamic radius:

$$R = (k T) / (6 \pi \eta D) \qquad \text{Equation 12}$$

Where parameters are similar to those in Equations 8-10.

This basic model assumes a single particle size distribution, the spread in sizes resulting in a lack of single exponential behaviour. Fitting the correlation to a high order polynomial results in the first term relating to mean size and the second term to the spread in size, with all higher terms zero for a log normal distribution (Koppel 1972). In most cases, the particles are assumed perfectly spherical. Where particles are non-spherical rotational diffusion leads to a second exponential and thus an effective bimodal solution (Pecora 1968, Tagami and Pecora 1969, Cummins *et al.* 1969).

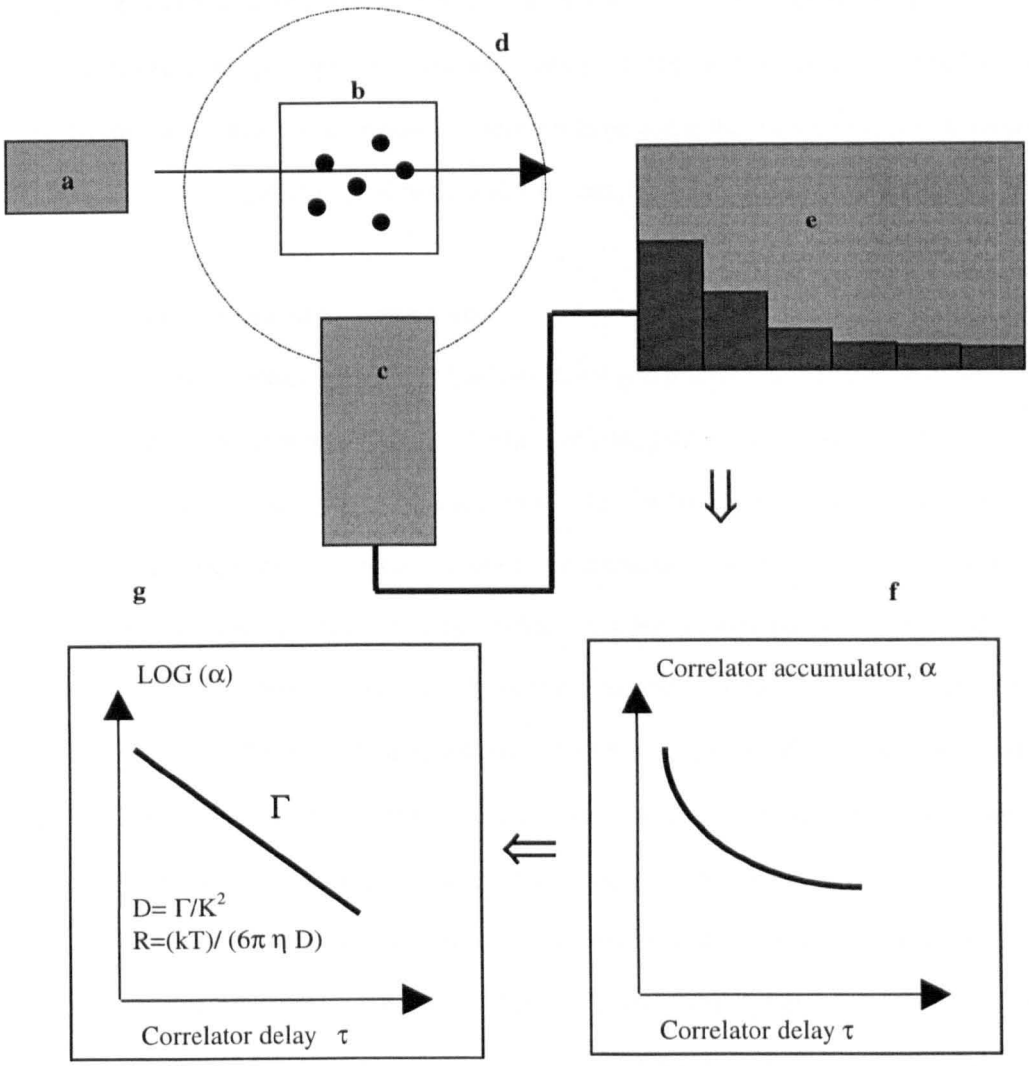

Figure 1 Photon Correlation Spectroscopy

The figure shows a typical PCS arrangement showing the laser (a), sample cell (b), detector (c) on a goniometer set at 90^0 (d), the correlator (e) and the analysis computer (f). The computer screen shows the correlation function of the suspended particles. The second trace of the computer screen (g) shows the correlation plotted log (α) versus τ and the analysis, where α is the correlator channel accumulator value and τ the correlator delay. The gradient of the straight line defines the decay rate of the exponential and thus the diffusion coefficient and size of the suspended particles.

1.4-8 Concentration Limits

PCS is generally limited to volume fractions (ϕ) of $1x10^{-4}$ and below. Above this a significant number of scattered photons may experience multiple scattering. The lower concentration limit is set by the requirement for more than 100 particles to be within the scattering volume to ensure the signal is not due to particles passing through the scattering volume (Number Fluctuation Spectroscopy).

1.4-9 Analysis of Dense Suspensions

Diffusing Wave Spectroscopy (DWS) has been developed primarily due to lack of suitable measurement techniques above volume fractions of 0.01. In this regime even double scattering models (Sorensen *et al.* 1976, 1978) and limited volume cells (Cummins and Staples 1981) are of restricted use. PCS has been carried out at volume fractions above 0.5 by the use of a small population of tracer particles. The particle refractive index of the larger population is index matched to the continuous phase and only the tracer particles generate a scattering signal (Russel 1981, Hoover and Ree 1988, Van Megen *et al.* 1985 Pusey and Van Megen 1992). Whilst the work allowed analysis and modelling of interactions, further developments were required to allow measurement of industrial samples where index matching is not viable.

Early work using DLS, in non-index matched concentrated systems, tended to follow the methods of Tanaka and Benedek (1975). Their method was aimed at measuring the rate of blood flow via measurement of the intensity spectrum of the scattered light, hence the term Fibre Optic Doppler Anemometry (FODA)[1]. The most common arrangements used a conventional heterodyne FODA and a single multimode fibre for both emission and detection (Ross *et al.* 1978, Dyott 1978, Dhadwal *et al.* 1980, Floy *et al.* 1988). Later workers used similar experimental arrangements but carried out the measurement in the time, as opposed to frequency, domain (Thomas and Tjin 1989, Thomas and Dimonie 1987). Macfayden and Jennings (1990) have reviewed the optical arrangements. Whilst allowing some analysis of size ranking, for a given material and concentration, no model existed for the systems under measurement until the work of Pine *et al.* (1988) and the development of DWS.

1) Similar experiment arrangements intended to measure particle size via measurement of the intensity spectrum are usually termed Fibre Optic Dynamic Light Scattering. Measurement of an intensity correlation is termed Fibre Optic Quasielastic Light Scattering (FOQELS), although the terms are not universal.

1.5 Diffusive Wave Spectroscopy

1.5-1 Analytical Solution

The first analytical model for light scattering in dense media grew from studies of localisation of light in random media. Previously workers tended to consider that the photons had been multiply scattered (a set number of times), leading to solutions only applicable to a single suspension type, size and concentration. Maret and Wolf (1987) considered that the range of different decays present, from the different sequences, sum incoherently to give:

$$g^{(1)}(\tau) \propto < E(0)\, E^*(\tau) > = \int I(L) \exp [\, -L\, \tau / (\, 4\, l_* \tau_0)\,]\, dL \qquad \text{Equation 13}$$

Where E is the amplitude of the field, τ the correlator delay time, τ_0 the characteristic fluctuation time, L the fluid thickness and l_* the photon transport mean free path. The latter is defined as the average distance a photon travels to lose all information on its original wave vector and is a function of concentration, refractive index and particle size. The model was unique in that it did not contain the mean scattering path (l), thus concentration, directly. Providing the particle sizes present in the sample were in the regime $L >> l >> l_*$, then the analysis would always be of the same form. This generic solution also suggested that, for samples of similar refractive index and concentration, relative size ranking was valid.

The main restriction of the model, which also applies to all the models described in this work, is that it assumes non-interacting spheres. This places a significant concentration limit of the models use in high concentration samples (ϕ= 0.1+) and disallows samples that are charged or gelled, as is the case in many industrial samples.

1.5-2 The Diffusion Approximation

Whilst Maret and Wolf (1987) had shown that analysis may always have the same form, Pine *et al.* (1988) described the motion of photons as diffusion. In this case the weighting of each scattering order, which is related to I(l) in Equation 13, was known and the integral was solved as a general case, independent of particle size. Thus particle size was defined by a single function. For a plane wave incident on a surface of thickness L they described the amplitude correlation function as:

$$g^{(1)}(\tau) = 1/[(1-\gamma\, l_*/L)]\, \{\sinh[(L/l_*)\, (6\tau/\tau_0)^{0.5}\, (1-\gamma\, l_*/L)] / \sinh [(L/l_*)\, (6\tau/\tau_0)^{0.5}]\} \qquad \text{Equation 14a}$$

Which, in retroreflection, reduces to:

$$g^{(1)}(\tau) = \exp[\,\gamma(-6\tau/\tau_0)^{0.5}\,]^{-1} \qquad \text{if } L >> \gamma l^* \qquad \text{Equation 14b}$$

Such that the analysis is independent of l^*. Where γ is a parameter that describes the crossover from ballistic to diffusive light transport. Their work suggested γ was 2 with very little variation with particle size. This was a significant advance as it not only produced an analytical solution but also a solution that, in the specific case of retroreflection, was not a function of l^*, and thus was concentration independent. If the sample volume is limited in size higher order scatter may be preferentially lost leading to line shape variation on the correlation. However, the requirement set for a minimum sample volume is not significant in most industrial applications, and not at all in pigment manufacture. Typical measurements of l^* (in milk and latex) are of the order of 1mm and thus the sample will normally be significantly larger.

1.5-3 Analysis of Size

The concept of diffusion of photons and thus random walk led directly to the simple solution of Equation 14b. The equation is not a function of l^* and thus no background measurements are required. Taking the logarithm of both sides gives:

$$\log g^{(1)}(\tau) = -1/[\gamma(-6\tau/\tau_0)^{0.5}] \qquad \text{Equation 15}$$

Thus plotting the correlation as log/square root gives a straight line, the gradient of which may then be related to the diffusion coefficient:

$$D = -\tau_0 / K^2 \qquad \text{Equation 16}$$

and thus the size obtained via the Stokes-Einstein relationship:

$$R = (kT)/(6\Pi\eta D) \qquad \text{Equation 17}$$

Where T is temperature and K the scattering vector. This equation assumes that the measured diffusion coefficient is the free diffusion coefficient, Section 2.3-3. The negative is simply due to the analysis of the intensity (as opposed to amplitude correlation) as discussed, Section 3.2-1. This work did not assume the whole model to be absolute from the project start. The value of the refractive index used in the analysis (and thus K) has been considered in detail, Section 5.3-5/4, 5.4-2. It has also been concluded that in DWS the Stokes Einstein relationship itself was of limited validity, Section 5.4-2/3. Thus, Equations 16,17 are given as how DWS conventionally would be related to size, as opposed to the method of analysis proposed by this work.

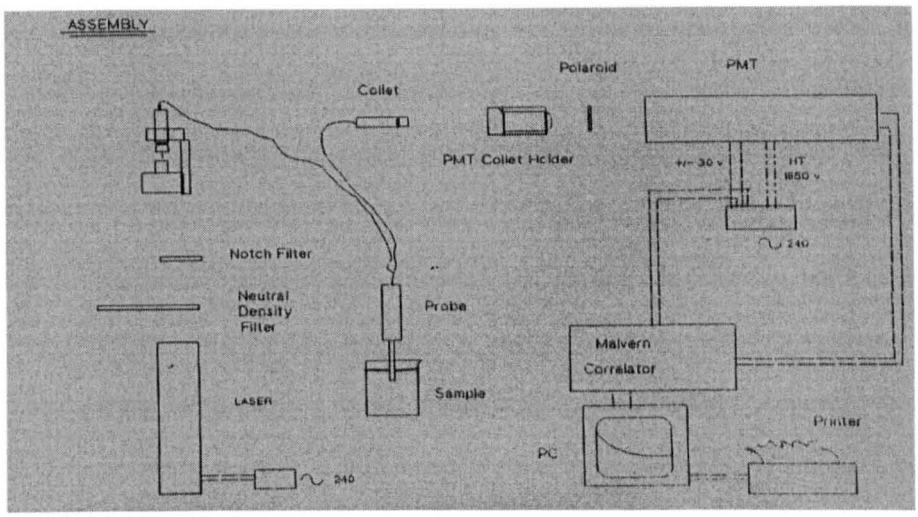

Figure 2 DWS Optical Arrangement

The DWS arrangement used prior to this work. Figure taken from MSc thesis (Lloyd 1991).

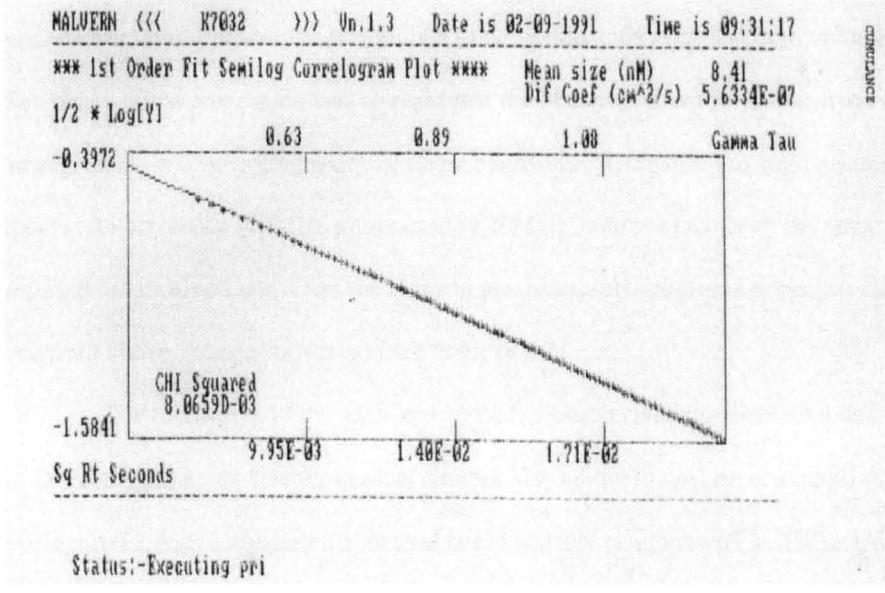

Figure 3 A DWS Correlation

The figure shows a DWS trace with the log of the correlator accumulator value (α) plotted versus the square root of the correlator decay ($\tau^{0.5}$) for a 300nm latex bead at a volume fraction of 0.02. The data appears suited to the model, with the data points not distinguishable from the fitted straight line. Analysis using a modified form of the Malvern autosizer package (Perkins 1990). Figure taken from MSc thesis (Lloyd 1991).

1.5-4 Hardware Development Prior to this Work

A basic fibre mediated arrangement, operating on a retroreflection approximation, had been constructed prior to this work being carried out (Lloyd 1991), Figure 2. Two cleaved optical fibres were glued into a hypodermic syringe used to produce a probe. One fibre was illuminated with a laser and the other directed at a photon detector connected to a correlator. On low refractive index samples at moderate concentration the correlation line-shape appeared to match the basic model well, Equation 14b, Figure 3. This earlier arrangement, whilst crude, demonstrated a robust technique that was insensitive to both vibration and contamination. The system was shown to rank latex microspheres linearly, at least for a size range between 200nm and 2 micron, Figure 4.

The ability to operate at a liquid interface (without Fresnel reflection) suggested the method could be employed in-line as a process monitor giving real-time feedback, Figure 4.

The system was evaluated for concentration dependence using a sample of white paint pigment, Figure 5. Whilst the original results suggested zero concentration dependence, at high volume fractions, the analysis was known to be significantly biased at high volume concentrations. The decay of the correlation was so rapid that the Malvern correlator (taken from a Malvern PCS arrangement) was operating near maximum bandwidth. To reduce this limit a second higher bandwidth correlator (40MHz as opposed to 20MHz) was used to check the results. In addition, information received later from the pigment manufacturers suggested imperfect mixing might have occurred above volume fractions of the order of 0.2.

The robustness of the technique to both vibration and contamination had shown the ability of DWS to operate on-line for process control. The ability to operate at a liquid interface (without Fresnel reflection) suggested the method could actually be employed in-line as a process monitor giving real-time feedback. To this end the system was evaluated for flowing systems[1]. Results on a laminar flow system showed a clear reproducible relationship between flow speed and the correlation gradient, Figure 6. Plotting the logarithm of the measured size against the logarithm of the fluid surface velocity gave a simple linear relationship allowing deconvolution. The correlation decayed faster with increased flow speed but no effect on the correlation line-shape was noted.

1 Since this work it has been shown DWS may be used as an analysis technique where the flow is three dimensional (Menon and Durian 1997).

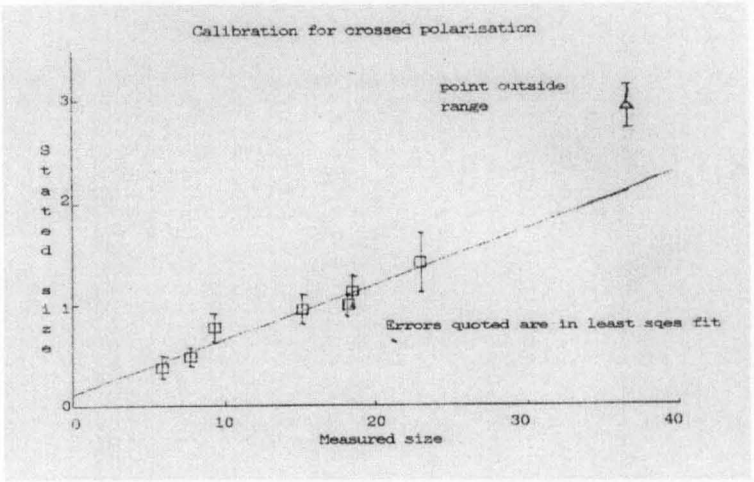

Figure 4 Size Ranking by DWS

The ranking of a range of polystyrene beads using the DWS arrangement, Figure 3. The 'measured' size is that given by the Malvern Autosizer using a modified form of the Autosizer package (Perkins 1990). The probe was placed on the sample/air interface. Figure taken from MSc thesis (Lloyd 1991). In this work, the inverse of the correlation gradient (from the log α versus $\tau^{0.5}$ plot) was used as a measure of size.

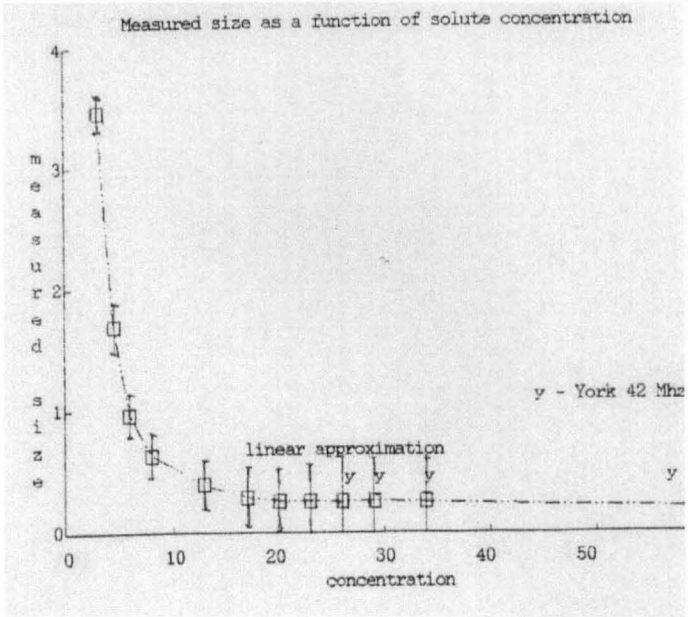

Figure 5 Concentration Dependence of DWS

The output parameter of the Step 0 software as a function of titanium dioxide pigment. The concentration is expressed as percent by volume. Figure taken from MSc thesis, (Lloyd 1991). Analysis using a modified form of the Malvern autosizer package (Perkins 1990), DWS size as Figure 4 but normalised to a volume fraction of 0.05.

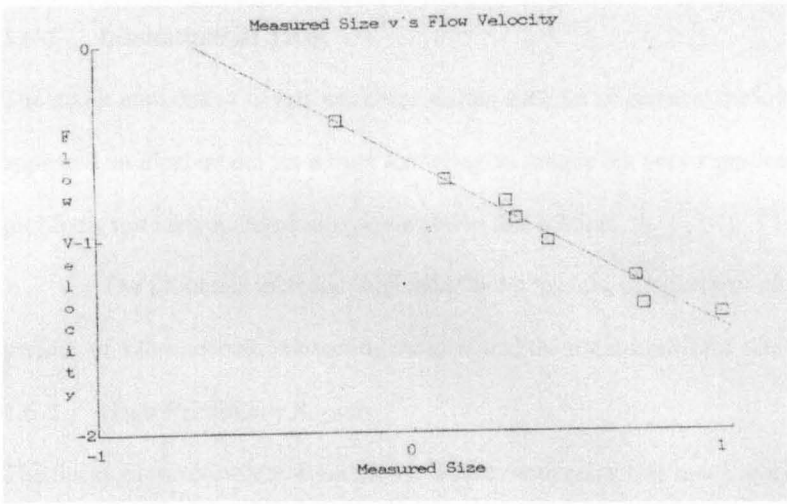

Figure 6 Flow Dependence of DWS

The 'measured' size is that generated by using a modified form of the Malvern autosizer package (Perkins 1990). The measured size was indirectly proportional to fluid flow speed when plotted log-log. Figure taken from MSc thesis (Lloyd 1991). The inverse of the correlation gradient (from the log α versus $\tau^{0.5}$ plot) was used as a measure of size. Measured size is defined as Figure 4.

1.6 The Application of DWS to Industrial Samples

1.6-1 Limitations of TiO_2

The major application of this work was in-line analysis of pigment during production. This initially appeared an ideal model for a light scattering technique but very significant sample specific problems were encountered as overviewed in this section.

The problems included: high bandwidth signals, samples that altered their properties over periods of a few second, interacting samples and the requirement for size distribution information.

1.6-2 High Frequency Signals

The decay of the correlation function increases with refractive index and concentration (scattering order) and inversely with particle size. Thus, the titanium dioxide pigments used in this work gave very high frequency signals, Section 2.5-4. The bandwidth placed significant demands on the hardware Section 3.2-2/4, to 7. Many of the assumptions used in PCS concerning instrument bias had to be questioned, as it was not known if they would be valid in this regime. The high frequencies involved also did not allow for conventional PCS fitting algorithms to be used in the analysis, where the region of the correlation function to be analysed is found automatically, Section 3.2-3/4,5.

1.6-3 Material Properties

TiO_2 has a relative density of 4 making even submicron dispersions sediment rapidly. The magnitude of this problem is shown by the use of the word stable within the pigment industry. The term does not denote a sample that remains the same, but that re-suspends in a similar way after a defined mixing protocol. Samples were shown to vary over timescales of seconds, such that most comparative measurement techniques were of little or no use in many situations, Section 2.3-2/3, 7.5-1/4.

The rapid sedimentation of the pigment was often compounded by the materials chemical stability. TiO_2 is inert material and requires boiling concentrated sulphuric to dissolve, Section 4.5.

Surface coatings to aid re-suspension are often difficult to apply and barely stable. Addition of other liquids to the continuous phase often caused an immediate collapse in the material and strong flocculation, Section 5.3-5.

The cross-linking materials, such as latex, added to these problems caused significant secondary issues. This made analysis even more complex, as the no-interaction model was obviously not valid. Many of the materials are added as coalescing agents, helping form a paint film, leading to instant build-up on the probe surface, Section 5.2-3/5.

The interactions were a significant issue as the model (Equation 14b) assumes no interactions occur. The concentrations and number of coatings and additives in a typical suspension suggested that the interactions would themselves be a complex mixture of types.

Thus this work undertook not merely to measure complex samples but samples that were known to be significantly outside the regime of the DWS model.

1.6-4 Material Processing

The major requirement for size analysis of pigment is in the final milling process, as opposed to the formation of the primary particles, Section 4.5. In the latter process there are significant benefits in terms of cost and final product quality. Whilst there is some commercial interest in analysis at the nucleation stage these processes have mainly been studied empirically by the industry. Once a 'recipe' has been formulated there is no requirement to alter it. DWS would only be of significant use in optimising new formulations. The equipment designed in this work would operate successfully in the majority (sulphuric process) of applications, provided the probe window holder was produced from glass as opposed to steel, Section 4.5-1/2. However, in the chlorine process nucleation occurs at temperatures of 500^0C, such that the probe would rapidly become unusable (diffusion of the fibre dopants). Thus, the probe would be required to be disposable or cooled. Both chemical processes for dissolution and re-crystallisation of pigments produce primary particles, typically of 220 nm diameter, Section 4.5. However, the resulting pigment mean size is typically in excess of 5 microns. The particles are formed of both strongly and weakly bonded collections of primary particles (aggregates, agglomerates and flocculates).

Milling a material with different types of primary particle binding may give rise to a complex multiple peak particle size distribution. In the final stages of milling, the vast majority of the sample is at the primary crystal size but a small percentage remains effectively unmilled.

The energy and time requirement for pigment reduction increases exponentially with reducing size. The sample would reach an effective plateau when all particles, that are capable of being reduced in size by milling, are at the base size and further milling has little or no effect.

Conventional analysis methods include turbidity and X ray sedimentation, both of which require dilution and are not suited to on-line analysis, Section 4.4. However, they both generate distribution information (sedimentation directly) whilst it was thought DWS would not.

In milling studies this was thought to be a significant problem as in the final stages the reduction in mean size may be minimal, the distribution is just narrowed. However, in early work DWS indicated that it had the necessary sensitivity to evaluate the milling process from the change in mean size alone Section 5.3-4. This work also suggests, that in specific conditions, a measure of polydispersity may be viable, Section 5.4-4/6. The measure was not based on size distribution but dispersion distribution, how well the sample was wetted to the fluid. This is a more significant measure in this type of application.

1.6-5 Environmental Limitations

Pigment factories, like most industrial process lines, are harsh environments. Temperature changes can be significant and rapid. Equipment may be subject to significant vibration and physical shock. Solvents, strong concentrated acids and alkalis are present. Typically, the environment is such that contamination, of any sample taken off-line, may be significant

Equipment for process work should not only be able to operate in such conditions but requires to be fully automatic, have minimum down time and pose no user hazards. Conventional dynamic and static light scattering arrangements are typically of little or no use. The equipment will not operate in the environment due to the temperature cycles, vibration and contamination. The operator needs to be trained to be capable of interpreting the results.

Furthermore, the large gas lasers typically required are too big, too dangerous and too fragile, as well as suffering significant failure and down time problems.

The project required to analyse real pigment samples in these conditions. Whilst this work touched on new concepts in dense media, such as shape determination (Section 5.4-3/7) and the dispersion index, the major project aim was strictly followed. This ensured that the project developed a viable method of industrial sample characterisation.

1.7 Optimisation of DWS for the Application

The introduction has discussed how dynamic light scattering is often a more robust and accurate method of particle analysis than simple intensity based measurements. However, only within the last decade has the analysis of suspensions of volume fractions of above 0.01 been practical.

The use of retroreflection DWS has been discussed as advantageous from both a theoretical standpoint, as no background measurements are required, and from practical aspects, allowing an in-line dip-in probe to be utilised. The most basic model of DWS was shown to give a reasonable calibration against known reference materials and to have low concentration dependence. The major application of the project, characterising TiO_2 pigment particles in dense suspensions, was shown to be a commercially viable application, as accurate particle size analysis may lead to improved product performance and/or reduced product cost.

The requirement for analysis techniques be operated in environments with temperature changes, noise, vibration, contamination, concentrated strong acids/alkalis and solvents has been discussed as making conventional DLS impractical in most process applications. The use of a dip-in probe suggested DWS was applicable to a wide range of industrial processes as the probe could easily be incorporated into a port into any pipe or vessel. The polarisation maintaining homodyne arrangement ensured vibration was not a significant problem, provided the probe was vibrating in conjunction with the sample, unlike conventional free space laser DLS experiments.

The production of an instrument and method that operated with the complex industrial TiO_2 suspensions produced generic hardware and methods capable of operating in almost all sample types. The solutions of the problems encountered required some of the basic assumptions underlying the technique to be questioned. This in turn gave rise to the possibility of analysis of a dispersion index (polydispersity) and even particle shape. Sensitivity was typically better than obtainable by most other techniques (below 1%, Section 6.3-2), even where sample pre-processing are conventionally required. Experimental set-up and control was automatic and measurement durations were typically 1-10 seconds. The system was capable of automated feedback every two seconds. The feedback was damped by previous results such that 'glitches' did not make the system unstable. The equipment could thus, be monitored by unskilled personnel and control the process directly.

CHAPTER 2

Models of Scattering for Industrial Application

2.1 Model, Method and Hardware Requirements

This project aimed at producing hardware, models and experimental methods to show that DWS could produce useful data in industrial environments and preferably in an automated way suitable for process control.

To this end the environment itself as well as the application specific limitations are considered first, Section 2.2. This is followed by a more detailed study of conventional light scattering. Whilst various techniques and methods have been used prior to DWS they are shown not to be suitable to the application, Section 2.3. The basic development and model of DWS is then considered along with its assumptions and limitations, Section 2.4. The final section details the theory and model used at the onset of this work and the approximations and limitations present.

The following chapter then considers the actual build of a DWS instrument and what, if any, of the approximations and assumptions made of the hardware for conventional DLS are valid for DWS, and this application in particular.

2.2 The Application and its Limitations

2.2-1 Industrial Requirements and Environment

2.2-1/1 Industrial Environment

This work was not aimed at a theoretical study of multiple scattering but establishing if a signal from a multiply scattering media could be utilised, for suspension characterisation, within an industrial setting.

Industrial environments are often ill-suited to optical methods due to significant variations in the temperature, humidity, electromagnetic fields and vibration. There is also a requirement for operation, of lasers, at safe optical powers on the shop floor. For process lines the equipment had to be used by unskilled personnel, if not be fully automatic. This section details the requirements of the application on particle sizing equipment.

2.2-1/2 Process Control Requirements

The major application of the equipment was seen as the active control of a process line. The pigment industry carries out continuous and batch processes which often last for days, such as pigment milling. There is a significant requirement for a method that can evaluate the concentrated suspension.

This would allow a reduction in processing, thus energy saving and increased plant throughput, without risk of product failure. The analysis requires not only to be on-line, but also to properly fulfil the requirements of process control it is required in-line. Thus the optics had to be compliant with operation through ports into pipes and the measurement and analysis capable of rapid operation. To generate an automated feedback loop the analysis had to be capable of producing a simple variable/s describing the process material's state.

2.2-1/3 Supporting Measurement Limitations

Incorporation of DWS into an existing process was made difficult, as no generic method for measuring diffusion, in dense systems, existed. Conventional measurements rely on dilution and thus measure a different property. Analysis by DWS is a measure of the actual sample characteristics, including interactions, Section 2.5-2.

DLS could be used as a generic reference technique, to DWS, only in specific conditions. The size had to be stable during dilution, such that only dispersions as opposed to emulsions could be considered. In addition the property being studied by DWS had to be a change in size, as opposed to change in other suspension characteristic.

This point has been discussed in some depth (Section 5.4-2/4) in comparison of DWS with the industry standard turbidity and sedimentation methods, Section 4.4. Often due to the limitations of the background measurements, they are either not carried out by industry or only carried out on final product.

This work has shown that DWS is highly sensitive (Section 5.3-4) and calibration to a standard technique will be limited to the accuracy of that technique. In most cases this will give an absolute accuracy that is very low compared to sensitivity. This can make a readout in absolute size misleading, the possible error being an order of magnitude, or greater, than the statistical variance.

This work suggests that, for generic industrial usage, DWS must be capable of some form of calibration, without reference to other techniques. Thus a method of calibration was required where calibration occurred against a reference sample, which is known to be ideal of that process, and variation from this used to determine the material or process characteristics.

2.2-1/4 Identification of the Correct Parameter

The majority of work on DWS has assumed, by necessity, that the dependant parameters required for the light scattering model are the same as those used for DLS. This work discusses that the refractive index used in the analysis is not merely that of the suspension but is that of the sample Section 5.3-5/4. An even more significant problem is that this may not be a simple percentage volume effect but a non-linear effect based on scattering cross section, thus a function of particle size itself, Section 5.4-2/1.

This work also considered the term viscosity could be defined differently in terms of interactions (Section 5.4-2/3) and how analysis of different regions of the correlation function could result in different effective viscosities being analysed, Section 6.3-4. The situation is further complicated as interactions (as well as continuous phase viscosity) are temperature dependent.

2.2-1/5 Dependent Variables

Even if the correct dependent variables for the model are identified, absolute sizing may not be practical. Many process industries buy in 'trade name' materials to add to their product. They may have little or no information on the optical properties of these materials, which are often trade secrets of a third party. There is little point in a robust on-line process system if analysis requires off-line examination of background measurements.

The lack of an 'absolute' size is frequently not a significant issue. Most industries are interested in maximising a certain property of a materials behaviour, as opposed to obtaining a size in microns.

In many instances this carries over to any supporting equipment, which is available to calibrate DWS. In industry the equipment is often not calibrated to absolute size, but to give a certain value for the product. This was shown to be the case in this work.

Pigments for UV scattering applications (sun tan cream) when measured by the conventional techniques gave a significantly larger size than theory would suggest was optimum. However, this 'absolute' size was then calibrated against empirical results on properties of the sample when applied as a film, Section 5.4-3/7.

2.2-2 Application Specific Limitations

2.2-2/1 Application Limitations

The previous subsection considered that general industrial process lines place limitations on analysis equipment. However, each application has its own subset of further limitations and it was found these were significant in the pigment industry.

2.2-2/2 The Pigment Industry Environment

The pigment production process is based on dissolving one of the most inert elements. The majority of process lines operate by dissolving the TiO_2 in boiling sulphuric acid, although the use of chlorine at over 500° C is becoming more widespread, Section 4.5-1/3. Following this the material is ground, typically over periods of 24-48 hours. The process produces significant vibration, heat and electrical noise. The product itself is used as an abrasive and is capable of damaging even hard crystal materials over a short period of time, Section 5.2-3/6. After production the pigment is usually mixed with solvents to form a paint material.

Thus, a DWS instrument for widespread use had to be capable of withstanding vibration, temperature and electrical noise. Any part of the material exposed to the sample also required to be capable of being immersed in both strong acids or alkalis, as well as a range of solvents. Any part of the reading face in contact with the sample had to be replaceable, as even sapphire will scratch quickly with the pigment material.

The basic retroreflection arrangement discussed earlier (Section 1.5-5) had obvious advantages. It allowed a dip-in probe such that only a small area of the equipment was exposed to the sample. In addition, by clamping the probe to the sample container, problems of vibration were minimised.

2.2-2/3 Adhesion

Many of the materials analysed were aimed at the paint market, i.e. intended to produce a film that dries on contact with air. Materials such as latex (rubber not as in conventional 'latex beads', which are now produced from polystyrene) were used as coalescent agents and were designed to bind to any exposed surface, Section 5.2-3/5,-8. This gave a requirement at the start of the project for 'non-stick' coatings to be produced and used.

2.2-2/4 Interacting Particles

Industrial milling is carried out at volume fractions between 0.125-0.25, thus the approximation of non-interacting particles that underlies DWS will not hold, Equation 14b. Whilst the final products may have a volume fraction lower than 0.125 the pigment coatings and coalescing agents again limit the approximation. Even when supplied in dried form the majority of, final product, pigments were coated with long alcohol chains to cause interactions between particles on re-suspension.

Thus this project undertook to evaluate a material which neither in production nor final product could the DWS model be assumed to be correct.

2.2-2/5 Time Dependent Behaviour

The reasons for the addition of crosslinking agents became obvious when uncoated pigments were analysed. The samples showed significant time dependent effects as to settling due to their high density (ρ=4gm/cm^3). This has led to the pigment industry to define the term stability to include samples that immediately settle/flocculate, providing they return to their original size and distribution following a defined mixing method.

It became obvious early on in the project that a technique for industrial usage would require to be capable of analysing rapidly changing samples. In addition, this work has discussed that in many cases the time dependent behaviour gives more information than merely a size, Section 6.3-5.

2.2-2/6 Range of Decays

The pigment field probably generates a wider range of concentrations and refractive indices, hence characteristic decay times, than any other industry. Materials vary from polystyrene beads (ri =1.5) at volume fractions of 0.01 to ultrafine titanium dioxide (design size 50nm) at volume fractions of 0.125. The project was supplied with samples that showed decays from the millisecond range to those that decayed more rapidly than 250ns.

The collision properties of the samples also ranged from the hard sphere of simple pigments to effective polymer gel structures due to long chain alcohol pigment coatings and the effects of coalescent agents. Material viscosities ranged from water to thixotropic non-drip paint samples.

2.2-2/7 Absolute Size

The limitations of the industrial environment and application would appear to make the term 'absolute size' irrelevant in many applications, even where the sizing technique itself was usually considered absolute. In this work the model of DWS (Equation 14b) was known to be a gross simplification, not only were interactions significant but also a range of types of interaction were possible. The high refractive index of most of the samples made the question of which refractive index should be used for a model significantly more important than in many other applications, Section (5.3-5/4).

When these factors where taken in conjunction with the equipment/experimental limitations (Chapter 3) it appeared that calibration of Γ was of greater validity. The sensitivity of the technique (Section 5.3-4) would appear to suggest the only method of particulate measurement for calibration would be electron micrographs and this would require significant assumptions on the effect of drying the pigment.

The consideration of Γ as the parameter to study had also been reached from theoretical reasoning. To calibrate the new technique it was considered that the measured parameter should be studied, not be a second order derivative (D, R) from a pre-existing model that was know to be inaccurate for the application. Instead the instrument output (Γ) should be monitored over a range of measurements and a new model generated, which may or may not fit with the accepted paradigm.

2.2-2/8 Size Distribution

The introduction (Section 1.6-4) gave an overview of the complex size distributions that can occur in a milled sample, as different types of particle collections break down at different levels of stress and in different rates. The distribution in the final stages of milling usually consists of two populations. The majority of particles have reached the primary particle size but a very small percentage remaining at a significantly larger size. These larger particles having an adverse effect on the material properties in final product and may effect the material shelf life (stability) as they will settle and may act as nucleation centres.

The mean size, or mean Γ, was of secondary importance in milling. Attempting to mill a sample to an 'ideal' size would result in extended, expensive and useless over milling, when the primary crystal size was slightly higher in a particular pigment batch. When the primary particle size was slightly smaller significant undersize and low specification product would be produced.

To allow milling to a correct mean size would also require the accurate measurement of the primary crystal size of that batch, prior to DWS analysis. This is a complex, costly, time consuming and inaccurate task.

In milling the rate of change of the mean size (or Γ) with processing time is the most significant measure. When the particle size ceases to decrease further the primary particle size has been reached. However, this requires an on-line sensitivity significantly greater than most DLS arrangements can produce, even in clean laboratory conditions, Section 5.3-4, Table 6.
In addition, the oversize population may be so low as not to be analysable within the much larger small population using conventional DLS methods, Section 7.5-1/4.

Any method of analysis of the quantity of oversize present was seen as key in assuring the instrument was a significant method of process characterisation for this application.

2.3 Conventional Methods and Models for Light Scattering

2.3-1 Photon Correlation Spectroscopy

2.3-1/1 PCS Operation and Limitations

The introduction gave a basic overview of PCS without study of its inherent limitations. The model requires that suspended particles do not interact with one another and that photons are scattered only once prior to detection. The latter is generally the most important assumption in defining the upper range of the concentration that may be analysed. The limit is strongly dependent on refractive index and may be as low as a volume fraction as $1x10^{-4}$, on highly refractive materials. At such low concentrations the first assumption, coupling of scattering particles, is not usually relevant.

2.3-1/2 Dilution

In the majority of PCS applications the sample must be diluted, this generally removes the possibility of in-line monitoring (Chowdbury *et al.* 1984, Carr *et al.* 1988, Chow *et al.* 1988) and of the study of the bulk properties of the sample. In many applications it is the bulk properties that are of interest and measurement of a free diffusion coefficient by dilution is either of no consequence, or at best, a second order measurement. In conjunction with the defined limits dilution also requires significant assumptions. Possibly the most significant assumption is that the sample will remain stable on dilution, which is not typical in many cases. This may be particularly true for hydrophobic materials such as pigment where complex coatings and additives are used to maintain stability, often by cross-linking. Also to be capable of dilution the exact make-up of the continuous phase must be known. In industrial environment, this may not be known and/or the recipe may vary to stabilise samples on a batch basis.

2.3-1/3 Operating Environment

The requirement for dilution has significant effects on the equipment and its operating environment. Typically lasers for PCS are rated in Watts, require three-phase power and water cooling.

Whilst smaller lasers may be used in specific applications, no operation has been found at or below laser classification 3. Thus, they must be only be operated by specific personnel.

In addition the strong scattering dependence on particle size (Equation 2) makes contamination by a dust a significant problem. The environment must be kept clean, the waterbath, and continuous phase used for dilution, stringently filtered.

2.3-2 Analysis of PCS data

2.3-2/1 Interpretation of Γ

The introduction detailed how a PCS analysis produces a single exponential, which allows direct determination of the characteristic decay rate, and hence size. However, the analysis is more complex, this is considered in more detail prior to consideration of effects of concentrated systems.

PCS is often stated to be an absolute measure of size. In the strictest sense this is incorrect, PCS measures spherical equivalent hydrodynamic radius to which no standard exists. Even if such a standard came into being the measurement would only be absolute when carried out in heterodyne mode (Section 3.2-1), unlike all commercial arrangements.

This section gives only a brief overview of PCS to allow development of DWS theory. The technique that has been reviewed extensively (Cummins and Swinney 1970, Cummins and Pike 1974, Chu 1970, Ford Jr 1970, Pusey and Vaughan 1975, Pecora 1985, Phillies 1990).

2.3-2/2 Analysis of the Correlation

The analysis of dilute suspensions is complicated by the limitation that the sample will be polydisperse in diffusion coefficient and/or refractive index. Thus the correlation is not an exponential but a curve produced from the summation of exponentials for each particle species. Koppel (1972) modelled polydispersity in PCS analysis by this lack of single exponential behaviour. The correlation is fitted to a set of polynomials and analysed as a series. It is important to note that the analysis assumes all deviation from single exponential behaviour are due to polydispersity of size alone.

The R^6 dependence of light scattering makes it highly sensitive to a small population of large particles, such as oversize in milling. However, the large particles are at least an order of magnitude greater than the incident laser wavelength. Even where the distribution was simple lognormal multi-angle measurements would be required due to the Mie scattering pattern, Section 1.2-3. This requires very precise angular alignments and such equipment would rarely be considered robust.

2.3-2/3 Distribution Analysis

Whilst the cumulants method, described previously, is often used to generate a distribution the technique merely gives a mean size and an index that is a measure of the non-exponential behaviour. Analysis software uses the simple quadratic fit to produce a distribution assuming a standard, typically lognormal, distribution. Whilst the method is a robust technique at analysing mean size it is limited to effectively showing that a sample either is, or is not, a narrow assumed distribution. To fully analyse the distribution would require fitting a large number of exponentials, where both the decay time and magnitude floats in the iteration. However, this problem is ill conditioned and no single solution can be found.

Methods of distribution analysis are based on either: force fitting the data to fixed size intervals or consideration of parsimony. The latter method assumes the simplest answer, that gives a reasonably low error, is the correct one. The methods are complementary.

The force fitting technique is good for measuring wide particle size distributions that cover many size intervals but is obviously limited where separate distributions are widely spaced and narrower than the interval. However, the floating method (CONTIN) can analyse narrow widely spaced distributions. These techniques were available as standard software on the Malvern 9600C PCS arrangement used in this work.

In pigment manufacture, at milling onset there is one large wide distribution that would be suitable for the interval technique but as milling progresses the presence of two discrete widely spaced populations will significantly bias the results.

Basic theory would suggest that whilst PCS may not correctly identify the oversize distribution it should be highly sensitive to it. However, experimental results in this work suggested that PCS ignored the oversize population, as it would have settled out before measurement. Even if this limitation was overcome there may be limitations, due to the relative size (particle number) of the larger distribution. This work suggested that the conventional methods of noise reduction may act to remove the effect of oversize from the PCS signal prior to data analysis, Section 7.5-1/4.

2.3-2/4 Rotational Diffusion

The previous section has shown that the interpretation of the correlation is complex for real samples. However, even if a truly mono-disperse sample could be produced and measured at a single angle there would still be a spread in exponentials.

The previous model assumed the particles have one degree of freedom, i.e. are spherical. However, particles are never perfectly spherical and a rotational diffusion coefficient is convoluted with the translational coefficient (Pecora 1968, Tagami and Pecora 1969). Thus a monodisperse sample of non-spherical particles will generate a tri-modal correlation similar to a sample containing a mixture of three monodisperse particle sizes (Cummins *et al.* 1969), Section 5.4-3-5.

2.3-2/5 Range of Wave Vectors

The introduction noted that it is necessary to limit the measurement volume of a DLS experiment to assure coherence between scattering particles. This itself does not limit the scattered intensity as high numerical aperture lenses may be used. However, as the numerical aperture increases so does the range of scattering vectors analysed, which gives rise to a range of exponentials in the final correlation. This is an effective size distribution. Thus the numerical aperture of the equipment will generate a falsely broadened distribution. However, it will not affect the mean measure provided the particles are small compared to the incident wavelength.

Where analysis other than mean size is required, the numerical aperture must be minimised leading to conflicting requirements.

DLS relies on single scattering from a small volume and thus a low intensity signal. The measurement of the distribution approaches ideal as the numerical aperture approaches zero, such that there is no signal. It is not possible to increase laser power beyond certain thresholds or laser heating becomes a significant problem, such that a compromise is required.

The situation defines that, where a sensitive measure of the size distribution is required, that DLS will always require high power lasers. This is a significant limitation for industrial usage.

2.3-2/6 Absolute Size

This chapter has already discussed that the PCS size cannot be considered absolute. The measure is also a complex function of the particle size distribution, refractive index distribution, particle shape and particle shape distribution.

In PCS, in the infinite dilution regime, the diffusion coefficient is termed the self diffusion coefficient, D_0. This approximation assumes the scattering particles have no interactions with each other. The measured diffusion coefficient is also affected by the surface tension between the particle and the solvent. The surface properties may lead to the particle carrying water molecules with it, as it moves, increasing its effective size. The analysis also uses a drag factor calculated from macroscopic analysis of the viscosity of the supporting fluid. Thus, the size calculated from PCS is a hydrodynamic size and a measure of the particle in a particular suspension as opposed to the particle itself. The measured size may be a strong function of additives such as dispersants or ions, even where these are at low concentrations. This has been discussed as significant in pigment applications. Even the simplest pigments used in thus work were typically coated to allow dispersion and many had a second overcoating to aid stability.

The information relating to size is detected by means of scattered light. When the particles are small compared to the wavelength, this may be approximated as varying as R^6, which defines the weighting of the particle distribution. This strong function leads to a distribution, and mean size, which is highly dependent on small populations of large particles.

The analysis is complicated for large or high refractive index particles, such as TiO_2. The scattering cross section (Equation 2) will be oscillatory with size and vary with scattering angle, Section 1.2-3. For PCS analysis of absolute size multiple angle measurements would be required

The actual measurement is therefore 'the mean, intensity weighted, spherical equivalent, hydrodynamic radius' and is based on assumptions of the rotational behaviour of the particles and assumes that no interactions occur. Underlying the entire technique is the assumption that the amplitude, not intensity, correlation function has been measured (Section 3.1-2/4) although in commercial equipment this appears rarely to be the case.

2.3-3 Operation Above the Infinite Dilution Regime

2.3-3/1 Diffusion

At high concentrations, particles will interact with one another and the self diffusion coefficient cannot be directly measured. The interactions are typically separated into three types: hard sphere collision, charge repulsion and momentum transfer *via* the continuous phase, as further discussed below.

Whilst these models may be limited in more complex pigment samples, they indicate the type of interactions arising in uncoated pigment materials.

2.3-3/2 The Electrostatic Model

The electrostatic model described by Pusey and Tough (1983) has an analytical solution and is thus suited to direct implementation in light scattering equipment. Whilst more detailed models of interaction have been considered (Pusey 1975, Pusey and Van Megen 1992, Russel 1981, Brady 1993), the results, and implementation in a practical light scattering system, are more complex. The correlation decay of particles diffusing in a harmonic crystal is given by:

$$\Gamma = [(k T) / M] \exp (-\tau / t_B) - A \exp (-t / t_I) \qquad \text{Equation 18}$$

Where t_B is the time scale of solvent/solute interactions, t_I the time scale of solute/solute interactions and A is a constant defining the electrostatic well. The particles will also interact with each other, the effect increasing linearly with the time-scale monitored. The average displacement, S, in time-scales over a few ns will be given by:

$$S = < x^2 (t) >_{(t>tb)} = 2 D_0 t - 2 A t [(t + t_I) \exp (t / t_I) - t_I] \qquad \text{Equation 19a}$$

Which may be approximated by the equations:

$$< x^2(t) >_{(tb<t<tI)} = 2 D_0 t - 2 B t^2 \qquad \text{Equation 19b}$$

$$< x^2(t) >_{(tI<t)} = 2 (D_0 - A t_I) t + 2 B t_I^2 \qquad \text{Equation 19c}$$

The long time self-diffusion of the particle can be defined as $D_s=D_0 - Bt_I$. This is a measure of the motion on time-scales $t>t_I$ where the particle is moving through a number of quantum wells. Pusey and Tough (1983) further analysed this model and showed that t_I first appears in the third cumulant and could thus be measured, in a monodisperse system.

2.3-3/3 The Hard Sphere Approximation

The electrostatic model assumes that the quantum well is a smooth single function, which may be reasonably accurate in dilute un-screened systems. However, it will not hold for counter ion-screened systems, where A may itself be a function of the distance from the ideal crystal spacing.

In more dilute (ϕ= 0.01 - 0.05) and less charged systems, when a large area of the correlation tail has been analysed ($t = t_l$), the term; $D_s = D_0 - B\ t_l$, may be more accurately replaced by the hard sphere equivalent $D_s = 1 - 3.06\ \phi$. This has been found to be the case for many of the polystyrene sphere type materials (Hoover and Ree 1988).

2.3-3/4 Application of Interaction Models to DWS

Even the simplest samples analysed by DWS are liable to involve interactions. In the case of pigments this situation is complex. In uncoated samples the hard sphere model should hold to a good approximation, however when dealing with coated product the alcohol coatings will hinder motion. It is probable that this will operate similar to the electrostatic model, the linkage having increased effect with particle displacement. In addition, real paint samples will contain cross-linking materials (coalescing agents). Where the pigment does not attach directly to them this would suggest a caged system, similar to the hard sphere model but over a different displacement range. Paints contain a range of different particle types with different surface coatings and undergoing different interactions. Real paints are further complicated as they tend to be thixotropic such that one or more of these interactions is a function of shear, and when the shear was applied.

The requirement for operation in single scattering has made experimental study of these interactions complex for conventional DLS and various techniques to allow operation at higher volume fractions have been devised.

2.3-4 Conventional Analysis of Dense Suspensions

2.3-4/1 DLS in Dense Suspensions

Whilst PCS is limited to very low volume fractions, attempts have been made to use modified PCS equipment and models in higher concentration samples. Thus, before consideration of DWS, these methods were studied to illustrate the need for the new technique.

2.3-4/2 Depolarised Photon Correlation Spectroscopy

The onset of double scattering inhibits conventional PCS measurements, as the ratio of different scattering orders requires to be known to allow solution (Russel 1981). However, novel approaches have included modelling the effects of double scattering (Sorensen *et al.* 1976, 1978).

The method requires that the particles scatter as the Rayleigh model and thus do not depolarise the light scattered at ninety degrees to the incident beam. Thus when only depolarised light is detected the analysis ignores single scattering. Whilst this model allows a very simple method of analysis of samples outside the infinite dilution regime, the increase in concentration range is limited. The concentration must be such that the number of photons scattered by three, or more, particles is insignificant. In addition, whilst in normal PCS it is possible to check the scattering regime by simple single dilution, this is not the case in this technique and prior knowledge of the concentrations is required. Obviously, pigment samples are far too dense to suggest only double scattering occurs and in addition the particles cannot be considered small compared to the incident wavelength. Thus the technique had no relevance to our application directly.

2.3-4/3 Tracer Analysis

A significant amount of work has been carried out using tracer particle analysis. The sample to be measured must be low refractive index such that it is possible to alter the continuous phase to the same value, at this point no scattering is evident. A small number of tracer particles, of a different refractive index but similar size, are added. This low concentration population may then be analysed by PCS. This made possible the study of many of the models of interaction (Ottewill and Williams 1987, Hoover and Ree 1988, Pusey and Van Megen 1992). However, the techniques are of little or no use as the generic methods of analysis for industry.

2.3-4/4 Restriction of the Measurement Volume

Direct PCS analysis has been carried out at volume fractions as high as 0.01, using a novel wedged cell (Cummins and Staples 1981) to restrict the analysis volume[1]. Many of the methods based on a similar theme, of restricting the area monitored, have been discussed extensively (Schatzel 1991). The restricted area is not defined by the cell but by the optics. This can be carried out by means of restricted overlapping scattering centres, cross-correlation of different frequencies and techniques based on colour coding and/or time coding[2].

These techniques allow the characterisation of small areas of dense suspensions but at significant added complexity. In addition, these techniques are based on analysis of single scatter, where the majority of the signal must be discarded. Laser powers are typically even higher than required for DLS and signal to noise may be lower. For dense suspensions, it would obviously be better to analyse the higher signal magnitude, multiply scattered light.

1 This appears to be the background of the ALV-NIBs systems that has become available over the past year (Peters *et al.* 1998)
2 Recent work (Urban and Schurtenberger 1998) has allowed DLS measurement size and PSD in samples of polystyrene at volume fractions of 0.2 using cross correlation.

2.4 Models of Multiple Scattering

2.4-1 Historical Development

2.4-1/1 Early Analysis Methods

The majority of the work predating the diffusive model of light can be traced back to the analysis of blood in vivo (Tanaka and Benedek 1975), which was aimed predominantly at measuring flow rates. Dyott (Ross *et al.* 1978, Dyott 1978) used a conventional PCS analysis, alongside a calibration for concentration based on the scattered intensity. Floy *et al.* (1988) analysed volume fractions as high as 0.4 where analysis was based simply on the area under the power spectrum curve. The correlation has also been analysed in terms of a bi-exponential where the long decay tail was considered due to single scattering (Thomas and Tjin 1989, Thomas and Dimonie 1987). Horne (1989) followed this approach as well as cumulants and straight line fitting to $\tau^{0.5}$. The work found the double exponential approach did not match the results but that the long time correlation tail could be used to estimate the size, as had been discussed earlier (Maret and Wolf 1988).

2.4-1/2 Solution of the Ill-Conditioned Signal

Until the advent of DWS it was assumed that the problem of analysis of light scattered from a concentrated system of particles was ill conditioned, i.e. that there was an infinite number of solutions that could match the data. Light would return from the sample with different orders of scattering at different times, due to path length differences, and from all directions. A solution for particle sizing came almost as a by-product of other advances in optics thus a brief review of the related advances in localisation is given.

2.4-1/3 Localisation & Enhanced Backscatter

The solution to multiple scattering analysis can be traced back to pioneering work of Anderson 1958). His theory suggested diffusion of electrons would not occur in the conduction band of semiconductors, due to the random spacing of the impurities, the interactions between impurities and the interactions between the electronic and nuclear spins. The theory suggested that at low densities of impurity the diffusion of the free carriers, as spin waves, cease. The wave functions are said to be localised.

The phenomenon was shown to exist in the scattering of electromagnetic waves from the atmosphere (De Wolf 1971). It was extended to include the localisation of visible light, within a random polystyrene suspension at a volume fraction of 0.3 (Van Albada and Lagendijk 1985).

The underlying theory shows that where light is detected at the same angle as launch (180° or retroreflection) two photons may travel opposite but identical paths prior to returning to the detector and thus generate an increase in intensity. They found an enhancement of 1.6 and 1.3 for light detected with a polarisation parallel to and perpendicular to the incident light compared to theoretical values of 2 and 1. Whilst the localisation of light may be of significant importance within the optics field, it is the 'randomness' within the theory that allowed solution for particle sizing.

2.4-1/4 Transport and Scattering Paths

The introduction has already shown that the work of Maret and Wolf (1987) gave a solution where a single equation could represent all types of suspension, Equation 13. This was extended by the concept that the light migration could be considered diffusive (Pine *et al.* 1988), Equation 14a.

Pine *et al.* (1988) used the effect of varying L to experiment, via transmission experiments, with photons that had traversed short paths, hence seen large particle movements. However, in this regime Equation 14a must be replaced by:

$$g^{(1)}(\tau) = L / (\gamma l_*) \{ \sinh [(\gamma (6\tau/ \tau_0)^{0.5}] / \sinh [(L / l_*) (6\tau/ \tau_0)^{0.5}] \} \quad \text{Equation 20a}$$

Which may only be reduced to:

$$g^{(1)}(\tau) = [(L / l_*)(6\tau / \tau_0)^{0.5}] / \sinh [(L / l_*) (6\tau / \tau_0)^{0.5}] \quad \text{Equation 20b}$$

Which, for $t << \tau_0$, still requires separate measurement of l_* (parameters as defined Equation 14).

The model of the diffusion of photons through a sample has been given qualitative support by work using both physical models (Garcia *et al.* 1992) and Monte Carlo simulations of the transport of light from an isotropic source in dense media (Zaccanti 1991).

In addition to the limitation of requiring a background measurement, transmission measurements are obviously significantly less useful for process control than retroreflection. Transmission requires a defined cell which must allow for the source-detector spacing to be moved to allow for samples of a range of l_*. It does not allow for a dip-in probe or simple incorporation through a sample port, as does the arrangement used in this work.

2.4-2 The Model and Analysis

2.4-2/1 Size Analysis

The introduction has discussed how the correlation line-shape (decay rate) may be related to the particle size and the limitations of this method, Section 1.5-3. For absolute sizing, where the sensitivity of the technique is reflected, the complexities of concentration in terms of ballistic scatter, interactions and suspension refractive index require more thorough consideration. In addition, the complex nature of the scattering vector needs to be accounted for in the case of particles of the order of three times the incident wavelength, such as 220nm TiO_2, Section 1.2-3.

To overcome the limitations of the unknown parameters, and small number of samples of each suspension type, this work studied the instrument function, Γ. This is defined as the gradient of the correlation when the logarithm of the accumulator is plotted against the square root of the delay time. This has the benefit of not assuming the validity of the scattering vector, the Stokes Einstein relationship or the accuracy of a calculated or measured ballistic to diffusive crossover factor, γ.

Even using this simplified variable the analysis may vary between different instruments due to different instrument parameters, χ, Section 7.2-1/3. To overcome any practical instrumental differences all data was always normalised to a particular sample size, concentration or temperature. Thus the ratios obtained should be valid for other instrument types and regardless of any model variations. A transform was given for each data set such that data from other instruments could be compared directly with the results in this work.

2.4-2/2 The Step 0 Model

This work carried out a series of advances in the way the data was collected and analysed. To differentiate them they have been defined as Step 0 to 3, Section 4.3.

This work stemmed from a brief feasibility study (Lloyd 1991), that generated the initial model and the analysis methods, Step 0, Section 4.3-3/1. Following Pine *et al.* (1988), it was assumed the photon migration could be modelled as diffusion and the correlation would decay as an exponential when plotted against the square root of the correlator delay:

$$g^{(1)} = -\exp(\Gamma \tau)^{-0.5} + B \qquad \text{Equation 21}$$

which, when plotted log g_1 versus the square root of the correlator delay, may be modelled as a straight line:

$$\log g^{(1)}(\tau) = -(\Gamma \tau)^{-0.5} + B \qquad \text{Equation 22}$$

Where $g_1(\tau)$ is the amplitude correlation function, τ the correlator delay time, B a constant and Γ a measure of the characteristic decay. After establishing Γ by means of a straight-line fit the signal decay was analysed as PCS signal, Equation 16, 17. Whilst this model took no account of complexities, such as the diffusive crossover, γ (Equation 14b) it allowed the instrument output to be compared with supporting analysis and thus establish the correlation in size ranking.

2.4-2/3 The Step 1 and 2 Models

It was known that this work would be comprised predominantly of analysing the variation of Γ for industrial samples at different points in the milling process. Parameters that underlie Γ, such as γ, could not be analysed in detail. Thus a major function of equipment and algorithm design was to keep the technique within the diffusive regime and thus limit variance of γ.

During this work advances where made in automatic selection of the area of the correlation to use in the analysis. The pigment samples altered significantly over short time periods and it was shown that this variation was an important measure, Section 6.3-5. This led a significant part of this work to methods of analysing rapidly changing systems, Section 4.3-5.

2.4-2/4 Selection of the Delay Time

The work prior to this project, Step 0, had utilised measurements using a fixed correlator delay, which was arbitrarily set, such that the measurement included the majority of the correlation function. Initial work showed that in many instances, particularly at low concentrations, the correlation tail curved significantly in agreement with the concept of increased low order scattering, Figure 12. Methods of reducing the effect of low order scattering, whilst maintaining a simple straight line fit, were considered for the first (Step 1) analysis method developed in this work.

2.4-2/5 Step 1 Delay Time Method

The quantity of correlation analysed was found by incrementing the correlator delay from a minimum setting and carrying out a straight line fit after each increment. The optimum portion of the correlation was selected as that correlator delay that gave the lowest fitting error to a straight line. When only a small amount of the correlation was measured, the correlation was a straight line but limited by noise. As the amount of correlation increased, the relative noise in each data point decreased, however, the correlation began to curve. The point of lowest error was considered a compromise between analysis of the linear part of the correlation and the increase in noise when the area of the correlation analysed was reduced. Whilst the method had no proven theoretical basis, it proved to be a robust and reproducible method of analysis of the most complex correlation line-shapes studied in this work.

The weighting of the data points, that occurred due to the fitting procedure, was later shown to aid the fitting method and gave some understanding of its stability, Section 3.2-4/3.

2.4-2/6 DWS Models and Error Analysis

Prior to consideration of limitations of the DWS model used this work considers the limitations of fitting data from any new technique to a model, with emphasis on the specific characteristics of the DWS model analysed. For real experiment situations the actual, theoretical and measured functions are all different ($F_T \neq F_A \neq F_M$), whilst force fitting assumes $F_A = F_M$ so the measured error will be the sum of the statistical uncertainty in the points and variation from the ideal fit ($E_M = E_S + E_F$). In applications where the model represents the data well, such as PCS, it is often assumed that $E_F=0$. In this case $E_M = E_S$, the measured error is assumed to be the variance error. This estimation may be confirmed using a simple runs test.

However, in the case where the model is, or may be, a poor representation of the data ($E_F > E_S$), then a different analysis method should be used. The measured error could be due to almost purely statistical variance or purely due to a poor fit (Figure 7). In this work the latter was shown to be the case $E_M \approx E_F$, Section 5.3-2.

However, the statistical variation is of significant importance as this defines the sensitivity limitation of the measurement.

In stable suspensions, we can obtain a measure of E_s simply by the statistical variation in the measured parameter over repeated measurements. To study the model itself, and carry out an accurate fit, the correlation accumulator values (channels) should be averaged. The variance of each channel being used to weight the fit. This can have a significant effect when measuring signals where the function decays to zero (or a baseline) as the errors cannot be assumed to be constant with channel number. This is the case in DLS where the relative error typically increases logarithmically with channel number.

This posed a serious problem when analysing the majority of the pigment samples as they exhibited complex time dependant behaviour. In this case errors from 'averaging' would have the statistical variation convoluted with the sample (as opposed to measurement) specific time dependant behaviour.

To allow fitting early methods (Step 0, 1) used the assumption, commonly in PCS, that the variance in the accumulator channel is related to the squareroot of its magnitude.

However, possibly more importantly, it was not possible to give the statistical variance of the measurement. It would be incorrect, and misleading, to give a statistical variation value from an error which was due to time dependant change of the sample itself.

The problem of having an unknown model (i.e. assuming one that was only crudely approximate) and having samples which where not stable was a significant complication of this project. The use of standard reference materials would have overcome this but been of limited use, as they do not behave as typical industrial samples. Many industrial materials are not stable during manufacture and many manufacturing processes dealing with dense media have significant effects of the sample characteristics, Section 6.4-2. For DWS to be a viable technique in the pigment industry, and to allow generic usage elsewhere, it was obvious these limitations would have to be overcome. This led to the Step 3 software (Section 4.3-4) which defined each sample not as a two dimensional correlation but as a three dimensional surface. This latter approach allowed E_s, E_F, time dependent shifts in Γ and the correlation line-shape changes to be properly separated.

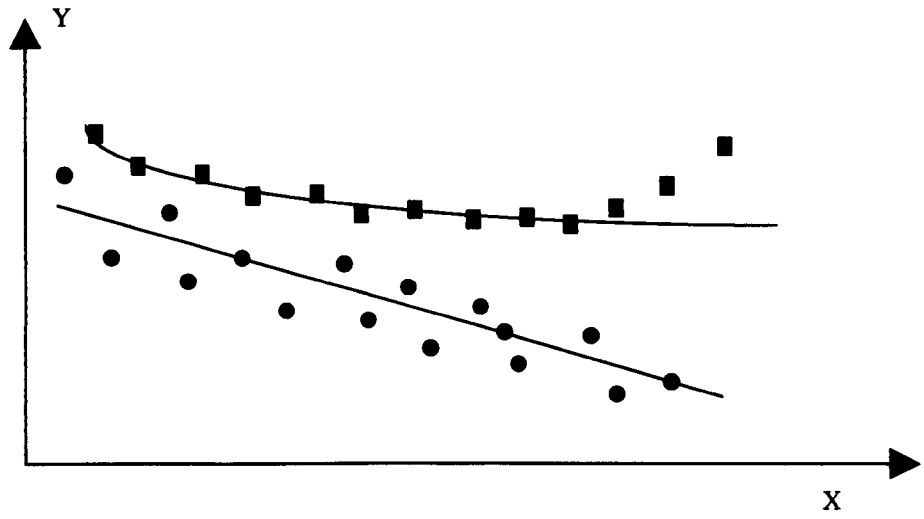

Figure 7 Limitations of Force Fitting

The trace shows two functions y=f (x) where the actual function (solid line) is measured with some statistical error. When force fitted to a straight line the polynomial trace (squares) may exhibit a better fit than the straight line (circles), due purely to the noise, although the lower trace is a better fit to the actual model. Thus force fitting takes no account of reproducibility (statistical noise) and actual model fit error. The suitability of the model can be assumed from a runs test, or similar statistical fit, but the limitation has significant effects when the data points must be weighted.

2.5 Limitations of the Models

2.5-1 Lower Concentration Limit of DWS

2.5-1/1 Range of DWS

The basic model of DWS was considered valid over only a narrow concentration range, the exact values dependent on refractive index and particle size but between volume fractions of 0.01 and 0.1. At low volume fractions it was understood that a significant portion of the returning light would be due to low order scattering. In this case the signal should be modelled as multiple, as opposed to diffuse, scattering. At concentrations above 0.1 the signal was considered to be a function of interactions between particles. In commercial pigments it has been stated that interactions may be present at much lower concentrations.

2.5-1/2 Retroreflection and the Low Concentration Limit.

The gap between the diffusive regime and the upper concentration limit of PCS measurement suggested that there would still be a significant concentration range not analysable by DLS methods. At low volume fractions the photon scattering path, and hence transport path, is highly concentration dependent. Use of a single fibre probe was not seen as viable. The probe would be highly sensitive to large particles in its immediate vicinity, as opposed to true diffuse scatter. In addition pure homodyne operation would not be possible due to reflection at the probe face and/or the beamsplitter/fibre fusion point, Section 3.4-4/4.

This section considers the conventional low order scattering limit of DWS and methods employed in this work to allow DWS to operate at lower concentrations.

2.5-1/3 Scattering Angle

The light leaving an emitter and entering a multiple scattering medium will begin to diverge with a delta shaped probability distribution, Figure 8. At a distance of one photon transport path the returning light may be roughly modelled as a diffuse spherical emitter. However, significant low order scattering is still detected and at low concentrations the variation in scattering orders will not be modelled by the diffusion approximation.

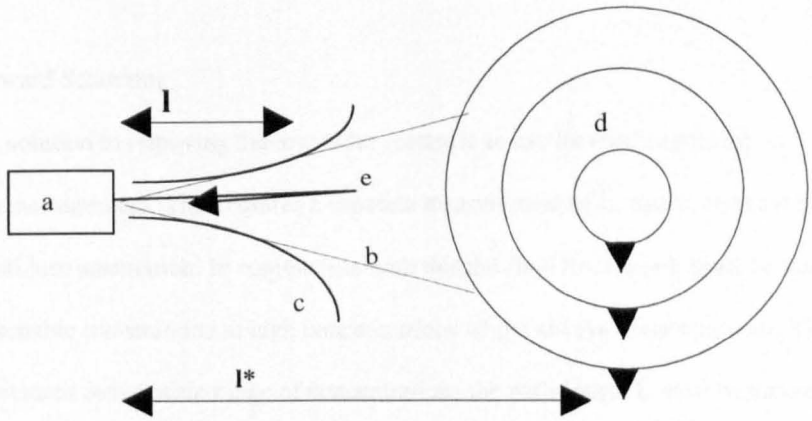

Figure 8 Retroreflection Arrangement

The figure shows a DWS arrangement in retroreflection. The emitter/detector has a NA (b) into which light is coupled, prior to 1 scattering path (l) the light will begin to spread into a delta wider than this NA due to scattering (c). Light returning that has travelled the equivalent of a photon transport path (l_*) may be modelled as a returning spherical wave (d). At low concentrations the signal will predominantly be due to low order scatter (e)

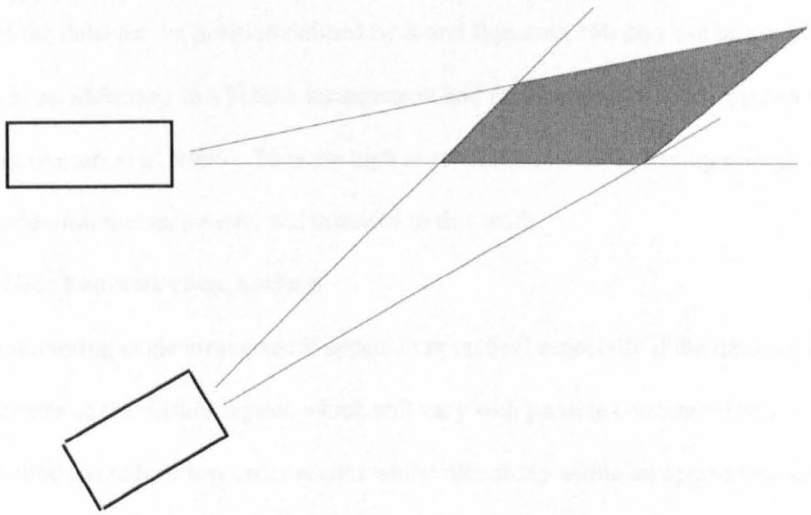

Figure 9 High Angle Scattering Cell

The definition of a scattering cell area is typically of many DLS arrangements. The NA of the emitter and detection fibre defines an area, shown in grey, from which scattered light is collected. This method has been used for the Brookhaven instrument and ensures light must have travelled a significant distance to enter the detector such that the light may be considered diffusive.

2.5-1/4 Forward Scattering

The obvious solution to removing the low order scatter is to use forward scattering, i.e. transmission measurement. This requires a separate measurement of l^*, which makes it less suited to commercial instrumentation. In conjunction with this the fluid thickness L must be thin enough to allow reasonable transmission at high concentrations whilst always remaining $>> l^*$. Thus to allow measurement over a wide range of concentrations the path-length L must be variable, this makes implementation in process significantly more complex.

2.5-1/5 High Angle Scattering Measurements

High angle scattering cells have been utilised to reduce second order scattering, an example is the Malvern HiC instrument with a fixed scattering angle of 150 degrees. This ensures all light has travelled a significant distance and removes low order scatter, Figure 9. This requires solution to Equation 14a, as the analysis is now a function of l^*. A second problem encountered is where the detector is at fixed angle and not directed at l^*, Figure 10. The diffuse spherical wave is not centred in front of the detector, its position defined by l^* and Equation 14b may not be applicable. This point has been addressed in a FODA arrangement and results showed an increase in the diffusion coefficient (Ansari *et al.* 1993). Thus the high angle cell was seen as having no significant benefits over transmission measurements, and unsuited to this work.

2.5-1/6 Near Retroreflection Analysis

The high scattering angle arrangement appears impractical especially if the detector is to be aligned with the centre of the diffuse region, which will vary with particle concentration size and refractive index. Methods to reduce low order scatter whilst remaining within an approximation of retro-reflection were thus considered. The simplest method appeared to be to use two fibres separated by only small distance, u. Provided this distance remains smaller than the transport path, l^*, (at all concentrations) the backscatter model should remain valid:

$$(l^* - u) / l^* \approx 1 \qquad \text{Equation 23}$$

This was shown to be case during this work (Vankeuren *et al.* 1993a). If the numerical aperture, NA, of the detector and emitter are low such that the crossover of their NA is of the order of, at least, the transport path:

$$l^* \tan (NA) =< u \qquad \text{Equation 24}$$

Then the possibility of single order scattering is negligible and low order scattering is also reduced such that predominantly diffuse light is detected, Figure 11. The numerical aperture of the fibres was 2 degrees (in water), and the spacing set at the minimum possible value of 125 microns, Section 3.4-4/7.

2.5-1/7 Polarisation Effects

Whilst the previous approach will remove all single scatter and reduce low order scatter it does not ensure only highly multiply scattered light is detected. This was carried out with a plane-polarised source and orthogonal polarised detection. Where only light polarised at 90 degrees to that incident was detected it was argued that the probability of detecting low order scatter was reduced. Previously workers had used polarisation in retroflection mode to study localisation (Van Albada and Lagendijk 1985) and the variation of the enhancement in retroreflection. This work utilised it as a means of increasing the validity of the DWS model and extending the concentration range of the technique. For practical reasons, of reducing vibration affects and to allow in-line analysis, this work used fibre optics and thus polarisation maintaining fibres, Section 3.4-3.

The method removed fifty percent of the diffusive signal, but the percentage of ballistic scatter remaining was negligible (Lilge and Horn 1991, Schmitt *et al.* 1992, Bicout and Brosseau 1992).

2.5-1/8 The Application

In much of this work the high refractive index of the pigments was a limiting factor. In this case the high refractive index of the particles could be argued to increase the low order scatter detected, as the light would become depolarised more quickly, thus closer to the probe. However, this would appear not to be the case. The high refractive index of the particles caused a significant increase in the forward scatter, and thus a decrease in low order backscatter. Whilst the particles were high refractive index they also were relatively small (1/3 wavelength) and during the project it has been shown that depolarisation decreases with particle size (Bruscaglioni *et al.* 1993). Thus, the material would appear ideal in aiding the physical methods used to limit the low order scatter. It is argued in this work that the complex scattering patterns of the high refractive index particles are only relevant at low scattering orders. When diffuse light is collected, light from all possible scattering angles is being analysed and the scattering pattern is irrelevant.

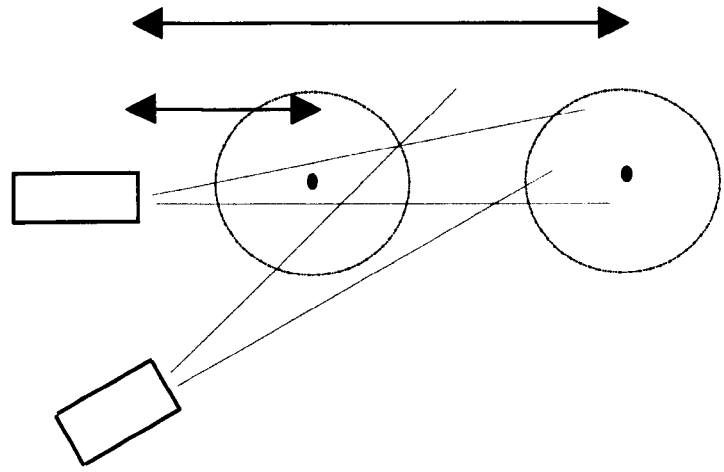

Figure 10 Complexities of a Defined Scattering Zones

The figure shows the scattering cell arrangement for systems where the transport mean free path (arrow) is shorter and longer than the distance from the laser to the defined scattering zone. When light is multiply scattered the scattering cell cannot be defined by the geometry of detection and emission. The diagram shows that the statistics of the detected light may be a strong function of the transport mean free path, depicted by the arrow. The simple diffusive approximation may not hold, as the detected light is not a plane wave incident from in front of the detector.

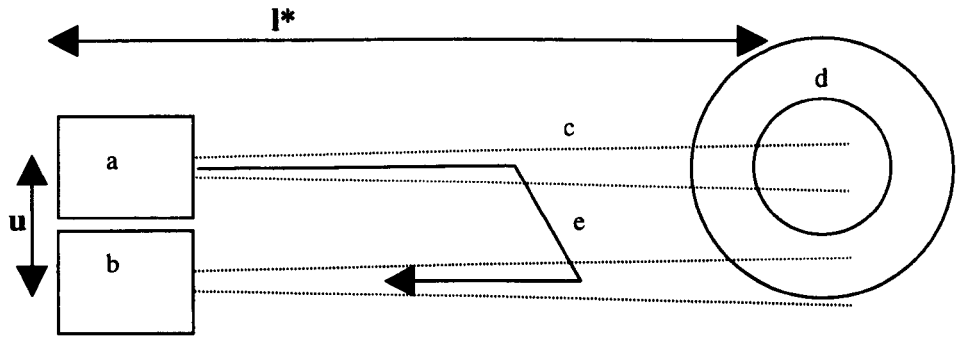

Figure 11 Near Retroreflection Arrangement

The figure shows a separate emitter and detector separated by a distance u. The numerical apertures of the detector and emitter (c) are low such that the crossover point>>l_*. Detected single scattering is negligible and low order scattering (e) strongly attenuated. Where the distance u is kept short, such that $(l_*-u)/l_* \approx 1$, the model of a spherical wave (d) of diffuse light originating a distance l_* from the detector is closely approximated.

2.5-2 Upper Concentration Limit of DWS

2.5-2/1 The Diffusive Correlation

The previous section detailed the lower concentration limit and methods of ensuring only diffuse photons were detected. This section considers the effects of interactions and how the parameter Γ may differ in a DWS analysis to that of a single scattering measurement, such as that measured in tracer systems.

2.5-2/2 The Conventional Measurement of Γ

In PCS the whole correlation is analysed and the correlation may be considered a trace of how the particles have moved the distance required to de-phase the incident light, $\lambda/2$. The free diffusion coefficient is only measured at volume fractions below 0.1, after this point the measured diffusion coefficient, D_m, decreases due to interactions and becomes zero at the glass transition point, volume fraction of the order of 0.5. The basic model of DWS assumes the gradient Γ is due to similar phenomena but this work suggested that this is not the case.

2.5-2/3 The Diffuse Measurement of Γ

The correlation due to diffusion can be viewed as the summation of many correlations due to different scattering orders, Section 2.5-2. The initial decay of the correlation is produced from the highest frequencies and therefore must be weighted by the diffuse scattering. Each photon has monitored many particles on its path through the system. Thus in the case of DWS each photon delay may be said to contain information on the average particle size, as opposed to a single particle in the conventional DLS case. It is only necessary that each particle, that the photon traverses, moves a few nm as the summation of this will give a path-length difference equivalent of $\lambda/2$. Thus the gradient of the diffusive decay, Γ, may be a significantly different measure to that measured by PCS.

This ensemble averaging that occurred for each photon delay is believed to be significant in the very high reproducibility shown possible by this technique, Section 5.2-3/4.

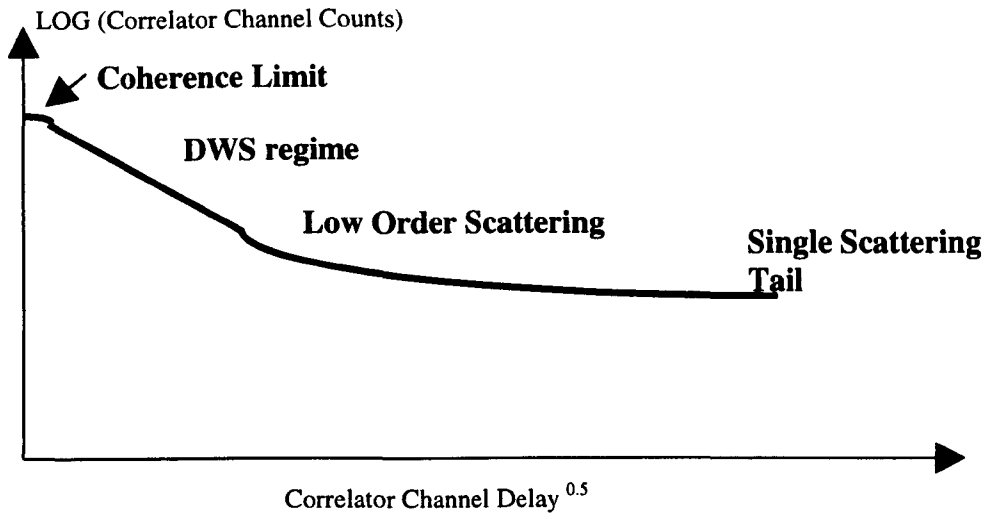

Figure 12 DWS Correlation, Scattering Regimes

The trace indicates different scattering regimes may predominate in different parts of a correlation function and that coherence may affect the initial decay.

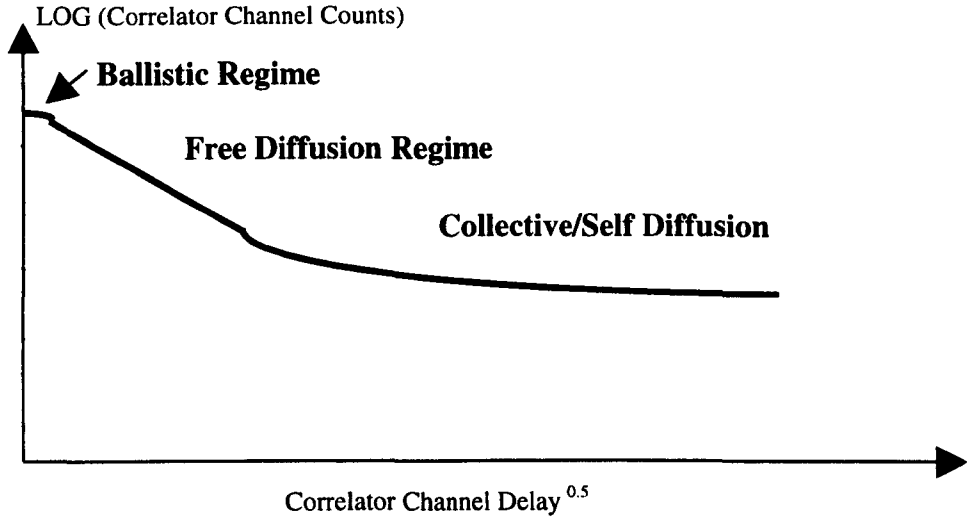

Figure 13 DWS Correlation, Diffusion Regimes

The trace is identical to the previous figure although now showing possible reasons why the same line-shape could be produced due to different types of particle movement. The two traces indicate the complexity of defining exact reasons behind a particular correlation line-shape, without consideration of the sample properties and equipment characteristics.

2.5-2/4 The Meaning of Γ

It is suggested that decay of the DWS correlation is a complex function dependent on the instantaneous ballistic speed of the particles, S_B, as well as the effective diffusion coefficient. The effective diffusion coefficient is itself a function of: the free diffusion coefficient D_0, the self diffusion coefficient D_S and collective diffusion coefficient D_C (Qiu *et al.* 1990).

This work suggests that, whilst the information is convoluted and not necessarily separable, different areas of the correlation will be weighted in favour of different parameters, Figure 13.

2.5-2/5 Evaluation of Short Time Γ

The initial gradient of the correlation, over the time-scales less than 1ns is considered strongly weighted to the ballistic movement of the scattering particles (Weitz *et al.* 1989, Zhu *et al.* 1992, Kao *et al.* 1993). The concept is further supported as a decay rates have been analysed above the glass transition where free diffusion is zero (Wang and Miller 1992).

Any photon that has seen diffusion will generate fluctuations of significantly higher frequency. Thus the next area of the correlation should obey Equation 14b, as this will be weighted most strongly to the free diffusion coefficient. At timescales over the order of 1ns each scattering particle has had more than one interaction with a water molecule (Qiu *et al.* 1990). In the diffuse regime, at concentrations below 0.1 and where only diffuse light is detected, this should predominate.

2.5-2/6 Evaluation of Long Time Γ

Where ballistic scatter has been detected, this will affect the long time measurement of Γ due to the much lower frequencies of low order scattering. This works suggests that in conjunction with this the gradient may decrease due to particles that have moved significant distances and thus are more likely to have interacted with other scattering particles.

MacKintosh and John (1989) have discussed that the long time tail will vary most significantly when analysing the unpolarised (or parallel) polarised reflected light, which our design has minimised.

2.5-3 Properties of Γ

2.5-3/1 Polydispersity

Photon Correlation Spectroscopy is capable of making some measurement of PSD provided certain assumptions on the material are known. Horne (1990) extended the work to the measurement of polydispersity in DWS and concluded that no polydispersity index could be extracted. The PCS correlation may be considered the sum of many exponentials due to different particle species. However, in DWS the correlation is the sum of exponentials due to different scattering orders, where each 'scattering order exponential' is itself the average over all particle species.

This argument is only valid for diffuse scattering, some polydispersity information could still be available in the long time tail of the correlation, when measuring dilute suspensions (Maret and Wolf 1989). However in our arrangement single and low order scatter was rejected, and it was believed unlikely significant useful PSD information could be de-convoluted.

2.5-3/2 Analysis of Ballistic Movement

The ballistic movement and the convolution of this data in the DWS signal has a significant effect on the analysis. Whilst ballistic measurement allows analysis of caged particles where D_0 is zero the analysis relies on different properties. The introduction discussed diffusion and showed that the measurement is dependent on cross sectional area and not mass, Section 1.4-4.

However, the ballistic movement of a scattering particle is a direct measure of momentum transfer and analysis requires the mass of the solute particle. This would give a result in terms of mass, as opposed to the radius, of the scattering particle. Thus it is possible that in certain circumstances DWS is a measure of a completely different physical property to DLS.

2.5-3/3 Temporal Coherence

The temporal coherence may appear to be a simple hardware limitation to be discussed later. However, results in this work suggested that the interactions in a homodyne analysis (Section 6.4-2/3) might give similar results to those where the coherence is limited. In addition the coherence requirements are shown to be maximised in the retroreflection arrangement. Thus, the theoretical effects of coherence are an important aspect of this work.

In PCS maximum path length differences between different scattering particles are clearly defined (Figure 10) and typically below 1mm. The temporal coherence requirement is not significant for most laser sources, Section 3.3-2/2. This is not the case in DWS as the maximum path-length differences cannot be defined. The multiple scattering allows the maximum path-length difference to be significantly larger than the sample itself.

Bellini *et al.* (1991) carried out both experimental and theoretical studies of the effect of laser coherence lengths on DLS. The experimental results were outside of the diffusive regime but they showed theoretically that reduced laser coherence would strongly effect the shape of the correlation, $G^{(2)}(\tau)$. Their model showed a preferential reduction in the gradient at short delay times:

$$G^{(2)}(\tau) = \exp (\tau / \tau_s)^{\alpha} \qquad \text{Equation 25}$$

where the time constant, τ_s, and the exponent, α, were functions of the radial distance between the parallel axis of the detection beam. They noted the reduction in α, with increased emitter detector spacing, was most noticeable in backscattering mode, the arrangement used in this work.

2.5-4 Effect of Diffuse Scattering on Optical Fields

2.5-4/1 Effect of Diffuse Scattering

Early results in this work suggested that DWS was more sensitive to the magnitude of the optical fields than is the case in PCS, Section 5.3-1. In multiple scattering each photon has undergone many collisions leading to the reduction in the measured decay, defined by the square root in Equation 20. Thus, the mean measured frequency is higher. In conjunction with this the high refractive index of TiO_2 increased the frequencies further. It is considered that the high frequencies place more stringent requirements on the intensity range DWS is valid over. Thus more significant requirements are placed on the hardware and conventional DLS approximations may not hold.

2.5-4/2 Photon Statistics of Light Scattering

Bandwidth limitations of light scattering equipment are often modelled assuming that the incident light is a Poisson distribution:

$$P(N)= (\langle N \rangle^N e^{-\langle N \rangle}) / \langle N \rangle! \qquad \text{Equation 26}$$

Where P defines probability and N a number of photons. In PCS the signal is random but has a characteristic fluctuation, which leads to photon bunching. Thus when analysing the statistics at time-scales small compared to the fluctuation time, such as a correlation, Bose-Einstein statistics should be used (Bertolotti 1973):

$$P(N) = \langle N \rangle^N / (1 + \langle N \rangle)^{1+N} \qquad \text{Equation 27}$$

Over short timescales $P_{BE} = 2\ P_{Possion}$. Whilst this may have little effect of PCS, in multiple scattering the probability of counts, for small t, is greater due to the more rapid decays.

Bertolotti (1973) has also suggested that multiple scattering fields may not be Bose-Einstein but a high order function. For a Gaussian beam scattered by a Gaussian particle system he suggested the more complex function where the m^{th} factorial moments are given by:

$$\langle N! / (N - m)! \rangle = m!^2 \langle N \rangle^m \qquad \text{Equation 28}$$

with m=1 Poisson, m=2 Bose Einstein, m=3 Multiple Scattering.

For the factorial moment m=0,1 the solutions are similar. However, for large m the squared factorial causes significant divergence of the results. This was shown to have significant effects in terms of bias if the detected intensity was too high, Section 5.3-1/2.

CHAPTER 3

Physical Limitations Imposed by the Hardware

3.1 Hardware Requirements

Chapter 2 detailed the theory of a near retroreflection arrangement with particular emphasis on the requirements of an industrial method. The theoretical limitations of the analysis and instrumentation were considered. This chapter details the practical limits of the hardware and the effect this had on the models used in analysis.

This work measured a correlation function that may have been affected significantly by both the hardware constraints of the components and the light scattering arrangement used to collect data. Thus the chapter opens with discussion of the amplitude and intensity correlation functions. Whilst correlation of amplitude is shown to be possible, it was considered impractical for industrial based DWS. This leads directly to consideration of the homodyne and heterodyne field arrangements. Heterodyne measurement is shown to be a direct measure of the amplitude correlation but to be less robust and requiring a more complex arrangement than the homodyne case.

Real-time signal processing by means of digital autocorrelation is overviewed with significant emphasis on the effects of high frequency signals, typical of DWS, on the validity of the digital approximation. The use of a digital processing defines the need for digital, and preferably quanta detectors. The properties of the two major types are addressed. Photon multiplier tubes are considered the optimum choice, for applications that are not intensity limited.

The extended coherence requirements of DWS, due to increased path-length difference, are considered. Single transverse mode lasers are shown to be adequate for most applications whilst diode sources require careful selection. Mode stability is shown to be a more significant concern than mode order.

This work considers the optics in some detail, the fibre type and arrangement are shown to have significant effects on the behaviour of the overall system. Bow Tie type birefringent fibres are shown to be the optimum type for optical probes ensuring high levels of stability.

The arrangement is then contrasted with single fibre and bifurcated fibre design in terms of the hardware limitations of each type, thus the practical benefits of the design selected.

This allows the behaviour and benefits, from both the hardware constraints and theoretical considerations (Chapters 2,3), to be summarised at the beginning of the results, Chapter 5.

3.2 The Correlation

3.2-1 Method of Correlation

3.2-1/1 Intensity and Amplitude

Solutions for the correlation have previously been given in terms of $g^{(1)}(\tau)$, the un-normalised amplitude correlation function, Equation 14b. However, it is only possible to measure the intensity of a photon, as the measurement is destructive. Therefore to analyse $g^{(1)}(\tau)$, the correlation must occur prior to detection, Figure 14. This is shown to be impractical in this application, resulting in analysis of the intensity correlation $g^{(2)}(\tau)$. This cannot be assumed to be a direct representation of the amplitude fields, Figure 14,15.

3.2-1/2 The Amplitude Correlation

Analysis of the amplitude correlation requires an etalon. This consists of scanning one, of a pair, of high reflectivity mirrors, over an accurately measured spacing. Thus, light is compared with itself over a set time delay and the intensity noted. Where the frequency is a solution of the cavity no transmission occurs, as the time delay increases the cavity becomes lossier and transmission increases. By scanning a number of delays a correlation built-up. given by: $g^{(1)}(\tau)_{\tau=0} = 0$, $g^{(1)}(\tau)_{\tau=\infty} = 1$, Figure 15.

The etalon is unsuited to our purpose as:

- a large cavity size is required for sub-GHz frequencies;
- the resolution of the etalon (finesse) is directly related to the mirror reflectivity, so operation with a high signal to noise results in minimal signal transmission;
- the etalon is of limited use within the industrial setting due to its fragility, the etalon must be isolated against all environmental variation.

3.2-1/3 The Intensity Correlation

It is not possible to measure the amplitude of a photon (A) only its intensity ($I=AA^*$), Figure 14. Thus, when correlation occurs after detection (Section 3.2-2.2) the intensity correlation function is analysed: $g^{(2)}(\tau)$, as opposed to the amplitude correlation $g^{(1)}(\tau)$, for which solutions have previously been found, Figures 14,15. Whilst the mean amplitude of the photon field equals zero, $\langle A \rangle = 0$, the mean intensity does not, $\langle I \rangle = \langle AA^* \rangle \approx |A|^2$ (Jakeman 1973).

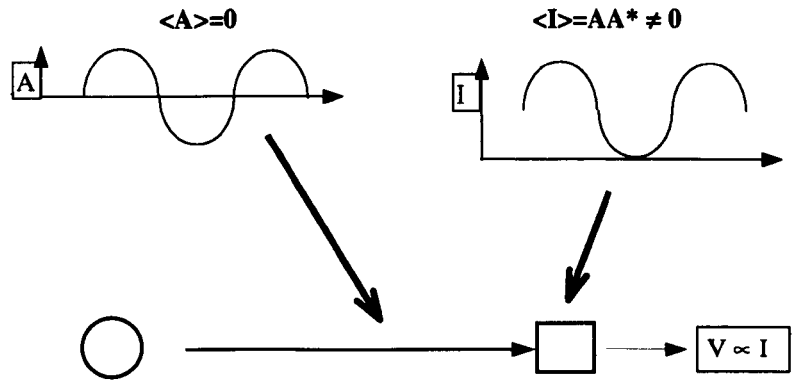

Figure 14 The Optical Fields

The figure shows light (solid line) leaving a source (circle) and incident at the detector (square) where a voltage is generated (dotted line). The amplitude fields prior to detection and the intensity fields at detection are shown.

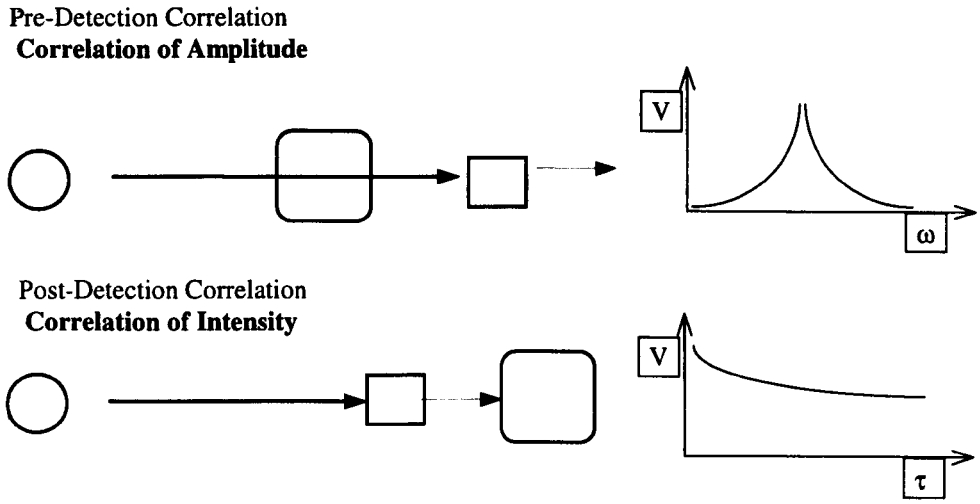

Figure 15 The Intensity and Amplitude Correlations

The intensity and amplitude measurement arrangements comprising a light source (circle), optical field (solid line), correlator (large box), detector (small box) and electrical signals (dotted line). The amplitude correlation is produced from a signal of mean value 0 varying between +A and -A leading to the correlation shown top whilst the intensity correlation is formed from a field equivalent to AA*. This varies between 0 and A^2 thus the mean is $\sqrt{}$ (AA*) or |A|

This leads to a reversal of the intensity correlation function varying from $\langle A \rangle^2$ to $\langle A^2 \rangle$ for full or no coherence, respectively.

The un-normalised intensity correlation is significantly different in shape to the amplitude function, decaying from: $g^{(2)}(\tau)_{\tau=0} > 1$ to $g^{(2)}(\tau)_{\tau=\infty} = 1$, Figure 15. The relationship between the intensity and amplitude correlation is dependent on the method of measurement.

3.2-1/4 Scattering Arrangements

There are three arrangements for measurement of the correlation. The scattered light may be mixed with itself, homodyne, with a portion of un-scattered light, heterodyne, or with a local oscillator from a different source, superheterodyne[1], Figure 16.

Pusey and Vaughan (1975) gave the general case, for classical heterodyne intensity correlation, in terms of the detected intensities, as:

$$g^{(2)}(\tau) = 1+(\langle I_s\rangle/\langle I_T\rangle)^2 [g_s^{(2)}(\tau)-1]+(\langle I_s\rangle I_L)/\langle I_T\rangle^2 [\exp\{i(\omega_L-\omega_S)\tau\}g_s^{(1)}(\tau)+cc] \quad \text{Equation 29a}$$

Where I denotes intensity, ω the frequency and the subscripts S, L and T are used to define scattered light, light from the local oscillator and total light respectively. In the conventional heterodyne arrangement the local oscillator is the same frequency as the scattered light, $\omega_L = \omega_S$ and the relationship reduces to:

$$g^{(2)}(\tau) = 1 + (\langle I_s\rangle / \langle I_T\rangle)^2 [g_s^{(2)}(\tau) - 1] + (\langle I_s\rangle I_L) / \langle I_T\rangle^2 g_s^{(1)}(\tau) \quad \text{Equation 29b}$$

In this case the overall correlation is a function of both the intensity and amplitude correlations, $g_s^{(2)}(\tau)$, $g_s^{(1)}(\tau)$ respectively.

3.2-1/5 Homodyne Measurement

In the pure homodyne case, $I_L = 0$, the scattered light has mixed with other scattered light and the signal is a measure purely of the intensity correlation, thus:

$$g^{(2)}(\tau,\tau+t) = 1 + 1(g_s^{(2)}(\tau+t) - 1) \quad \text{Equation 29c}$$

The homodyne intensity correlation must be related to the amplitude correlation by means of the Siegert relationship, which has been shown to be valid for Gaussian scattering fields and non-coupled particles leading to (Jakeman 1973):

$$g^{(2)}(\tau,\tau+t) = 1 + | g_s^{(1)}(\tau+t) |^2 \quad \text{Equation 30}$$

However, the validity of the Siegert relationship is questionable in multiple scattering. At high concentrations the particles may couple, thus in DWS Equation 30 cannot be assumed for all sample types.

1 This may lead to confusion as the terms are not universally accepted. In the communications field (and some older light scattering literature) the following terms are used: autodyne [for homodyne], homodyne [for heterodyne], heterodyne [for super heterodyne].

In this work interactions occurred in most pigment samples. Thus Equation 30 could not be assumed and the only the intensity correlation can be considered. This is not a significant problem in the analysis of Γ but limits any analysis of absolute size.

3.2-1/6 Heterodyne Measurement

When $I_s << I_L$, the heterodyne approximation, an intensity correlation is measured but scattered light is present in only one path. The signal is therefore a direct measure of the amplitude correlation regardless of the scattering field.

$$g^{(2)}(\tau) = [1+(<I_s>I_L) / <I_T>^2] \, g_s^{(1)}(\tau) \qquad \text{Equation 31}$$

As the heterodyne arrangement allows a direct measure of the scattering field the experimental duration should be more rapid. For accurate heterodyne analysis I_s must be small, typically 0.01 of I_L, where I_L has no information of the suspension (Figure 16). The photon detector is limited in the maximum count that may be applied. This is particularly the case where high frequency signals are analysed such as in DWS, Section 2.5-4/2. Thus I_s may be significantly lower absolute magnitude than optimum and the signal may be swamped by detector noise significantly increasing the experimental duration. This work showed that the detected intensity should be limited to 70Kcps (Section 5.3-1/2, 3), suggesting a maximum I_s signal would be 700cps. The heterodyne arrangement also places more stringent requirements on coherence, as the optical path-length differences are increased.

In our work the purity (homodyne to heterodyne) was better than 99.8 percent, Section 5.2-3/3. In the heterodyne case, this level of purity would require an intercept 0.2 percent higher than the baseline.

However, the most significant drawback in DWS has been shown to be the lack of control of the relative portions of I_s and I_L in fibre mediated systems. In this case, the analysis is solution to Equation 29b and requires fitting of two separate exponentials for the homodyne and heterodyne components. This requirement for bi-exponential analysis, in conjunction with the arrangements used, increased sensitivity to vibration, because I_s and I_L have travelled different paths, which limits the applicability of the heterodyne method in industrial environments.

3.2-1/7 Normalisation

The measurement of the intensity correlation thus generates a baseline $\langle I \rangle^2$ which must be removed, this may lead to significant biasing if the scattering model is not correct (i.e. the photons are not uncorrelated). The intensity correlation, heterodyne or homodyne may then be normalised

$$G^{(2)}(\tau,\tau+t) = g^{(2)}(\tau,\tau+t) / \langle I \rangle^2 \qquad \text{Equation 32}$$

Any bias will be more pronounced when intercept $<<$ 1, as in the case in heterodyne analysis.

3.2-2/8 Statistical Variance

If the scattered intensity is not limited, such that I_s may be selected for an optimum value, then the error in measurement is approximately:

$$\text{Error} = [(\text{experimental duration}) / \tau_0]^2 \qquad \text{Equation 33}$$

Early analysis methods used conventional fixed experimental durations whereas the final software package used this relationship to produce measurements of equal statistical variance for samples of differing correlation decay time, Section 4.3-5/2.

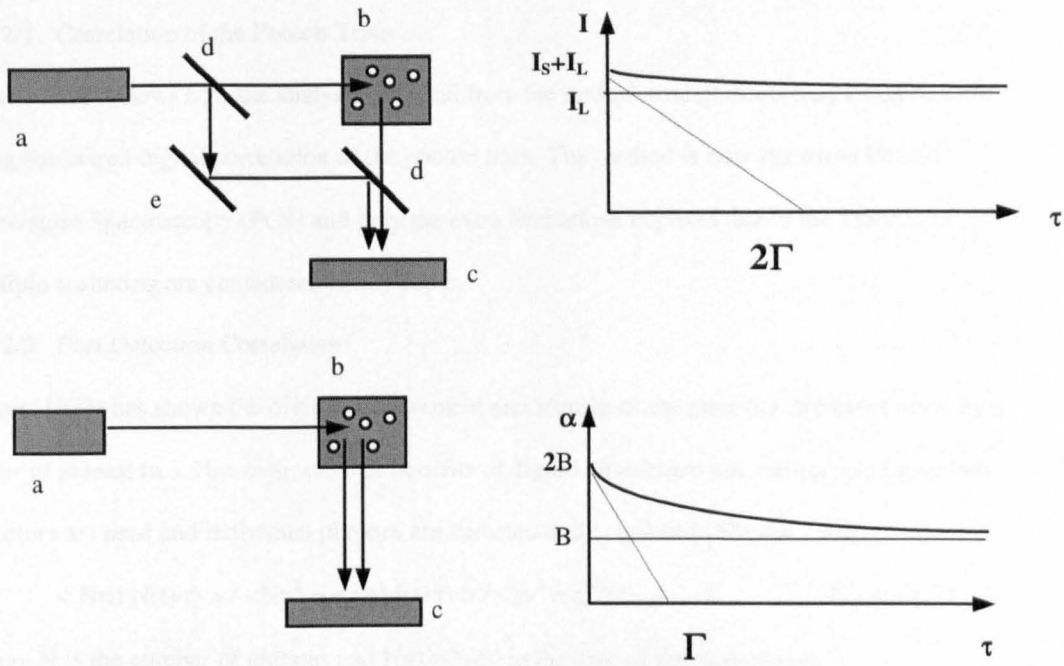

Figure 16 Heterodyne and Homodyne Scattering Arrangements

The heterodyne arrangement, top, with laser (a) directed at the sample (b), which scatters light to the detector (c). The local oscillator is defined by two beamsplitters (d) and mirror (e). In the simpler homodyne arrangement, lower, only scattered light is detected. The traces to the right show the lower intercept values of the heterodyne case and the reduced correlation gradient.

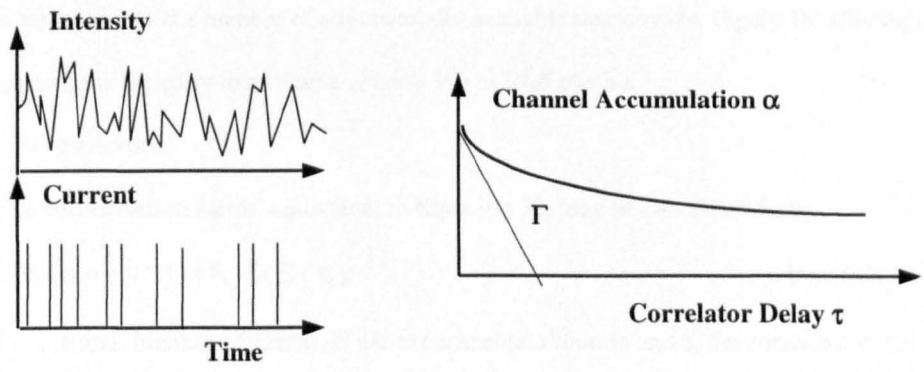

Figure 17 Analogue and Photon Counting Signals

Correlating the number of photons in a specific time, lower trace, is equivalent to measurement of an analogue signal, upper trace, except noise levels may be reduced by up to 8 fold as uncertainty in signal measurement, storage and multiplication is removed.

3.2-2 Photon Correlation

3.2-2/1 Correlation of the Photon Train

This section reviews how the analysis of signal from the optical arrangements may be carried out using hardwired digital correlation of the photon train. The method is now known as Photon Correlation Spectroscopy (PCS) and only the extra limitations imposed due to the analysis of multiple scattering are considered in any depth.

3.2-2/2 Post Detection Correlation

Oliver (1973) has shown the digital measurement and storage of the intensity decreases noise by a factor of at least two. However, the true benefits of digital circuits are not realised until quantum detectors are used and individual photons are detected and correlated (Mandel 1963):

$$< N(t)\, N(t+\tau) > / <N>^2 = < I(t)\, I(t+\tau) > / <I>^2 = g^{(2)}(\tau)_{\tau \neq 0} \qquad \text{Equation 34}$$

Where N is the number of photons and $N_1(t)=N_2(t)$ in the case of autocorrelation.

Thus correlation of the number of photons within a sampling period is equivalent to a measure of intensity, Figure 17. Oliver (1973) also showed that this reduces noise by up to a factor of eight, when considered with the purely analogue measurement and that the analogue correlation function may be replaced by:

$$G^{(2)}(\tau) = \Sigma\, N_1\,(t)\, N_2\,(t+\tau) \qquad \text{Equation 35}$$

Jakeman (1973) discussed how correlation might be carried out using simple digital shift registers, which resulted a number of commercially available instruments, Figure 18, although channel spacing is typically logarithmic (Figure 19) in DLS studies.

3.2-2/3 Normalisation

The digital normalisation factor, equivalent to Equation 32, may be calculated from:

$$\text{Norm} = (N / E)\, (E)^{-1}\, (E / \tau_s) \qquad \text{Equation 36}$$

where N is the total number of counts, E the experimental duration and τ_s the correlator delay time. This may lead to significant biasing if the scattering model is not correct (i.e. the photons are not uncorrelated). The normalised intensity correlation may thus be defined:

$$g^{(2)}(\tau,\tau+t) = G^{(1)}(\tau,\tau+t) / \text{Norm} \quad |^{\text{for all t}} \qquad \text{Equation 37}$$

Oliver (1973) has shown that the line-width will be affected by three times the mis-normalisation fraction. Any bias will be more pronounced when $I_{intercept} << 1$, as in the case in heterodyne mode.

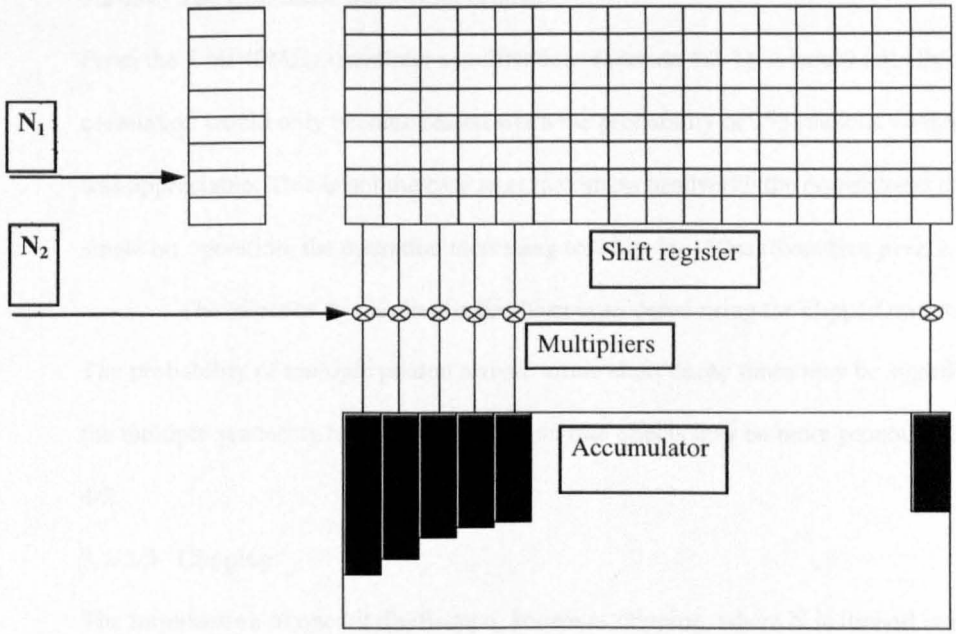

Figure 18 The Use of Shift Registers for Correlation

A 16 channel 8 bit correlator, in single clipping mode where the shift register is single bit but the multiplier is still eight bit. In double clipping mode, the multiplier is an AND gate (Jakeman 1973).

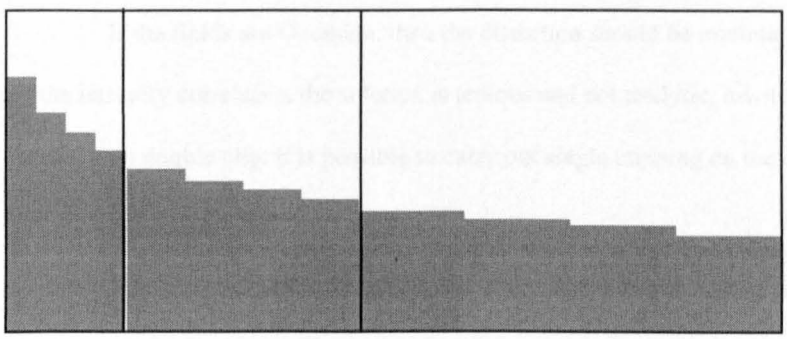

Figure 19 The Dilated DLS Correlation

A 12 channel correlator, where a dilation of two occurs every fourth channel leading to a temporal coverage of the equivalent of 28 linearly spaced channels. The decrease in resolution with correlator delay can be seen to match the decrease in gradient of the correlation.

3.2-2/4 The Correlator Bandwidth Limitation

From the 8 bit 40MHz correlator specifications (Section 4.2-1), it would initially appear that the correlation would only become biased when the probability of 255 photons within 25nanoseconds was appreciable. This is not the case as at maximum bandwidth the correlator is capable of only single bit operation, the operation increasing to 8 bits by 150ns (Svendsen *pers. comm* 1990).

The effect of this limitation has been considered using the clipped correlator as a model. The probability of multiple photon arrival within short decay times may be significantly higher in the multiple scattering regime and thus count rate effects may be more pronounced, Section 2.5-4/2.

3.2-2/5 Clipping

The introduction of one bit digitisation, known as clipping, where N is limited to the values 0 or 1 significantly simplifies the electronic circuit required. The multiplication is now of ones and zeros and can be carried out simply by AND logic gates. Jakeman (1973) has shown that the clipped autocorrelation function can be related to the amplitude correlation by:

$$g^{(1)}_{clip}(\tau) = (2 / \pi) \arcsin g^{(1)}(\tau) \qquad \text{Equation 38}$$

If the fields are Gaussian, then the distortion should be minimal. However, when related to the intensity correlation the solution is tedious and not analytic, involving a triple sum. Rather than double clip, it is possible to carry out single clipping on the electronic signal, such that:

$$V_{clip}(\tau) = < V_c(\tau)\, V(t+\tau) > \qquad \text{Equation 39}$$

This incorporates much of the electronic advantage of double clipping and allows a simple analytical solution. The multiplications are now the product of 0 or 1 times the multi-bit number, per sample period. The simple relationship between the single clipped correlation and the unclipped correlation is given by:

$$g^{(1)}_{Sclip}(\tau) = [\, g^{(1)}(\tau) \,] / (2 / \pi) \qquad \text{Equation 40}$$

Which has an analytical solution for the intensity correlation

$$g^{(2)}(\tau) = 1 + [\, (1 + k) / (1 + <N>) \,] < g^{(1)}(\tau) >^2 \qquad \text{Equation 41}$$

Where $N_k = 1$ if $N > k$ and $N_k = 0$ if $N =< k$. This is identical to the Siegert relationship for the situation, $<n>$ = clip rate (k).

Obviously, when clipping occurs due to bandwidth limits of the equipment the latter equality will not hold. A more significant problem is that the quantity of biased clipping that will occur will be function of the correlator delay used in the analysis. In addition, depending on the exact architecture of the correlator, the clip rate may be a function of the correlator channel position.

This suggests bandwidth limitations may give rise to significant differences in the analysed correlation. The effect of the bandwidth limitation could also be considered as pre-scaling, where N is incremented only after a pre-set number of photons. Analysis by Muller and Muller (1984) suggested that real experimental errors are similar for scaling as for clipping.

3.2-2/6 The Derandomiser Circuit

The clipped incoming count rate is generally processed by a simple 'flip-flop' arrangement. At the start of each sampling period, the 'flip-flop' is reset and any incoming pulse within the sampling period will make the output positive. However, the Sensor Dynamics correlator, used in this work (Section 4.2-2) was not de-randomised leading to unspecified behaviour when two more photons within a 25ns period were present. An even number of photons would generate a logic low and an odd number of photons would generate a logic high, until the photon arrival rate exceeded the bandwidth of the circuit and the logic output would be undefined, erratic. This limitation was overcome by ensuring the detector output pulse was in excess of 12.5 nanoseconds full width half maximum, such that two photons with 25ns would simply trigger as one, introducing some bias, Section 4.2-3/5. Use of a better derandomiser, thus allowing detectors with shorter pulse-widths would significantly improve the effective instrument bandwidth.

3.2-2/7 Pseudo Cross Correlation

In many applications the detectors used in the analysis have a lower bandwidth than the correlator used for the analysis. Even where the detector bandwidth ≈ the correlator bandwidth, the detector may bias high frequencies. Whilst the correlator is truly digital, and gives a step transfer function, the photon detector contains analogue effects such as dynode recharge time, envelope charge build-up.

These effects may bias measurements even of photons occurring at a higher frequency than the detector bandwidth. In the final design used in this work the detector bandwidth limitations were overcome directly with detector pulse width being reduced from 65 to 12.5ns, Section 4.2-3/5.

However, the work carried out on cross-correlation proved useful in showing the probe design reduced low order scatter to an insignificant level, Section 5.2-3/2.

To remove the effects of detector bandwidth the quantum nature of light is used directly. When the scattered light is split equally between two detectors a cross correlation of the data may be carried out (Equation 34, 35, $N_1 \neq N_2$), Figure 20. A photon will either travel to one or other detector but cannot travel to both. Thus the photon rate to each detector is halved but more importantly a photon is detectable on the second detector almost immediately after a photon is incident on the first. Thus a pair of photons may be detected that are closer than the inherent pulse widths of each detector.

The signals occurring on each detector are not identical, photons being shared between detectors on a random basis. However, with each detector measuring the signal as if it had merely been attenuated by 50 percent, each signal contains the same phase and frequency information.

Thus detection, of sparse events, is possible at frequencies that are higher than the detector bandwidth, provided the signal is analysed as quanta. The limitation that the events must be sparse is often not significant in the analysis, as shown in this work, Section 5.3-1/2,3.

A more significant limit of the technique, for industrial application, is that two optical paths exist. Thus the technique is sensitive to any vibration between the detectors, which may result in either a false signal and/or the actual signal being washed out.

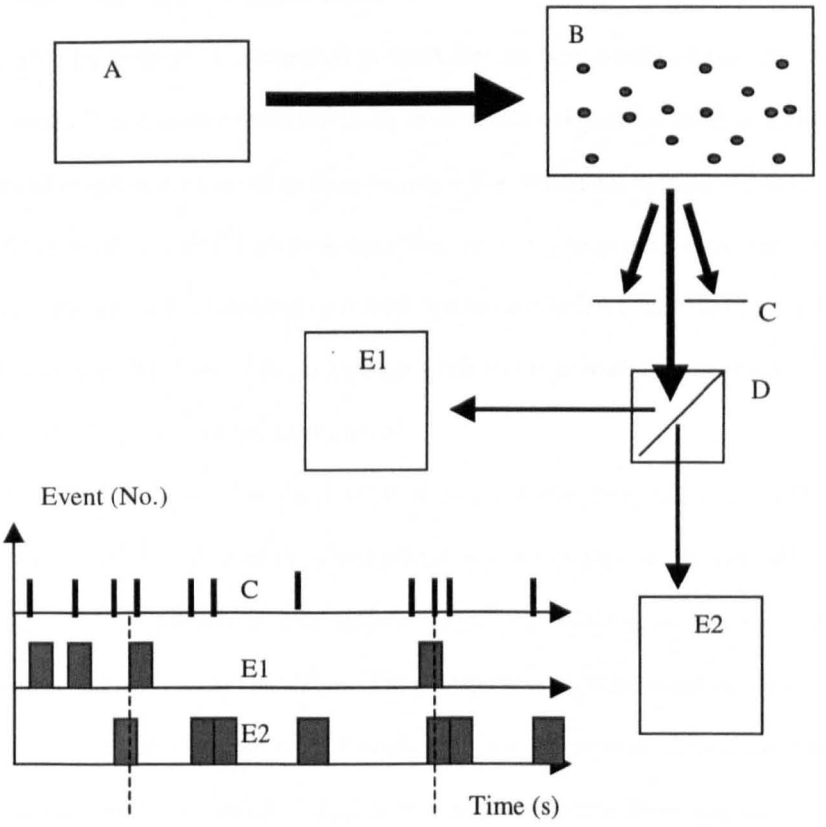

Figure 20 Pseudo Cross Correlation

The figure describes the basic pseudo cross correlation arrangement. A laser (A) is directed at a sample (B). The signal is collected at a fixed angle and either a pinhole (C) or monomode fibre is used to ensure only a single coherence area is monitored. The light is directed at a beamsplitter (D), which shares the light equally between two detectors (E1, E2).

The graph shows the photon stream at C and how the sharing of the photons between the detectors is a random process. On detection the electron pulses are spread by the PMT and its output circuit, giving rise to wide electron bursts. The two dotted lines shows closely spaced photon pairs that would have been ignored using a single detector. Such photon pairs giving rise to the initial fast decay in the correlation.

Both detectors must be identical optical path-lengths from the sample and any vibration occurring in only one arm of the signal will give rise to a false signal.

3.2-3 Analysis and Setting of the Correlation

3.2-3/1 The Far Point Measurement

In PCS experiments it is common to check that the normalisation calculated (Equation 36) is correct. This may be carried out using an extended delay of the last few channels such that the correlation has decayed to an insignificant value. Where the measured and theoretical baselines do not agree, to around 0.1 percent, significant bias may be present in the measurement. The far point measurement was considered of critical importance in DWS as it defines if the entire correlation has been analysed and if the assumptions behind the normalisation remain valid.

3.2-3/2 Force Fitting the Correlation

The previous chapter (Section 2.4-2/6) discussed force fitting and the differences between the variance and the fitting error. The problem is more complex as the correlator channels are conventionally linearly spaced, thus plotting $\tau^{0.5}$ causes a bias in the weighting of the fit toward the long time decay of the correlation. The channel spacing may be taken into account in the fitting but this requires an assumption in the model such that the error is taken as the difference between the measured parameter and the fitted parameter. Where the model is accurate the approximation, that the fitting error is equivalent to the statistical variance, is valid but this is not the case for DWS experiments, Section 2.4-2/6.

Their appeared little point in attempting to remove the bias due to channel spacing, as this could cause a more complex bias due to the fitting of an incorrect model. The unusual channel spacing also proved useful in stabilising the analysis.

3.2-3/3 Complex Correlation Line-shapes

The unusual weighting of the data, due to the fitting, $\tau^{0.5}$, was initially seen as a problem. However, early results on the analysis of complex line-shapes showed it had significant intrinsic benefits. The square root arrangement allows the fitting procedure to ignore any initial curvature in the correlation as it forced the majority of data points onto the linear, diffusive, part of the correlation, Figure 21. In principle it could be argued that a correlator with channels spaced at the square of the delay time was required, Figure 22. Thus when plotting the square root, this would give a linear relationship. However, the practical bandwidth limits of correlation would give too few correlator channels on the exponential decay in this application.

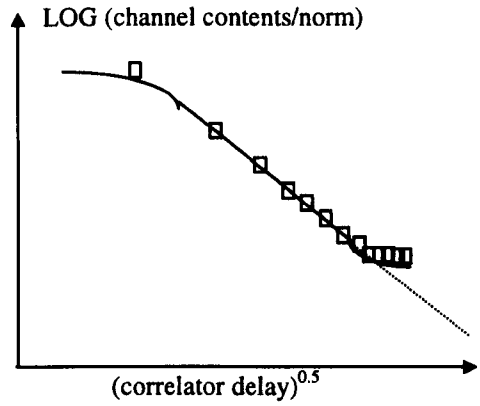

Figure 21 The Conventional DWS Trace

The trace shows a normalised DWS correlation plotted LOG (contents) versus $(delay)^{0.5}$ and thus the compression of the data points at long delay. The trace shows the continuation of the fitted line (dashed) after the long time delay. The initial curvature is not significant in the analysis as only a few points lie in its regime. Provided the points on the long time tail are discarded the analysis is thus strongly weighted to the linear part of the correlation

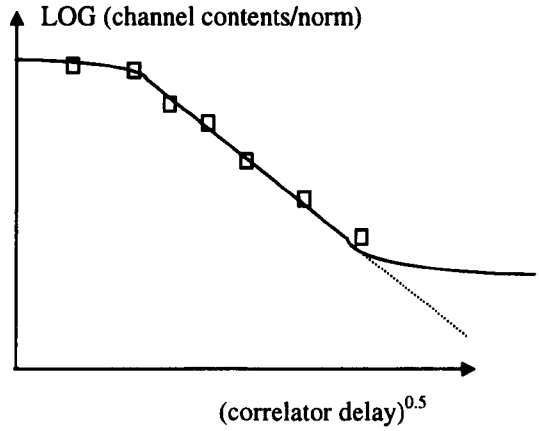

Figure 22 The Ideal Dilated DWS Trace

The figure shows the use of the non-linear channel spacing to promote measurement of the diffusive part of the correlation. Ideally the channels would be $(delay)^2$ although a true log function would give a reasonable approximation. The initial short time non-linear portion of the curve receives little weighting due to the few data points. Unfortunately practical bandwidth limits would give few data points on the trace when analysing high bandwidth signals.

3.2-3/4 Dilation

This concept underlying the far point delay has also been utilised to increase the effective number of correlator channels, Figure 19. The digital correlator is typically produced from a number of sub-circuits each of which has a number of channels. Placing a delay between these units causes the portion of the correlation analysed to be extended.

Little information is lost as the quantity of information contained in the correlation may be considered a function of its instantaneous gradient, which reduces logarithmically with correlator delay for a linear plot, Figure 1,19.

This method is typical of PCS analysis methods and allows the correlator delay time to remain constant for most sample types, as the correlator now covers thousands of 'effective' channels.

3.2-3/5 Theoretical Limitations of Dilation in DWS

Whilst the ability to produce dilation was maintained within the software it was found in very early experimental work that it was of limited applicability, due to both practical and theoretical limitations. Aside from the clipping limit, where the dilation leads to an initial correlator delay of below 150 nanoseconds, the fitting/statistical variance error problem becomes significant.

The correlator channels are laid out linearly with a dilation factor every 16 channels (shown as 8 in Figure 19 for clarity), when the channel positions are plotted as square root the channel spacing is complex.

For calibration of the DWS parameter, even where all data is analysed using the same dilated channels, it is liable to produce a non-continuous function, Figure 23. The function may be double valued at every Γ where a dilation between integrated circuits is present, Figure 24. Where the dilation and correlator delay time is varied, the measured Γ may vary for each dilation/delay time pair used in analysis. Thus all DWS measurements would be required to be carried out with the first sixteen channels at 25ns with the correlation acting as single clipped, Section 3.2-2/5. Even in this case many samples would decay too rapidly for more than a few of the correlator channels to lie on the linear regime of the correlation. The unsuitability of the logarithmic dilation required this work to operate with a correlator delay that was individually set for each measurement, Section 2.4-2/5.

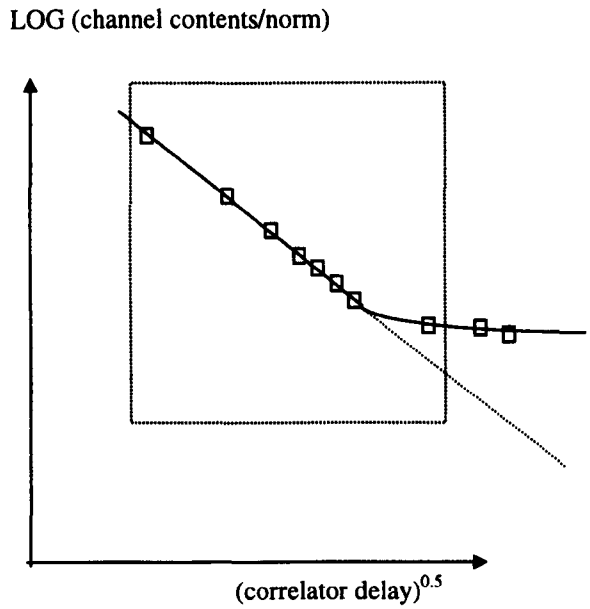

Figure 23 Actual Dilated DWS trace

A dilated correlation plotted log (channel contents) versus (correlator delay)$^{0.5}$. The solid trace shows the line of best fit whilst the dotted line is a continuation of the gradient of the fitted straight line. The last data point may strongly bias the result as it is does not obey the standard model, upper trace.

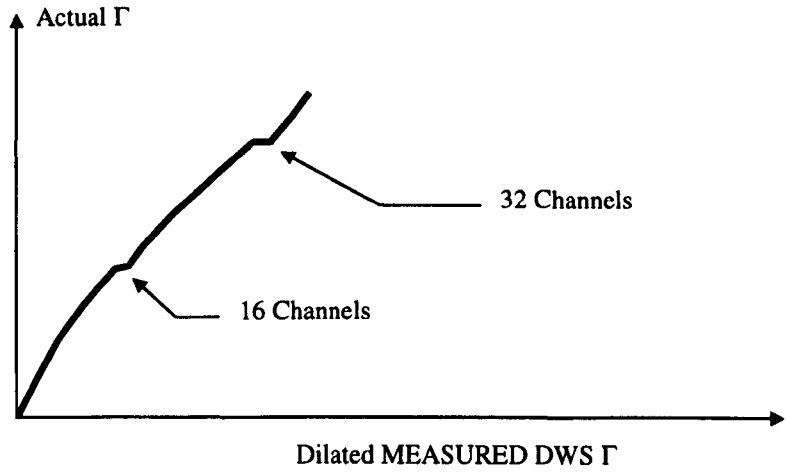

Figure 24 Dilation Effects

The dilation may cause a non-continuous trace, for the function measured Γ versus actual Γ, when using a constant correlator delay. The situation is exacerbated, as the position of the step is a function of the correlator delay time. An analysis with delay time τ, using X channels, may give a different response to a measure of the same sample using a delay of $\tau/2$ and 2X channels.

3.3 Requirements of the Source and Detector

3.3-1 Detection of Quanta

3.3-1/1 Amplification

The previous section has detailed the advantages of digital operation without consideration of the practical limits of detection. A single 633nm photon has energy of 3 $x10^{-19}$ J, which is less than 100kT at room temperature. To produce a measurable signal, above the noise band, some type of amplification intrinsic within the detector is required. This section covers the two detector types currently capable of single photon resolution together with their operating and noise characteristics.

3.3-1/2 PMT Operating Principles

A single electron, generated by a photon incident on the phosphor cathode, is accelerated towards the first dynode by a potential of the order of 100V. The kinetic energy of the electron is sufficient to free δ more electrons ($\delta > 1$) from the first cathode on collision. These are accelerated towards a more +ve dynode generating a geometrical increase of the signal with dynode number.

Typically the single dynode amplification (δ) is of the order 4 and 12 dynodes are utilised. This gives a massive amplification 4^{12} or $1.7x10^{7}$

This level of amplification allows a single photon to generate an electronic signal that is readily measurable above the background noise by use of a single threshold. Thus each photon produces a standardised digital electronic pulse

3.3-1/3 Avalanche Photodiode Operating Principles

This section will discuss the basic principles of Avalanche Photodiodes (APDs) when operated above their breakdown voltage (in reverse bias) known as Geiger mode. A lightly doped silicon photodiode will not exhibit tunnelling even when the voltage bias across it is above breakdown.

However, any optically generated free electron/hole pair in the diode will move rapidly towards the anode due to the high bias voltage, typically 300kVcm (Lightstone and Macintyre 1988). At a high bias, a rapidly moving electron may cause impact ionisation and release more electrons, which themselves will be accelerated towards the detector and may cause more ionisation. Thus the generation of a single electron/hole pair by a photon may cause an avalanche effect of charge across the diode.

Streetman (1990) gives the empirical APD multiplication factor, M, as:

$$M = 1 / (1 - (V / V_{br}))^{n} \qquad \text{Equation 42}$$

Where V is the reverse bias voltage and V_{br} is the breakdown voltage.

The factor *n* is always larger than 2 and dependent on material. Verdeyen (1981) suggests the parameter *n* varies between 2-3, whereas Streetman (1990) suggests 3-6. This high amplification factor appears beneficial but it is shown that it is also a limitation of the APD.

3.3-1/4 Pulse Height Distribution

For experiments where the signal intensity is higher than that required, then the fundamental limit of the signal to noise is a function of the pulse height distribution, of the electron pulses.

If there are sufficient photons for analysis, then signal to noise improvements can only come about by better discrimination of noise from photon pulses, this discrimination being purely a function of the pulse height distribution.

Foord *et al.* (1975) discussed the pulse height distribution of a PMT in terms of the secondary emission as a geometric distribution, but also allowing for a spread in gain across the dynode face. This gives a pulse height variance in terms of numbers of electrons given by:

$$\text{Var } N_e = [(\delta b + 1) / (\delta + 1)] \delta^2 \qquad \text{Equation 43}$$

Where N is number of electrons in the photo pulse number, δ is the dynode amplification factor and b a factor defining the PMT quality. The situation b=1 gives Poisson statistics and b<1 gives a measure of the dynode inhomogeneities. The dark count distribution should be of the same form unless the dynodes are contaminated. A detector with $b \ll 1$ is liable to cause bias in the correlation which may be a function of frequency.

However, in the APD case the pulse height distribution is wider (Equation 42, $n>2$) as the depth of the absorption of the photoelectron in substrate is random. Thus, photoelectron pairs are generated at different depths in the detector. The gain of the APD occurs as the electron causes an avalanche as it passes through the substrate. The difference in path-length travelled, by each photoelectron, leading to different level of amplification for each photon pulse. Verdeyen (1981) suggested the increase in shot noise for an APD might be as high as M^4.

To reduce background noise PMTs may be 'electronically focused', as used in this work, Section 4.2-3/5. A magnetic field is applied which allows only a small area of the cathode to generate an electron pulse at the anode, as photons incident outside this 'sweet spot' are not incident on the first dynode. This focusing also limits the different paths an electron pulse may take, during its amplification through the dynode structure, further reducing the width of the pulse height distribution.

3.3-1/5 Bandwidth Limitations

Most PMTs will operate to at least 40MHz and many allow sparse events at much shorter pulse spacings. However APDs are more limited as the APD requires to 'recharge' before a second pulse can be emitted. Allowing the re-charge to occur passively, gives rise to detectors limited to frequencies below 1MHz (Brown *et al.* 1986) and unsuited to this application.

Actively recharging the circuit gives rise to detectors capable of operation at up to 20MHz (Brown *et al.* 1986). Grant (1993) illustrated the bandwidth may be increased to at least 40MHz by the use of discrete component comparators. However, the feedback loop inherent in active quenching suggests very high frequency operation is not possible.

3.3-1/6 Choice of Detector

The preceding section would suggest that PMTs are preferred over APDs in most DLS measurements. However, the opposite is generally the case.

Conventional DLS measures low frequencies which removes the bandwidth limits, of actively quenched APDs. More importantly, the scattered signal usually has a very limited intensity, due to single scattering. In analysis of small particles this is a significant problem as laser powers cannot simply be increased to any limit, due to effects of thermal heating. The APD has a gain which is an order of magnitude higher resulting in either an order of magnitude increase in signal or an order of magnitude decrease in laser power, depending on the application.

The gradual improvements in laser diodes (discussed in the following section) suggest that the high red sensitivity APDs will replace PMTs in most DLS applications. PMT efficiency decreases rapidly with wavelength due to the photoelectric effect, such that they are unsuited to laser diodes typically operating at above 635nm. Standard phosphors cease to operate at around 600nm, although operation up to 1.2 microns is possible with noisier materials at low efficiencies, Figure 25.

Thus APDs outperform PMTs in most DLS arrangements but a peculiarity of DWS reverses this situation. DWS operates with a high intensity, multiply scattered, signal which makes the higher APD efficiency of little significance. Thus a higher signal to noise can be achieved with a PMT, even with laser powers below 5mW (laser pointer classification), Section 3.3-1/4. Additionally, the high frequency components of DWS, particularly in this pigment based application, would also increase the bias of the more bandwidth limited APDs.

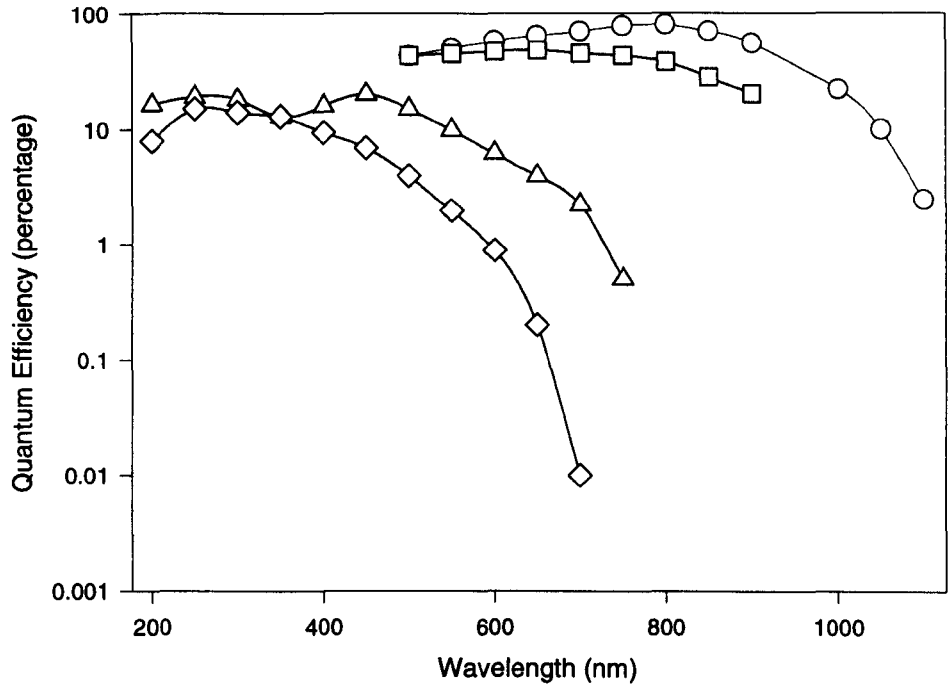

Figure 25 Manufacturers Stated Quantum Efficiencies of Detectors

The quantum efficiency of various PMT and APD detectors as quoted by the manufacturers.

Key

Dark Circle	PMT type 98310-Q, produced by EMI
Triangle	PMT type R6500U-04, produced by Hamamatsu
Square	APD type CS 30902, produced by RCA
Circle	APD type SPCM 100, produced by RCA

3.3-2 Source Requirements

3.3-2/1 Intensity Fluctuation

DLS monitors variations in intensity with time and a source of constant amplitude is required. Lasers with intensity stability, over time-scales of a few minutes, are readily available. This sub-section initially discusses the requirement for coherence prior to effects due to modal and polarisation fluctuations, which may cause instability in the nano to microsecond range. This work noted complex correlation line-shape changes that would normally be considered due to a coherence, or limited sample thickness, effect. Thus this aspect is covered more fully.

3.3-2/2 Coherence

The introduction stated that two different light sources might be considered coherent (Forrester *et al.* 1955). This can also be shown in terms of coherence of particles (Verdeyen 1981). In terms of the Heisenberg uncertainty principle, the ranges of momentum, p, and position, x y z, of a photon within any mode are given as (Martiensen and Spiller 1964):

$$\Delta x\, \Delta p_x = \Delta y\, \Delta p_y = \Delta z\, \Delta p_z \geq h' \qquad \text{where } h' = h / (2 \pi) \qquad \text{Equation 44}$$

or, in terms of angular apertures of radius u and using $\sin u_x = \Delta p_x / |p|$ and $|p| \lambda = h$, the spread and loss of phase, or spatial coherence, of an ideal source is given by:

$$\Delta x \sin \phi_x \geq \lambda \qquad \text{Equation 45}$$

This requirement defines the use of a pinhole in conventional DLS experiments to ensure only a single coherence area is monitored. In DWS a single coherence area must also be monitored but this was carried out using a monomode fibre. This has significant practical advantages for equipment required for industrial usage Section 3.5.

We can also define $\Delta p_z \geq (h\, \Delta\omega / c)$ and $\Delta z \geq (c\, \Delta t)$, and thus the temporal coherence in terms of frequency and temporal speed:

$$\Delta\omega\, \Delta t \geq 0.5 \qquad \text{Equation 46}$$

Thus at low light levels the light scattered by different particles at different times may still exhibit a level of coherence and thus interfere constructively. In photon correlation spectroscopy the coherence requirements are typically of the order of a millimetre and lasers are frequently only required due to their unidirectional output. In DWS more stringent coherence requirements are set, due to the increased path-length differences, although lower laser intensities may be used.

3.3-2/3 Longitudinal Cavity Modes

The gain of most laser mediums is low, 0.6 percent cm^{-1} for a helium-neon mixture at 633nm. To generate the population inversion, which is a prerequisite to lasing, an optical capacitor or resonator is required. The cavity now causes some restrictions on the laser beam. The wave front of the generated single mode must match the mirrors of the cavity and the characteristics of the beam (i.e. minimum spot size) are now functions of the cavity as well as the wavelength. The cavity will thus oscillate at any frequency, ω, for which nodes exist on the mirrors

$$\omega = (x\ c) / (2\ S) \qquad \text{Equation 47}$$

Where x is an integer and S is the optical length of the cavity, Figure 26. The gain of the medium may cover a wide range of frequencies, as the energy levels of the active species are not discrete. Thus lasing may occur on a few longitudinal modes around the main laser line. As PCS is commonly carried out using 20MHz bandwidth correlators, this only limits cavity length to below 7m.

3.3-2/4 Transverse Cavity Modes

Each longitudinal mode, given by Equation 47 for q=0, has a family of associated transverse modes (m, p), Figure 26. The transverse mode frequencies for a cavity may be calculated:

$$f = [\ c / (\ 2nS\ )\ ]\ (\ q + \{\ (\ 1 + m + p\ ) / \pi\ \}\ \cos^{-1}\ (\ g_1 g_2\ )^{0.5}\ ) \qquad \text{Equation 48}$$

Where the cavity parameter g is positive for a stable cavity and given by:

$$g_{1,2} = 1 - S / R_{1,2} \qquad \text{Equation 49}$$

Where R is the mirror diameter and S the cavity length. They are much more closely spaced than longitudinal modes and thus cause significant noise and bias in a DLS signal. However, the probability distribution of the modes (mode order) increases with radial distance and may be limited by the use of a pinhole. Frequently, in helium neon lasers, high order transverse modes are restricted by simply limiting the diameter of the laser tube.

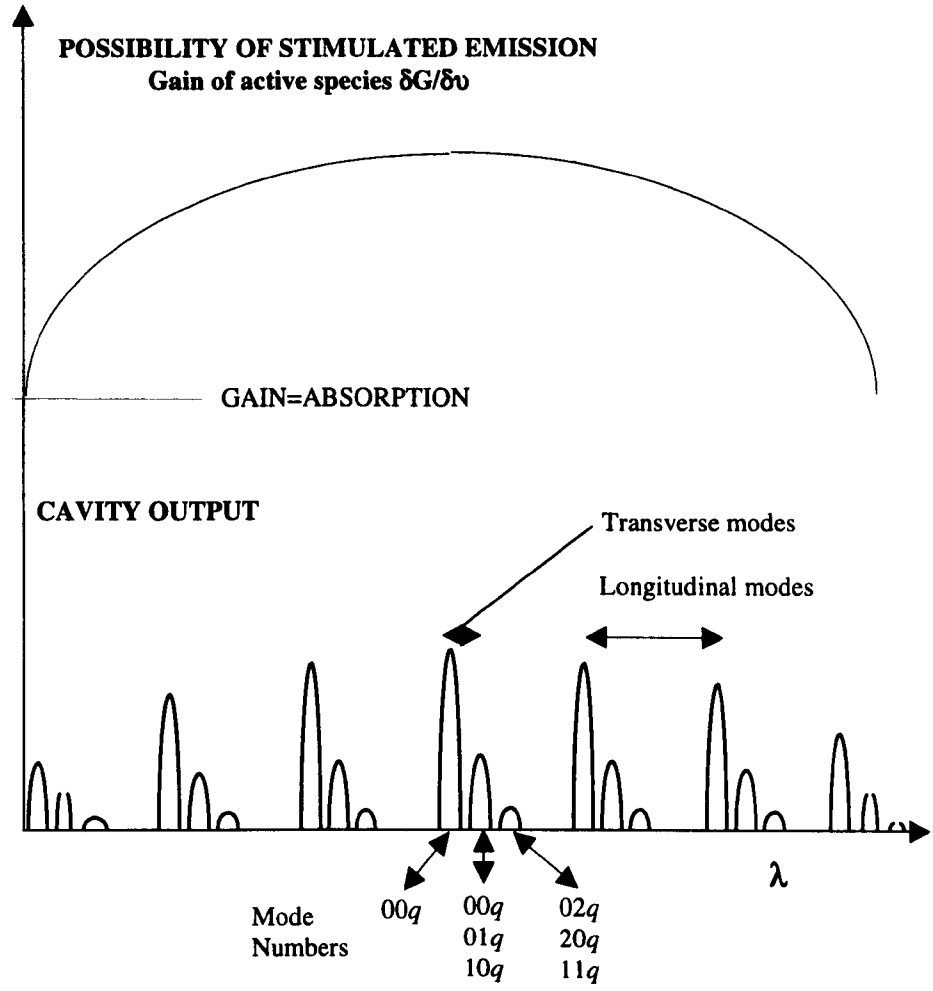

Figure 26 Cavity Modes and the Active Medium Gain Curve

Laser output for a hemispherical cavity with $S/R_2 = 1/2$ (Verdeyen 1981). Each longitudinal mode has a family of three transverse modes. These transverse modes reduce in intensity as their increased laser spot-size makes a cavity of finite mirror diameter lossy. Thus reduction in the mirror diameter or intra-cavity pinhole is generally used to limit their existence.

A large number of longitudinal modes may exist at different intensities, which is a function of the active medium gain curve. An intra-cavity etalon may be used to ensure all longitudinal modes but one are highly lossy. The modes are degenerate (lie on top of each other) for $p+q=5$. In the case shown the mirrors are small so only modes with $p+q=3$ oscillate.

3.3-2/5 Stability

The basic theory suggested that any single transverse mode laser may be used for DWS and even a certain quantity of higher order transverse modes may be tolerated. However in many laser types, particularly diode lasers, mode stability may be a problem.

A laser may operate on only single longitudinal mode, but switch the absolute mode number (mode jumping). This gives rise to intensity fluctuations and coherence reduction. In addition in transverse mode lasers 'spatial hole burning' may lead to alternating transverse mode patterns giving similar problems.

It is also noted that the TEM_{00} mode is really a family of modes of different polarisation angles. Where a laser is unpolarised, within the cavity, the laser will give rise to rapidly and erratically alternating polarisation output. A laser may be polarised by setting the output coupler at the Brewster angle, Figure 27. A polarisation ratio of between 100 and 500:1 is typical of gas lasers providing they are running at gain saturation (Oliver 1973).

Most lasers are capable at operation at a number of different levels, over 100 being identified for neon to date. A colour filter would be too lossy for most lasers and thus a diffraction grating may be used at one end of the laser or different gas mixtures/pressures used. This work used the standard 633nm neon line, Figure 28.

Mode and polarisation must be selected intra-cavity. Use of an extra-cavity polarising filter and/or pinhole to cause single mode operation will actually intensify amplitude fluctuations. This limits the use of many 'single transverse mode' diode lasers where an extra-cavity pinhole is used.

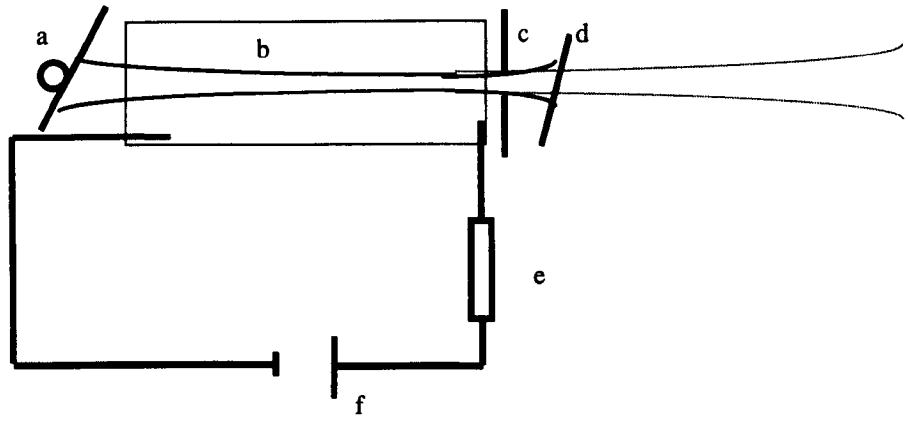

Figure 27 Typical Medium Power Gas Laser

A typical medium power laser showing the wavelength selective Bragg reflector (a), active species (b), pinhole (c), Brewster window (d), ballast resistor (e) and 1-6kV supply (f).

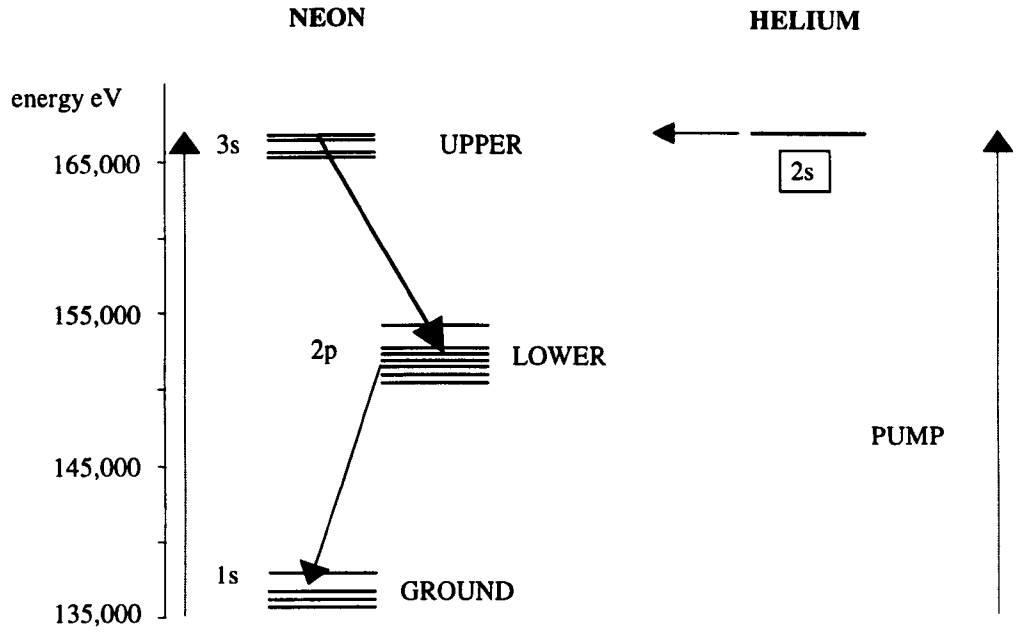

Figure 28 The Simplified Helium-Neon Laser Operating at 633nm

The basic three levels involved in 632.8 transitions of the helium neon laser. The lasing transitions, as well as the decay to ground, are shown for the active neon atom. Only the lower transfer state is shown for the helium atom, many more exist and most are short lived and decay to the long lived 2s state rapidly. This allows the helium to act as a long lived upper level reservoir, transferring energy to unexcited neon atoms by collision.

3.3-2/6 Laser Selection

In conventional DLS arrangements argon ion lasers are the typical source used with powers (single laser line) between 25 and 1000mW. The higher power types are used to analyse small particle sizes, where the signal magnitude is limited. At lower powers helium neon lasers are a more conventional choice although diode lasers may be used in specific applications (Brown and Grant 1987). Whilst argon and neon lasers are typically below 1percent efficient the small area of the diode cavity, and thus massive power density, allows efficiencies of 40 percent to be achieved.

However in this work a helium neon laser was selected. Whilst larger and less efficient than diode lasers, a helium neon laser gives better intensity stability and a greater coherence length. The most important consideration is not the order of the modes contained within the laser but that the mode pattern is stable. The level of coherence required by DWS allows most experiments to be conducted with lasers that have many longitudinal modes and often even low order transverse modes of low intensity will be acceptable. In addition, helium neon lasers are very robust devices compared with their diode counterparts, and better suited to an industrial environment.

When the laser is operating well above threshold, the amount of spontaneous emission will usually be negligible; however, where the intensity incident to a DLS experiment is set by reducing the pumping of the cavity, the signal to noise ratio will vary, as the spontaneous emission may not reduce significantly. In conjunction with this, gain fluctuations in the active medium, typical of gas lasers, will affect the correlation (Oliver 1973). Slow drifts in mirror alignment are liable to give small increases in the baseline error, this has little effect on homodyne operation but may require correction in heterodyne schemes. The helium neon laser was fixed at maximum power such that this limitation did not require further consideration.

3.4 Optical Components for DLS

3.4-1 Bulk Optics

3.4-1/1 The Requirements of Optics

The optics, and most notably the fibres, used in the arrangement had a significant effect on the behaviour of the system, especially in respect to the near-retroreflection model. This section details the requirements of the bulk optics and fibres in general prior to a more detailed overview of polarisation maintaining fibres and shows their advantages in a pure homodyne near retroreflection model.

3.4-1/2 Isolation

The optical configuration must exclude light of a similar wavelength, to that of the laser, from entering the cavity. External light may act as a seed causing rapid changes in intensity and mode structure as the light may be out of phase with the emitted field and the wavefront will no longer match the cavity mirrors. This leads to out of phase stimulation and fluctuating lossy cavity modes. Thus optical isolation of the emitted beam must be ensured. To overcome this opto-isolators should be used, however, a more economic option is to place the first optical component at least 5cm from the laser source at a very small angle. In this manner the reflected laser light will not re-enter the cavity.

3.4-1/3 Control of Intensity

The intensity of the laser must be correctly set, particularly at the high frequencies and high count rates found in DWS, to avoid pulse pile up, Section 3.2-3/4. For optimum signal to noise the laser should be operated near its maximum output, in gain saturated mode. In any case, in many low power lasers the output intensity is fixed at this level. A variable neutral density filter is typically placed in front of the laser.

This text argues that the reduction in intensity should occur immediately prior to detection. When the input intensity is reduced the signal decreases whilst the noise remains constant. However, reduction of the detected intensity maximises the signal to noise. This also has the effect of applying lower optical power to the filter and thus avoiding filter heating effects.

3.4-1/4 Types of Lenses

There are various types of lenses that may be used including convex-convex, plano-convex, achromatics, and Graded Index (grin). Conventional lenses rely on shape and the air glass refractive index difference whilst grin lenses have flat ends and rely on radial parabolic change in refractive index. The optimum lens is the achromat, even for monochromatic light, as spherical aberration is minimised. However, they are costly and significantly more complex to mount and align than the grin type. The latter may be butt coupled directly to a fibre and glued in place. This ensures vibration will cause neither misalignment nor intensity fluctuations.

Brown and Jackson (1987) have discussed the benefits of grin lenses over planoconvex and gave the equation for the blur circle radius, R_b, as:

$$R_b = x\, f(\,NA\,)^3 \qquad \text{Equation 50}$$

Where x is 0.65 and 0.54 for grin and planoconvex lenses respectively. Thus a grin lens is capable of a 20 percent smaller spot than an equivalent plano-convex lens.

Sakamoto (1992) has made a complete theoretical study of grin lenses for both monomode and multimode couplers and connectors. Whilst results show a minimum spherical aberration for the SLW1.8 lens, the SLS2 is recommended to reduce losses.

This work used achromatic lenses for optical launch, this ensured minimum spot size and thus maximum launch into the small core diameter optical fibres used. Grin lenses were used for light collection at the detector end of the probe, where diffraction limited performance is not required. This simplified the probe design considerably.

3.4-1/5 Polarisers

A polarising filter is required for detection and may be required on the source, depending on the degree of natural polarisation of the laser. Glan-Thomson polarisers operate on the Brewster principle, containing an air or glue gap between two wedges set at the Brewster angle. The gap causes the beam to deviate, which is troublesome when the polarising filter must be rotated. Where a polarisation of 1000:1 is acceptable the simple method of overcoming this is to use a polarising cube relying on a thin dielectric film as opposed to air gap so almost no offset occurs between the incident and emitted beam. Since fibres will not practically maintain a polarisation of better than 1000:1(Section 5.2-2/2), this is the preferred method.

Varnham *et al.* (1983b) suggested that Bow Tie fibres used well above their cut-off could be used as polarising filters, by making one mode lossy via bending. To produce a reasonable extinction a considerable length of fibre must be coiled, increasing the probe length and thereby reducing the signal to noise ratio. Fibre polarisers are expensive and larger than their bulk optic counterparts and do not allow the polarisation to be switched through 90 degrees easily. There would appear to be no good reason to use fibre polarisers in DWS. In the longer term further developments of the side pit single polarisation fibre (Zing) may make it practical and economical for the fibre probe to itself act as the polarising filter.

3.4-2 Fibre Optics

3.4-2/1 The Waveguide

This work used a fibre optic probe for direction and collection of laser light. There are a variety of fibre types available and the choice of which to use has a significant effect on the stability of the equipment, and on the evaluation of the correlation line-shape.

Fibres are based on the principle of total internal reflection. It is possible to produce a waveguide simply from a cylinder of high refractive index material, Figure 29. To reduce losses and increase mechanical strength this is typically coated with a low refractive index glass and a plastic coating.

Fibres may be separated into two major types single mode and multimode. Whilst multimode fibres transmit significantly more light single mode fibres are shown to have a higher signal to noise in DLS experiments as they detect light from only a single speckle (Ricka 1993).

3.4-2/2 Multimode fibres

Where the refractive index difference occurs as an abrupt transition, step index, the difference in optical path each mode may take causes a significant variation in the velocity each mode propagates within the fibre. This problem may be alleviated by the use of graded index fibres, which operate in a similar manner in grin lenses. The core has a parabolic refractive index profile equalising the optical path-length of each mode.

However, minor changes in the environment cause the mode structure of the fibre to fluctuate. This is termed modal noise and results in loss of coherence and drowning of the signal (Brown 1987). Thus, even where a pinhole is placed immediately prior to the detector, multimode fibres are not stable in the industrial environment.

Whilst the pinhole ensures that only a single coherence area is monitored, the light reaching the pinhole is scrambled by the fibre before this, any slight temperature variation or vibration causes a fluctuation in the detected intensity. If the noise is repetitive then a false signal is generated at the detector whereas if the noise is random the correlation intercept will be reduced, as the signal is washed out.

3.4-2/3 Single Mode fibres

It is not possible to produce a symmetric waveguide that only supports the equivalent of the TEM_{00} laser mode. However, the summation of the hybrid modes, LP_{01} and LP_{10}, is generally accepted to be equivalent to the TEM_{00} mode for first order analysis, although a more formal description has been given by Cherin (1983). To operate as single mode the refractive index, numerical aperture and core diameter of the waveguide must be accurately controlled.

Thus the pinhole occurs immediately at laser launch and, effectively, immediately prior to detection. Vibration and environmental fluctuations cannot give rise to the same modal noise that occurs in multimode fibres. However to act as monomode the fibre core must be very small, typically 3 micron for visible light. Thus launching light into the fibre can be inefficient. Whilst the quantity of light launched is low, only light from a single coherence area is detected and thus the signal to noise is maximised.

3.4-2/4 Launch Conditions

When light is launched into a fibre both the focusing power and the spot size should be matched to the fibre. This is not only to maximise the input intensity but also to ensure mode stability. The monomode laser has been described as not truly monomode and with short fibre lengths incorrect launch conditions can give rise to modal noise as previously described for multimode fibres.

Brown (1987) calculated a theoretical launch efficiency of 0.8 for monomode fibres, although he suggests 0.3 - 0.5 is more typical. The lens should be chosen such that the point spread function of the Airy disk, A_d, matches the numerical aperture of the fibre.

$$NA = A_d = (2.44 \lambda F) / D \qquad \text{Equation 51}$$

Where F defines the lens focal length and D its diameter.

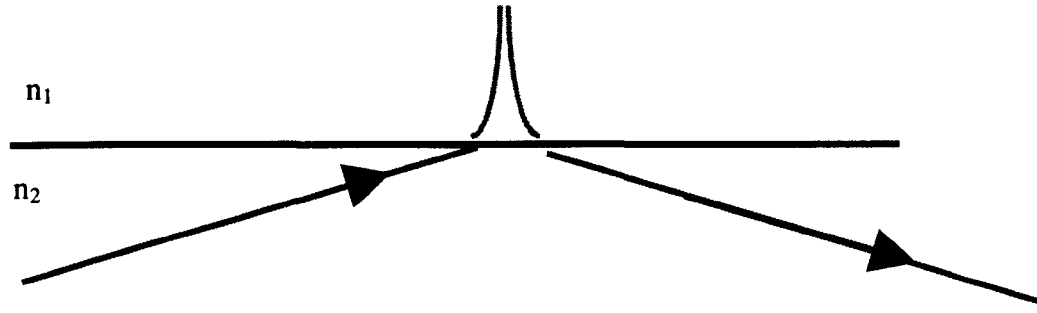

Figure 29 Total Internal Reflection and the Evanescent Field

Total internal reflection at an interface where $n_1 > n_2$ and incident angle is greater than the critical angle. The ray enters the cladding for a short distance and is transferred as stationary evanescent wave prior to re-emerging further down the fibre. The evanescent field decays exponentially with distance from the interface.

Typically the lens will be selected to have diameter of twice that of the collimated beam to ensure power loss is or the order of 1 percent.

The ideal condition of critical launching (NA = A_d) is unstable, in practice it will tend towards the conditions termed under-fill or over-fill, Figure 30. A fibre is said to be over-filled when the launch NA is greater than the fibre NA, this results in a significant reduction in the launch efficiency. Whilst a significant amount of light will not couple into the core, high NA photons may couple into the cladding area and travel down it as a helix, known as skew modes. These may re-enter the fibre causing dispersion and subsequent loss in coherence

In the under-filled condition, the launch has a lower NA than the fibre. This may appear beneficial but in practice the focus is liable to be larger than the fibre core leading to significant loss, and again significant light is launched directly to the cladding (Yang and Mickelson 1992).

3.4-2/5 The Use of Mode Scrambling

In under-fill conditions light may travel a significant distance prior to the LP_{11} mode becoming stable. The short length of fibre used in DLS makes equipment susceptible to this problem. This may result in intensity fluctuations at the output, which are environmentally sensitive. In communications these modes are generally removed by mode scrambling. The fibre is subjected to microbends via either a special roller arrangement, or more typically coarse sandpaper and pressure in the research laboratory. This ensures the modal pattern is stable on output even if the launch was in the under-fill condition. Mode scrambling is not practical using polarisation maintaining fibres, where the birefringence is produced via asymmetric stress patterns.

In light scattering arrangements to ensure mode stability this work suggests fibres should be kept as long as is practical and launch should be over-filled.

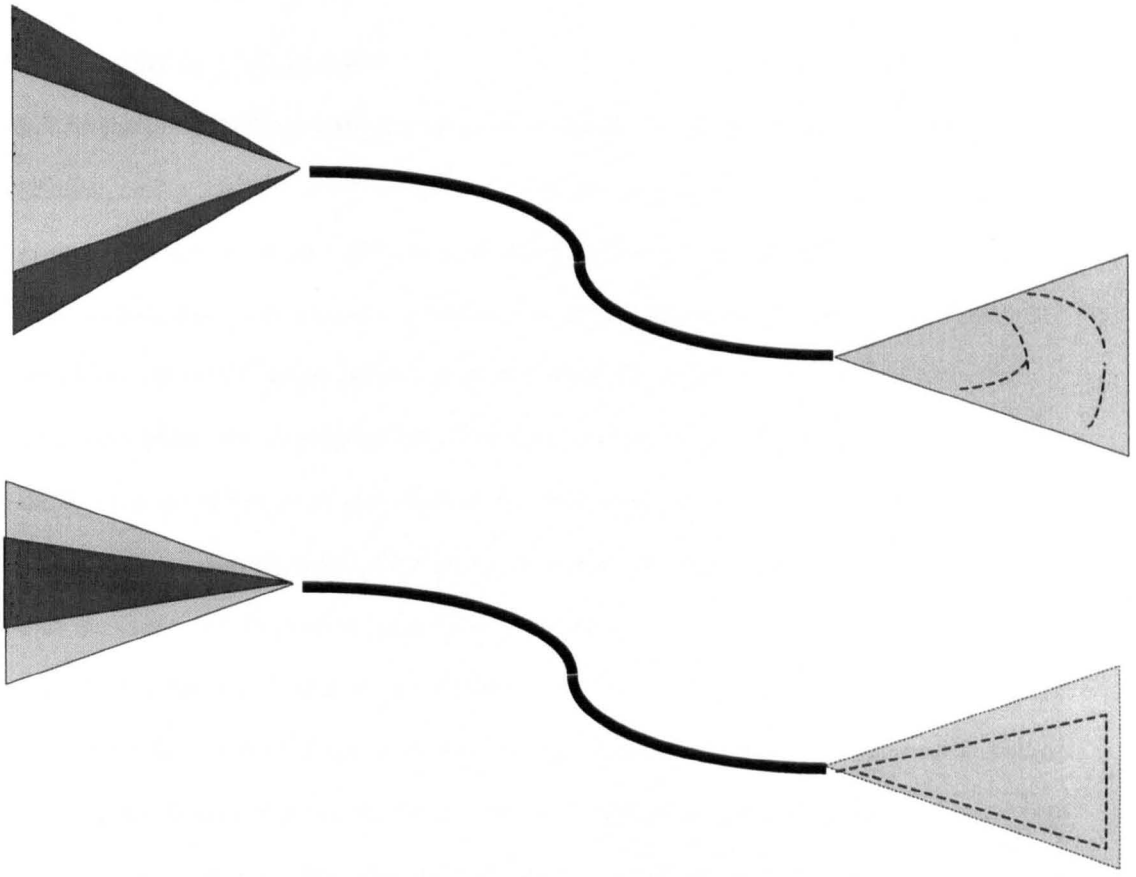

Figure 30 Over-fill & Under-fill Launch Conditions

For ideal launch we require the NA of the fibre to equal the NA of the lens whilst ensuring the laser spot size is less than the core diameter. The requirements are contradictory for single mode fibres and either the laser spot size or NA will tend to be too large. Dark areas signify input lens NA and light areas signify fibres NA.

Upper Trace- Over-fill: The light is incident such that $NA_{lens} > NA_{fibre}$. Significant light is beyond the cut-off angle for total internal reflection within the fibre core leading to both increased light loss and significant cladding modes leading to coherence loss.

Lower Trace- Under-fill: The light is incident such that $NA_{lens} < NA_{fibre}$. Whilst all the light is below the critical angle for TIR within the fibre the focus is larger and significant light may be coupled directly to the cladding. The amount of light launched and the emission pattern is sensitive to small vibrations.

3.4-2/6 Effect of Cladding Modes

In both launch conditions cladding modes may be generated. Under-fill may result in more cladding modes, whilst over-fill may gives rise to a high weighting of skew modes and thus greater dispersion. Since the modes travel a different optical path to the core they rapidly lose phase. This is particularly true of skew modes, which travel a significantly different distance. Cladding modes should be removed at launch as bends in the fibre may allow them to re-enter and travel as LP_{11} now out of phase with the original light. This may be achieved with high attenuation by stripping the first few cm of fibre of its protective coating and painting the surface black. The fibre only poorly supports cladding modes. Provided the launch is near critical fill and the fibre lengths of 5m+ are used it is unlikely to be a significant problem.

3.4-2/7 Evanescent Coupling Between Fibres

Basic ray tracing suggests that on reflection the light leaves the same point it was incident without entering the cladding material. Solution of Maxwell's equations shows this not to be the case. The incident photon generates an evanescent field within the cladding medium prior to re-transmission further down the fibre. When two fibres are held in close proximity leakage, known as cross-talk, will occur between the fibres due to evanescent coupling, Figure 29. This forms the basis of the fibre coupler, where two fibres are fused together. The degree of coupling will vary linearly with the length of the fibre held in proximity and exponentially with the cladding thickness. This suggests that the emission and detection fibres should be kept separate as much as is possible to ensure the excitation fibre does not couple into the emission fibre.

In practice the use of monomode fibre significantly reduces the degree of cross coupling between fibres. A monomode fibre typically has a cladding thickness of over 60 microns (per side), while for a multimode fibre this may be as low as 12.5 microns. This is highly significant, as the cross talk effect is an exponential function.

3.4-3 Polarisation Maintaining Fibres

3.4-3/1 Polarisation Beating

Section 3.3-2/5 discussed that only polarised lasers should be used for DLS, as unpolarised lasers gave rise to erratically changing polarisation beating. A similar situation occurs in non-polarisation maintaining fibre, which generate fluctuations in the emitted polarisation state when illuminated with a plane polarised source. This beating is a function of environmental variations and thus susceptible again to either generate false signals or wash out the signal of interest. Obviously if unpolarised light is used the problem in removed.

However, this would assume the sample scattered light of both polarisation states equally in retroflection. This is known not to be the case even in simple systems as depolarisation takes many scattering events (Lilge and Horn 1991, Schmitt *et al.* 1992, Bicout and Brosseau 1992, Brugscaglioni *et al.* 1993).

This work attempts only to give the background theory required to describe the fibre selection made in this work, as opposed to considering more advanced fibre models (Cherin 1983).

3.4-3/1 Polarisation Modes of Fibres

The level of polarisation preservation may be described in terms of the normalised birefringence, *B*, which is the propagation difference between the two modes:

$$B = 2(\beta_x - \beta_y) / 2(\beta_x + \beta_y) \qquad \text{Equation 52}$$

$\beta_{x,y}$ is the birefringence of each mode, or in terms of the beat length, L:

$$L = \lambda / (n B) \qquad \text{Equation 53}$$

Where n is the fibre core refractive index.

Barlow *et al.* (1981) have shown that natural birefringence of monomode fibres may be reduced by spinning the fibre during the drawing process. This reduces the chance of polarisation beats, which are often seen in a monomode fibre, but it does so by scrambling the polarisation information and increasing the pulse spread due to the combination of β_x and β_y.

This suggests that it is not possible to separate different polarisation states, after transmission by a standard monomode fibre. Using a very short length of fibre could actually generate an environmentally sensitive waveplate, as the fibre length will have a certain number of 'twists' from the drawing process.

3.4-3/3 Preservation of Polarisation

A more useful method of reducing polarisation noise is to increase the natural birefringence to such a point that the modes will not mix. This may be carried out in variety of ways and leads to four major Polarisation Maintaining (PM) fibre types. PM fibres have two effective NAs giving an elliptical spot. Whilst launch to the low NA, or fast axis, is more difficult the light travels a shorter distance hence coherence may be improved.

3.4-3/2 Elliptical Fibre

Elliptical fibres operate by separation of the Eigen modes (fibre axis) using physical shape of the fibre core. Okoshi (1981) gives an approximate measure of the birefringence as:

$$B = e^2 (2\Delta)^2 z(\omega_n) / \omega_n \qquad \text{Equation 54}$$

Where Δ is the refractive index difference and z is a function of the normalised frequency (ω_n) and takes into account change of refractive index with frequency.

Since there are obvious limits to the magnitude of Δ, the only method of obtaining a large B is by reduction of the core size. The small core of a high B elliptical fibre makes launch difficult and attenuation is significantly greater than standard single mode fibres.

3.4-3/3 Side Pit Fibre

Okoshi (1981) showed the possibility of producing a single Eigen mode fibre using non-symmetric radial changes in refractive index. By correct manipulation of the parameters it is possible to make a fibre that will be beyond its cut-off, for one of the two modes. Unfortunately, analysis shows that the difference in cut-off frequencies will be very low making it unsuitable for most purposes where stress is present.

3.4-3/4 Stress Induced Fibres

The polarisation properties of fibre were been known to be very stress dependent. Okoshi (1981) discussed the use of the material mismatch of the cladding and core to induce stress by using a circular core and elliptical cladding. If stress was sufficient this would cause a true birefringent fibre. In principle these fibres could be very low loss. However, the quantity of stress appeared limited, as beat lengths over a centimetre were typical. Another method of inducing stress is by inclusion of materials of different thermal expansion within the fibre cladding.

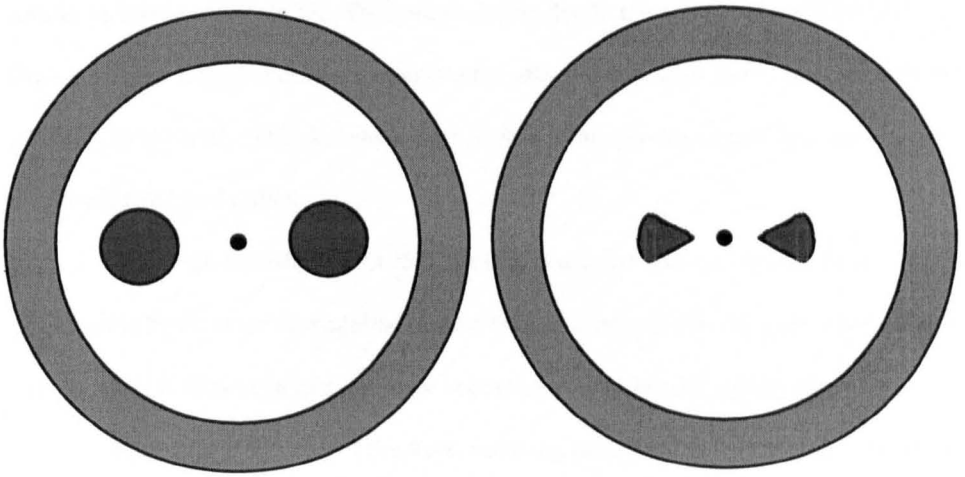

Figure 31 Bow Tie & Panda Fibres

Cross-sectional view of Bow Tie (right) and Panda (left) fibres. The black central spot is the fibre core, the white the cladding, the light grey the plastic coating and the inserts are shown dark grey. Panda fibres give low attenuation, as the insert is some distance from the core, whilst Bow Tie types give an order of magnitude better extinction (for similar stress levels).

The evanescent field is a standing wave, which decays exponentially with radial distance and is not dispersive, for an infinite cladding. In practice some light is lost due to the finite cladding thickness

This allows the stress to be centred around the core producing a very high birefringence for quite low stress levels. There are two types of this fibre on the market at present commonly known as Panda and Bow Tie. Their names given due to the appearance of their cross section, Figure 31. The Bow Tie design maximises the effect of the stress due to the insert shape (Birch *et al.* 1982, Saski *et al.* 1982, Varnham *et al.* 1983a). This gives a very high B for a given stress value compared to a Panda fibre.

Rashleigh and Marrone (1982) have reported that a stress induced fibre maintains polarisation by an order of magnitude better than an elliptical core in areas where vibrations are present. This is obviously of significant importance for industrial equipment.

Whilst the proximity of the stress inducing inserts to the core increases attenuation, this is not a significant problem for the short lengths used in DLS. Bow Tie fibre appear the most suitable type for use in light scattering measurements within industrial environments, although Sasaki (1982) reported that some of the hybrid types presently under investigation, such as elliptical cored Panda, may eventually prove more suitable.

3.4-4 Fibre Arrangements

3.4-4/1 Arrangements for DLS

This work has aimed at describing the necessary theory for the two fibre system used in this work. However, prior to considering the overall benefits of the arrangement, the hardware constraints detailed in this section are considered with respect to more conventional fibre probe designs.

The most obvious fibre arrangement, for a near retroreflection model, would be the use of a single fibre for both incident and detected light. This is not only limited as single scattering is preferentially detected but physical constraints suggest it has a secondary disadvantage in terms of homodyne, heterodyne operation.

3.4-4/2 Heterodyne or Homodyne Operation

The fibre end of a fibre beamsplitter will act as a local oscillator. The Fresnel reflection of around 1 percent, when immersed in water, will propagate back down the fibre. The magnitude of this reflection is fixed but the signal due to the scattering particles varies with concentration. At low concentrations the signal is near perfectly heterodyne but, if the transport path decreases, the signal becomes a more complex mixture of homodyne and heterodyne signals. This complex mixture requires bi-exponential fitting, even for purely diffusive light (Bremer 1993).

This work suggests that, since the correlation may be biased in shape due to other effects, the heterodyne signal should be calibrated in the equivalent continuous phase of the suspension. Thus re-calibration for every suspension type is required.

Where this does not occur it may be questionable if the homodyne contribution may be properly extracted.

In addition, it is known from the communications field that any fibre splice or fusion causes a reflection. Thus fibre beam splitters should not be used. Whilst this reflection may be low, light returning to the detector will have travelled a path-length many centimetres different to that of the local oscillator of the fibre face itself.

3.4-4/3 Coherence

It has been stated that the single fibre arrangement acts in a near heterodyne mode at low concentrations. Unfortunately at these concentrations and using this scattering arrangement the source coherence requirements are most stringent.

The average path-length difference between the local oscillator light and the scattered light being $2l_*$ whereas in the variation between path-lengths of the scattered light (homodyne) is merely $l_*^{0.5}$ as the photons are diffusive.

3.4-4/4 Polarisation

Unpolarised single fibre probes (using a fibre beam splitter or beamsplitter prior to the fibre) will suffer the polarisation problems discussed previously, Section 3.4-3. In principle it is possible to generate a pure homodyne arrangement using a polarisation maintaining fibre optic beamsplitter. However, these items are expensive and of limited extinction. The typical detected intensity in a DWS experiment was the order of 75kcps for a launched laser power of 2mW. Assuming a 1 percent Fresnel reflection on the probe face, and a requirement for below a 0.25 percent heterodyne signal, this equates to a minimum required extinction of 10^{12}.

Even polishing an angle on the fibre to remove reflections will not produce monomode single fibre system. On laser launch at least 0.1 percent of the light will enter the incorrect fibre axis and 1 percent of this will be reflected on the fibre face. This signal is significantly greater than the detected light intensity.

3.4-4/5 Pure Heterodyne Operation

In applications of high concentration, and/or high refractive index particulates, pure heterodyne operation is not possible using the fibres tip as a local oscillator, unless it was coated to increase reflection. The latter has not been carried out in the literature to date, and is probably due to the fragile nature of reflective coatings.

Even where heterodyne operation is possible then an unpolarised fibre beamsplitter must be used. Again giving rise to possible limitations of polarisation beating, Section 3.4-3/1.

3.4-4/6 The Bifurcated Fibre Bundle

The high extinction requirement between emitted and detected fields defines a single fibre system is unsuitable for pure homodyne operation. In addition, pure heterodyne operation cannot be assumed for sample concentrations, and polarisation effects may limit data validity.

The earliest multiple light scattering arrangements were based around bifurcated fibre optic bundles of multimode step index fibres. This arrangement allowed a simple homodyne set-up using commercially available parts but suffers a number of serious drawbacks.

The pinhole used to select a single coherence area is after the fibre delivery, from the sample. Modal noise, due to vibration or temperature, may cause a significant quantity of noise within the correlation. Where the pinhole is not chosen to exactly define a single coherence area the correlation intercept, hence signal to noise, is reduced or the quantity of detected light is below the optimum level. The high numerical aperture of the multimode fibres also makes them unsuited to the near-retroreflection model, Figure 11, Equation 24.

3.4-4/7 The Near Retroreflection Model

The theoretical benefits of the retroreflection model (Figure 32) have previously been discussed, Section 2.5-1, and this section details the impact of practical constraints on that model. The homodyne arrangement made the least coherence requirements on the source and reduced the errors due to laser instability and environmental instability. The stress induced fibres allow the exact separation of polarisation. (Bow Tie variety) and ensures polarisation stability.

The large core of the stress induced fibres, with respect to the elliptical core type, reduced the numerical aperture of the emitted light to around 2 degrees when immersed in water. This is a near ideal match to the near-retroreflection model with a 125 micron fibre core to core spacing and gave a numerical aperture cross-over around 2.5mm from the probe tip, strongly reducing low order scattering, Figure 33. This spacing is limited by the fibre cladding thickness and thus it would not be possible to obtain a smaller spacing without machining the fibres themselves.

The design suggested pure homodyne operation was possible, as no local oscillator signal would be present. However, publications during this work suggested other workers considered pure homodyne DWS not viable (Bremer 1993).

The 125 microns fibre spacing gave a crossover of the NA significantly greater than required for operation in high refractive index concentrated samples. It would be beneficial to use a smaller spacing such that the retroreflection approximation (Equation 14b) would be more valid. However, this would require production of speciality fibres, which the DWS application would be unlikely to financially support. Use of larger fibre spacing was not considered beneficial in this application. This would merely reduce the retroreflection validity and there was no theoretical or practical reason to suggest it would be beneficial, as pigment samples will not exhibit a photon transport path greater than 2.5mm.

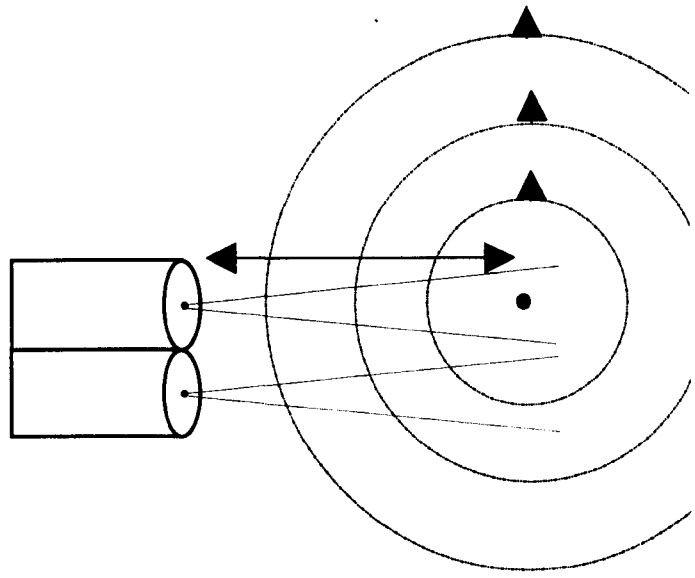

Figure 32 Schematic of the Theory Used in System Development

The light must travel a displacement equal to half the wavelength of the incident light before the light may be considered diffusive. The incident and detected NAs are such that the ballistic crossover will generally be a greater distance than the transport path hence little low order scattering is detected. The scattered light is crudely modelled as a sphere originating a distance 1 transport path into the suspension. The relatively close spacing of the fibres and very small aperture of the fibre allows the existing wave to be considered as an infinite plane wave originating directly in front of the fibre.

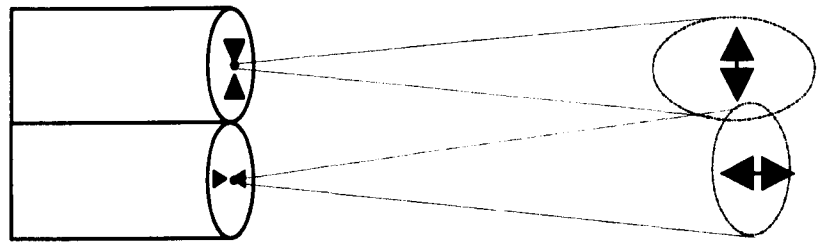

Figure 33 The Effect of NA on Detected Scattering Orders

The figure shows two fibres aligned orthogonally giving the distinctive ellipse output of a HiBi fibre. Orientations of fibre NA and polarisation detected may be made to weight towards high order or low order scattering. The low or high Numerical Aperture may be used for detection and emission. Detected light may be polarised perpendicular or parallel to the source.

3.5 Hardware Limitations

This section has discussed the hardware limitations placed on DLS equipment, with emphasis for use in DWS and high refractive index suspensions. It has shown that the homodyne (intensity) correlation cannot be assumed a direct measure of the amplitude correlation, Section 3.2-1. Whilst direct correlation of amplitude is possible it requires large fragile scanning etalons, which are cumbersome, expensive and unsuited to this application.

In conventional DLS the heterodyne measurement method is often used to obtain an intensity correlation, which is a direct measure of the amplitude correlation. However, the heterodyne technique cannot produce a piece of generic DWS equipment unless the local oscillator magnitude may be controlled. A fixed local oscillator will tend give too little or two great a scatter signal when the sample concentration, or refractive index, varies.

The signal to noise of the heterodyne signal is significantly lower than the homodyne case and the correlation intercept should always be less than one percent of the baseline, to ensure no homodyne component.

This work has argued that the bandwidth limits of the hardware suggest the detected DWS intensity should be kept constant and at a relatively low value for all measurements. This would set the actual signal containing information of very low intensity in heterodyne mode, Section 5.3-1/3. This suggests the signal will be noise limited and the baseline errors due to any laser noise will be significantly higher than in the homodyne case.

Overall in this application there would be little value in attempting heterodyne operation. The samples analysed were typically interacting such that even an absolute heterodyne analysis will not relate to the DWS model. Thus this work aimed at producing a robust, environmentally stable and highly sensitive sample characterisation technique.

This work has suggested that in most DLS applications APDs are the best choice. When analysing intensity limited signals, typical of small particles, their high efficiency gives rise to an improved signal to noise. However, it has been stated that in DWS the signal is not intensity limited and the efficiency increase is not of significant benefit. In this specific case, the reduced width of the PMT photoelectron pulse height distribution gives signal to noise benefits over the APD.

In addition the PMT offers superior high bandwidth performance that is important for high refractive index, high concentration samples, typical of this work.

Laser selection suggested that mode stability, as opposed to mode order, was the most important parameter, Section 3.3-2/5. Small gas lasers were shown to be well suited to the application.

This section also reviewed the optics required for DLS and indicated achromatic lenses should be used for laser launch but that grin lenses may be used for light collection. It also considered that polarising beamsplitting cubes give adequate extinction for the detected light.

The fibre optics used in this work were discussed in some depth. It was suggested that monomode fibres should be used where possible to reduce noise and increase stability and remove the need to align secondary pinholes, Section 3.4-2/3.

This work also suggested that polarisation maintaining fibres should always be used for detection of scattered light. Even where a circularly polarised excitation laser is used the returning light will not have equal polarisation components due to preferential scattering, thus polarisation beating may occur.

The low numerical aperture and maximum extinction ratio, for a given stress, of the selected Bow Tie fibres, suggested they were optimum for the near retroreflection system. The fibres gave a crossover of the NA of the fibre a significant distance from the fibre face limiting low order scatter, even when the fibres were placed as close as possible. It was discussed that increased fibre spacing would merely reduce the retroreflection models validity without improvement in data quality.

Single fibre and fibre bunches were discussed and limitations shown for operation in either pure heterodyne or pure homodyne mode.

The sub-components of the instrument are listed as materials (Chapter 4) and an overview of the developed system precedes the experimental results, Chapter 5.

CHAPTER 4

MATERIALS AND METHODS

4.1 Materials for DWS

This section details the components and suppliers for components and consumables used in this work. The building of the equipment is outlined, making note of alterations made early in, or at the onset of, this work.

Sample preparation methods are provided, methods involved in taking and analysing experimental data are presented.

It was the nature of this work that significant software development was undertaken. The basic methods used, and the refinements required for the final analysis package, are presented in this chapter. The development of the algorithms, together with the experimental results required to validate DWS, follow in Chapters 5,6.

Brief descriptions are given of the reference measurements and methods, used to validate DWS. This chapter concludes with a summary of the processes involved in the manufacturing of titanium dioxide and details of the material properties of the pigments.

4.2 Components and Build

4.2-1 Parts List

The laser used in this work was a plane polarised 15mW Spectra Physics tube operating at 633nm, TEM_{00}. This laser was over-rated for this work but available within the laboratory. Polarising filters, laser bandpass filter, neutral density filter and sapphire probe windows, when used, were purchased from Ealing ElectroOptics.

The probe was designed at CAMR and Sensor Dynamics and constructed at Sensor Dynamics and Point Source. The bow tie type fibres with a cut-off wavelength of 600nm were procured from Newport. The equipment jig was designed and built at CAMR with parts produced by Tioxide and single axis translation stages purchased from Ealing.

The correlator was supplied by SensorDynamics. The device had 256 channels with a minimum correlator delay of 25ns and was capable of dilation at every 16^{th} correlator channel[1].

The Photon Multiplier Tube (PMT), housing and power supply were removed from a Malvern PCS arrangement and were modified at CAMR. Buffers and water filters were purchased from Sigma-Aldrich. Optical windows were produced from microscope coverslips, which were purchased from Ealing with coatings supplied *gratis* by Peptide Products.

Quarter pitch grin lenses, when used as optical windows, were purchased from Newport, lenses used in the probe were supplied by Sensor Dynamics.

The LabWindows Software was purchased from National Instruments. QuickBasic version 4.5, Microsoft word, Wordstar and Sigmaplot were purchased prior to this work by CAMR. Compiled software will be supplied on demand, subject to license agreements (C Lloyd, Drug Delivery, School of Pharmacy, Manchester University, Oxford Rd., Manchester, M13 9PL). The software was run on IBM 386 and 486 compatible clones. Ancillary items, such as electrical components and glue, were procured from RS components.

Pigments and dispersants, for in house production of samples, along with ready produced samples were supplied by Tioxide.

1 The correlator listed was supplied later, a wirewrap prototype being used for the first 18 months.

4.2-2 Suppliers

Ealing Electro-Optics plc
Greycaine Rd.
Watford
Herts
WD2 3PW

EG&G Electronics Distributors
Pacer Electronics
Pacer Components Ltd.
Unit 20
Horseshoe Park
Pangbourne
Reading
Berkshire
RG8 7JW

Hamamatsu Photonics UK Ltd.
Lough Point
2 Gladbeck Way
Windmill Hill
Enfield
Middlesex
EN2 7JA

Laser 2000 (UK) Ltd.
Wooton Grange
Barn Owl Close
East Hunsbury
Northampton
NN4 OUA

Malvern Instruments Ltd
Spring Lane South
Malvern
Worcestershire
WR14 1AT

NewPort Corporation
1791 Deere Ave.
Irvine
CA 92714
USA

Peptide Products Ltd
Saddleworth Business Park
Huddersfield
Delph
Oldham
OL3 5DF

Point Source Ltd
Leylands Park
Colden Common
Hampshire
SO21 1TH

RS Components
PO Box 99
Corby
Northants
NN17 9RS

SensorDynamics
Ichen Abbas
Winchester
Hants
SO21 1BQ

Spectra Physics
see Laser 2000

Sigma Aldrich Company Ltd.
Fancy Rd.
Poole
Dorset
BH12 4QH

Tioxide Group plc
West Site
Haverton Hill Rd.
Cleveland
TS23 1PS

4.2-3 Design and Build of Equipment

4.2-3/1 Equipment Design

This section gives the optical arrangement that was initially designed, with the exception of the addition of the optical window and the detector drive electronics. The detector's drive circuits were modified prior to the experimental work (Section 4.2-3/5) whilst the window and coatings were added later, Section 5.2-3/5, -8. A schematic and photographs of the equipment is given, Chapter 5, along with the engineering drawings for all of the jig and the probes, Appendix 1.

4.2-3/2 The Probe

The probe head consisted of three low Numerical Aperture (NA) highly birefringent 'Bow Tie' fibres with a 600 nm cut-off. Mean fibre half angle was calculated at 2-3 degrees in water. Light was launched into a single axis (eigen mode) of the fibre using an achromatic lens.

Practical limitations meant the fibre was not mode stripped, to remove cladding modes immediately after launch. The fibre was placed into a suitable narrow steel capillary along with two similar detection fibres, aligned and set with epoxy. One detection fibre was aligned similarly to the emitter fibre and one with its optical axis set at 90 degrees. The fibres were encased in a flexible stainless steel jacket supplied by Point Source.

4.2-3/3 Detection Fibre Coupling

The detection fibres were terminated using a 1.8mm, 0.25 pitch, anti-reflection coated (633nm) Gradient Index (grin) lenses, set within aluminium cylinders. The cylinders were locked on the detector axis within aluminium rectangular prisms. These were produced such that the fibre remained on axis even when the cube was turned through ninety degrees. The output from the detection fibre coupled directly to a Glan Thomson polariser and then to a 633nm bandpass filter (20nm full width half maximum), with the mirrored surface facing the detection fibre. The polarising filter was mounted such that it could be turned accurately through ninety degrees.

4.2-3/4 Laser Coupling

A polarised (100:1) helium neon laser operating at 633nm TEM_{00} was launched into the output fibre after passing first through a 633nm, 20nm FWHM laser line filter, a Glan Thomson polariser and polarisation rotator. The laser line filter was placed with the mirrored surface facing the laser, to reduce heating effects. The filter was placed a few centimetres from the laser such that a slight angle, 1-2 degrees, ensured reflections did not re-enter the laser. The polarising filter was mounted such that it could be accurately turned through ninety degrees. Light was coupled into the fibre using an achromatic lens set within a cylinder. The cylinder was set in a Point Source laser diode stage (5 contact point type) allowing lateral translation as well as yawl and pitch.

4.2-3/5 Equipment Upgrade

The engineering drawings for the probe head and detector/laser assembly are shown in Appendix 1. The detector assembly allows for two PMT's to have the optical signal split between them. Cross correlation of the detector outputs was considered necessary when the Malvern PMT output pulses were noted to be 75ns (3x the correlator bandwidth), however the electronic upgrade made this use unnecessary and only a single detector was used.

The output from the filter passed directly to a Malvern PMT removed from a PCS arrangement. The red sensitive PMT was an electronically focusing type, reducing dark count (Model EMI 98310). The drive electronics were slightly adapted, the amplifier being replaced by a higher speed 'pin for pin' compatible device. The 50 ns delay line was replaced with a 25 ns unit that passed directly to the correlator via a high speed 50 Ohm voltage follower. This allowed a Full Width Half Maximum (FWHM) pulse of 12.5 ns, 25 ns pulse spacing (+/-2.5 ns).

4.2-4 Attachment of the Optical Window

4.2-4/1 Window Attachment

The optical window was glued to the front face of the probe sheath using two part epoxy (fast setting Araldite). The windows were cleaved into square sections slightly larger than the probe sheath, to ensure glue was not present on the front face.

The background signal from the front face was regularly checked to ensure that wear did not cause a heterodyne signal. This was carried out with the probe pointed at free space such that any signal was due to a reflection. Adhesion to the probe was regularly checked by both visual inspection and, after dipping into the sample, by monitoring the count rate for a cyclic signal.

4.2-4/2 Window Cleaning Prior to Coating

The slides were coated with silane to reduce adhesion to the probe. This was used for the majority of the work. Prior to the coating process, the slides required stringent cleaning. The slides were individually dropped into a 30ml vial of dichloromethane. This vial was sealed and shaken well at regular intervals until the slides were thoroughly wetted with the solvent. Whilst still immersed in the solvent the slides were treated with ultrasound for 30 minutes and soaked overnight.
Slides were then removed from the solvent and cleaned with filtered deionised water to remove the excess dichloromethane. The slides were then dropped into concentrated hydrochloric acid and allowed to soak overnight. They were then removed and the excess acid removed with double filtered deionised water prior to treatment with ultrasound for 30 minutes, whilst immersed in double filtered deionised water. They were then covered with a lens tissue and allowed to dry.

4.2-4/3 Silane Coating

The slides were introduced to a sample of silane individually and allowed to stand for 12 hours. Excess silane was removed using a dichloromethane wash bottle, prior to dipping in two baths of dichloromethane to remove any remaining residue.

4.2-4/4 FC405 Coating

The slides were introduced to the coating solution individually and allowed to stand for 12 hours. The coating solution was composed of a 20 percent by volume FC405 pH 5.3, made up with a 1 percent by volume aqueous solution of acetic acid buffer. After removal they were washed in the same buffer. Slides were stored in buffer until immediately before use.

4.2-4/5 FC315 Coating

The slides were introduced to the coating solution individually and allowed to stand for 12 hours The coating solution was composed of FC315 at a concentration of 500 ppm in an aqueous solution of 10 percent by volume isopropyl alcohol. After removal they were washed and stored in the same buffer until immediately before use.

4.2-4/6 Use and Cleaning

The probe was introduced to the sample whilst inclined and re-dipped a number of times to ensure air bubbles were not present on the probe window. After removal from the sample the probe was immediately placed into a beaker of water and swirled to remove the majority of contaminant. The probe was then thoroughly cleaned using a wash bottle filled with deionised 0.22micron filtered water prior to drying the window face by gentle application of an optical tissue. The glass face was then cleaned using isopropanol alcohol applied to an optical tissue that was gently slid across the slide face. This was repeated until the laser output from the probe was a clear elliptical intensity profile.

4.2-5 Suspension of Samples

4.2-5/1 Sample Preparation

The majority of the samples utilised in this work were commercial pigments and extenders used in paint products. The industrial processing of the materials and the pigment specifications are detailed later, Section 4.5.

Milling was carried out, using Tioxide's in-house protocol, on a small scale sand mill supplied and calibrated by them. Prior to use the water was passed through a double 0.22micron filter. The initial few drops of filtered water, from each syringe load, were discarded to reduce the possibility of fines passing to the sample.

Where dilution occurred, additives such as dispersants were introduced to make the solution similar to the continuous phase of the sample under dilution, where these additives were known.

Parameters for water, viscosity and refractive index were taken from the CRC Handbook, Weast (1979). The measurement software contained these values as a look up table, intermediate values were automatically calculated using a straight line fit between the two nearest known values.

4.2-5/2 Sample Pre-treatment and Storage

The samples were generally inverted and placed in a water bath to bring their temperature to within 0.5 ^{0}C of the bath before final mixing. The detected intensity and the correlator delay time were crudely set on the sample prior to mixing. Samples were mixed with a vortex mixer and two minutes ultrasonic treatment. When swirling, the samples were maintained in the inverted position. The sample was then returned inverted in the water bath for up to five minutes. The sample was turned the correct way round and the probe introduced. This was carried out by dipping the probe into the sample twice, while at an angle to ensure no air bubbles remained on the probe window.

Industrial samples were stored at room temperature whilst polystyrene reference materials were kept in a domestic refrigerator at approximately 8 ^{o}C.

4.3 Data Collection and Analysis

4.3-1 Measurement Protocols

4.3-1/1 Development of Methods and Protocols

This section refers to the Step 3 (final) measurement procedure and algorithms and the methods used in the analysis.

This chapter includes explanation of the algorithms for Step 1-3 data analysis methods but the reasons why these procedures were developed are considered in the results, Chapters 5,6.

4.3-1/2 Initialisation

The Photon Multiplier Tube (PMT) voltage was set at 1700 volts and the probe pointed at a non-reflective surface. The laser and PMT voltage supplies were switched on. The output of the probe was checked to ensure an elliptical output spot with a smoothly changing spatial intensity profile. The window was cleaned or replaced as necessary. The computer and tape streamer were switched on. At the DOS prompt the batch file that operated as programme control, INDWS, was executed. The time and date were set. The file manager module then allowed settings of default directories. The correlator settings and then parameter settings were changed or accepted in the correlator setting module. In the count rate module the background/heterodyne signal was checked to be below 100 photons counts per second with the probe pointed towards the ceiling or wall. After this point the modules could be operated in any order, a typical measurement sequence is described. A schematic of the initialisation method is given in Appendix 2, whilst the algorithms are considered in Section 4.3-4, 5.

4.3-1/3 Measurement

Running 'T.exe' as the mixing/milling finished set the experimental start time. The probe was introduced to the sample and gently re-dipped. The count rate module, 'C.exe', allowed the intensity to be set by altering the neutral density filter that was placed in front of the laser. After setting the count rate roughly the count rate graph was enlarged, to allow accurate setting to 75kcps and to allow inspection for possible heterodyning/adhesion. Running 'D.exe' then set the correct correlator delay time and experiment duration. This automatically found and loaded the correct values without operator intervention.

The measurement module, 'Z.exe', was then run. This carried out a pre-set number of experiments. When the count rate altered significantly the measurement module was stopped, the count rate reset and the measurement module restarted. A schematic of the measurement method is given in Appendix 2, whilst the algorithms are considered in Section 4.3-5.

4.3-1/4 Analysis

When a sufficient quantity of data had been collected, typically 50 correlations, the data was analysed by running 'R.bas' from within the LabWindows environment. Data sets were typically between 10 and 100 individual correlations, dependent on sample type and experiment purpose. A schematic of the analysis method is given in Appendix 2,

The data was then saved to the tape streamer using the 'b.bat' program. The program '9.bat' was used to remove only the last data set whilst '99.bat' removed the entire correlation set, '8.bat' removed only the three dimensional fitting information.

The correlation data could be stored from the temporary drive to the hard disk and then reloaded to the temporary file later using the '2.bat' and '3.bat' programs respectively.

The correlator was closed using the 'q.bat' program. The analysis method schematic is given in Appendix 1, with the algorithms considered in section 4.3-5

4.3-2 Software Development

4.2-2/1 Development Method

Software development was continuous throughout the project. This section defines three major methods (defined as Steps 0-2) that led to the final method (Step 3, Section 4.3-4). Step 0 was the analysis method used prior to the project (Lloyd 1991) whilst Step 1 was the initial work carried out prior to experimentation and was thus covered in Chapter 2. Later steps were developed due to limitations in measurement and thus detailed in Chapter 5.

This section details the methods used to carry out the analysis as opposed to reasons behind the development. The reasons for development and operation of the Step 0, 1 software are covered in Chapters 1,2 whilst the developments within the work are considered predominately within the results, Chapter 5.

The software (Step 1-3) was produced with LabWindows environment and programming produced in Quick Basic 4.5 on 386 IBM compatible clone equipped with a 40MB hard disk and 8MB of RAM equipped with the SensorDynamics correlator capable of a 25ns minimum delay time. The program included the SensorDynamics correlator driver module.

4.3-2/2 Software Listing

The final software package runs to tens of thousands of lines of code, 9MB in the Step 3 analysis module alone. A significant part of the size was due to the code that was automatically generated by the Graphical User Interface (GUI) as well as the code relating to the correlator driver supplied by SensorDynamics. These had to be repeated in each module, each of which required to be below the 640Kbyte DOS limit.

4.3-3 Initial Analysis methods

4.3-3/1 Step 0 Analysis Method

The original Step 0 software package was a modified copy of the Malvern automeasure package (Perkins 1990).

After initialisation of the correlator, using the SensorDynamics module, the intensity of the laser was set. The count rate setting module was a simple module that ran a series of experiments with pre-set durations and delay times, default 1 second and 100ns respectively. After each measurement the count rate per second was plotted on a graph.

The log of correlator channel value (α) was plotted versus the square root of the correlator delay time (τ) and a straight line fit carried out to find the characteristic decay rate (Γ), and intercept value (K): $\log \alpha = -\Gamma \tau^{0.5} + K$ Equation 55

The error between the theoretical values of α and the actual values were calculated, E, and a runs test, Ω, carried out. A series of experiments were carried out and the mean values, and errors, of Γ and K calculated. The theory behind Step 0 analysis is discussed in Section 2.4-2/2.

4.3-3/2 Step 1 Analysis

The Step 1 analysis was similar to Step 0 except that the correlator delay time was allowed to 'float'. The requirement for this is discussed in Section 2.4-2/3. After setting the count rate the sample setting module was run. Experiments of pre-set time, 3 second default, were automatically taken with the correlator delay time doubling after each experiment. This continued until the error, E, increased or the modulus of the runs value, Ω, minus 0.5 increased. The process could then be repeated but over a reduced range of correlator delay times with geometric or linear steps of a pre-set value, default 25ns. A pre-set number of experiments, default 10, was then carried out and stored. The average values for Γ and K were calculated automatically.

4.3-3/3 Step 2 Analysis

The Step 2 analysis differed from Step 1 in that the analysis was not tied to the resolution of the correlator delay time. A series of measurements with a geometric increase in correlator delay time from pre-set values, default starting delay 25ns, finishing delay 15microseconds, were taken. A straight line fit was carried out of log accumulator values versus the square root of the correlator delay. The error E from the fit was then plotted against correlator delay time for each measurement and a cubic spline interpolation carried out in Sigmaplot, Figure 34. The theoretical delay that gave the minimum error was then calculated; this was not limited by the actual correlator resolution (25ns steps) but could be an intermediate value. The calculated parameters for each correlation (E, Ω, Γ and K) were then plotted against the correlator delay time used in each measurement and a quadratic fitted. This allowed the generation of the parameter values at the previously calculated optimum correlator delay time. The cycle was then repeated automatically a pre-set number of times, default 20 cycles, or until a key was pressed.

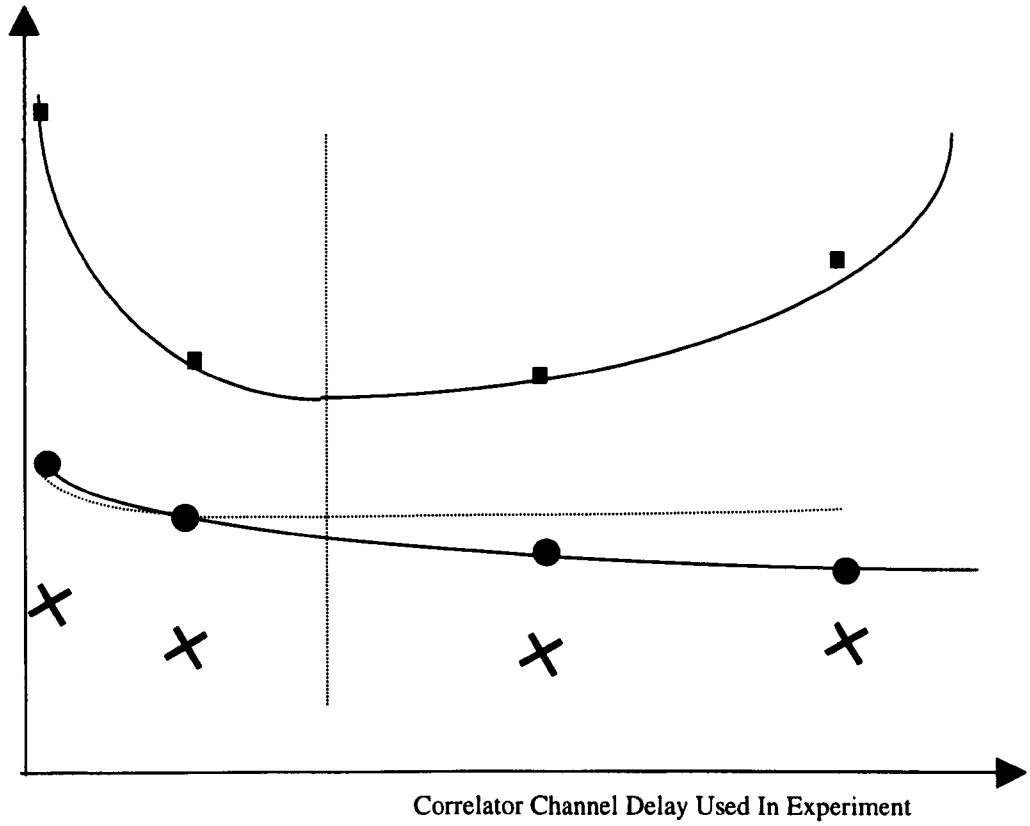

Figure 34 Step 2 Analysis

The figure shows a series of 4 experiments at increasing delay time, where the magnitudes of various parameters are plotted versus against the delay time. The top trace (squares) shows the error in fitting for each experiment $E_\Gamma(\tau)$. The mid trace (circles) represents the decay whilst the lower trace (crosses) represents the intercept value. All the traces are fitted with a cubic spline interpolation. The values taken for final analysis were those at the delay time that were at the minima for the cubic spline fitted to the fitting error $E_\Gamma(\tau)$ as shown by the vertical dotted line.

4.3-4 Final Initialisation Methods

4.3-4/1 Software Listing

This section details the function of each module in the Step 3 package whilst the design, and results of the design, are considered in Chapter 6. Flowcharts were not used in planning of the software but a basic schematic showing initialisation and first measurement is given for the final software package, Appendix 2.

4.3-4/2 File Systems

The file procedures were written to be able to utilise a RAM drive device. The RAM files could be saved permanently or temporarily to hard disk. Standard DOS batch commands were written to allow a tape storage device to behave as a standard floppy device for longer term storage of entire correlation sets.

One temporary data file was generated on a RAM drive for each: channel, dependent variable and analysis parameter, 356 in total. After each experiment the measurement procedure requiring to open each file consecutively and append the data to it, unless a new measurement was requested.

All data for each correlation, including suspending fluid codes, temperature, refractive index was saved individually for each correlation.

Batch files were generated that allowed the software itself to be loaded to the RAM drive and run from it for all modules except the final analysis package, which was too large for the memory available.

4.3-4/3 Programme Control

The package was constructed of many different programs and DOS batch programs were written to allow operation as a single program. A separate autoexec.bat in the DWS directory allowed the software to run from start-up. This called the ancillary procedures required for initialisation. After this modules could be called in any order and made to loop via batch files. All parameters and defaults were passed between modules via DOS files on the hard and RAM disks allowing the modules to run in any order after initialisation.

4.3-4/4 Correlator Initialisation

The initialisation module was a modification of the module generated by SensorDynamics. Major functional changes were such that the correlator returned set values, as opposed to those requested, to the algorithms. All correlator defaults were now kept on a hidden file on the hard disk root directory. The module did not load a Graphical User Interface (GUI), but operated in the background unless the correlator was not found at the stored address when a GUI was loaded to allow input of the interrupt and input/output space the board was set for[1]. Calling the initialisation reset all the correlator settings, with the defaults that were again stored in a hidden file on the hard and RAM disks.

4.3-4/5 Correlator Control Module

The correlator module allowed setting of any of the available hardware configurations. Settings not usually altered were colour coded. The module also allowed for delays between experiments that could be fixed, or part fixed and part random. The set delay between experiments could also be set to be constant or increase/decrease logarithmically. The correlator control module also allowed setting of dilation between every 16 correlator channels.

4.3-4/6 Suspension Coding Module

All data entered with regard to the sample suspension (refractive index, viscosity, concentration, etc) was stored in order to allow for later re-analysis. A method of coding was developed that allowed the pigment, continuous phase and dispersant to be noted. The continuous phase parameter was coded as a three digit code. The first number or letter defined the type, that is, '1' denoted an aqueous propylene glycol continuous phase. The second two digits denoted the concentration. The software could then read from files, such as: vis.100 and ri.100, and calculate the viscosity and refractive index of the continuous phase from coding.

The algorithm could then be used to set the bulk refractive index from the pigment and continuous phase refractive indices concentration. Similar algorithms and files were generated for pure liquids at various temperatures. The algorithms used a single data point above and below the requested value, from the requested file, and extrapolated a value, at the temperature required. This allowed for the data points in the files to be randomly spaced.

1 The original software design was for the software to search for the correlator board in the PC input/output space. However this was strongly recommended against, due to possible hard disk errors that could be generated (J. Baker *pers. com.* 1991).

Algorithms were also generated to allow the inclusion of a thermocouple, hence, automatically compensate for refractive index / viscosity changes prior to each experiment. The parameter files were designed to allow easy input from the DOS editor so different materials can be added.

4.3-4/7 Count Rate Setting Module

The original count rate setting module was included in this package. Changes included that the module picked up all defaults used for the measurement module, except the experiment duration, instead of having its own defaults.

4.3-5 Final Measurement and Analysis Methods

4.3-5/1 Selection of the Correlator Delay Time

The baseline of the correlation was calculated theoretically (autocorrelation). The sub-section of the correlation curve used was defined in terms the area above of a fraction of the baseline (f_b, i.e., 1.27 * baseline). Initially, the correlator was set with a long correlator delay time, S_D set at 1 microsecond by default, at a pre-set experiment time, E_D set at 3 seconds by defaults After the first measurement, the correlation was analysed from channel 1 to the first channel that was below the f_b point. The computer then calculated which correlator delay would make f_b occur as close as possible to requested channel, RC, which was set at 128 as default.

The model accepted a pre-selected number of channels around RC, +/-lim default 5 channels to stop hunting. The software was required to find the best correlator delay time a number of times (NT). When the software initially found the correct correlator delay time (within RC+/-lim) it flagged the event, but also continued to calculate and set a new RC from the last experiment. If the limit could not be achieved after a pre-set number of attempts, NQ default set at 5, the module stored the parameters used in the final correlation and finished. The module only loaded a GUI if a key was pressed during running, in this case the GUI allowed setting of all default values.

4.3-5/2 Selection of the Experimental Duration

The experimental duration used was based on the number of correlator decays (Γ) measured so all measurements should have the same statistical variance:

$$\text{Experimental duration} = ND * RC * \text{correlator delay} \qquad \text{Equation 56}$$

where ND is a variable, default 10^6, that allowed the operator to set a suitable experimental duration for a particular suspension and experiment type.

The maximum experiment duration was set at a reasonable value to ensure statistical noise did not cause impractical measurements, ME default 15 seconds. A second variable was used to define the longest measurement duration allowed within the correlator delay selection module, MSE default 5 seconds, but had no effect on the measurement module detailed later. Minimum measurement duration, MMD default 1 second, affected all modules.

4.3-5/3 Measurement Feedback

The operation of this module is difficult to explain in text, as the software's current action depended on its the previous action. The previously collected correlation was analysed and saved, whilst a new one was collected. Prior to each correlation start, the absolute time and date, as well as time in seconds since the timer was started, was noted. Real-time plots of the correlation under analysis were displayed, as soon as the previous fitting and storage procedures had concluded.

After the correlator had flagged finished, it was rechecked until the calculations have actually finished (hardware fault Section 7.4-3/4). The final correlation was displayed, and the RC point was used to set the sample/experiment time for the next experiment. Any pre-set delay occurred prior to the start of the next correlation. Hunting was reduced using a separate set of limits to those of the correlator delay module. The limit mlim, the allowable error in positioning of RC in the measurement module, was set at a default of +/-1 channel. When a key was pressed during the collection of a run of correlations, the system paused and required user input to stop or continue. When 'quit' was selected the same loop was adhered to, except that a new correlation was not initiated. The default number of experiments per measurement was 10 and could be via the correlator control module. After analysis, the data was stored (appended) to 340 files. A file was used for each individual channel of the correlator and a file for each material parameter, fitting parameter, material code etc.

The actual time and date, as well as time since timer reset at time + (0.5 previous experiment duration), were stored to file. Experiments could be re-started even after analysis.

4.3-5/4 Three Dimensional Parameter Fitting

Section 2.2-4/6 discussed the limitations of analysis of samples that were altering with time. When the decay of correlation trace is time dependant, due to settling or flocculation, it is not possible to establish if the error in the fit is due to variance in the data or due to use of a model that poorly represents the physics of the measurement.

In addition, it is shown in the results (Chapters 5,6) that the way the correlation varies with time may be used as a powerful analysis tool in determining if a sample has been properly milled. This required that 3 dimensional fitting was carried out to allow variance to be separated from modelling errors, and the information on the manner and rate of sample change to be established.

When the measurement module was running, the data from the correlator channels up to f_b were separated from those beyond this value. Straight line and quadratic fitting occurred and root mean square errors and a run test were calculated. The linear fit for the region of data above f_b was used to define the instrument response and an error E was calculated that included both variance and lack of fit generated for each correlation, Figure 35. The parameters for all fits were displayed in real-time along with the count rate and the trace of last correlation analysed.

However, to carry out a true three dimensional analysis, the three dimensional fitting module allowed large data sets to be analysed in detail following data collection, although data sets could be added to later as previously described.

On initialisation, the analysis module gave displays of mean gradient, curvature, intercept and count rate versus time of measurement, using the data from all the correlation. The displayed parameters were then fitted versus time of measurement by a quadratic function, and the values calculated for a time in the middle of the experiment set[1] which, for the example of linear fit of the correlations[2] above the f_b threshold, gave:

$$Z(t)= A_1 t^2 +B_1 t +C_1 \qquad \text{Equation 57}$$

$$\Gamma(t)= A_2 t^2 +B_2 t +C_2 \qquad \text{Equation 58}$$

$$Y(t)= A_3 t^2 +B_3 t +C_3 \qquad \text{Equation 59}$$

$$E(t)= A_4 t^2 +B_e t +C_4 \qquad \text{Equation 60}$$

Where Z is the count rate, Γ the gradient, Y the intercept, E the root mean square error and t the time of measurement.

1 The results were displayed on a graphical GUI and movement of a cross hair gave the value of the polynomial at the time selected. The parameter files were linked to a simple array of binary flags, which allowed selection of the first and last correlation to use in the analysis, as well as removal of correlations affected by glitches.

2 This software used modified versions of polynomial fitting procedures supplied by, and remaining, the intellectual property of, Dr D Svendsen. Use of these algorithms within the project, and his consideration and suggestions in the development of the software, are gratefully acknowledged. The correlator control module was a modified version of the software supplied by Sensor Dynamics.

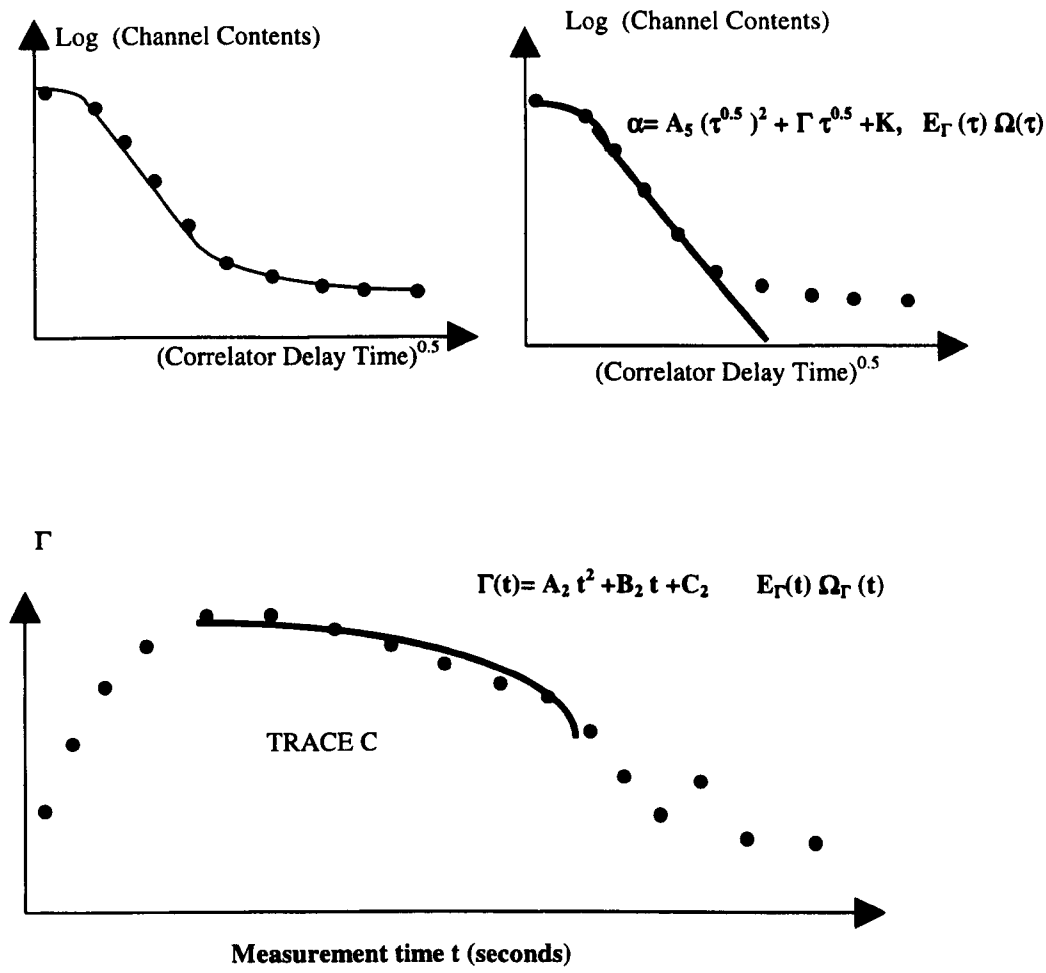

Figure 35 Three Dimensional Parameter Fitting

The data points of an arbitrary DWS correlation function, plotted log α versus $\tau^{0.5}$, along with a line of best fit, top left. A selected area of the correlation function was force fitted to a suitable function generating the decay time, $\Gamma(\tau)$, and an error, $E_\Gamma(\tau)$, trace, top right. The decay times from a selected number of a series of experiments were then fitted against a suitable function generating a three dimensional description of the decay time $\Gamma(\tau,t)$, lower. Where the number of experiments is chosen to suit the fitted function the error, $E_\Gamma(t)$, was termed the variance in this work.

The results of Equations 57-60 were substituted into Equation 22 to generate a three dimensional surface described by the linear fit of the correlation above f_b plotted versus decay time and time of measurement:

$$\log (A_1 t^2 + B_1 t + C_1) = 1/[(A_2 t^2 + B_2 t + C_2) \tau^{0.5}] + (A_3 t^2 + B_3 t + C_3) \qquad \text{Equation 61}$$

This analysis was also carried out for the polynomial fits to the correlation data above f_b and the linear and polynomial fits of the data below f_b.

The entire package was interactive as the movement of the cursor, or removing a data point, caused the automatic update of all the fits and displayed parameters. No automatic glitch detection was established during the work, and the usual method was to select the nine results (from each set of 10) that were closest to the fitted polynomial.

4.3-5/5 Three Dimensional Data Fitting

The methods in the previous section could be applied to the data collected for each correlation and thus produce a correlation with errors in each channel for a pre-set time (default mid point in experiment duration), Figure 36.

This included the 256 channel files as well as fits to every parameter and stored variable. This generated a further two temporary files, one of which contained the fitted parameters and one containing the result, error and runs test for each correlator channel and stored parameter, Figure 37.

After analysis and/or saving more data could be collected in the same data file for re-analysis if required.

4.3-5/6 Other Fitting Options

A third analysis module was available the analysis package. This allowed any file parameter to be plotted versus any other. The diffusion coefficient could be plotted versus stored temperature values or experimental count rate. Linear and quadratic fits and runs tests being carried out for each fit. Data was analysed only over the range selected as previously and data points again ignored, if previously flagged as such.

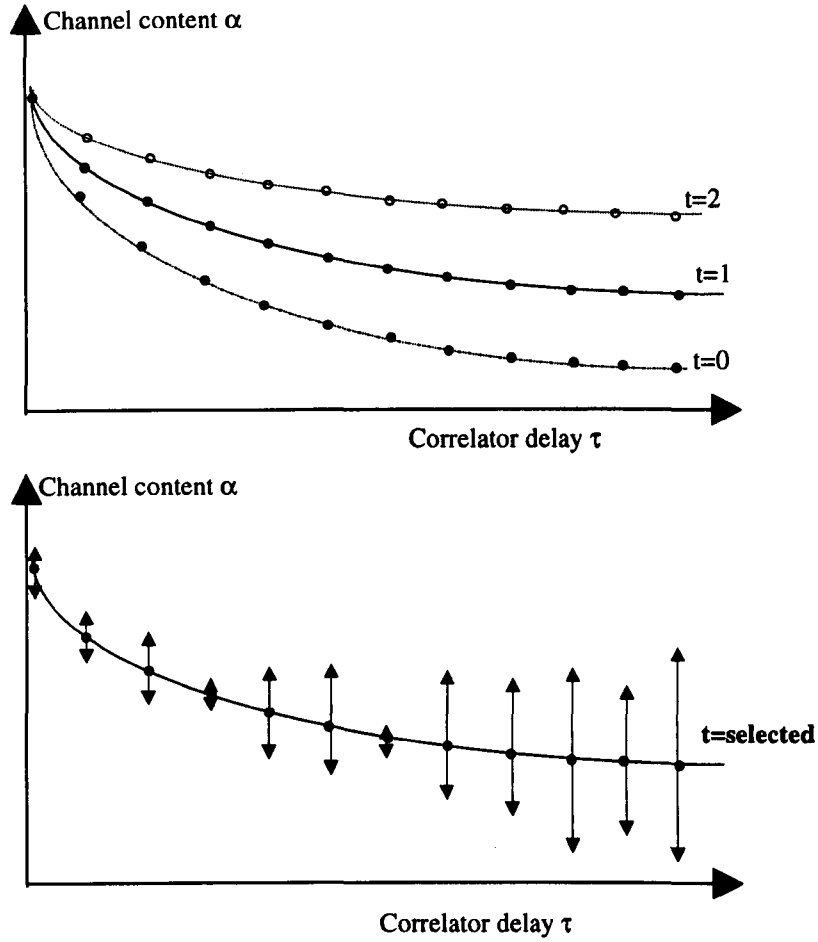

Figure 36 Three Dimensional Data Fitting

The top trace shows three arbitrary correlation functions taken at different times t=0, t=1 and t=2 which suggests a correlation changing in a continuous and systematic way over the time period selected. Each individual correlation was analysed as it was collected generating the decay time, $\Gamma(\tau)$, and an error, $E_\Gamma(\tau)$. The accumulator values for each channel were then fitted against time of measurement assuming a quadratic fit. This was carried out for every correlator channel and the functions saved to file. The value for any correlator channel at any time (time of measurement) could then be produced along with an error, $E_\Gamma(t)$. Thus provided the variation in an accumulator channel with time of measurement was smooth and continuous (and could be approximated by a quadratic fit) then this gave the statistical variance of the channel, as it was independent of the DWS model or the sample variation.

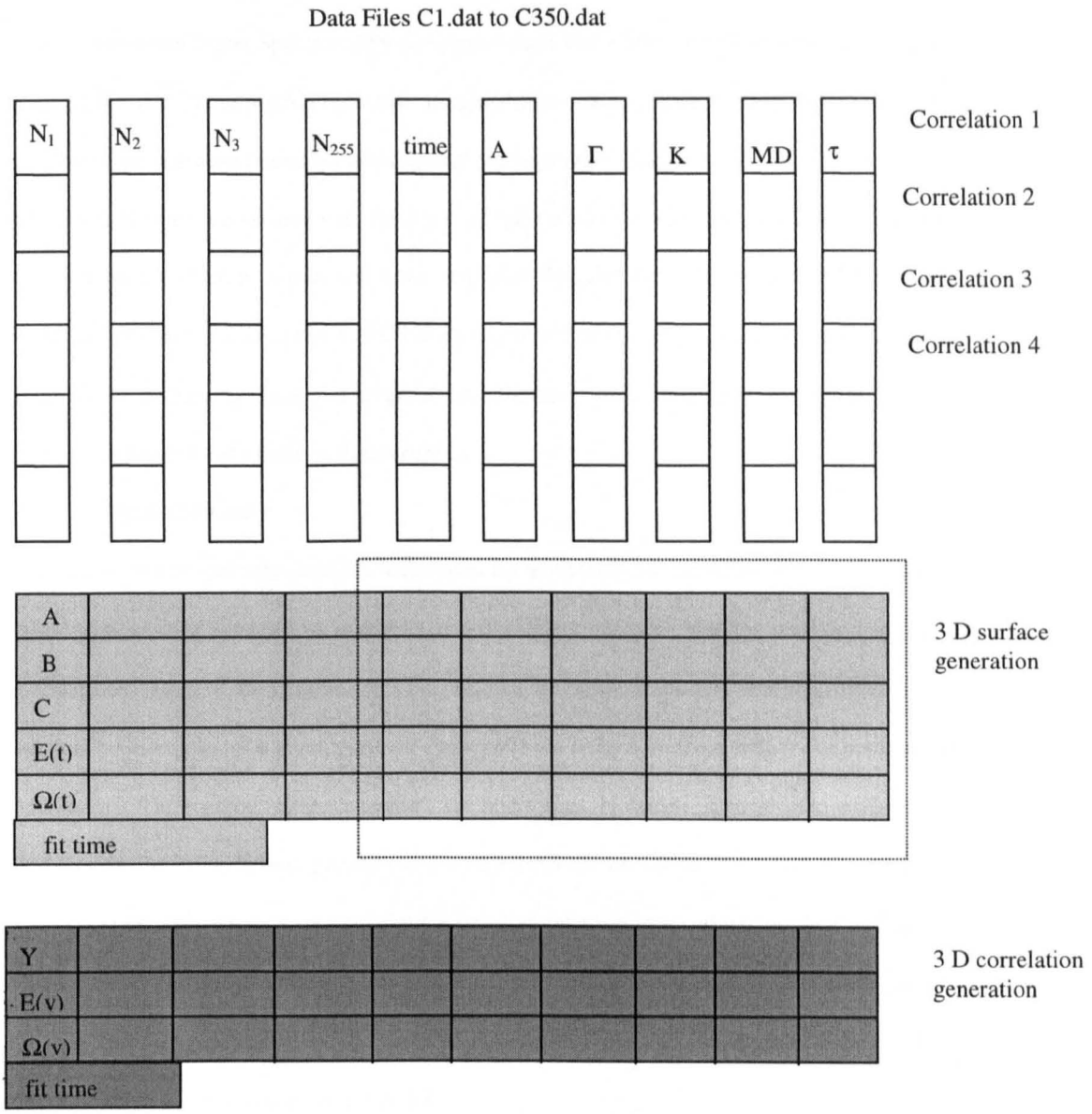

Figure 37 Step 3 Data and Results File System Schematic

The 350 files comprising the data system are shown top (white), one file for each correlator channel and one for each fitted parameter and stored constant. Fitting each file versus time (of measurement) generates a function showing the variation of that parameter with time (light grey). The parameters within the hatched area both define a three dimensional surface. The functions generated for each correlator channel were then be used to generate a true 3D correlation (dark grey).

4.4 Supporting Measurements

4.4-1 Photon Correlation Spectroscopy

The Photon Correlation Spectroscopy equipment used was a Malvern 6800 series utilising a Spectra Physics 2W argon ion laser operating at 488nm TEM_{00}. The 'automeasure' software was used with the software operating without user assumptions on particle size.

The curettes were pre-washed with double 0.22 micron filtered deionised water, which was also used for sample dilution, where water was required. Samples were allowed to equilibrate in the waterbath for five minutes prior to PCS analysis. Where TiO_2 sample were measured they were removed from the water bath and inverted, such that they were the correct way round, and replaced in the bath immediately prior to measurement.

4.4-2 Optical Density

Tioxide have a proprietary turbidity technique. By analysis of the turbidity of a dilute pigment suspension at three separate wavelengths, it is possible to measure both the particle size and standard deviation of the suspension. This requires the ratios of the scattered intensities of the various wavelengths, at a given pigment concentration, to be compared with those predicted by Mie theory. The method is simple to carry out and robust. However, it requires significant dilution and tends to be insensitive to particles above about 0.5micron due to their forward scattering.

The measurements were carried out using a standard operating procedure supplied by Tioxide (Tunstall 1980). Results indicated mean size and standard deviation assuming a refractive index of 2.7 and that no particles above 0.5 micron were present. Samples were measured when absorption at pre-set wavelength was the order of 0.1.

4.4-3 Brookhaven Centrifugal X-Ray Sedimentation

Sedimentation is a useful particle size measurement technique for TiO_2 due to the high density (4) of the material. The technique is based on the analysis of the time required for each detected particle to fall a set distance thus generating a full particle size distribution. Calculations are only valid for volume fractions up to around 0.01. At higher concentrations all particles tend to settle at the same rate, a phenomena known as subsidence. The small size of the particles involved in pigments make it usual to use forced sedimentation, via centrifugal force, to ensure the results are not affected by Brownian motion. The method is rapid and accurate and most importantly gives a direct measure of size distribution. There is no requirement to assume a distribution model.

However the method is not based on light scattering, which is the most significant factor for pigment. Tioxide carried out all sedimentation work to their internal procedures. Whilst the Brookhaven centrifuge (BIDCP Brookhaven Instruments 750 Blue Point Road, Holtsville, NY 11742-1896 U.S.A) gave the entire distribution curve, typically only mean, median and standard deviation were quoted.

4.5 Production and Properties of Titanium Dioxide

4.5-1 Production of Titanium Dioxide

4.5-1/1 Production of Primary Particles

This work studied TiO_2 extensively and thus the properties and method of manufacture are briefly covered. The process initially requires the production of pure TiO_2 as small primary particles and then processing of these to produce stable monodisperse pigment materials, Table 1.

4.5-1/2 The Sulphate Process

Two production processes for TiO_2 currently exist. The more conventional sulphate process relies on dissolving the ore in concentrated (80-95%) sulphuric acid. The process is exothermic reaching a temperature of 200^0C.

$$FeTiO_3 + 2H_2SO_4 \rightarrow \quad TiOSO_4 + FeSO_4 + 2H_2O \qquad \text{Equation 62}$$

Following this reduction and settling, crystallisation, filtration and concentration, the pigment (TiO_2) is precipitated by hydrolysis prior to calcination and milling. Commercial pressures, which appear to be predominantly due to environmental issues of waste production, have made the process expensive and the chloride process is becoming increasingly popular.

4.5-1/3 The Chloride Process

The titanium is extracted from the ore by chlorine at 950^0C after which the solid wastes are extracted before the titanium tetrachloride is condensed and purified.

$$\text{“}TiO_2\text{”} + 2Cl_2 \quad \xrightarrow{C} \quad TiCl_4 + CO_2 \qquad \text{Equation 63}$$

The tetrachloride is then oxidised at temperatures of around $1000\text{-}1200^0C$ where nucleation and crystal growth occurs: $TiCl_4 + CO_2 \rightarrow TiO_2 + 2\,Cl_2$ Equation 64

4.5-1/4 Coatings

Coating of pigments is generally carried out with precipitation of small quantities of colourless oxides, Table 2. The coating is tailored to suit each application and their varying requirements, such as dispersability, dispersion stability, opacity, gloss and durability in paints. Judin (1993) has also suggested that the oxide coating has a role in reducing photocatalytic activity, due to the semiconductor nature of TiO_2. Organic materials, such as polyhydric alcohols, alkanolamines or siloxanes, are often then overcoated to further enhance dispersion characteristics.

PARAMETER	ANATASE	RUTILE
Crystal Structure	Tetragonal	Tetragonal
A (nm)	0.3875	0.4593
B (nm)	0.9514	0.2593
Density (kg/m^3)	3890	4260
Refractive Index	2.54	2.75
Dielectric Constant	48	114
Bandgap (eV)	3.25	3.05
Melting Point (C)	converts to rutile	1830-1850
Solubility	insoluble in water & organics	insoluble in water & organics

Table 1 Properties of TiO_2

Physical properties of the two major crystal types of TiO_2 used in the pigment industry (Lawson 1992).

MATERIAL	PERCENTAGE VOLUME
TiO_2 as anatase or rutile	80-99
Aluminium Oxide coating	0-10
Silicon Dioxide coating	0-10
Zirconium Dioxide coating	0-2
Organic treatment over-coating	0-0.7

Table 2 Titanium Dioxide Pigment Composition

Typical pigment make-up for a paint (Lawson 1992).

4.5-2 Milling & Dispersion of Pigments

4.5-2/1 Aggregation, Agglomeration, Dispersion

Pigments are not monodisperse when produced and must be processed to maximise their scattering and dispersion characteristics. The definitions of aggregates, agglomerates, and flocs follow the work of Sato (1979). Aggregates are clusters of primary particles joined at crystal faces and thus more tightly bound than agglomerates, which are joined only at the edges or corners. The particles require to be broken down by stress that is applied by milling. The degree of stress required is a function of both the strength of the joint and the wettability of the material. Dispersion is the process of wetting the material to the supporting liquid and, generally, in the case of TiO_2, inorganic coatings are required to lower the interfacial tension of the solid-liquid interface.

4.5-2/2 Flocculation & Stabilisation

After producing a pigment dispersed in a fluid it may flocculate, if not properly stabilised. Flocculation is the phenomena of particles binding, after dispersion, whilst in solution. The particles are both attracted by Van der Waals forces and repulsed electrically and/or sterically.

The difference in the range of these forces may lead not only to a deep primary energy minimum, behind a repulsive barrier, but also to a secondary energy minimum some distance from the particle. This, in turn, leads to two types of flocculation, termed strong and weak. Weak flocculation is usually open network and may be broken by stirring. However, strong flocculation is often irreversible without high mechanical shear.

4.5-2/3 Milling of a Pigment

The raw pigment is generally supplied dry in the form of agglomerates, up to a size of 100micron, of primary particles between 50 and 400nm with mean size varying between 150 and 240nm. The pigment is generally dispersed, and the agglomeration and aggregation broken down in a single milling stage. Various types of grinding mill may be used, including sand mills, ball mills, Silverson mills and high speed stirrers, Figure 38. For research purposes, small sand mills operating at volume fractions of 0.0125 model the large commercial mills, which operate at higher concentrations. This low concentration allows the milling to be carried out much more rapidly than in the industrial case (15mins as opposed to 48 hours).

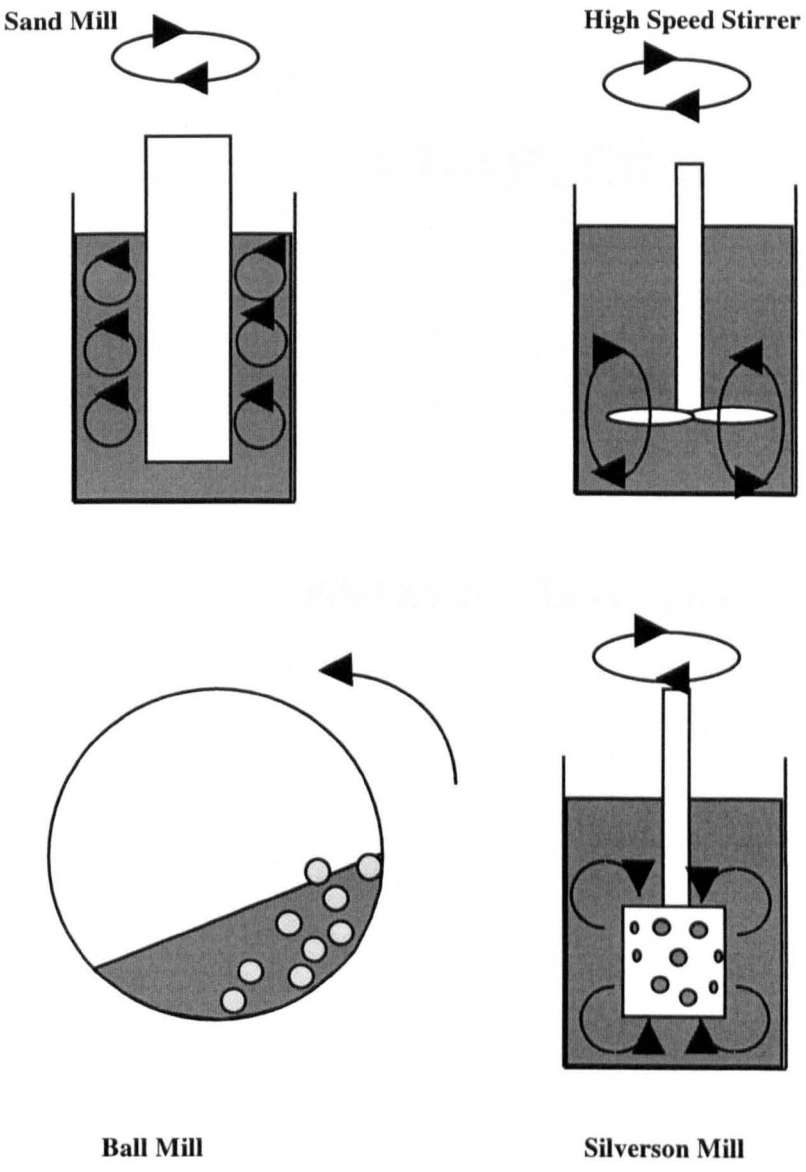

Figure 38 Types Of Mill for Pigment Dispersion

The four major mill types showing fluid flow during operation.

When the sandmill is fitted with a cylindrical rotor all stress is imparted by friction between the pigment, the container walls and the rotor, following Lawson (1992), as used in our work. It is noted that for breakage of agglomerates, the high speed stirrer is actually fitted with a blade as opposed to paddle as shown.

CHAPTER 5

Pilot System Development

5.1 Development, Calibration and Testing of DWS

The theoretical and practical limitations of DLS equipment, of individual components have been discussed with emphasis on their use in DWS, Chapter 2, 3. The advantages of a near retroreflection pure homodyne system based on birefringent optical fibres were proposed.

This chapter details the practical implementation and evaluation of the system produced, emphasising application for industrial measurement and particularly the analysis of pigments. This work led to significant developments in the methods used to collect data as well as the routines and algorithms required, Section 4.3. Thus a major part of this work is involved in detailing why and how these advances came about.

The chapter is split into three sections; the first section details the equipment along with practical experimental and hardware limitations. Whilst absolute size is shown to have limited meaning, in characterisation of high concentration materials, the DWS parameter is defined (Γ) and concluded as being more useful in many applications. Normalisation of the data to master samples allowed relative sizing and reduced the effect of the instrument transfer function on the data obtained.

The second section considers calibration of the arrangement. To ensure that it was differences in sample characteristics, not bias, that generated the results; the effects of experimental duration and scattering intensity were studied. After establishing sensible experimental durations, instrument variance was analysed. This ensured results were statistically significant and evaluated the quality of the arrangement produced. The concentration dependence of the Step 1 method was then evaluated, to ensure differences measured were not purely concentration effects. It was shown that both concentration dependence and fitting error halved (compared with Step 0), which gave greater confidence in the Step 1 method.

This finally allowed the system to be calibrated to a set of industrial pigment samples. It was shown that the sensitivity of the technique was at least as good as industry standard techniques. In addition, the level of reproducibility indicated sensitivity greater than any system capable of analysing liquid samples available at that time. The dependent parameters, temperature, viscosity and refractive index were finally considered.

The final section discusses limits of the pilot system and analysis in terms of advances in methodology to overcome correlator bandwidth limits, sample instability and more complex limits due to refractive index and particle shape.

It is shown that refractive index is a complex function for DWS. At low concentrations, the refractive index used in modelling should approximate to that defined by the relative volumes of pigments and the continuous phase. At moderate concentrations, the refractive index is more complex and is also a function of particle size. However, at high volume fractions of high refractive index materials, it is suggested the effective refractive index of the sample may be independent of concentration of the suspended particles. Furthermore, it is considered that the phenomenon that leads to concentration independence may also lead to a reduction in light absorption by the continuous phase.

5.2 DWS Development and Experimental Limitations

5/2-1 The DWS Measurement

5.2-1/1 Normalisation of the Correlation

The correlation produced in a DLS experiment is an exponential decay superimposed on a background. In pure homodyne mode, with ideal equipment, the baseline is equivalent to half the interpolated accumulator value at a correlator delay of zero, Section 3.2-2/3. Thus, the correlator accumulator values used in the analysis were given by:

$$\alpha = (\alpha_I - \alpha_{baseline}) / \alpha_{baseline} \qquad \text{Equation 65}$$

Later work showed differences in correlation shape (Section 5.4-3/2) and normalisation was evaluated using the highest accumulator value (approximate to the zero delay value):

$$\alpha_i = (\alpha_I - \alpha_{baseline}) / \alpha_{MAX} \qquad \text{Equation 66}$$

This gave a correlation always decaying from 1 to zero and allowed differences in correlation shape to be visualised. However, it was found to give biased results if used for analysis.

5.3-2/2 The DWS Parameter, Γ.

This text has argued that any analysis of DWS should first be based on analysis of the parameter actually generated by the instrument. Thus the correlation gradient, as opposed to second order parameters such as diffusion coefficients or size, should first analysed, Section 2.2-2/7. This parameter has no direct meaning in itself and requires to initially be normalised to a 'master sample' and variations of different samples considered relative to it. If samples are similar to the master, in all properties except size, then the result is a direct measure of how DWS responds to variation in size. Thus, Γ was defined to be the modulus of slope of the correlation when the logarithm of the correlator of the accumulator is plotted against the square root of the correlator delay time, Equation 22. A normalised decay rate Γ_N was then defined, where N defines the sample the decay is normalised to and is calculated as a direct ratio:

$$\Gamma_N = (\Gamma_{mes} / \Gamma_{ref}) \qquad \text{Equation 67}$$

Thus the normalised parameter clearly demonstrates sample to sample differences. From the model (Equation 14b) a large value of Γ corresponds to a smaller 'effective size', or lower viscosity. This method of defining the result as ratio was also thought to reduce the effect of instrument bias and removed limitations caused by parameters which were unknown, Section 1.5-4.

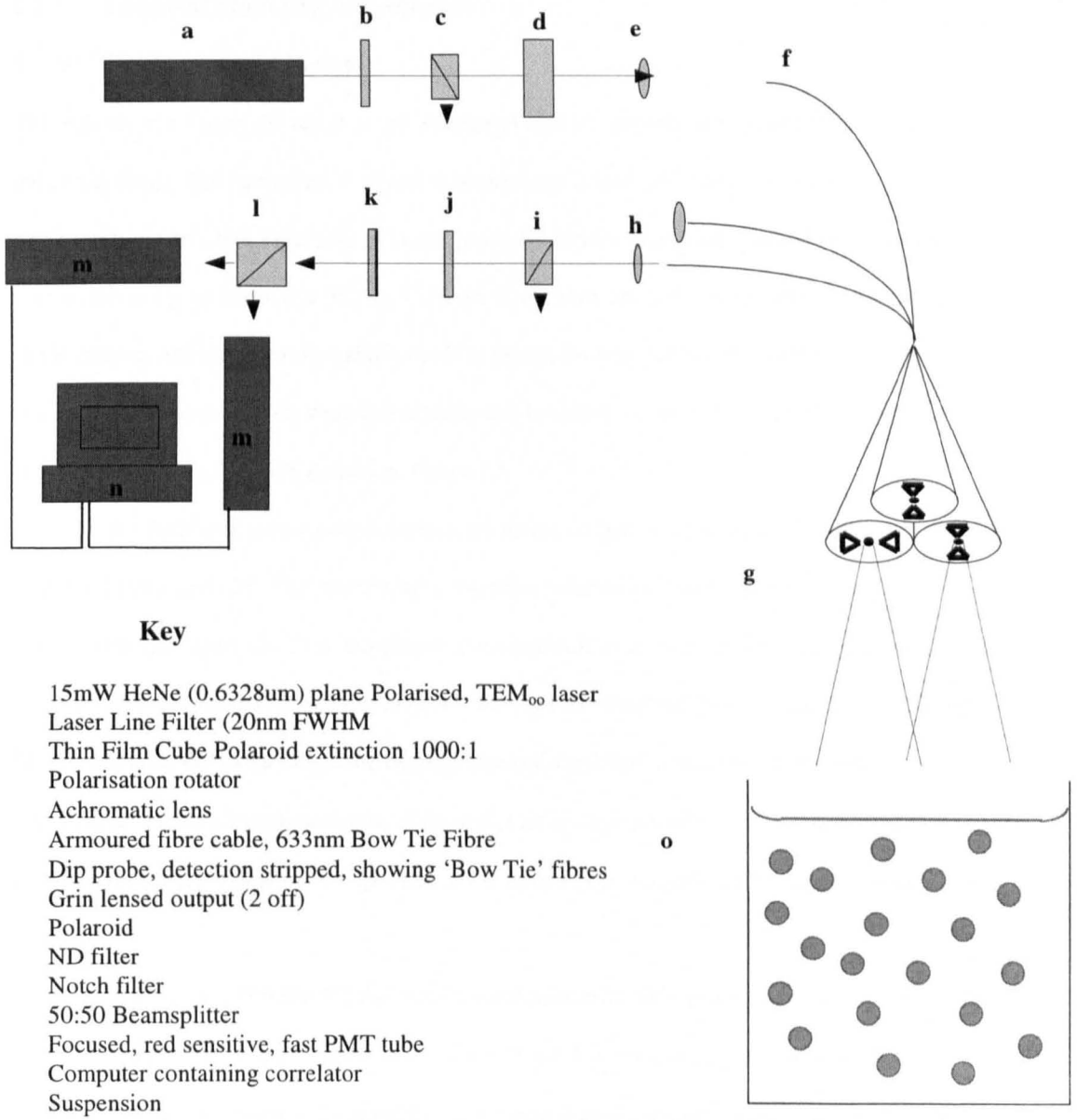

Key

a	15mW HeNe (0.6328um) plane Polarised, TEM_{oo} laser
b	Laser Line Filter (20nm FWHM
c	Thin Film Cube Polaroid extinction 1000:1
d	Polarisation rotator
e	Achromatic lens
f	Armoured fibre cable, 633nm Bow Tie Fibre
g	Dip probe, detection stripped, showing 'Bow Tie' fibres
h	Grin lensed output (2 off)
i	Polaroid
j	ND filter
k	Notch filter
l	50:50 Beamsplitter
m	Focused, red sensitive, fast PMT tube
n	Computer containing correlator
o	Suspension

Figure 39 The Optical Arrangement

The schematic shows the DWS equipment and arrangement developed in this work.

5.2-2 The Light Scattering Arrangement

5.2-2/1 The Arrangement Design

This sub-section details the result of the equipment build in producing a system suitable for industrial usage. The equipment is shown schematically, Figure 39, and photographs of the equipment are included, Figure 40. A linear polarised helium neon laser was utilised. This type of laser exhibits a pure and stable TEM_{00} 633nm output. They are multi-longitudinal mode but of a stable pattern, and do generally exhibit mode hopping, Section 3.3-2/5. Suitable diode lasers available at the project onset were less reliable and tended to operate at longer wavelengths, a significant problem for PMT detection, Figure 25.

The laser was intra-cavity polarised, by means of Brewster windows, ensuring polarisation stability, Section 3.3-2/5. The emitted light entered a polarisation rotator allowing simple alignment to the fibre axis. This was placed approximately 5cm from the laser at a small angle to the fibre axis and ensured no reflections could re-enter the laser and cause instability. A laser line filter and a laser line polarising cube beamsplitter followed this. It has been stated neither polarisation nor wavelength selection of the laser can occur extra cavity, for a stable emission. However, the components reduce spontaneous emission launched to the fibre, thus increased signal to noise.

In the design (Figure 39) the variable neutral density filter is shown on the detection fibre, this arrangement improving signal to noise, Section 3.4-1/3. However, practical mounting constraints of the arrangement required this to be placed on the source, immediately following the polarisation rotator.

The polarisation beamsplitting cube was placed in a holder that allowed it to be accurately rotated through 90 degrees, Appendix 1. This type of cube was selected as virtually no beam offset occurred (Section 3.4-1/5), thus the laser spot position would remain fixed regardless of the polarisation shift. The mirrored side of the laser filter was set facing the laser to reduce heating and the Polaroid was the last optical element to give maximum extinction of the emitted light.

The light was coupled into a single mode fibre using an achromat, effective magnification x25, this lens type giving the smallest possible spot size, Section 3.4-1/4. The fibre had a low NA, such that an over-fill condition ensured mode stability would occur over short fibre lengths, Section 3.4-2/4, 5.

The use of single mode fibre ensured that at all times a single coherence area was analysed and thus the signal to noise was maximised, Section 3.4-2/3. It was not practical to mode strip the fibre at launch (Section 3.4-2/6), as the flexibility of the probe would cause the fibre to break. To reduce cladding modes 10 meters of fibre were coiled in the box where the detection and emission fibres came together. This was also carried out for the detection fibres.

Bow tie type polarisation fibres were selected due to their high extinction ratio (Section 3.4-3/4), the design allowed a polarisation of 1000:1 to be achieved in a stable environment. Grin lenses were attached directly to the detection fibres and the output light passed through a Polaroid and laser line filter as previously described. The light was shared between the detectors by a 60:40 beamsplitter. This gave a near 50:50 split for the vertically polarised light. Each output beam was directed at a lensed photon multiplier tube (Figure 39) and path-lengths were kept similar to within 1mm.

The probe contained one launch fibre and two detection fibres, Figure 39. The detection fibres where aligned such that any combination of polarisation and numerical aperture possible could be obtained, Section 5.2-3/4.

The Photon Multiplier Tubes were red sensitive and electronically focused, Section 3.3-1/6. This gave a background count of around 25cps when the PMT voltage was reduced to its minimum setting (Malvern PCS PMT and supply). PMTs have been argued as having a more determinate gain than APDs due to their dynode structure, which should give a higher signal to noise when the pulse discrimination is taken into account, Sections 3.3-1/4.

The correlation was carried out on the fastest commercially available real-time auto-correlator with a bandwidth of 40MHz and 256 correlator delay channels. Correlator channels were set up linearly to ensure the measured function was continuous and not significantly biased, Figure 23, 24.

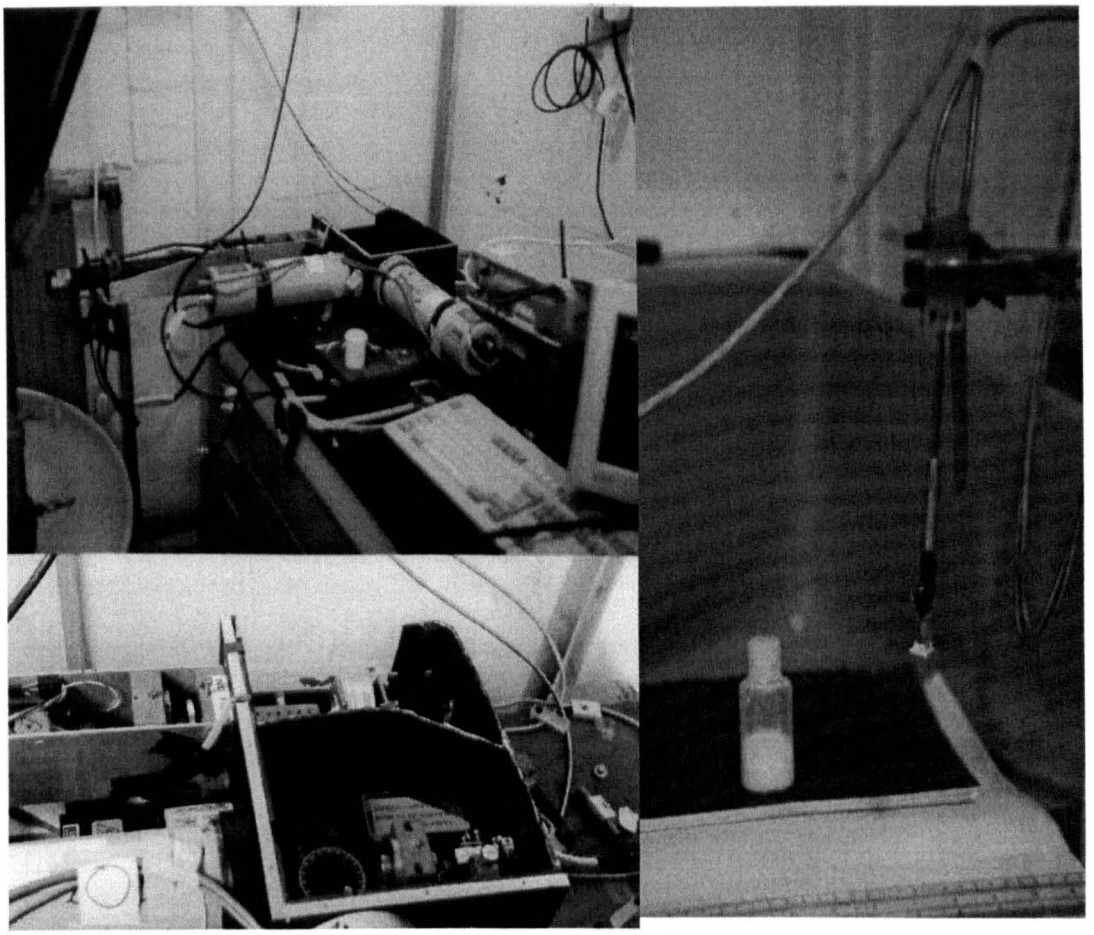

Figure 40 The Equipment Produced

The figure shows the DWS equipment and arrangement used for this work.

Top left: The two PMT housings are clearly visible along with the laser bracket connected to the main box. Lower left: The main unit with the laser launch (upper). The laser bracket contains the laser filter and an interlock system, which cut the laser power when the lid was removed. This had to be fitted to allow the instrument to be used at the industrial partners site.

The edge of the Polaroid beamsplitter table can be seen and the polarisation rotator (silver). This is separated from the detection side by a black card spacer. In the detection axis (lower) the input fibre cube/clamp is visible and the rotating Polaroid. The beamsplitter rotating table (used to align for cross correlation) is empty. This unit was fitted with a lid with 2 curtained slots to allow for the input/output fibres. Right: The near retro-reflection dip-in probe with the optical window holder and window attached. The apparent 'wedge' on the end of the probe is Araldite that holds the window in place, pigment can be seen to have adhered to the glue. The book shown is A4 giving an indication of scale. The robustness of the measurement is illustrated by the ability to use a simple clamp stand to hold the probe.

5.2-2/2 Industrial Requirements

The near retroreflection model was obviously ideal for industry, as the probe would simply fit into any sample or pipe, Figure 40. The probe was produced from high grade stainless steel making it suitable for use in areas where solvents, acids and alkalis would frequently be spilt on it, Section 2.2-2/2. The probe design allowed for sample contact on only a single glass interface where required. The fibres were coupled back to the main laser/detector unit by armoured cable.

The typical launched power of below 1mW also made the unit a Class 2 laser ensuring a suitable safety limitation for shop floor usage. The fibres used ensured that no modal noise (nor polarisation beating) could occur. The fibre probe achieved an extinction of at least 500:1 even when the probe cable was vibrated, typical of an industrial environment. This level of extinction was believed to be significantly better than would normally be considered possible for fibre instruments.

The simplicity of the monomode fibre design also removed the requirement for a pinhole, which itself can cause noise if it vibrated relative to the detector and or input fibre. The robustness was further enhanced by the homodyne design such that any vibration present would occur in both optical paths and not generate a false signal, Section 3.2-1/6.

This arrangement allowed operation in a pure homodyne mode in all concentrations evaluated, unlike conventional arrangements where this has been considered impractical (Bremer *et. al.* 1993). In addition no background measurements of transport mean free path were made, making the technique suitable for generic usage.

The detectors used in this work were rated to 20MHz, although scope traces suggested even this was optimistic as the pulse width was of the order of 65ns, full width half maximum. Thus, in the original design the collimated light from the detection fibres was split and sent to two different photon multiplier tubes. Any photon could travel to one, or the other, detector but not both. This allowed cross-correlation of the two signals to act as an autocorrelation but removing the limitations of detector response, Section 3.2-2/7. To ensure that environmental variations between the optical paths did not give rise to a vibration sensitivity, similar to a heterodyne arrangement (Section 3.2-1/6), the detector arrangement had be highly stable. The detectors were mounted on an L bracket which itself was locked to the base, Figure 40.

5.2-3 Modifications of the Arrangement

5.2-3/1 Modifications Required

Three major modifications of the hardware were required at, or near, the onset of this work. These had significant impact, both positive and negative, on what studies could be carried out during the lifetime of this project. These modifications are considered prior to the experimental results obtained using the system.

5.2-3/2 Change to Autocorrelation

Early in this work it was possible to upgrade the detectors by replacement of the amplifier and internal delay lines with compatible but faster silicon chips. This generated a pulse of around 15ns FWHM, ideal for the 25ns correlate minimum delay time and allowed the arrangement to operate with only one detector. This made the arrangement simpler and also removed any problem that could occur due to vibrations between optical paths, Section 3.2-1/6.

As the detector pulsewidth was shorter than the correlator delay the only bandwidth benefits for DWS (using cross correlation) would occur when operating at very high photon rates, where analogue parts of the PMT could bias high frequencies. However, this work showed very early on that there is no benefit at operating at high count rates, Section 5.3-1/3. This appeared to negate any significant benefit of the cross correlation arrangement, although it proved useful in analysis of the fibre spacing, discussed in the following section.

5.2-3/3 Fibre Spacing

Using both detector fibres (one into each PMT) allowed the quantity of low order scatter detected to be monitored. This was not pseudo cross correlation, where only a single coherence area is monitored, as the light being split from a single fibre. Instead two different coherence areas are monitored and the resulting correlation is due to the level of overlap between the fibres, Figure 32. If no overlap occurs the two signals will exhibit no coherence, and thus similarity, between them.

Launching plane polarised light into 1 fibre and connecting the other 2 detection fibres into separate detectors (unpolarised) gave no correlatable signal from a sample of Tioveil CS94, a standard pigment product at volume fraction 0.12. It was believed this was because the light became diffusive before the crossover of the numerical apertures of the fibres (Figure 33) and thus different coherence areas being monitored. This was a clear indication that in this type of material the fibre spacing was either optimum or too great. There appeared no benefit in analysis of larger fibre spacing, which could only detract from the retroreflection model used and require higher power lasers.

Evaluation of reduced fibre spacing would have been beneficial, Section 2.5-1/6. However, in the arrangement the fibres were as close as possible (125 micron core to core), the cladding in contact, Figure 32. To obtain closer fibre spacing would require specially produced fibres, which would be very costly. DWS experiments were carried out at an intensity that generated a scattered signal of 75kcps. Typically this required 1mW of light to be launched into the fibre. When the probe was pointed at free space this signal reduced to 75cps. The extinction between source and detected light being of the order of 1 part in 10^{12}, this was 10^{6} better than could be supported by any Polaroid and impractical for single fibre arrangements. The use of an optical window suggested that reduced fibre spacing would significantly reduce this extinction, Figure 41.

The application used for this work used samples of both high refractive index and high concentration materials, minimising l^* and therefore reducing the validity of the retroreflection approximation, Figure 11. As the concentration and refractive index of the particles increase, Equation 24 loses validity and becomes non-physical if l^* falls below 125 microns, the fibre core spacing.

5.2-3/4 Selection of Polarisation and Numerical Aperture

The detection polarising filter was mounted in a holder capable of 90 degree rotation, which, along with the polarisation rotator, on launch, allowed any of the five possible static orientations to be aligned V_sV_s, V_fV_f, V_fH_f, V_sH_s and V_sH_f. Where V, H denotes the polarisation state and f, s the fast or slow eigen mode of the fibre. The number of effective orientations increases to 12 for a flowing system. Lloyd (1991) suggested this might allow the study of various parameters including:

- the effect of polarisation (VH, VV) on measured D, particularly where a small percentage of large particles are present in a suspension that generates Rayleigh scattering;
- the effect of numerical aperture on measured diffusion coefficient, particularly with respect to ballistic to diffusive cross-over and the effect of large particles near to the probe tip;
- the effect of numerical aperture on flow, measurement at two separate numerical apertures allowing separation of the measurement of flow speed and size.

However, in practice it was not possible to adjust the polarisation without misaligning the system. For 633nm light the fibre had a core size of 3 microns, such that even a 300nm offset was significant. In addition the low NA of the fibre (3/5 degrees) meant that even optics aligned to 0.5 degrees gave a significant offset when rotated.

Realignment took considerable time and made relative measurements of different NAs impractical, especially as most samples analysed in this work were not stable with time. VH polarisation of the fast eigen modes was used for experiments. As considered theoretically, Chapter (2), this arrangement was designed to ensure:

- low concentration dependence due to both the deep ballistic crossover of low NA fibres and the requirement for multiple scattering to cause depolarisation, by small particles;
- pure homodyne operation as no Fresnel signal is present from lens/window reflections;
- reduced effect of large particles near or adhered to the probe giving an effective Fresnel reflection.

Whilst measurement of different NAs may have been an interesting point it was given low priority in this work, as no worker has suggested a different orientation to that used would give data more representative of our model, Section 3.4-4/7.

5.2-3/5 Requirement for an Optical Window

It became apparent as the probe was built and tested that an optical window was required to protect the adhesives that had been used to lock the fibres in place. These were epoxy based and cannot be immersed long term in water.

In addition to this problem the abrasive nature of the sample required that the probes be re-polished to an optical surface frequently. In industrial applications this would mean probe replacement on a daily basis. This requires complete re-alignment of the system, which took considerable time. This would seriously limit the use of DWS for any application.

A third limitation was imposed by many of the pigment samples that adhered to the probe surface. This binding was time dependent and led to an increasing heterodyne component. As the layers built up on the probe, the detected intensity exhibited a sine wave function, as the layer acted as an optical filter which gradually increased thickness, Section 6.4-3/2. A non stick coating was required and it was not viable to recoat after each probe polishing process.

5.2-3/6 Window Material

A large number of different types of window were evaluated during the project. The optimum window initially appeared to be 1 mm thick sapphire windows. This was found to show less adhesion to the pigments than glass and the material is exceptionally hard, resisting scratches. However, over a matter of a day or two of use it was found that TiO_2 would significantly scratch the surface and a large heterodyne component became present. Grin lenses were tested, as it was believed this might have improved the characteristics of the instrument, in terms of a coincident source and detector, Section 3.4-4/7.

However, they also generated a Fresnel reflection. This was not suitably alleviated by Anti-Reflection (AR) coatings or grinding a 5^0 angle in the axis of the emitter fibre polarisation. Calculation of the level of extinction required between the input and scattered light (Section 5.2-3/3) suggested this could not be achieved. Attempts were made using solid plastic and polyethylene film windows but both surfaces caused a significant heterodyne signal.

The most suitable window materials were found to be 0.2mm thick soda glass microscope coverslips, where no Fresnel signal was generated until they were very heavily abraded. These windows operated well as the low refractive index soda glass index matched between the continuous phase and the window itself minimising reflections. The narrow thickness of the windows meant that even when scratched emitted light would not enter the detection fibre unless multiple reflections, and thus attenuation, had occurred, Figure 41.

5.2-3/7 Evaluation of Non-Stick Coatings

Whilst a probe allowing an extinction of $1:10^{12}$ between emitted and detected light had been produced, this was shown to fail when samples adhered to the probe. Initial attempts at coating the probe centred on dipping the probe in a filtered sample of the continuous phase, before the inserting it into the suspension. This was aimed at reducing the possibility of the probe acting as a seeding point but was unsuccessful. Various commercial wax polishes and solvent-oil mixtures were also tried with no success.

A coating procedure (Tinsley-Bown 1991) was adapted to suit DWS operation. To select the most suitable coating tests were carried out with windows coated with different low adhesion materials. Two types of perfluorocarbons and one liquid silanisation coating were compared with a control set of cleaned slides. Each treated set was split into two subsets, one of which was used in its treated state and one of which was given 3 simulated cleanings. The probe windows were sent to the Tioxide site where they were exposed to various pigment materials, washed, dried and studied by Electron Microscopy (EM). Over 40 EM photographs were taken showing various degrees of adhesion of different materials. In most cases, it was difficult to see a significant difference due to the abrasion.

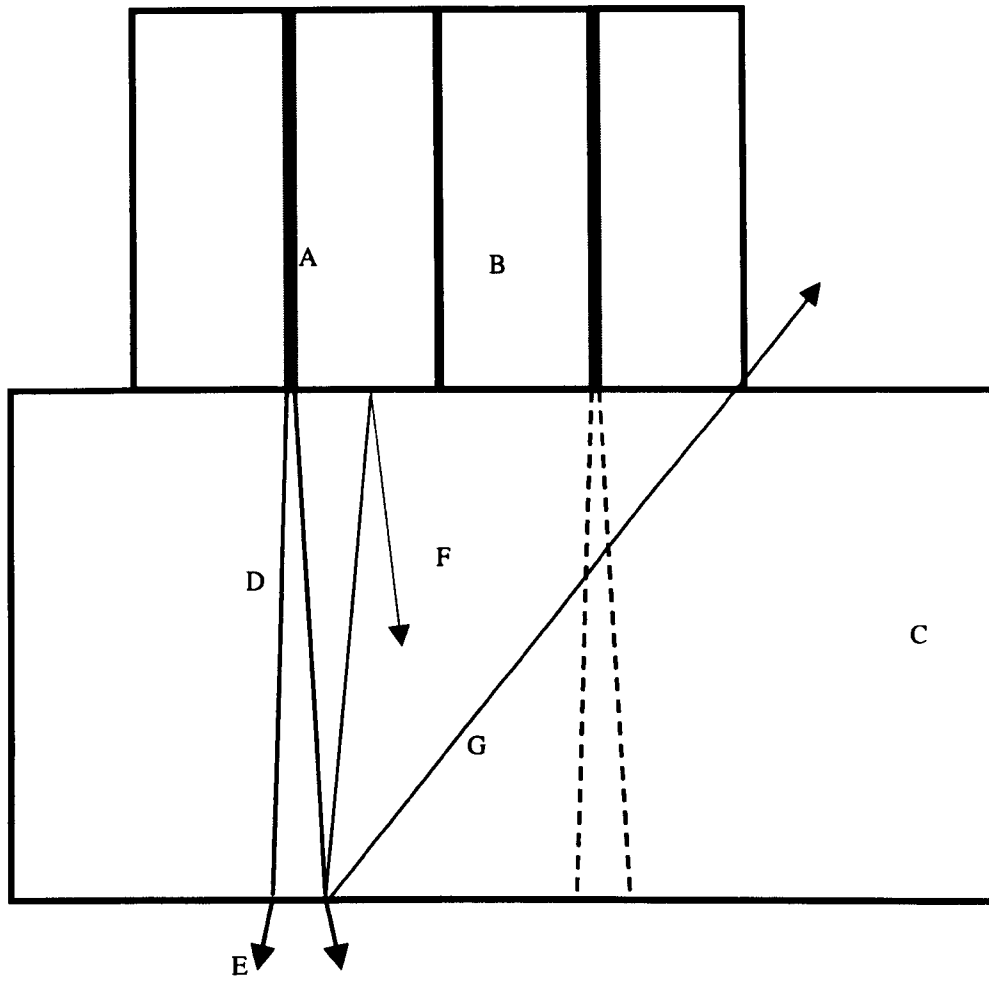

Figure 41 Probe Window Schematic

The figure shows the two fibres mated to the window. The fibre core (A), fibre cladding (B) and probe window (C) are shown to scale, 3μm diamter,125μm diameter and 200 μm thick respectively. The numerical aperture of the fibres has been shown greater than actual size for clarity. Laser light emitted by the emission fibre will output in an ellipse with Numerical Apertures (D) equivalent to 1 and 2 degrees (in soda glass) until it reached the far side of the window when the angles will increase (E) to 2 and 3 degrees (in water). The reflection on both sides of the coverslip is minimal, as the coverslip is index matched to the fibre using microscope immersion fluid and the opposite side is index matched by the continuous phase of the sample. Thus, the reflections are highly attenuated after only a few passes (F). Orthogonal polarisation of emitted and detected light reduces any signal that enters the detection fibre to insignificant levels. Whilst scratches may give rise to sharper angles of depolarised reflection (G), these are outside the numerical aperture of the fibre. This allowed an extinction of $1{:}10^{12}$ between emitted and detected light.

5.2-3/8 Comparison of Types of Coating

The silanised slides appear to show the least adhesion of TiO_2 particles, as concluded by qualitative examination during earlier DWS measurements, Figure 42, 43. While clumps of material may be seen, they are large and clearly delineated, indicating that they are not strongly adhered to the surface and may simply be dried-on, due to incomplete washing before electron microscopy. The abraded silanised slides showed smaller and less clear groupings, indicating some degree of adhesion.

Little difference between the two perfluorocarbon slides can be seen at high magnification, Figure 44. Individual and small clumps of TiO_2 are unclear and obviously well bound. At lower magnification, the 315 material exhibits unusual patterns, not apparent on the other slides. Whilst this could be a drying effect, its presence on only this material suggests the coating may be patchy. Measurements on latex materials were ambiguous. This was believed to be due to the coalescing of the latex on the surface, giving a continuous film, as opposed to discrete particles, as indicated by the fuzzy EM. Attempts to carry out DWS suggested that latex adhered to all the coating types.

The adhesion could obviously have occurred after the probe was removed from the sample, on air contact. However monitoring the output of the DWS probe suggested adhesion occurred within the sample itself.

Study of the polystyrene beads again showed the silanised surface to have only large, clearly delineated, clumps of material, while the control indicates individual bound particles, Figure 43. All subsequent work was carried out using silanised windows, Section 5.2-4/8.

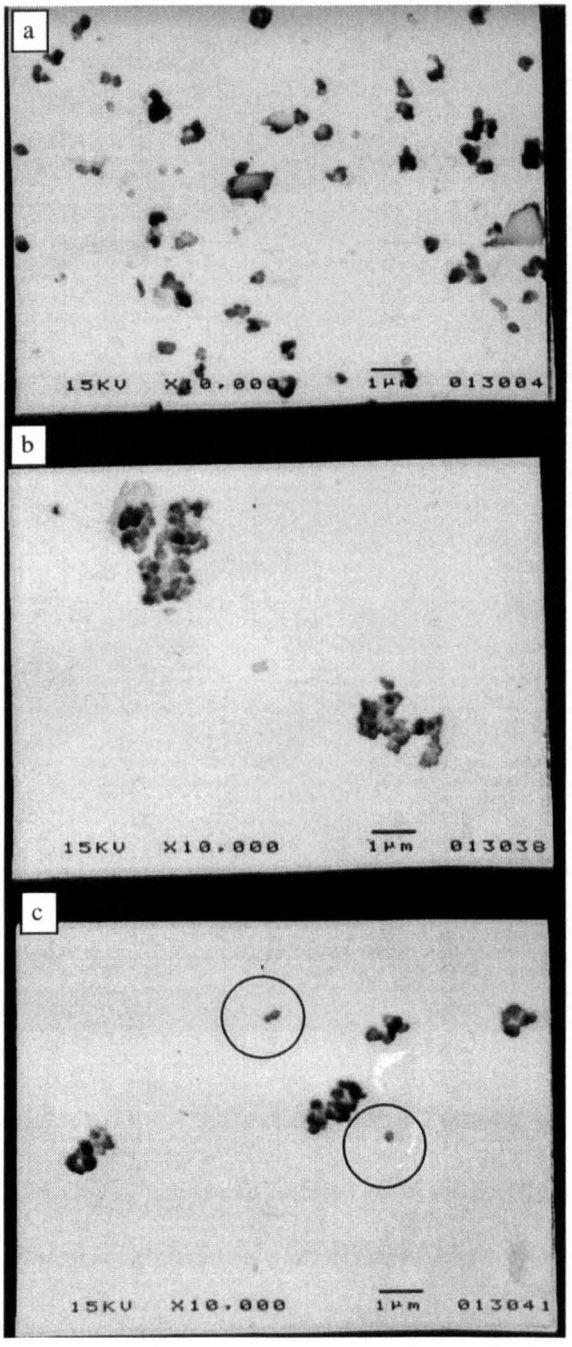

Figure 42 Effect of Silane Coating on TiO_2 Adhesion

The silane coat dramatically reduced the adhesion of TiO_2 to the slide surface. The silanised slide showed only cleanly focused clumps due to drying whilst the glass indicated many single bound primary particles. After significant wear of the coating some adhesion was noted of primary particles (circles) and smaller flocs. Key (a) un-coated glass exposed to TiO_2, (b) silane coated glass (new) exposed to TiO_2, (c) silane coated glass (worn) exposed to TiO_2. Greyscale inverted for clarity.

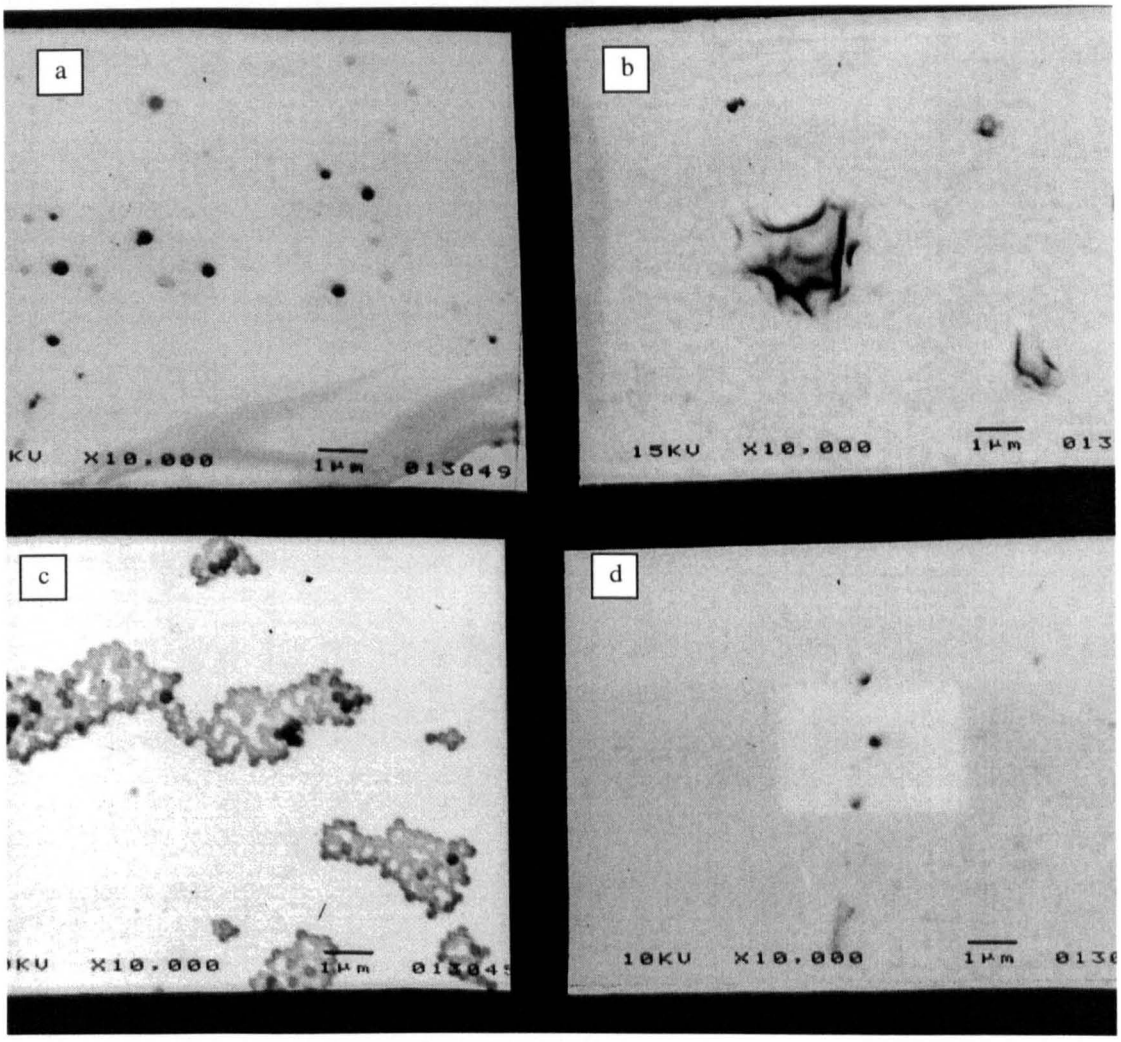

Figure 43 Effect of Silane Coating on Polystyrene and Latex Adhesion

The latex adhered to all surfaces whilst the polystyrene beads showed little adhesion to glass and none to silane. Even the edge of a worn silane coated slide showed only clear focused clumps of polystyrene, probably due to drying. Grey scale inverted for clarity.

(a) un-coated glass exposed to polystyrene, (b) un-coated glass exposed to latex, (c) silane coated glass exposed to polystyrene beads (worn edge of slide), (d) silane coated glass (new) in latex

All images scaled at 10,000:1. Grey scale inverted for clarity

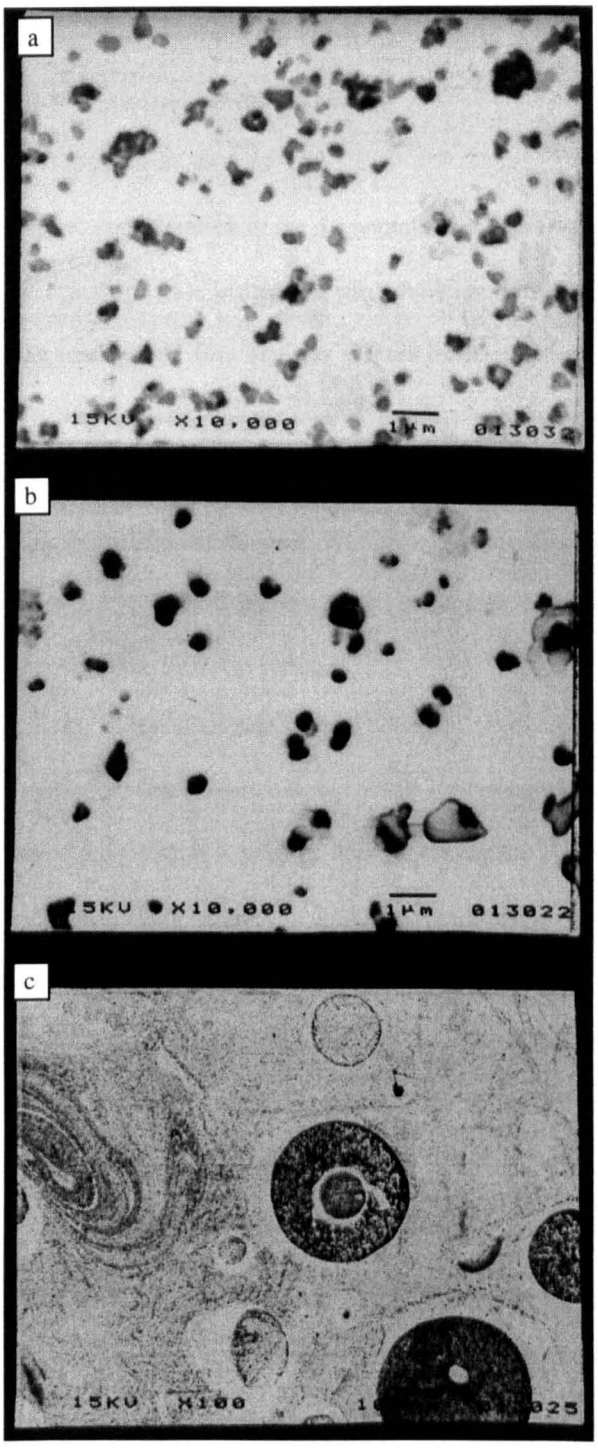

Figure 44 Effect of PFC Coating on Adhesion

The FC405 showed clear signs of adhesion, although the sharp focus indicates only loose binding. However, the FC 315 showed a reduced focus and, at lower magnifications, it appeared the coating was not uniform. Key (a) FC405 coated glass (new) exposed to TiO_2, (b) FC315 coated glass (new) exposed to TiO_2, (c) FC315 coated glass (new) exposed to TiO_2. Greyscale inverted for clarity.

5.3 Evaluation of Pilot System

5.3-1 Analysis of the Hardware

5.3-1/1 Instrument Bias

Prior to consideration of the data obtained on the DWS arrangement it was necessary to show that the signal from the instrument was a function of the sample measured (Γ), as opposed to the instrument itself. Bias analysis was not trivial as effects could occur due to experimental duration, detected intensity, voltage bias or an inter-related combination.

The most obvious method that bias could be introduced is by means of differing count rates from different samples. Whilst two samples may give different correlation decays, it was necessary to check that this was due to dynamic properties as opposed to simply different count rates from the different samples.

5.3-1/2 Count Rate Bias

The frequencies present within a DWS photon train are higher than those typically found in PCS due to the multiple scattering, thus generating the square root dependence in Equation 20. In addition it has been discussed that the frequency envelope may be significantly different, leading to more significant biasing than would be expected in conventional DLS, Section 2.5-4/1, 2.

A stable sample of pigment material (volume fraction 0.125) was studied (Tioveil CS94). This was selected as it was specified as being the smallest particle size of the pigments supplied. It was known that a small particle size, high concentration and high refractive index sample would give a high count rate bias, Section 2.5-4. The instrument response was studied at a range of illumination intensities, using a fixed PMT voltage. Experiments of different durations were made and interleaved in a non linear sequence, to ensure the plotted function was not a product of total measured counts, or experiment duration. The trace clearly show scattering intensities of 500kcps or greater generate significant decrease in the measured gradient, Figure 45. This has been discussed as an effective low-pass filter due to multiple photon arrivals within a single correlator delay, Section 3.2-2/5. This suggested the count rate should be low to reduce bias and fixed to ensure bias is constant. At low intensities the bias introduced may be crudely estimated as a reduction of 7.7 percent per million counts per second intensity, using a quadratic fit. This was shown to be significant compared to the instrument sensitivity, Figure 46.

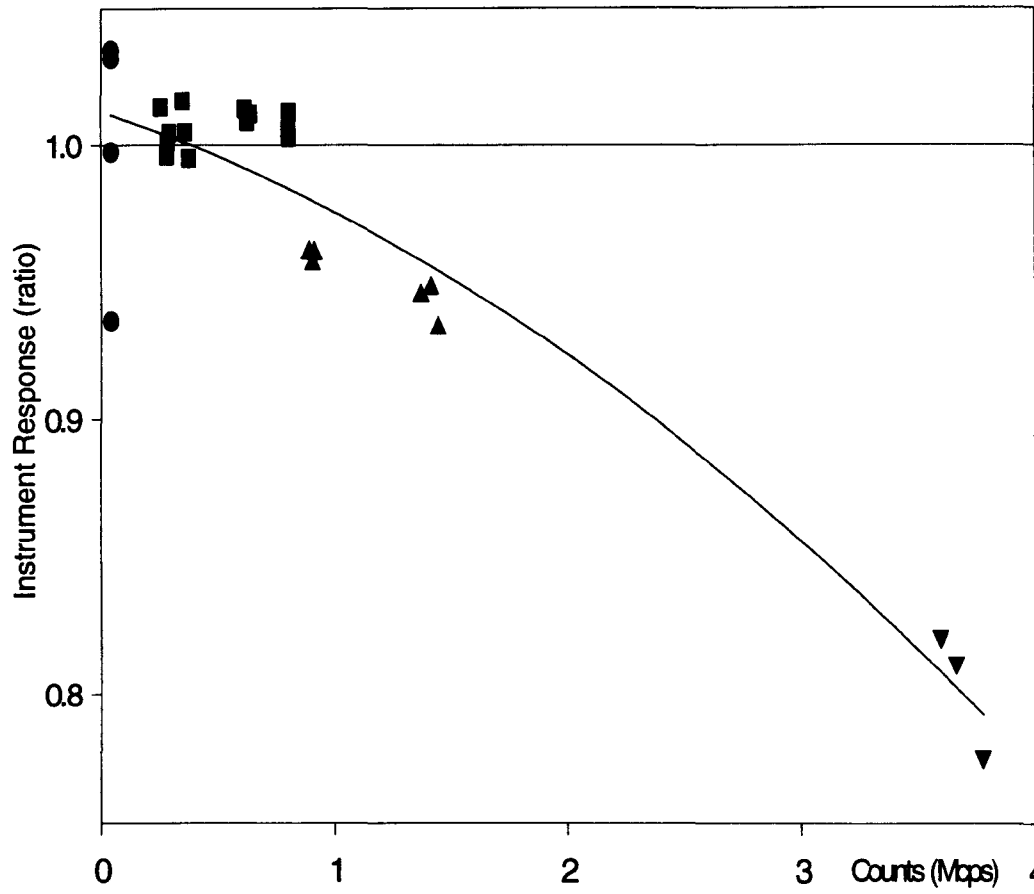

Figure 45 Count Rate Bias

A sample of Tioveil CS94 at 20C at a volume fraction of 0.125 measured via the Step 0 method, correlator delay 200ns, linear spaced channels. The instrument response, Γ, was normalised to the mean value at 40kcps. Γ defined as the magnitude of the correlation gradient when plotting log (α_N) versus $\tau^{0.5}$, where α_N is the correlator accumulator value when normalised according to Equation 65. Key, circles: 5s experimental duration, squares: 30s experimental duration, triangles: 15s experimental duration, inverted triangles: 1s experimental duration.

Transform for Γ: $\Gamma = \Gamma_M / \Gamma_{40}$, where Γ_{40} is the mean value at 40kcps and Γ_M the measured instrument response.

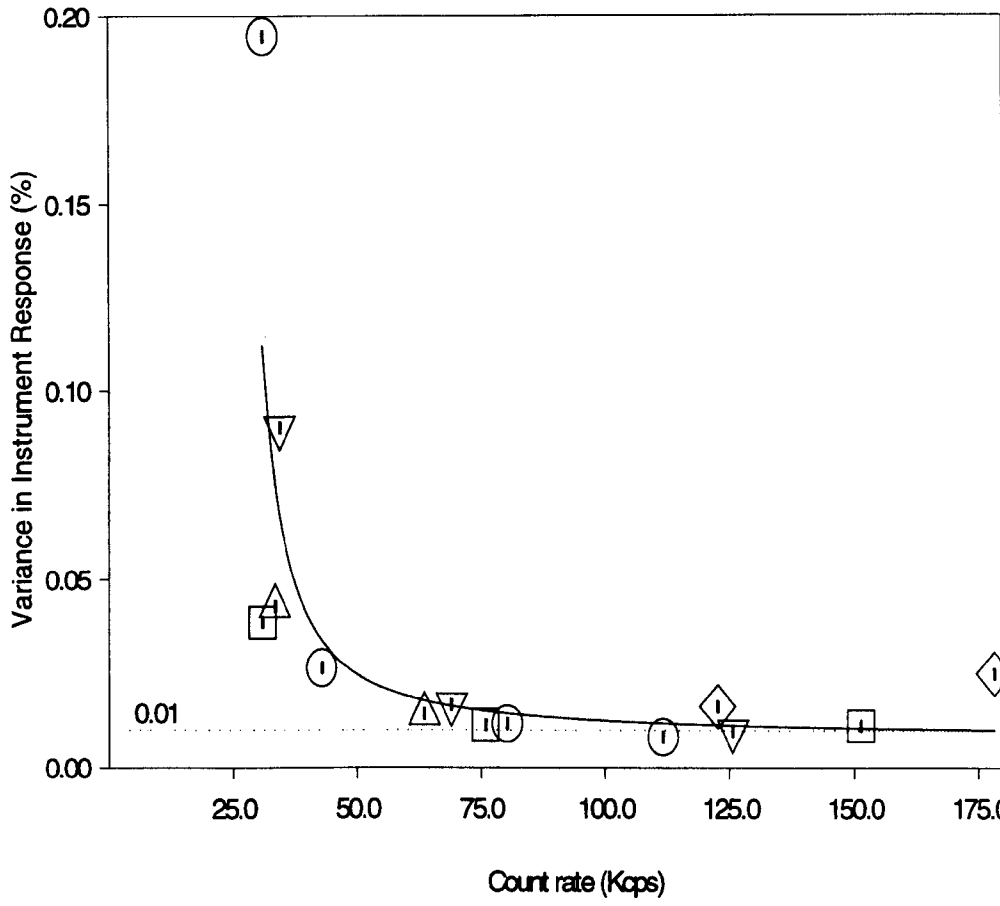

Figure 46 Variance as a Function of Count Rate

Each data point is the mean RMS error in instrument response for three 30 second measurements. Sample details as Figure 41. The measurements were taken at a number of voltage and laser intensity settings to ensure the analysis was a function of count rate only. The trace indicates that the minimum variance in the measurement of Γ occurs at an intensity as low as 75Kcps (for this sample) and equates to an error of the order of percent error. There appears no significant improvement in data quality above this level.

Curve shown - 3 parameter single exponential decay (Sigmaplot).

Errors in count rate (horizontal) are shown, in all cases too small to be significant or visible.

Key triangles: 1650v, circles:1700v, inverted triangles: 1750v, squares: 1800v, diamonds: 1900v.

5.3-1/3 Optimum Count Rate

The previous section shows that the count rate should be minimal to reduce bias. However, reduced intensity prolongs experimental duration and increases statistical variance of the measurement. Thus it was necessary to evaluate the function of statistical variance versus count rate such that a sensible compromise could be reached.

The previous sample of material was measured with different laser intensities. Each measurement was carried out three times and the correlation gradient and statistical variance for each measurement calculated. The mean of each data set was used, as opposed to mean of all measurements. Thus, the analysis shows only statistical variance and ignores bias due to count rate.

This was carried out for various detector voltages (detector gain) such that the data presented (Figure) gives a pure measure of the statistical variance as a function of detected intensity. An experiment duration of 30 seconds was known to be sufficient, Figure 45.

The trace indicates a rapid exponential decrease in statistical variance with intensity reaching a plateau at 75kcps. The strong non-linear function is illustrative that maximum signal to noise is approached when one photon is detected per 'decay time' and there is little benefit in detecting many photons in timescales.

It is suggested this trace is only valid for homodyne analysis. In heterodyne mode only the homodyne component, carries information on the sample. For a system allowing a sensitivity of the order of 0.1 percent then the intensity requires to be 1000 fold higher than that required for a homodyne analysis of a similar experiment duration[1].

Thus the optimum count rate in heterodyne mode is liable to be 75Mcps, which is impractical. The significant reduction in intensity required would increase experimental durations exponentially.

1 As previously discussed (Equation 29a), the frequency component in the heterodyne component is half that of the homodyne case. Thus the bias may only be less than that given by Figure 14 (approximately half). However, this difference is insignificant in comparison with an effective decrease in count rate of 1000 fold.

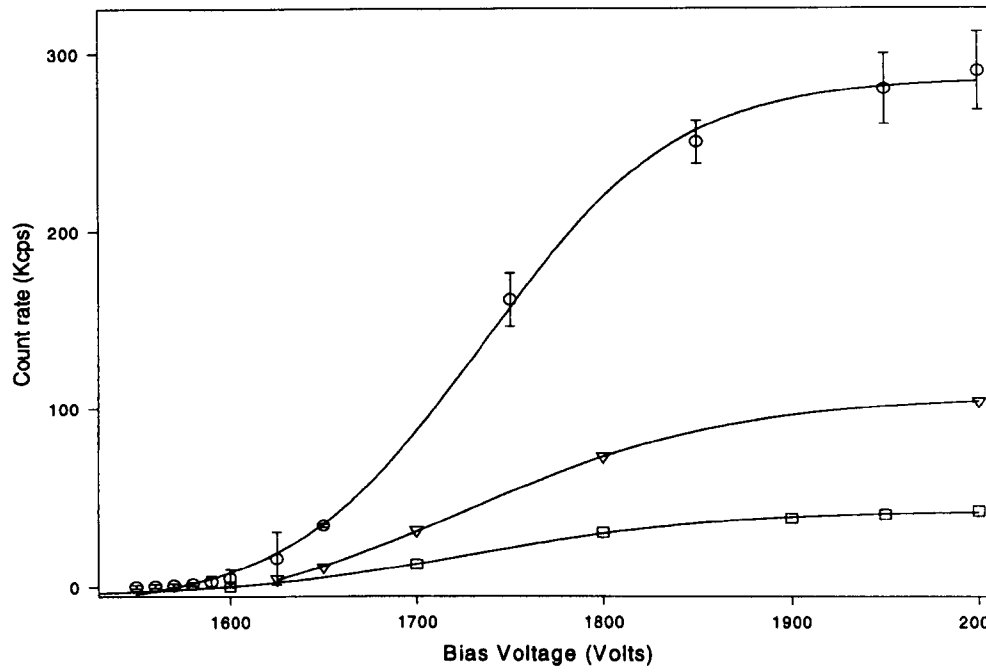

Figure 47 Laser Intensity and PMT Gain

The trace shows a sample measured at three different illumination settings and range of bias voltage settings. Error bars shown on one trace indicate dark count rate of detector when sample is not illuminated (similar for all plots). Key, circles: sample illumination 1mW, squares: sample illumination 0.5mW, triangles sample illumination 0.25mW.Four Parameter Sigmoid (Sigmaplot) shown fitted to data. Sample Tioveil CS94 at a volume fraction of 0.125 and temperature of 20°C.

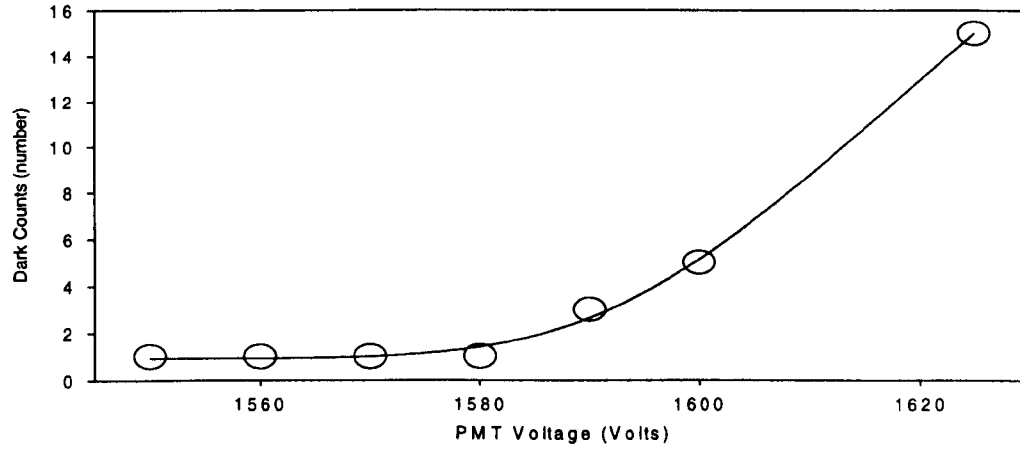

Figure 48 Dark Counts as a Function of PMT Voltage

The figure shows the exponential rise in dark counts, of the PMT, with applied bias voltage. Sample as Figure 47.

5.3-1/4 Bias due to Detector Gain

The level of amplification of a PMT is a non-linear function of the bias applied to the dynode structure. As the amplification is geometric quite small effects in bias voltage have a significant effect on the detection efficiency. The pigment sample previously described was measured at three separate excitation energies and a range of bias voltages between 1.54 and 2KV (the limits of the Malvern PCS PMT supply). There is an obvious significant increase in detector efficiency above 1650 volts, Figure 47. The error bars shown are not errors but the dark noise generated by the PMT (the number of counts generated when the PMT has no light applied). This dark count was noted as increasing significantly above 1650 volts, Figure 48.

DWS is not limited by intensity, as is the case in single scattering. A bias voltage of merely 1580 volts gave a high signal to noise [(signal-dark count)/dark count)] whilst allowing the 1mW of launched laser to generate over 75kcps of scattered light on all samples presented. For this reason the voltage setting was used in all future experiments.

5.3-2 Reproducibility

5.3-2/1 Variance in DWS Measurements

Consideration of the reproducibility of DWS is not simple. The previous section detailed the instrument settings required for a DWS analysis to allow sample characterisation that is unbiased. Bias will effect the accuracy of a system as this term defines an error in a known absolute parameter. In DWS exactly what parameter was being studied was not fully understood and could vary between sample types, Section 2.2-1/4.

This would suggest sensitivity would be an optimum measure of the system. However, calibration would require comparison to a secondary measurement of a higher sensitivity. DWS is shown to have a variance of as little as 0.15 percent, equivalent to the order of 0.3nm. Methods such as PCS will allow at best an accuracy of a few percent on average size even in ideal conditions, with distribution analysis the result is even less quantitative.

The only technique available that could allow such sensitivity was electron micrographs. However, these are based on dried samples where frequently the sample processing has significant effects on the analysis. In addition the analysis is not of dynamic motion, nor of light scattering making the analysis of limited use for this work.

This impasse was overcome by consideration of the reproducibility in measuring the same sample a number of times. The error analysis allowed a measure of statistical variance as well as the fitting error. The latter is the error between the calculated and actual measured correlation functions, Section 2.4-2/6. Thus assuming two samples similar in all properties except size Γ_1 and Γ_2 may be measured respectively and Γ_2/Γ_1 calculated. The statistical variance of Γ_2 was known ($\Delta\Gamma_2$). Thus the ratio gave the change in DWS response for that change in size, and the error the minimum change in size that DWS would be capable of reporting, whilst allowing for DWS to be more sensitive than the technique it was calibrated against.

Thus, even where the background measurements of the sizes of $\Gamma_{1,2}$ were of lower sensitivity than that of DWS, the method allowed an approximate measure of DWS sensitivity in absolute size units.

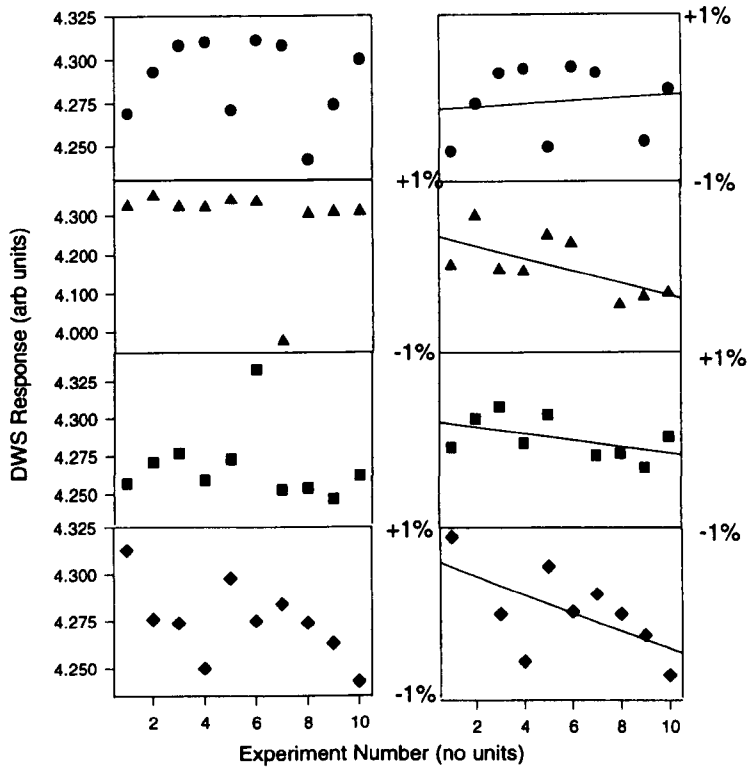

Figure 49 The Reproducibility of DWS Measurements

Four sets of 60 second experiments on Tioveil CS94 (probe removed and cleaned between each set). Data included all errors due to probe cleaning and adhesion. Traces on the right are to a similar scale and show only the 9 points closest to the mean, data is not normalised to Γ_{mean} to allow this selection.

All Data Points				
Mean	4.28860	4.28880	4.26860	4.27499
Std Err	0.02343	0.11083	0.02458	0.02070
Std Dev	0.00741	0.03505	0.00777	0.00654
9 Selected Data Points				
Mean	4.29378	4.32356	4.26144	4.27488
Std Err	0.01777	0.01514	0.01017	0.02195
Std Dev	0.00592	0.00505	0.00339	0.00732
Mean+1%	4.33700	4.36700	4.30500	4.31760
Mean-1%	4.25100	4.28000	4.21900	4.23200
Ratio (9/all)				
Mean	1.00121	1.00810	0.99832	0.99997
Std Err (%)	0.75866	0.13662	0.41399	1.06050

Table 3 Reproducibility Data

Ratios suggest that by removal of one data point the error is reduced (3 of 4 cases) and that no bias is introduced (the mean of 2 data sets increased in magnitude and 2 decreased).

5.3-2/2 Experimental Samples

The selected reference material, Tioveil CS94, was known by the industrial partner to be stable and was available at high concentrations (volume fraction, ϕ, of 0.125) and was understood to have a particle size of the order of 50nm[1]. In order to ensure the reproducibility test was a fair test of the equipment, when used in different samples, the probe was removed between each set of ten consecutive experiments, cleaned and re-inserted.

5.3-2/3 Data Analysis

Whilst each set of measurements showed a high level of reproducibility, runs 2 and 3 showed single points obviously unrelated to the data set, Figure 49. The statistical nature of light scattering generates occasional 'blips' and it is a valid procedure to de-select a smaller number of points by a common statistical rule. The correlations of each set of ten experiments were averaged and the instrument response calculated from this mean correlation. The nine correlations closest to the mean were then reanalysed to produce a mean instrument response and error. It was possible to plot the nine selected points, from each data set, on graphs which had a size range equivalent to less than +/-0.7 percent of the mean value of each set, Figure 49. Thus removal of a single data point reduced the mean statistical variation by approximately 40 percent, Table 3.

The data was then reanalysed to find the theoretical minimum variance that would occur for an infinitely long experiment but including the 'errors' due to insertion of the probe into new samples and cleaning. Thus, this is a measure of the reproducibility, not simply of a measurement but that expected between measurements on different samples. When all the data points (none de-selected) were plotted on a single trace the statistical variance was 0.22 percent. The point furthest from the mean (now mean of all data not of an individual set) was de-selected. The mean was then recalculated (data re-normalised to one in this case) and the next data point furthest from recalculated and removed, Figure 50. This process was carried out 7 times. The variance in the data decreased in a geometric fashion as data points were removed, with the exponential plateau at a value below 0.1 percent. This is at least an order of magnitude lower than would be expected using any conventional DLS technique. This exceptionally high reproducibility required bias and errors to be accurately known and analysed. The difference in variance using the technique is clearly illustrated comparing all data points and selected data points, Figure 51.

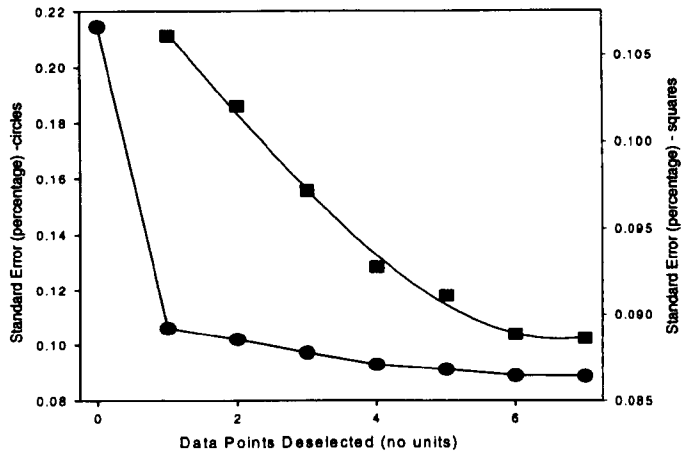

Figure 50 Data De-selection Technique

By analysing all 40 data points as a single analysis allowed the statistical variance between measurements to include all errors in involved in re-dipping and cleaning the probe. The data point furthest from the mean was deselected from the analysis. The mean recalculated (re-normalised to one in this case). The process repeated seven times. The upper plot (expansion of the lower plot disregarding the first data point, right hand axis) shows an exponential reduction in the statistical variance of the analysis to below 0.1 percent when 7 (17.5 percent) of the data had been deselected.

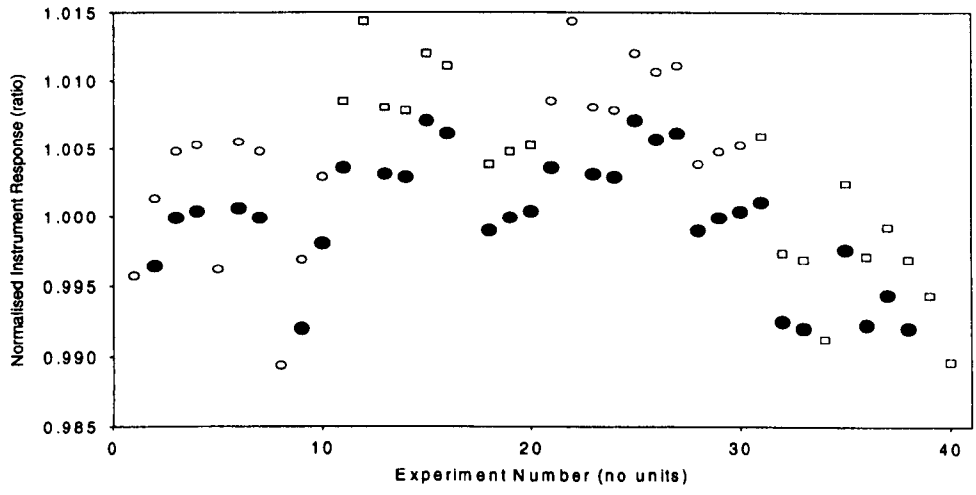

Figure 51 Selected Data

The empty squares show the original data and the full ones the re-normalised selected data. The selection allowed all data points to lie within 1 percent of the mean.

It has already been suggested that this level of statistical variation would not be viable using a heterodyne analysis method. The count rate and/or experimental duration required to allow this sensitivity would be impracticably large (Section 3.2-2/6) and the correlation intercept would require to be below 0.1 percent of the baseline, where baseline errors would predominate, Section 3.2-2/7.

5.3-2/4 Level of Reproducibility

In conventional PCS using properly diluted samples and ultra clean techniques a reproducibility of around one percent may be viable in a 5-40 minute period. This would only be true for a simple mean size, with distribution information far more qualitative. DWS has shown to be capable of an improvement in reproducibility in 60 seconds. Furthermore the variance of below 0.1 percent was possible, without any sample pre-treatment or dust control/filtering.

This improvement in variance, over conventional DLS, was believed to be due to three separate factors:

- in PCS each photon sees a single particle whilst in DWS the random walk allows each photon to contain information on the entire ensemble average;
- the difference in volume fractions between DWS and other techniques made a set quantity of contamination typically an order of 10^5 lower, as a volume fraction;
- in PCS only single scattering occurs such that a dust particle may have occluded the majority of the light path.

The stability of the measurement alone suggested that DWS would be an ideal process control monitor and allow evaluation of small changes in pigment size during milling which would usually require distribution information to analyse, Section 1.6-4.

The method of data removal, although theoretically sound, was not used in the data presented throughout this work. The overall variances and errors of complete data sets are given and thus should be viewed as 'worst case' measures.

5.3-3 Concentration Dependence

5.3-3/1 Diffuse and Ballistic Scatter

Whilst this work had designed the hardware to minimise the affect of varying concentration (Section 2.5-1/6), it is only possible to reduce the concentration dependence and not eliminate it.

Prior to calibration of size, viscosity and temperature it was necessary to show that measured differences were due to these functions and not due to errors in the concentration of different samples.

This work progressed through four different iterations, of experimental method, to produce a system with minimum concentration dependence. This chapter describes the method carried out prior to this work (Step 0) and first two method iterations of this work (Step 1,2).

5.3-3/2 Effect of Concentration on the Correlation Line shape

In PCS the range of decays measured is quite a short range and pseudo logarithmic delays may be used such that a single correlator delay suits almost all samples. In DWS the range of decays may be much wider (Section 2.2-2/6) and pseudo logarithmic channel spacing was found to give discontinuities when attempting to calibrate different samples, Section 3.2-4/5. In addition in PCS it is necessary to analyse the entire correlation line-shape (Section 2.3-2/3) for stable distribution analysis, whilst this work suggests that the section of correlation used in analysis should not include the long time tail, Figure 12,13.

Earlier work (Lloyd 1991) had set the correlator delay using a suspension at the original concentration arbitrarily selecting a correlator decay that gave a linear trace whilst statistical variance, in the correlator channels, was low, the same correlation delay being used in measurements on the subsequent dilutions, Figure 4. Thus, where the correlator decay changed dramatically, different 'portions' of the correlation were analysed.

A robust and reproducible analytical method of selection of the portion of the correlation to analyse was required. The analysis module has been covered previously (Section 4.3-3/2), thus the basic function is merely reviewed here. The software automatically took a series of measurements at different correlator delay times. A simple straight line fit was carried out to each correlation (Equation 22) and the average decay and the average error calculated. The error included both the statistical variance and the fitting error (Section 2.4-2/6).

At short delay times the statistical variance was significant and at longer delay times the fit error increased, as the curved correlation tail was analysed.

The method gave a single valued function for error versus correlator delay allowing a unique solution. Whilst having no theoretical basis, aside from the assumption that the linear part of the correlation was due to diffusive light, the technique was rapid and reproducible.

5.3-3/3 Comparison of Step 0 and Step 1 Techniques

The Step 0 method was set at a volume fraction (ϕ) of 0.125 (the undiluted sample) such that it was obvious the Step 0,1 data was identical at this concentration. The low concentration dependence of DWS ensured that this was the case to ϕ=0.025. At dilutions below this, the difference between the two methods is significant, Figure 52.The variation in magnitude of the instrument response, with reducing concentration, is half that using the new method. The reason for this was believed to be that the earlier method analysed the long time tail of the correlation, which contained non-diffusive information at low concentrations.

This was shown to be correct by analysis of the fitting error, Figure 53. This shows the error between the correlation function and a straight line fit and is related to how well the model represents the data and not reproducibility, Section 2.4-2/6. Using the new technique the error in fit between theoretical and actual correlation line shape was also halved. Thus it appeared the new technique was shown to select the diffusive part of the correlation automatically.

The form of the functions of Γ versus concentration were similar form, which supported the concept that the same parameter was being measured but with different weightings.

The plateau region in this pigment sample was typical of most samples measured, occurring around 12 percent. This would appear to be where the diffusion approximation becomes truly valid for this system. This assumption is supported by studies carried out by the pigment industry. Pigment surfaces decrease in scattering power with concentrations of TiO_2 above volume fractions of around 0.12 (*pers. com.* Lawson 1992). This process is known as clouding and is considered due to be due to multiple scattering, reducing the light leaving a paint surface (Judin 1993). The concept appeared analogous with localisation models of light, where photons begin to travel a substantial random walk within the media at higher concentrations, leading to the theoretical possibility of localisation and complete photon trapping at high concentrations.

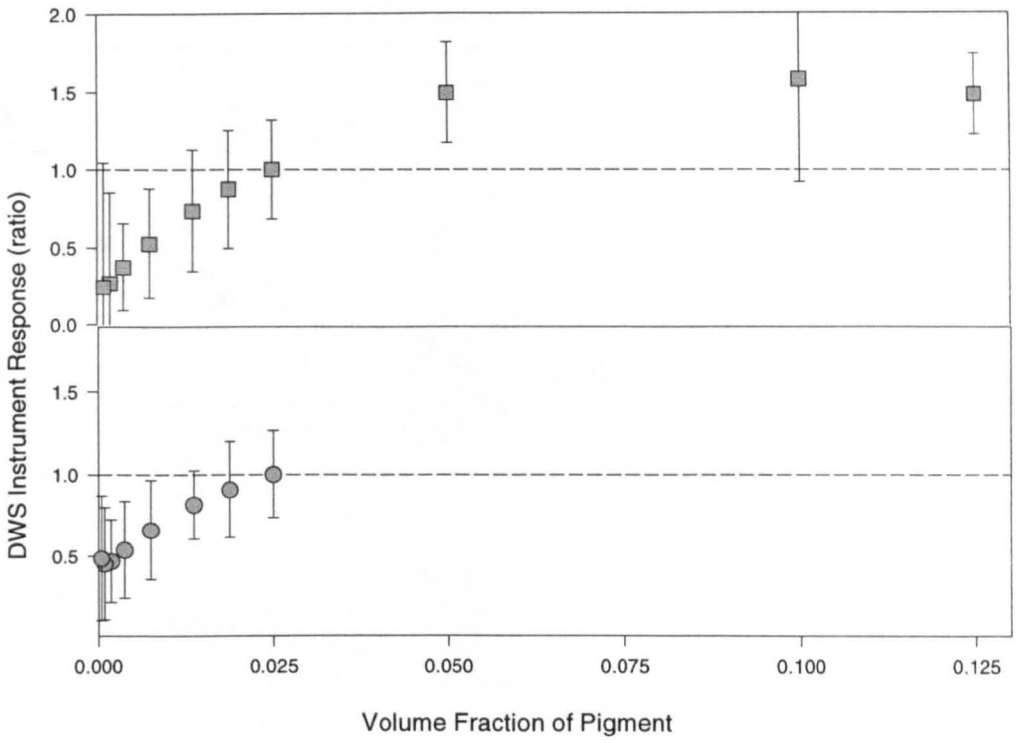

Figure 52 Comparison of Step 1 Analysis

A sample of anatase pigment (Tioveil CS94) was diluted in stages. After each dilution the sample was swirled for ten minutes prior to treatment for ten minutes with ultrasound. The sample was then held in a water bath for ten minutes prior to measurement. The automatic sampling time procedure was used to find the optimum correlator delay prior to ten experiments of sixty seconds.

Upper trace, squares: DWS instrument response using a fixed correlator delay of 100ns, Step 0

Lower trace, circles: DWS response using a variable correlator delay, Step 1 Values above 0.025 are not shown in this trace. The definitions of Step 0,1ensured the same data was collected and analysed in the same way for both techniques and the data was identical.

In both traces the instrument response was normalised to that generated by a volume fraction 0.025

Errors are mean fitting error and do not indicate reproducibility, statistical variation typically below 1 percent, Figure 50.

Transform for Γ: $\Gamma = \Gamma / \Gamma_{25}$, where Γ_{25} is the mean value at a volume fraction of 0.025.

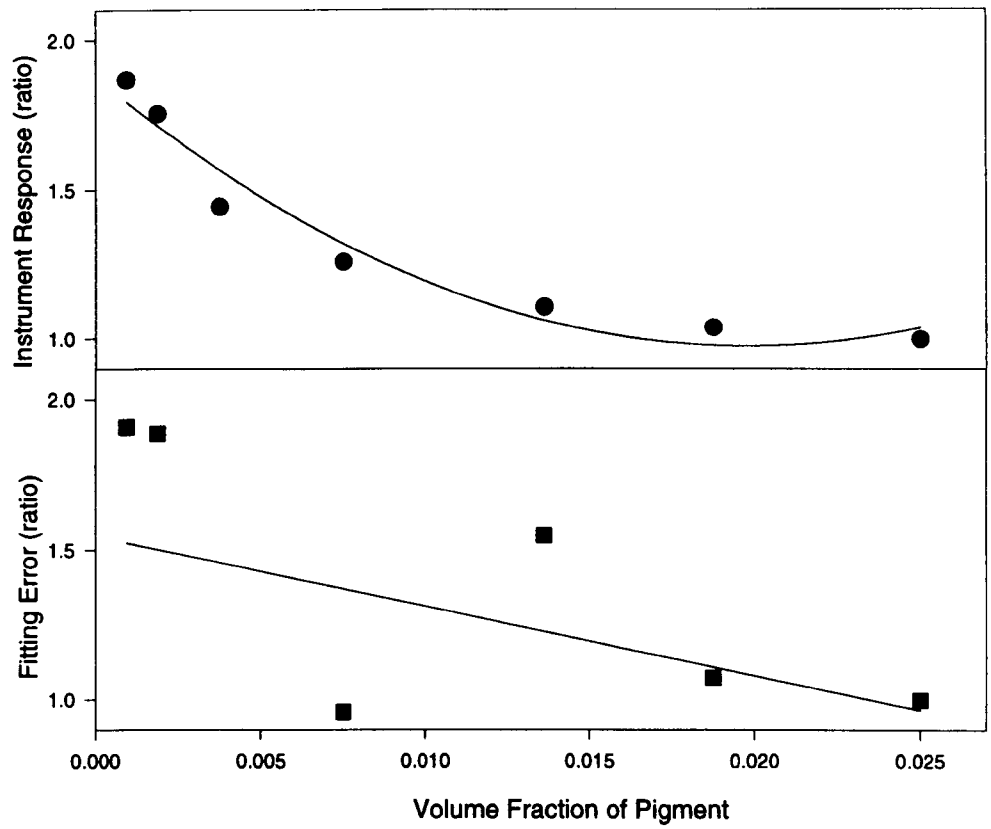

Figure 53 Reduction in Concentration Dependence and Error

The ratio of the variation in the magnitude and the reproducibility of the instrument response for Step 0 and Step1 methods for the data as Figure 52. Step 1 and Step 0 analysis were identical for concentrations between 0.025 to 0.125 (ratios are all 1).

Top trace, circles: Γ_N ratio, 2nd order polynomial fit:

$$\Gamma_{ratio} = 2297\phi^2 - 90.72\phi + 1.873, r^2=0.954,$$

Lower trace, squares, fitting error ratio, linear fit:

Instrument response fitting error ratio $=23.17\phi-1.545$, $r^2=0.209$

Transform for Γ ratio: $\Gamma = [(\Gamma/\Gamma_{25})^{Step0} / (\Gamma/\Gamma_{25})^{Step1}]$

Transform for error ratio: error ratio $= (error^{Step0}/error^{Step1})$

Where the subscript 25 defines Γ for a volume fraction of 0.025, ϕ denotes volume fraction and the superscripts define the measurement method.

The results indicated that Step 1 analysis was valid over volume fractions of at least 0.08 to 0.125.

However, the concentration would need to be known, or estimated from the count rate for a single point measurement

5.3-3/4 Step 2 Concentration Dependence

The Step 2 analysis is discussed later (Section 5.4-5). However, as the method has no direct effect on the concentration dependence these results are included at this point. The only difference between Step 0 and 1 results, in a stable suspension, was that the correct correlator delay was set with finer resolution. The main advantage of the Step 1 method being that it allowed analysis of unstable samples.

Concentration studies were carried out on latex/polystyrene materials but adhesion of the material to the probe caused significant problems, notably a sinusoidal variation in both measured diffusion coefficient and count rate as the adhered film built up. The variation was superimposed on a slow decrease in count rate and reduction in Γ. This was only partially alleviated with the addition of the silane window and disallowed Step 1 analysis. One sample of 180nm polystyrene beads[1] at volume fractions up to, approximately, 0.4 (0.48 w/w) are shown for example, Figure 54. The trace is broadly similar trace to the TiO_2 except that the diffusive regime appears to occur at a lower concentration. These results were not in agreement with the 'stated size' of the TiO_2 of 50nm as a particulate of this size with a refractive index of 2.7 would be expected to show significantly more scattering than the polystyrene. This irregularity is discussed in Section 6.4-2/3

Additional problems encountered were due to the limited sensitivity of the correlator setting. A sample of approximately 0.22 micron sized anatase pigment, which could not be analysed by the Step 1 method, was re-evaluated. The Step 2 method allowed analysis to a volume fraction of 0.1 but, above this, the correlator had to be set on its shortest correlator delay. The trace is similar to Tioveil up to $\phi = 0.05$, after which the results were known to be strongly biased due to the correlator bandwidth. The effect of refractive index normalisation (Section 5.3-5/4) is also shown on this trace.

1 Industrial sample used as a paint filler, supplied by Tioxide. Sample showed slow binding to the probe and could not be analysed by the Step 1 method.

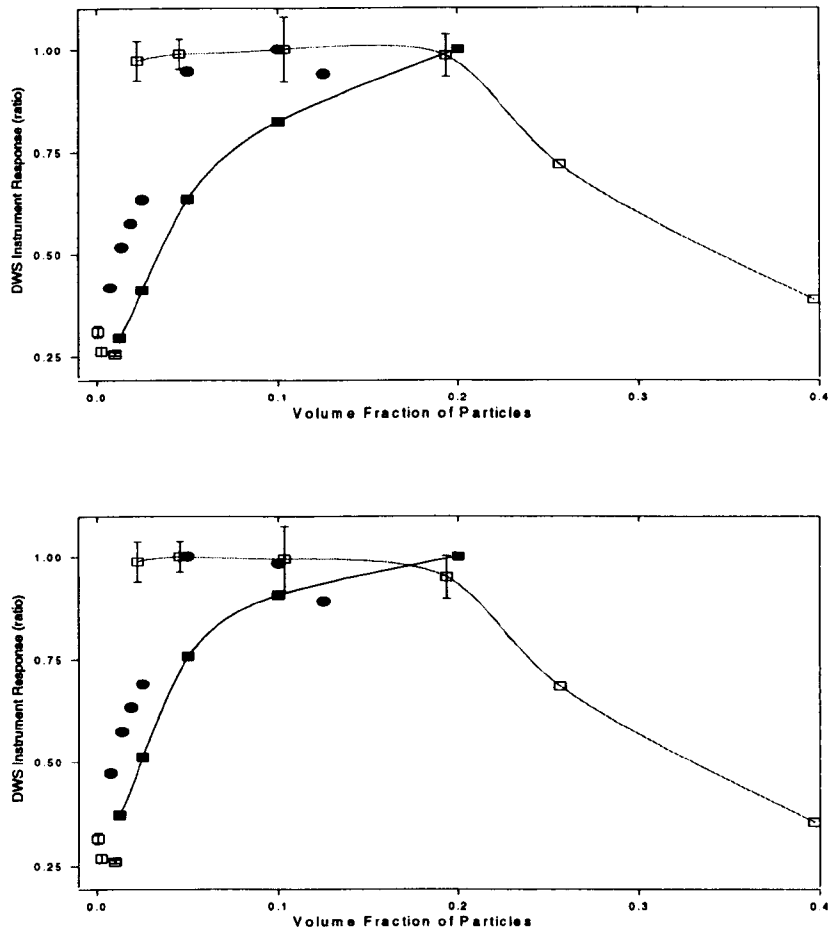

Figure 54 150nm Polystyrene Concentration Experiment

The instrument response as a function of concentration, for measurement of 180nm polystyrene, empty squares top trace. A number of experiments were taken and the correlations were averaged, one data point at ϕ =0.125 that was obviously erroneous was ignored on the plot. The curve shows the line of best fit (cubic spline) between volume fractions of approximately 0.02 and 0.4. The results for the TiO_2 sample from Figure 52, are also displayed for comparison normalised by a similar method, solid spheres, and a 0.22 micron anatase pigment where the Step 1 method failed due to lack of correlator bandwidth, solid squares.

Transform for Γ (upper trace): $\Gamma = \Gamma/\Gamma_{max}$ where Γ_{max}, is the maximum value of that data set.

The lower trace shows the anatase sample normalised for refractive index, Section 5.3-5/4.

5.3-4 Ranking and Sensitivity of the Pilot System

5.3-4/1 Experiment Method

The first major test of the basic Step 1 DWS model, and method, was the (blind) measurement of 10 industrial pigment samples. The experiments were aimed at showing the relative ranking ability and reproducibility, relative to the two well established commercial techniques currently in use. These were an in-house triple wavelength optical density technique and Brookhaven X-ray centrifugal sedimentation, Section 4.4. The optical density technique generated a size and a polydispersity index whilst the Brookhaven gave a distribution trace with mean and median.

Whilst industrial pigment milling occurs at high concentrations, the model samples used by the industry are generally at volume fractions of 0.0125. This regime is obviously at the lower range of DWS measurement (Figure 54 shows DWS becomes double valued at low concentrations) and where significant errors may result from any slight variations in concentration.

Whilst ten samples of pigment were produced by Tioxide, only eight were in the range of one of their comparative methods (Optical Density), Figure 55. However, the full data set is shown for DWS versus sedimentation, Figure 56. The sample set contained materials directly from a reactor discharge, as well as finished pigments coated with inorganic materials. Each data point is the mean of ten experiments of sixty seconds. Variance values are shown as errors on both graphs but are such that they were not visible on the traces when using symbol points, Figure 55.

5.3-4/2 Milling Calibration

The mean variance from the DWS measurements on all samples corresponded to a ranking sensitivity of +/-3nm, which is significantly better than would be expected for most hydrodynamic measurements. The result of the correlation between DWS and OD was greater than the correlation between DWS and Brookhaven analysis (0.9/0.65). In addition, this correlation was stronger than that between the two commercial techniques themselves, Table 5.

The larger difference between the two commercial techniques can probably be explained in that the OD analysis is strongly weighted toward smaller particles, unlike the Brookhaven technique. The correlation coefficients were calculated for both quadratic and linear fits between the data sets, to ensure results were not due to non-linearity in the functions. The effect of pigment coatings appeared to give no significant effects, Table 4.

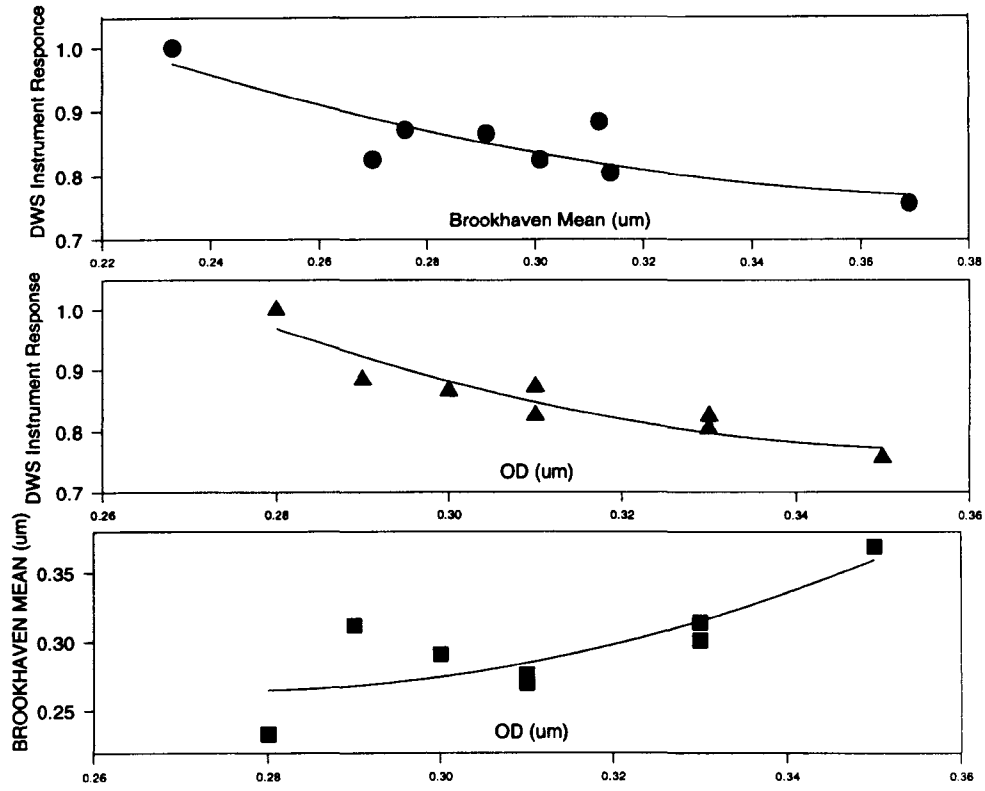

Figure 55 The Ranking Ability of DWS

DWS response versus measurements by Tioxide's Brookhaven sedimentation equipment (circles) and optical density techniques (triangles), on eight pigments. The correlation between DWS and OD was significantly higher than between Brookhaven and OD (squares). Instrument responses (Γ) were normalised to the sample of size of 0.233microns (OD), 0.28microns (Brookhaven) Statistical variance of DWS cannot be seen on this scale. Figure 56 shows DWS errors. Mixing carried out as per methods, Chapter (4).

Transform for Γ: $\Gamma = \Gamma / \Gamma_{23}$ where Γ_{23} is the mean value for analysis of a sample generating sizes of 0.233 and 0.28 microns when measured by OD and Brookhaven respectively.

Vertical Axis	Horizontal Axis	Polynomial Cor. Coeff.	Linear Cor. Coeff.
DWS	**Brookhaven**	**0.726**	**0.711**
DWS	**OD**	**0.8806**	**0.862**
Brookhaven	**OD**	**0.6545**	**0.6071**

Table 4 Correlation Coefficients for Figure 55

The DWS response is in better agreement with the Optical Density technique than the Brookhaven sedimentation method. The DWS-OD coefficient is also significantly better than the coefficient between the existing conventional techniques, for both linear and quadratic fits.

The similarity between linear and quadratic fits suggests a linear relationship with significant statistical error.

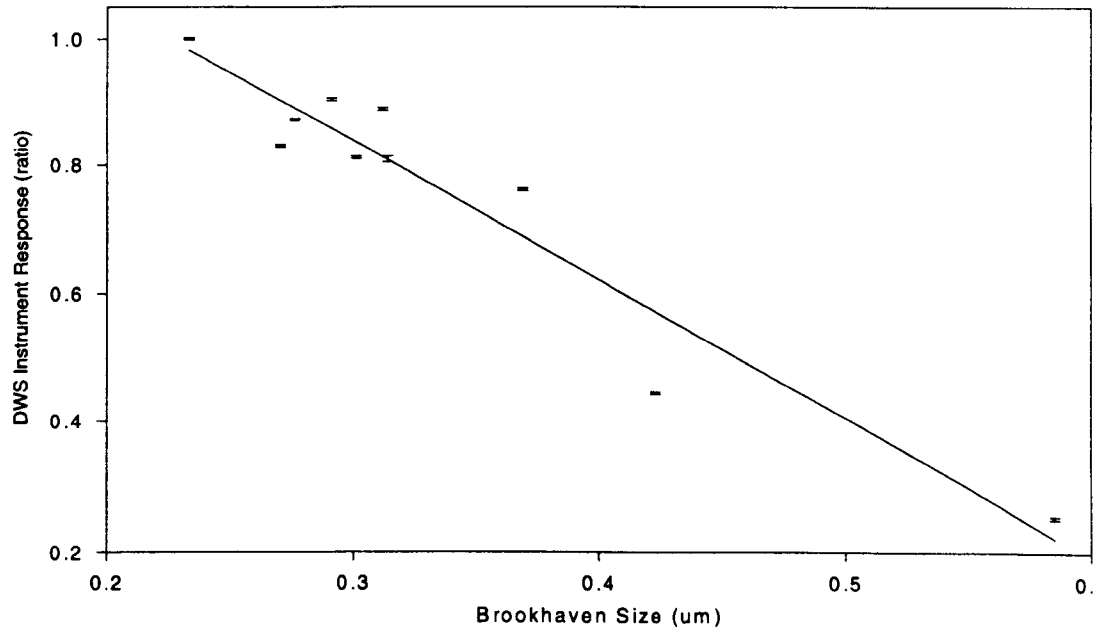

Figure 56 DWS and Brookhaven Results

The full set of ten samples measured by DWS and Brookhaven X ray Centrifuge. DWS does not have the upper size limitation of the OD technique. DWS statistical variance errors are shown. Transform as Figure 55.

5.3-4/3 Temporal Variation

It is suggested that the results indicate DWS is a highly reproducible and accurate technique since:

- this was the first set of experiments and no optimisation had taken place;
- the samples were measured blind;
- the sample concentration was slightly too low for DWS;
- the samples showed significant variation with time, Figure 57.

The latter point was viewed as the most serious as generally the instrument response of the sample was effectively used to set the correlator delay prior to a set of experiments. In the event of a change in the effective diffusion coefficient the results will be biased, as an unsuitable delay is being used for the measurement, Figure 52, 53. The variation with time was shown to be reproducible, within experimental limits, every time the samples were mixed and inverted. Mixing was required as the samples visibly settled over periods of the order of 30 minutes.

It was noted that the samples all underwent a similar temporal change in the first 400 seconds and there are no significant differences, of the time dependence, for different particle sizes. The most milled (smallest) sample was still the same stable value even 50 minutes after mixing. However, the less well milled samples changed to a two phase mixture at around 30 minutes where analysis became unstable. The trace shows that immediately prior to this, the instrument value for this sample rises, indicative in a reduction in particle size.

After a preliminary measurement run the Step 1 correlator delay was set for the plateau region and then remixed. The sample was then reanalysed, using this correlator delay. Reanalysis of the suspensions (not shown) had no significant effect on the ranking, or on the statistical variance. It appeared that the time to set up the sample and find the correct correlator delay had probably led to the previous measurements inadvertently being measured during the plateau region. However, in most measurements this phenomenon obviously increased statistical variation, when analysis was carried out by simple averaging.

5.3-4/4 Limitations of Step 1 Analysis

The statistical variance of 0.3nm analysed in this work is an overestimate of the real variance. This along with the reproducibility (Figure 49-51) and the ranking curves (Figure 55,56) suggested size ranking to sub-nanometer sensitivity is possible.

However, in unstable samples, the Step 1 method of analysis required plotting Γ versus time from mixing (to find the plateau region). Further re-mixing and analysis was then required to find the optimum correlator delay (in this region) before final remixing to collect data for analysis. This was time-consuming, could not be considered real-time and in addition only the plateau region was then analysed using the 'correct' correlator delay, the method then suffering similar limitations to that discussed between Step 0 and Step 1 for concentration variation, Section 5.3-3/2.

It was this initial time dependant problem that led to the start of the development of the Step 2 technique, Section 4.3-2/3. This required collection of vast quantities of data to be collected and did not give real time analysis. However a single measurement run could now analyse a changing sample, in a robust and reproducible manner.

This work now required to find a method of calculating the variance of the individual correlator accumulator's values on samples which were unstable and thus could not be calculated by averaging. Without these errors proper data fitting and analysis was not possible (Chapter 6).

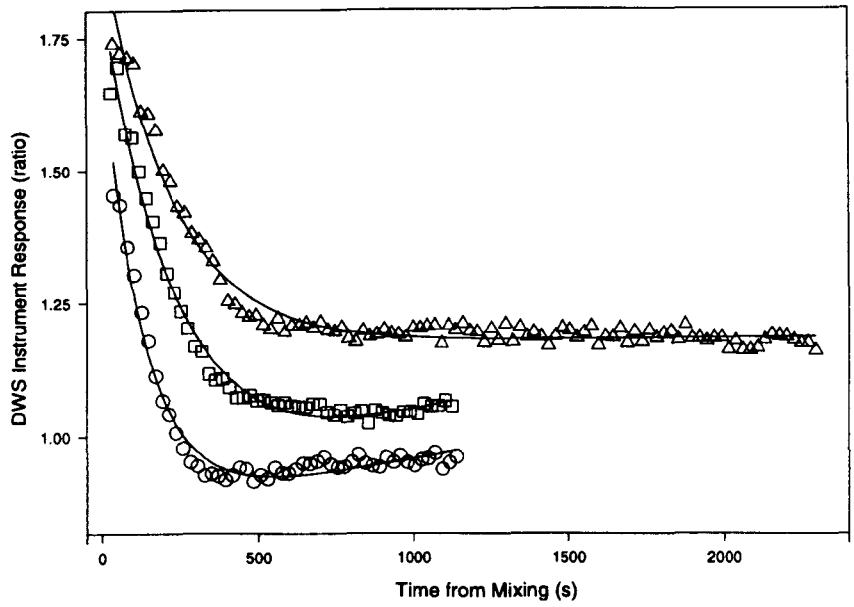

Figure 57 Temporal Variations of Milled Pigment Samples

Three of the pigment samples used in the analysis (Figure 55) are shown. The full set is not displayed for clarity. The samples show a decrease in Γ rapid prior to stabilisation with a slow settling effect, thus increase in Γon sample 26 (decrease in effective size). Γ normalised to the mean value measured on sample 26. The samples were preheated in a waterbath to 20 ^{0}C, mixed in a vortex mixer for one minute then placed immediately back into the waterbath for analysis. All measurements were taken using the Step 1 correlator delay for the plateau region of the curve. Table 4 gives a description of sample types.

Key Circles: Sample 26, Squares: sample 28, Triangles: sample 32

Transform for Γ: $\Gamma = \Gamma/\Gamma_{26}$, where Γ_{26} is the value from a 0.35/0.369 micron pigment, measured by optical density and Brookhaven respectively.

Sample	Material	Description	DWS Response	Optical Density	Brookhaven Mean
			(arb unit)	(um)	(um)
26	E-4698-3	Reactor Discharge	0.494	0.35	0.369
27	E-4698-8	Reactor Discharge	0.537	0.33	0.301
28	E-6614-3	Reactor Discharge	0.568	0.31	0.276
29	E-4637-2	Reactor Discharge	0.576	0.29	0.312
30	E407-71/2	Coated	0.524	0.33	0.314
31	/5	Coated	0.538	0.31	0.270
32	/29	Coated	0.564	0.30	0.291
33	/32	Coated	0.636	0.28	0.233
34			0.164	N/A	0.585
35			0.288	N/A	0.423

Table 5 Milled Sample Results

Sample data for Figures 55,56 and 57

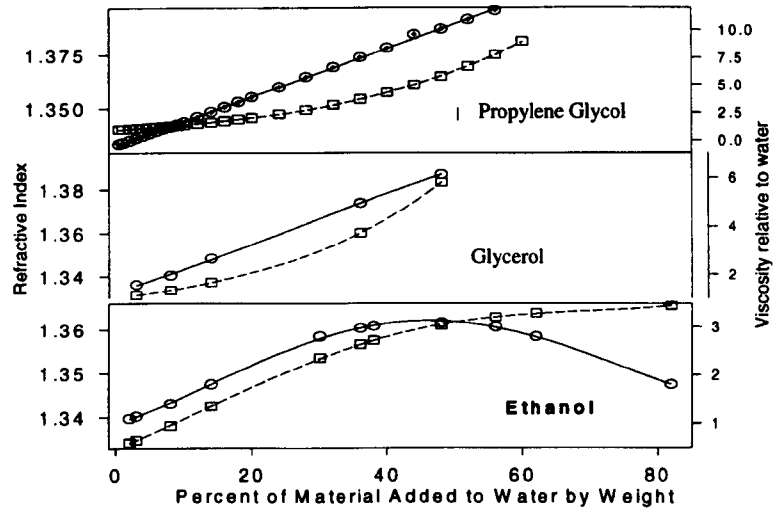

Figure 58 Properties of Aqueous Solutions

Properties of aqueous solutions, top trace propylene glycol, mid trace glycerol, lower trace ethanol. Circles refractive index, squares viscosity

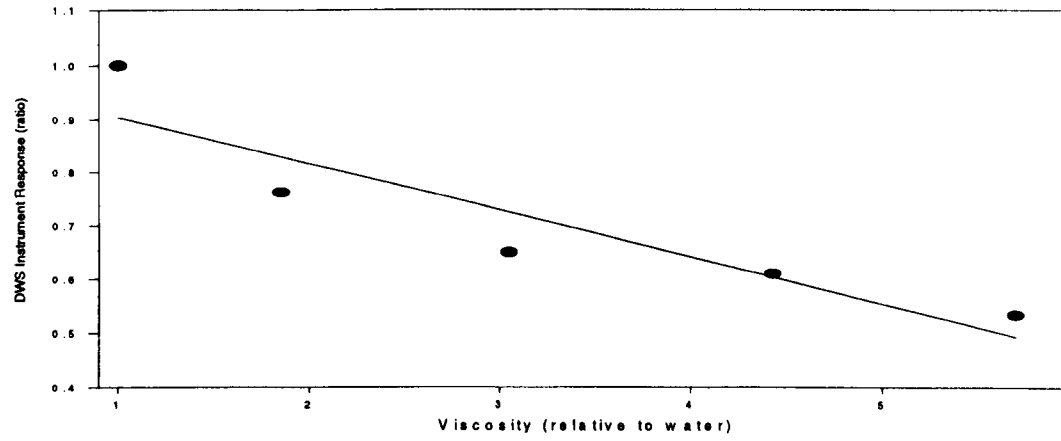

Figure 59 Viscosity Dependence

Samples of 0.22 micron anatase pigment in 0,15,30,49 and 50 percent by weight propylene glycerol. Γ= -0.0874 relative viscosity + 0.991. Analysis of 16 correlations per data point. Sizes given are linear extrapolation to measurement at probe insertion.

Transform for Γ: $\Gamma = \Gamma / \Gamma_0$ where Γ_0 is the mean value for the sample with no propylene glycerol.

5.3-5 Calibration of Dependant Variables

5.3-5/1 Dependent Variables.

In the literature a mean size is produced from a DWS response using the model previously described, Equation 15-17. Whilst this work has already considered that calibration to absolute size had significant limitations (Section 2.2-2/7) it was obviously necessary to be able to model the response of Γ to these variables. Calibration ideally required samples where only a single parameter is altered. To this end samples of TiO_2 were produced in various concentrations of ethanol/water mixtures. Aqueous ethanol mixtures are unusual in that the refractive index is double valued with concentration, such that it is possible to produce samples of differing viscosity but constant refractive index, Figure 58. Many samples were produced, both in-house and by the industrial partner, but the instability of TiO_2 made this a significant problem. No surfactant mixture could be found where no flocculation occurred over the range of high ethanol concentrations required (20-80% by weight). Sample collapse typically occurred over a matter of a few minutes. Similar work was carried out using the 180nm polystyrene beads but they appeared to 'swell' and flocculate over a matter of hours, thus the concept of using alcohols was not followed further.

5.3-5/2 Viscosity Dependence

In applications involving pigments the viscosity is obviously of significant importance and can vary dramatically from near water (whitewash) to gel (non-drip gloss).

Whilst it was not possible to maintain the refractive index a study of material showed propylene glycol (Figure 58) would allow an order of magnitude change in viscosity for less than a 5 per cent increase/shift in refractive index. Suitable pigment based samples were produced by the industrial partner. This led to a second set of problems as the material interacted with the alcohol chains used to stabilise the pigment, which made it stick to the glass windows regardless of the non-stick coating used. Further work with aqueous glycol solutions, which have similar viscosity/refractive index dependence, gave similar problems.

However, it was noted that the instrument response variation (with time after insertion to the material) was reproducible, when the probe window was replaced and the probe re-inserted. Thus the probe was inserted into each sample and the Step 2 correlator delay was calculated. The probe was removed and the window replaced.

The probe was re-inserted and measurements taken. Γ was extrapolated to 'probe insertion time' using a linear fit, as quadratic fits were unstable due to the large scatter in the data-points. The complex off-line data analysis is given as an example of Step 2 Analysis, Appendix 2.

The results (Figure 59) are at best limited but indicate a reduction in correlator decay with increasing viscosity as expected. Further work was not carried out and the extrapolations are not discussed in detail as a second limitation was found. Background measurements (centrifugation and optical density) suggested the particle size itself increased with increase in the propylene glycol concentration. This background data was itself limited, as it required samples to be diluted thus changing the sample properties. In the case of optical density the dilution was significant and these results were erratic and ignored. However, the fact that the samples adhered suggested that propylene glycol molecules had bound to the long alcohol chain coatings. This would lead to a significant change in hydrodynamic particle size but no significant change in the static light scattering size.

Thus, the data on viscosity may suggest a stronger relationship for viscosity (as increased particle size will also reduce the correlation decay) than actually occurs for viscosity alone.

5.3-5/3 Simple Temperature Model

The Stokes-Einstein relationship defines the diffusion coefficient's linear relationship to both temperature and viscosity, Equation 17. When the temperature increases the correlation decay thus increases directly with temperature and indirectly as the viscosity of the continuous phase decreases. In addition the refractive index of the material may increase decreasing the correlation decay and partially compensating for the viscosity variation (in water). The DWS instrument response for a sample of anatase pigment (Tioveil CS94, ϕ= 0.125) in water, as a function of suspension temperature, was studied, Figure 60. The trace shows a linear relationship over the 20 °C range that gives an instrument response variation of 1.3 percent per Celsius, which is linear over the range studied. This variation could be modelled and attributed to the three effects known to be occurring: direct temperature dependence, refractive index change with temperature and viscosity change with temperature. However, as discussed in the following section the model (Equation 17) was not believed valid and such an analysis would be misleading. The high level of reproducibility that this technique had shown suggested that samples should be stabilised (or measured) to a sensitivity, if not accuracy, of at least 0.1 °C.

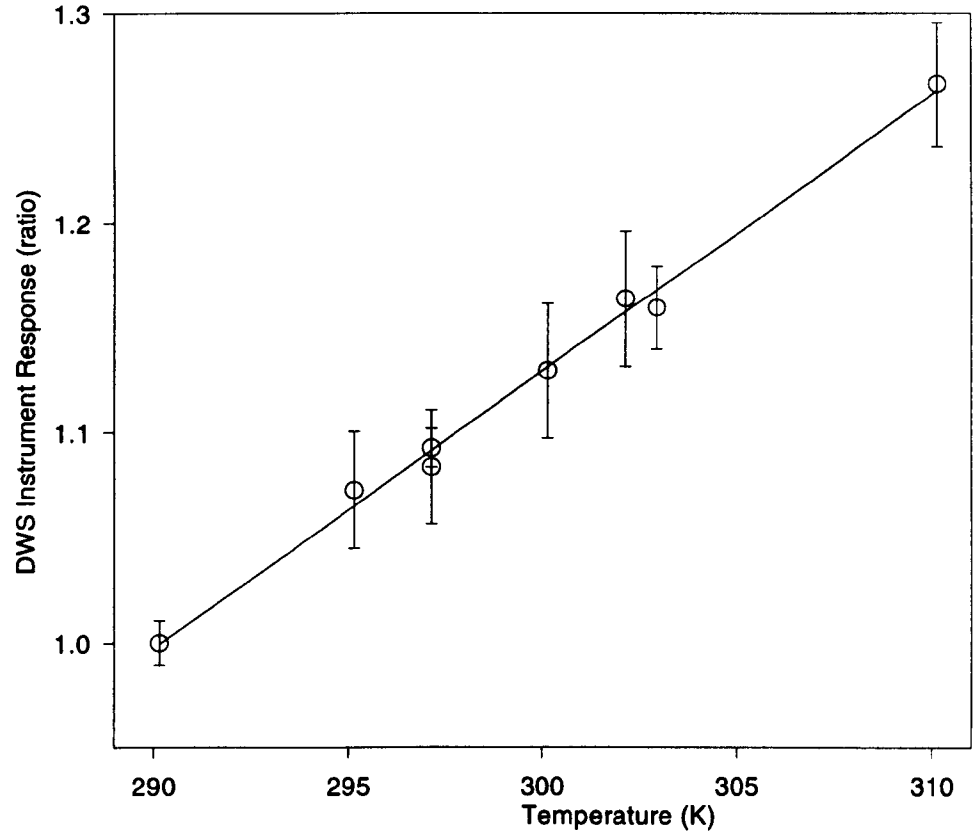

Figure 60 Effect Of Temperature

The effect of temperature on the apparent diffusion coefficient of a sample of Tioveil (0.125 ϕ TiO_2) normalised to 20C values taken during heating, except one data point (double valued) taken on cooling. Correlation coefficient 0.994, Gradient 0.0131. Each point mean of 6 experiments of 30 seconds. Dwell time before measurement 5 minutes. Statistical variance shown. Transform for Γ: $\Gamma = \Gamma / \Gamma_{20}$ where Γ_{20} is the mean value at 20^0C.

5.3-5/4 Calibration for Refractive Index

The refractive index dependence initially appears trivial when DWS is approached using conventional DLS theory. The refractive index is that of the fluid used and in most cases this will not vary significantly. The model for the scattering vector dependence assumes the refractive index of the continuous phase. This is correct, for conventional DLS experiments, where low concentrations are measured. However, in the development of PCS theory literature the ideal gas solution is modified to allow for the permeability of the particle (Pecora 1964). The difference is shown to be small, such that the permeability of the suspension may be used as an approximation.

It follows from this model that the refractive index of the suspension must be calculated by consideration of relative volumes:

$$n = n_1 + \%(n_2 - n_1) \qquad \text{Equation 68}$$

Where n is the effective refractive index, % is the percentage by volume of n2, and n1 the refractive index of the remaining volume. The relationship with refractive index is not linear but a square function due to the scattering vector. The difference is pronounced for high concentration materials, giving a variation of 100 percent in the scattering vector for a volume fraction of 0.5 TiO_2. However, the difference is only a 15 percent variation for polystyrene, at the same volume fraction, Figure 61.

Taking the scattering vector into account reduced the DWS concentration dependence, shown by analysis of the anatase pigment, considerably, Figure 62.

These results appeared, in part, to show why polystyrene beam samples gave a 'plateau region in concentration dependence at a lower concentration that titanium dioxide pigments. In the latter case the concentration dependence is a strong function of refractive index. However, consideration of the nature of diffuse scattering and in particular the phenomena of localisation suggest this improved model itself may be gross simplification, Section 5.4-2/1.

These results also showed a serious experimental limitation. The correlation decay of the most concentrated sample (ϕ=0.2) generated decay below 3.2us such that the step 1 technique was highly inaccurate and biased in analysis of the higher volume fraction samples.

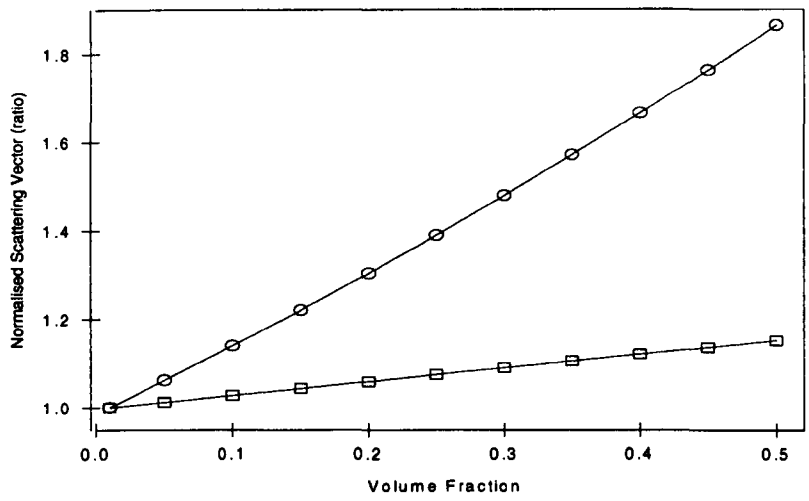

Figure 61 Theoretical Effect of Refractive Index

The effect of refractive index on the scattering vector for particles of refractive index 2.4 (anatase, circles) and 1.5 (polystyrene, squares) suspended in water.

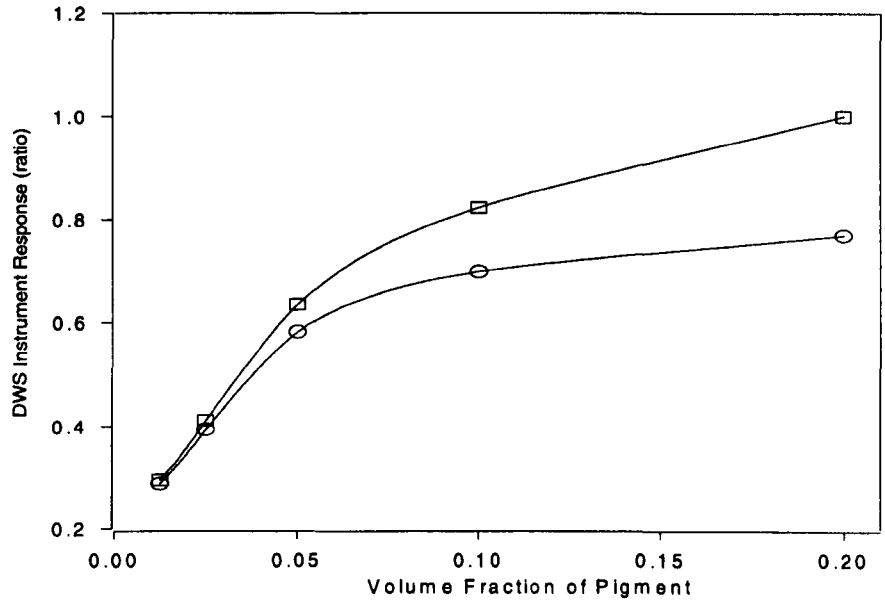

Figure 62 Experimental Effect of Refractive Index

Anatase pigment between ϕ =0.01 and ϕ =0.2. In this plot Γ' is modified to assume continuous phase refractive indices (square) and mean suspension refractive index (circle). Each point mean of 10 sixty second measurements, errors not shown for clarity.

Transform for Γ, $\Gamma = \Gamma / \Gamma_c$ where Γ_c is the value obtained for continuous phase viscosity at a volume fraction of 0.2.

5.4 Pilot System Development

5.4-1 Reasons for Development

Whilst DWS had shown itself to be highly sensitive and reproducible technique, significant developments were required. The instrument response had been shown to be a linear relationship with temperature and, to a more limited extent, with viscosity. However, the necessary sample materials to allow modelling had been shown to be limited and the model itself appeared inaccurate and required further attention.

Anomalies had occurred where different types of sample would not rank in size relative to each other and no physical understanding of why certain samples gave a 'reduced' decay rate could be found. These included stable, simple pigment in water, samples that also gave a curved correlation line-shape, which also could not be explained theoretically.

Many samples had shown themselves to be unstable and required complex repeated measurement procedures, unsuited to industrial analysis and process control, such that new measurement methods and procedures were required.

5.4-2 Failures of the DWS Calibration

5.4-2/1 Refractive Index

The basic calibration concluded that the refractive index to use in the DWS model was not that of the sample but of the bulk phase. Provided the concentration was known this would be simple to calculate and in operations such as milling, where the volume fractions of particle material remains constant, would remain fixed for a sample.

However, consideration of light scattering models suggested that this might have been a gross simplification at high volume fractions, especially of high refractive particles. In the pigment industry it is known that a volume fraction of 0.12 gives maximum opacity (when dried) and that increasing concentration above this is not only wasteful but may actually reduce the paint efficiency (*pers. com.* Lawson 1992). This has already been described as analogous to localisation where photons become 'trapped' within the lattice. A particle scatters light not only from the volume it physically occludes but also from the entire scattering cross section it defines which is significantly larger that the particle itself, due to the R^6 dependence, Equation 2.

At a sufficiently high concentration the particles would be spaced such that their scattering cross sections overlap and in the most basic sense it is questionable if the photon was 'in' the continuous phase at any point. At concentrations where any photon was always within a scattering cross section the refractive index of the sample may be a complex function.

This would prove a significant problem in applications such as milling where the conventional particle volume concentration is constant but the particle number concentrations, and size, are altering. Thus, to define refractive index, the equation may be of the form:

$$n_\phi = f(n_1, n_2, \phi, R) \qquad \text{Equation 69}$$

Where n is refractive index, R the particle size, ϕ the volume fraction (subscript 1 and 2 denote the particle and continuous phase respectively). In samples that exhibit polydispersity R may not be a simple mean size, depending on how polydispersity affects localisation, Section 7.2-3.

Whilst no other authors have reported this effect in DWS this may be due to the effective inclusion of this dependence into the 'instrument factor' γ (Equation 14b) and thus the variation in instrument factors reported. Most of the literature has been based on low refractive index particles at volume fractions around 0.1 where the effects may be minimal, Figure 61.

5.4-2/2 Temperature Effects on Refractive Index

The complex nature of clouding or localisation is not the only complexity of a true calibration. The refractive index is itself a function of the temperature. The refractive index variation with temperature of the continuous phase is generally known and is trivial to measure. However this may not be the case for the suspended particle. Thus the refractive index at a volume fraction ϕ may now be given by a function of the form:

$$n_\phi = f(n_1(T), n_2(T), \phi, R') \qquad \text{Equation 70}$$

Where n is now a function of temperature and R' is used to define the 'effective size parameter' in terms of localisation, which will be a function of the size distribution. This assumed that temperature did have a direct effect on localisation that appeared reasonable, as it is a static light scattering phenomenon.

5.4-2/3 Effective Viscosity

In DLS the Stokes-Einstein model (Equation 17) is adequate for most applications. The range of particle movements monitored is well defined (Section 1.4-5) and rarely allows any interaction to occur. However in the case of DWS particle displacement is not defined, Figure 13. A wide range of displacements may be analysed, from a few nanometers up to half the wavelength of the incident light, each photon delay being an ensemble average and thus suggesting that true separation of different displacement ranges is not possible.

In DWS the volume fraction is typically 2 orders of magnitude greater than that of conventional DLS and thus all interactions may be present. The effective viscosity is now a function of the continuous phase viscosity (η) as well as containing effective viscosity component due to: hard sphere interactions (η_{HS}), electrostatic interactions (η_E), hydrodynamic interactions (η_H), and any cross-linking (η_L). All of these viscosities, aside from electrostatic, are liable to be functions of temperature[1]. This gives an effective viscosity of the form:

$$\eta_T = f\ [\eta(T) + \eta_{HS}(T) + \eta_E + \eta_L(T) + \eta_H(\eta_T)] \qquad \text{Equation 71}$$

During this work Horne and Davidson (1993) suggested that for a first order correction $\eta_{eff} = \eta_{suspension}$ for a limited concentration range, up to $\phi \approx 0.2$ assuming hard sphere interactions.

For most paint systems all components, except for electrostatic, are liable to be significant including the most complex interaction function due to gelling agents. This work would suggest that for a first order approximation the harmonic electrostatic well model would be the best approximation of this non-linear effect, Equation 18.

5.4-2/4 Effect of Calibration Failure

The complex nature of the dependant parameters, which varied significantly for every sample type, defined that DWS was not a viable technique to use for absolute sizing. However, this limitation was due to the fact that DWS was capable of analysing complex functions not directly analysable by any other technique. This suggested that provided that DWS was calibrated to a 'master sample' then it would provide significant data for both process/industrial control, where absolute size is rarely important and as a research tool to investigate material properties.

1 In the hydrodynamic case, if the viscosity of the continuous phase at that temperature is considered then this dependence is taken into account.

5.4-3 Failure of the DWS Model

5.4-3/1 Size Ranking

DWS had shown itself to be a technique highly sensitive to particle size but ranking between measurements from samples of Tioveil on small (50nm) pigment, produced to scatter UV light, and other materials were not as expected. In addition, the polystyrene/latex 180nm beads (Figure 54) measured previously appeared to show a significantly slower decay than other samples analysed later. These also had a slight curvature in the front end of the correlation. It was noted that the 180nm beads tended to coalesce on the probe tip over time.

The decay rate of the Tioveil was much lower than that of that of an anatase or rutile pigment at similar volume fraction, whilst it should have been the reverse of that. As the Tioveil was uncoated unlike many of the anatase samples (which could causes a significant increase in hydrodynamic size), no reasonable explanation was initially evident. The highly stable nature of the sample suggesting aggregation was not the cause. It was also noted that the Tioveil sample gave a slightly curved line shape in the correlation when fitted as a straight line. As the sample volume measured was typically 20ml it was known that this effect was not due to a limited path-length cell leading to a loss of multiple scattered photons (Vankeuren *et al.* 1994). As the effect was not noted in many low refractive index (and thus high l^*) samples, such as polystyrene, it was obviously not a laser coherence limitation. Whilst the industrial partner believed no light absorbing species were present, this appeared to be the only reasonable explanation for the line shape and reduced correlation decay time.

5.4-3/2 Absorption of Light

The effect of limited mean free path may be studied by limiting the sample thickness, or by absorption by the suspension. Absorption by the suspending fluid should lead to significant concentration dependence, as the total distance travelled by the photon will effect the result. This will vary with the mean free path, of the photon, and as such may be highly concentration dependent. This work suggests the results should be compared to absorption by particles, suspended in a fluid of a purely real refractive index. Absorption by the particle should give a less concentration dependent result, especially at low concentrations. In this case absorption is simply a function of the number of scattering events, not the optical path travelled.

Obviously the control measurement (non absorbing suspension similar in all other respects) is required such that differences can be shown to be due to absorption and not concentration.

5.4-3/3 Experimental Samples

It was considered that by analysis of two samples at various concentrations (one containing dye bound to, or within, the particle and one with dye in suspension), it could be ascertained if the curved correlation line-shape was due to absorption.

It did not appear significant whether the particle absorbed light due either to surface absorbed or homogeneously dispersed chromophores. In both cases, the absorption would occur within the scattering cross section of the particle. In both cases absorption by the sample should not be a function of concentration (or scattering path) merely the mean number of scattering events.

Samples of polystyrene were tested with two dyes He32 and Rezarin. The particles were then forced into pellets by centrifuge at 15,000 rpm for 15 minutes. Neither sample showed significant quantities of bound dye, nor it was it possible to re-suspend the particles with either an ultrasonic bath or more energetic ultrasound probe. Similar work on TiO_2 (Tioveil) indicated the inert nature of the material would not allow for a dye to be absorbed.

Whilst absorbent polystyrene samples are available it was too costly to purchase sufficient quantities at high concentration for this work. The study was finally carried out on the worst case scenario: that of an absorbing continuous phase. A suspension of Tioveil had quantities of HE32 dye added consecutively, Figure 63. This blue dye was chosen as it showed high absorbency of the helium-neon 633 line, Figure 64.

The results were surprising since they showed that the dye had very little effect on the DWS response until quite high concentrations, where the previously white sample had turned dark lilac. This analysis was carried out using Step 2 analysis so no 'curve' function is given (as is the case for Step 3 results, Chapter 6).

However, the instrument response for Step 2 analysis is strongly decreased by front end curvature in the correlation, due to its method of selection of the portion of the correlation to analyse, Section 4.3-3/3. The trace shows the measured correlation gradient, and hence line-shape, remained constant to high dye volume fractions. The statistical errors for this work were significant, Figure 63. This was considered due to the incremental addition of dye and possible only partial mixing after certain additions.

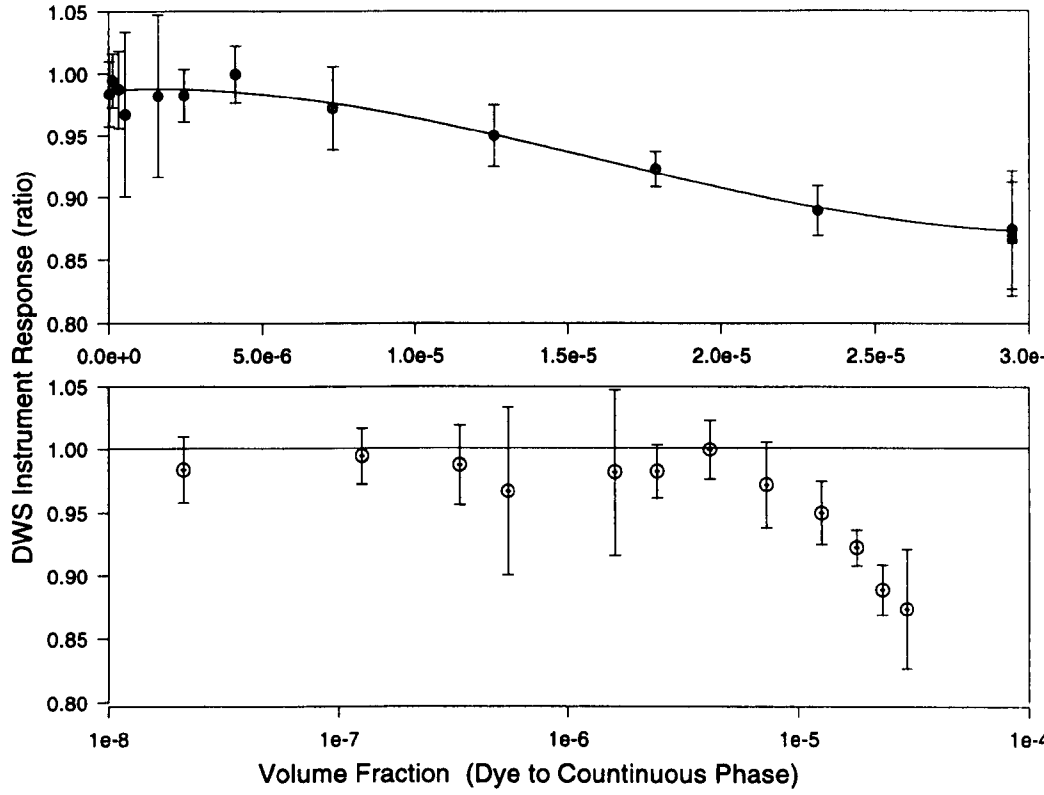

Figure 63 Effect of Absorption on Γ

The top plot shows the effect of addition of absorbing dye to a sample of Tioveil with the vertical axis showing $\Gamma/\Gamma_{no\ dye}$. The doubled value point indicates a test measurement taken one hour after this experiment was carried out to ensure the materials were stable and the results unaffected by flocculation and/or settling. Each data point is the mean of 15 experiments of 30 second duration. Statistical variance is shown. The trace includes a third order polynomial fit

$\Gamma(\phi)=[9.259\times10^{12}vf^3 - 4.471\times10^{8}\ vf^2+1280\ vf+0.9869]\ \Gamma_{no\ dye}$

Which is approximate for volume fractions above 10^{-6}.

The lower trace is similar data to the first but shown on log spacing to illustrate the curvature in the correlation is minimal until ϕ is of the order of 1×10^{-5}

Transform for Γ: $\Gamma=\Gamma/\Gamma_0$ where Γ_0 is the value with no dye

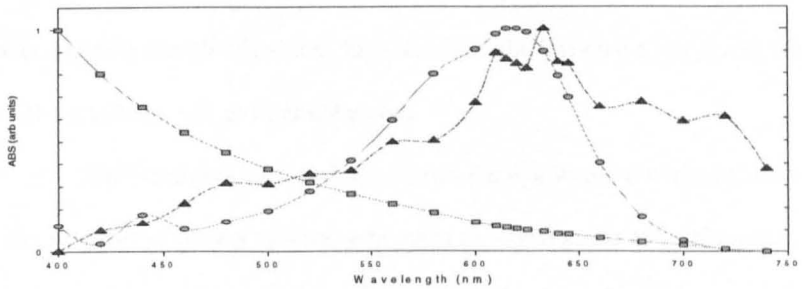

Figure 64 Spectral Scans of Tioveil and Suspended Dye

The spectral scans for the Tioveil (square), the dye in suspension (circle) and the final mixture (triangle). Results for the final mixture were normalised to the initial Tioveil results, as the effect of the dye could not be seen due to the high scattering power of the pigment. The trace indicates the dye was unaffected by addition to the suspension

Z average	Poly	Intensity D	SD	Mass D	SD	Number D	SD
238.700	0.286	382.700	132.700	415.900	90.700	348.300	98.100
242.500	0.280	482.200	256.900	636.000	191.800	301.700	201.600
237.000	0.278	361.100	181.600	510.200	145.000	289.600	159.700
234.900	0.277	526.500	217.400	554.500	201.500	314.600	163.300
231.700	0.289	397.400	171.100	452.800	124.700	311.600	136.900
237.500	0.265	390.700	156.900	462.400	142.000	317.500	130.200
ANALYSIS OF PARTICLE SIZE DISTRIBUTION							
	PEAK1	PEAK2	PEAK3		(2 from each set of 3 results selected)		
	170.6	385.0	560.0				
	160.0	390.0	627.0				
	148.0	380.0	620.0				
	156.6	375.0	650.0				
MEAN	**158.8**	**382.5**	**614.3**				
STD ERR	**4.674**	**3.227**	**19.185**				
VOLUME RATIOS							
Size	4/3 * Pi	r^3	Size	Volume ratio			
158.800	4.187	4.00E+06	1.68E+07	**1.000**			
382.500	4.187	5.60E+07	2.34E+08	**13.975**			
614.250	4.187	2.32E+08	9.70E+08	**57.874**			

Table 6 PCS Analysis of Tioveil CS 94

The standard Malvern 'automeasure' software was used allowing the correlator delay to be independently fixed for each set of ten experiments and reducing the possibility of operator bias. Three sets of ten experiments were carried out, each experiment of a duration of ten seconds. The system was calibrated with 40nm gold sol that gave a distribution mean of 38.7nm. Multi-exponential fitting procedures were used. The range of the exponential being adjusted until the analysis was at the point of over-resolving.

The quantity of dye required to significantly alter the correlation line-shape suggested that the curvature could not be considered due to absorption. The results on the majority of low concentrations samples (and thus high l^*) where the line-shape was linear with the fit also indicated the effect was not due to laser coherence

While the previous work has shown the dye would not interact with the simple TiO_2 in water suspension control spectra were taken as a final precaution. The high scattering power of the Tioveil made the effect of the dye indistinguishable from that of the control pigment sample. Normalising the trace, to that of the control sample, allowed the absorbance peak to be visualised. The trace suggest no unforeseen chemistry had significantly shifted the absorbance peak of the dye to a point that it had an effect on the 633nm light, Figure 64. The slight variation of the absorbency above 633nm was considered to be due to the magnification in errors from the normalisation.

The results thus showed that the correlation shape and long decay rate of the sample was not due to loss of diffusive photons. Further analysis of the theory and the material was required to explain both the correlation line-shape and the low decay rate.

However, this work also indicated that DWS was operable in highly absorbent materials.

5.4-3/4 Experimental Results

The previous work had been unable to identify reasons for the unusual behaviour of the Tioveil sample and the material was studied by cytometry[1], photon correlation spectroscopy and finally by electron micrographs.

PCS analysis was initially ambiguous. Results indicated a mean size of 425nm intensity distribution (or 230nm Z average). This suggested the pigment was significantly larger than its 50nm design size but still less than the few microns predicted by DWS. The PCS results indicated a distribution of three distinct separate peaks of 614, 382, 158nm. These were highly reproducible (to within 2.5 percent) on repeated measurements and with new samples, Table 6. This level or reproducibility (of the distributions) was noted as highly unusual for PCS distribution analysis. This reproducibility also indicated that the sample mean size and distribution was unlikely to be due to shock flocculation occurring on dilution and thus a PCS artefact.

1 The cytometer was designed to analyse cells (3-100um) and results were ambiguous and thus not included in this work

Initially it may appear that the distributions were due to a simple particle monomer, dimer, trimer distribution. However, light scattering measures volume (Section 2.3-2/3) and effective diameter. A dimer is only about 1.2 times the volume, hence effective diameter, of a monomer.

For flocculation to produce these peaks would require flocculates composed of 14 and 58 particles of 158nm respectively. This would be an unusual distribution to occur from a milling process.

The R^6 dependence of light scattering meant that the sample could contain a large 50nm population, which would not have been visible in this data. To check for a smaller distribution the samples were 0.22 micron filtered prior to further measurement. The initial results were disappointing, as a significant amount of material around 240nm appeared to have passed through the 0.22 micron filter. A new sample was prepared with the water being triple 0.22 micron filtered prior to addition of the Tioveil after which the sample was 0.22 micron filtered twice. The results were surprising, the 614nm peak was removed but the previously smallest distribution itself appeared to be the sum of two other distributions, of peaks 82nm and 155nm. Giving in total distributions of 614, 382, 158 and 85nm.

The analysis suggested that significant material of 300nm had passed through two 0.22 micron filters although this was considered unlikely. The distribution of distinct populations of each double the radius of the previous was considered unusual, leading to the theory of PCS being considered in more detail.

5.4-3/5 Rotational Diffusion

Pecora (1968) has given the PCS amplitude correlation function for rotational diffusion:

$$G^{(1)}(t) = NA^2 [B_0 \exp(-D_T q^2 t) + B_2 \exp(\{-D_T q^2 + 6D_R)t\} + B_4 \exp(\{D_T q + 20D_R)t\} \quad \text{Equation 72}$$

Where R_2 is the major aspect ratio, Q the scattering vector, B_{1-4} the relative weighting of each component, D_R the rotational diffusion coefficient and D_T the translational diffusion coefficient. The equation is valid provided $Q < 10$. The amplitude correlation may be related to the intensity correlation by:

$$g^{(2)}(t) = 1 + [B_0 \exp(-2t\Gamma_0) + 2B_0B_2 \exp-(\Gamma_0 + \Gamma_2)t + B_2^2 \exp(-2t\Gamma_2)]/[B_0 + B_2)^2 \quad \text{Equation 73}$$

If this is analysed as a conventional PCS signal it results in a triple population (although this may be reduced to 2 by plotting square root as opposed to the usual logarithmic style).

Notably the centre term consists of $\Gamma_0+\Gamma_2$ which would appear to coincide with the 'doubling' in intensity distribution we observed. In addition the fact that three distributions were always present in our analysis, regardless of what was filtered out, indicated probable rotational diffusion. A series of Electron Micrographs (EMs) were requested from Tioxide, Figure 65. These agreed with the rotational diffusion postulate. The EMs of the Tioveil showed individual crystals of the order 60x10nm (water based) and 100nm x 18nm (oil based). The physical aspect ratio of 6:1 may actually have been greater (optically) due to the birefringence of TiO_2 crystals.

Software, or a goniometer for multi-angle work, was not available to analyse the PCS data for rotational diffusion. In any case, the failure of the assumption QL<10 would appear to make any analysis questionable as the B coefficients, which have been calculated for Rayleigh Gans scattering, are unsuited to TiO_2, Section 1.2-2.

5.4-3/6 Effect of Rotational Diffusion on the DWS Line-shape

Rotational diffusion is a slow process compared with translational diffusion, particularly when impeded in concentrated samples, and thus this would explain the reduced correlation gradient obtained in analysis of the Tioveil material. However, this did not explain the variations in correlation line-shape. The same process of ensemble averaging which removes polydispersity information should also remove any effect on the correlation line shape.

It is suggested that the effect is probably due to hydrodynamic interactions. Rotational diffusion is liable to lead to longer range hydrodynamic coupling. The DWS model (Equation 14b) assumes no interactions and thus such effects would be expected to alter the correlation line shape.

The more unusual results of the 180nm latex beads can probably also be explained due to similar effects. These beads included a large amount of latex causing them to coalesce on the probe (and thus requiring Step 2 type analysis) thus coupling was occurring even at low concentrations. While the probe coatings reduced adhesion, it was not possible to eliminate completely, Section 5.2-3/8. This was unsurprising as the material is added to paint to act as a coalescence agent and ensure the pigments form a bound smooth surface after the continuous phase has evaporated. It was shown later in this work that the reduced size and correlation line-shape differences were encountered for other interacting spherical samples, Section 6.4-2.

5.4-3/7 Analysis of Shape

The previous work suggests that curvature in the correlation is probably a function of particle shape, as well as laser coherence and absorption. This would suggest that it might be possible to get a measurement of shape from DWS. However, this would be limited to an "index of sphericity" or, assuming an ellipsoid, the aspect ratio. Possible applications may be limited as the same type of correlation line-shape may be found in systems of spherical particles, when either coupling occurs or laser coherence is short compared to mean photon transport path.

Possibly more importantly for this project was that it indicated one failure of dynamic light scattering as a tool for the pigment industry. While the flocs of pigment are obviously larger than 50nm, the EM show them to be aligned and thus probably acting as 50nm Bragg grating. While dynamic methods indicate the suspension characteristics, they do not exemplify the static light scattering properties of the resulting dry film where further alignment may have occurred due to application method.

Whilst DWS may be a useful tool for process control within the pigment industry it must referenced to a static light scattering measurement. Complementary static light scattering analysis techniques are proposed based on the dependant scattering model of dense high refractive index suspensions, Section 7.2-3/6.

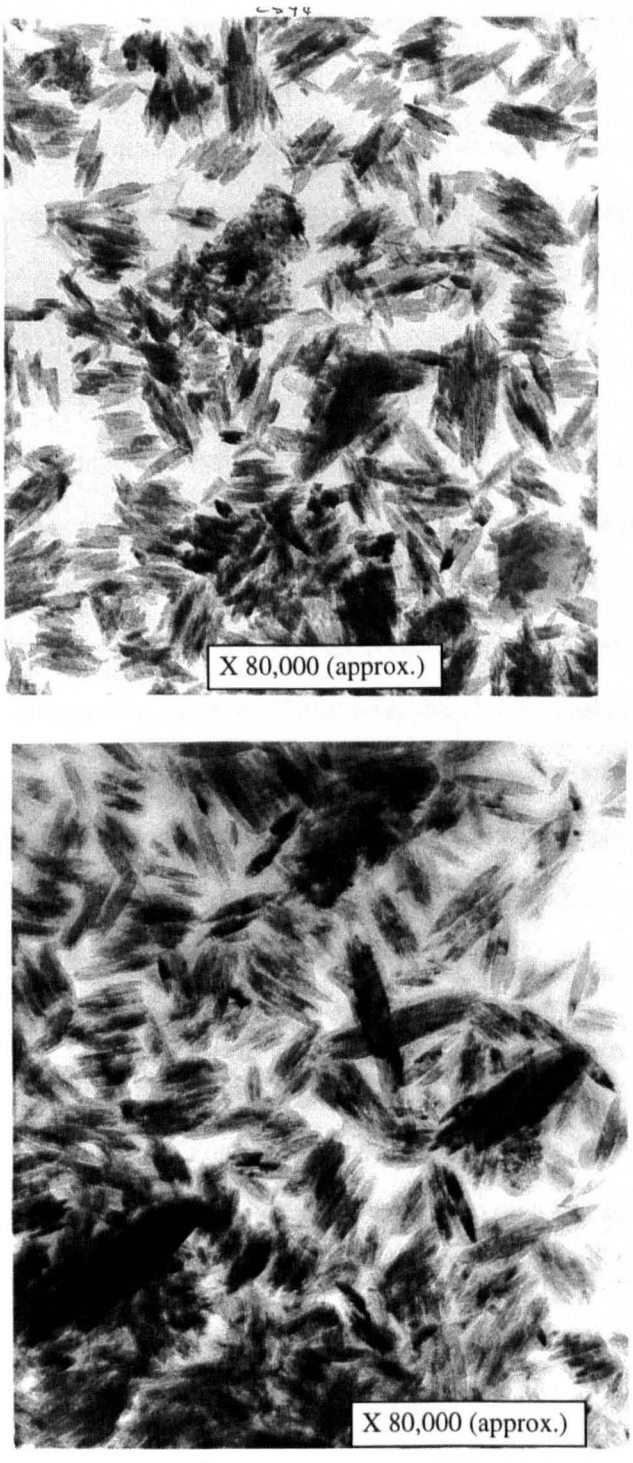

Figure 65 Electron Micrographs of TiO_2

The Tioveil material appears to have an aspect ration of the order of 6:1, for both oil and water based types. It is not practical to state if the flocculation is due to microscopy sample pre-treatment or is present in the undiluted sample. Top plate: water based Tioveil CS94 (as used as a reference in this work), Lower plate: oil based Tioveil. Images taken by Tioixde Ltd using their in-house standard procedures and methods.

5.4-4 Alterations in Methodology for Unstable Samples

5.4-4/1 Limitations of Sample Materials

The high density (4 relative to water) and complex nature of many of the pigment samples suggested that there was little point in production of equipment that would only operate in stable suspensions. In addition, it was considered that there might be more data available from a sample if the time dependant nature could be properly analysed.

5.4-4/2 Types of Temporal Variation

The temporal effects could be split into 2 categories, reversible and non-reversible. The milled pigments exhibited the same trace after each mixing and thus, whilst they may settle over a 10-15 minute period, they were stable in pigment terminology.

The second form of temporal response occurred when samples flocculated or bound to each other or the probe. Whilst reversible changes could be measured by repeated analysis (Section 5.3-4/3), this became even more complex for irreversible changes, Section 5.3-5/2. In many industries it may be an irreversible process that forms product and as such this was seen as an important problem to overcome. The Step 2 methods of analysis (Section 4.3-3/3, Appendix 3) operated well measuring both types of phenomena. This section concentrates on the analysis of the reversible changes, typical of pigment samples although the measurement method obviously would allow irreversible changes to be followed.

5.4-4/3 Milled Pigment Samples

Two forms of reversible temporal changes were noted. Immediately after milling (or mixing) the instrument response reduced in a smooth near exponential manner to a plateau region (short term time dependence). Over longer periods the instrument response again increased (long term time dependence). It was initially considered that the initial decrease in Γ, typical of milled pigment samples (Figure 57) might have been attributable to:

- the low percentage of 'oversize' pigment typically 0.5 percent, between 2-5 micron preferentially settling from the sample area;
- air bubbles rising, again generating a false high frequency signal;
- structuring at the probe interface;
- structuring in the bulk medium.

Previously samples had been produced by Tioxide and characterised by the Optical Density and Brookhaven centrifuge techniques prior to dispatch to CAMR for DWS analysis. It was considered probable that some or all of the temporal effects may have been due to the transport and storage of the samples, thus making Tioxide's measurements irrelevant. To overcome this problem a pigment mill and OD spectrophotometer were commissioned at CAMR, allowing measurements immediately after the milling process. The mill was a sandmill variety and Tioxides in-house milling protocols were used, Figure 38.

Samples of pigment milled on site (Figure 66) showed both short and long term time dependence as previously, Figure 57. It was noted that the long term time dependence was similar to earlier results, being most notable in the less milled pigment samples. However, the short term time dependence was significantly different. In previous work all samples, regardless of how long they had initially been milled, exhibited similar short term time dependence after mixing. However, measurement just after milling gave a short term time dependence that increased with the quantity of milling.

This suggested the most likely cause for this effect was included air. However, the other possible causes were also studied. Adhesion/structuring on the probe surface was discounted as no sinusoidal variation occurred in the count rate, which is typical of adhesion due to an effective etalon build-up, Section 6.4-3/2. Structuring of the bulk medium was discounted. This could only occur if complete gel disruption had failed to occur on the samples milled for shorter periods. In these simple water, pigment and dispersant mixtures no reason for significant gelling was considered feasible, particularly as most pigments are uncoated at this stage. In addition sand milling is a very energetic process and it was considered gel disruption would occur almost instantaneously.

As a final proof various experiments were attempted where the sample was degassed before and then during milling. However, a seal could not be maintained between the rotator and mixing pot to allow a sufficient vacuum. Degassing of the final milled sample took considerable time making the process useless.

5.4-4/4 Long Term Time Dependence

Whilst the short term time dependence was shown to be a function of the quantity of agitation applied (included air), the long term time dependence was not, provided the sample had been properly re-suspended. Therefore, it was evident that this was probably an effect due to the pigment particles themselves. It was noted in all milling results that the well milled samples tended to show little long term time dependence whilst the poorly milled samples (Figure 57, sample 26, Figure 66, sample after 5 minutes milling) showed an increase in Γ with time after milling or mixing. This is equivalent to a reduction in particle size. For well processed samples, analysed immediately after milling, the short term time dependence predominates for a full 10 minutes (Figure 66), until the samples collapsed and further analysis was not possible by this method. Analysis of highly instable milled samples is considered later in this work, Figure 79.

As less milled samples are polydisperse, and less well dispersed, this suggested that the effect was probably due to settling. This hypothesis was supported visually as less well milled samples could often be seen to settle (form a 2 phase mixture with a clearer eluant at the top) over 20-60 minute periods. It was considered that this could due to one, or a mixture, of three different settling phenomena:

- Increased settling due to lack of proper wetting;
- The velocity component of large particles as they pass through the probe detection area;
- The loss of the velocity component of large particles as they left the detection area;
- A reduction in the effective mean size due to the loss of large particles in the detection zone;

The first two points could be disregarded immediately as they would cause a bias and not time dependant behaviour.

If the sample initially contained a signal due to flow then this would combine with the scattering signal and would decrease Γ with time. This is the opposite of the effect noted and, in any case, it is suggested that the settling was so slow that the frequency component would not generate the magnitude of change noted. Whereas the loss of larger particles leads directly to a smaller particle size being analysed and thus an increase in Γ as seen in poorer milled samples, Figure 66, 5 minutes milling trace.

This was initially seen as unusual it was known that the phenomena of subsidence (Sato 1992) was expected in these samples, where weak hydrodynamic interactions cause all particles to fall together. This phenomenon of a two phase mixture (after 20-60 minutes) was visually noted in the samples, which suggested against any effect due to preferential settling.

It was believed that this could be explained due to the complex nature of milling materials such as pigments. In many reduction processes a sample of flocculates is reduced in mean size by milling. The statistical nature of the milling gives rise to an assumed log normal distribution whose mean size initially reduces (until the primary crystal size is reached) and the major effect of further milling is merely to reduce the distribution width.

However, a pigment sample contains a mixture of flocs agglomerates and aggregates, Section 4.5-2/1. The majority of flocs will breakdown almost instantly under the high stresses caused by sand milling but the agglomerates (particles joined at the edges) will taken significantly more energy. This reduction of the agglomerates to primary particles is the major purpose of sand milling TiO_2. The aggregates (particles joined at the faces) may survive the full milling process due to their strong bonding. These are liable to produce a second log-normal distribution superimposed on the first. The aggregates, which are known to be present in milled pigments (termed oversize) can have significant effects on sample stability and scattering characteristics, Section 2.2-2/8. Thus in milled samples we can consider the majority of the sample is a dispersion of flocs which are reduced in size and well wetted to the continuous phase during processing. These should follow the subsidence model and settle as a single unit. However, also present are a population of particles which may be an order of magnitude greater in size. These much more massive particles may preferentially settle through the subsiding flocs, particularly as they are liable not to be correctly wetted to the continuous phase.

This phenomena of three distinct populations, or more correctly three families of populations, each of which have different elements of preferential settling and subsidence appeared to explain the initially contradictory results: visible subsidence but with measured preferential settling of larger particles.

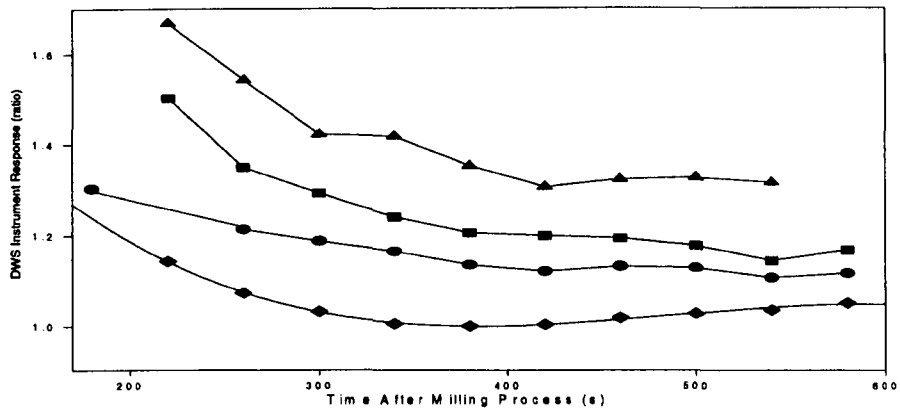

Figure 66 Γ as a Function of Time from Milling

The organically coated rutile pigment samples were milled at volume fractions of 0.0125 at CAMR using one of Tioxide's pigment mills. The time is referenced to switch off of the mill. The lower trace is fitted to a 3rd order polynomial. Other traces: straight lines join points. Γ is normalised to the longest decay from the sample milled for 5minutes at a time from milling of 380 seconds. Key, Diamond: 5 minutes milling, Circle: 10 minutes milling, Square: 15 minutes milling, Triangle: 20 minutes milling Transform for Γ: $\Gamma=\Gamma/\Gamma_5$, where Γ_5 is the lowest value from the 5 minute trace.

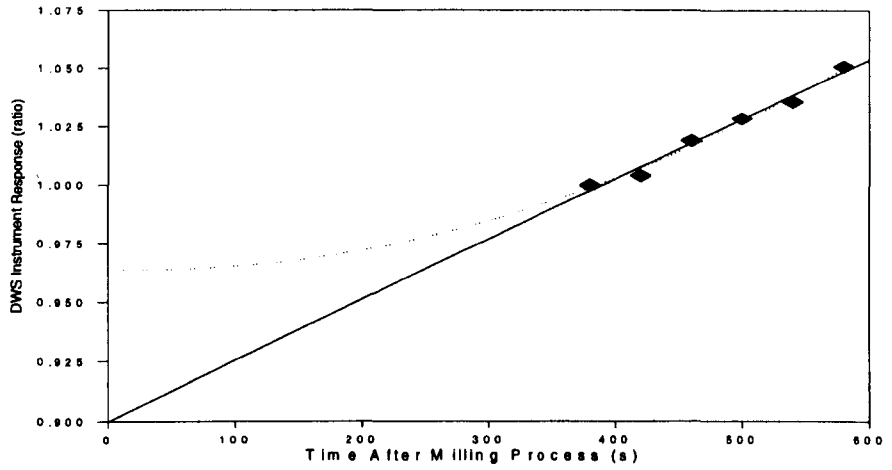

Figure 67 Limitations of Extrapolation of Size

The trace shows the data for the long time temporal variations for the sample milled for five minutes of Figure 66 (reduced data set, expanded axis). To show limits of extrapolation the data is fitted with both second and 3rd order polynomials. The latter allowing for smooth continuous changes. Quadratic fit: $\Gamma(t) = 2.837\times10^{-7} t^2 - 1.555t + 0.9637$, $r^2=0.986$, Linear Fit $\Gamma(t) = 2.568\times10^{-4}t + 0.8997$, $r^2$0.981 where t is time from milling. Transform as Figure 66.

5.4-4/5 Correct Value of Γ

In well milled samples the long term time dependence is low, leading to a slow smooth turning point between short and long term time dependence (Figure 57), termed the plateau region in this work. However, for poorly milled samples, the increased short term time dependence, reduced this to a simple turning, Figure 66.

The settling obviously begins as soon as milling is finished and thus the 'correct' value of Γ, as it has been decreasing since mixing or removal from the mill. This is not evident in the traces as the short term time dependence is a stronger function. Thus to obtain the t=0 value an extrapolation was carried out, ignoring short term time dependency area of the graph in the analysis.

However, even with samples that had been milled only a short time, and with a measurement spanning 10 minutes, the extrapolation is limited, Figure 67. The short term time dependence is significant and its removal does not allow sufficient data for extrapolation. This was clearly indicated by extrapolation with both linear and quadratic functions, where the turning point was assumed the end of the short term time behaviour.

A longer series of measurements was not possible as subsidence leads to the probe being left in only the continuous phase, thus much larger samples would be required. In addition, it is questionable when the short term behaviour finishes and thus which data should be excluded. The temporal variations of DWS could have been viewed as a disadvantage but the ability to monitor this effect made DWS unique, allowing the study of change in complex media without sample pre-treatment.

The different methods studied for obtaining a single value from the response included the measurement at some fixed arbitrary time and the minima of a curve fit (Γ plotted versus time from milling), Figure 68. Both traces appeared to be measuring the same parameter (Table 7) as the correlation between optical density and Γ were similar (within experimental errors) for both methods, Figure 69, 70. The use of a fixed measurement time obviously requires all the sample traces to be measured and viewed in advance and is a qualitative technique. To quote a single value for a DWS measurement, of a high density polydisperse material, the size or instrument response should probably be defined from the plateau or turning point simply for reasons of reproducibility..

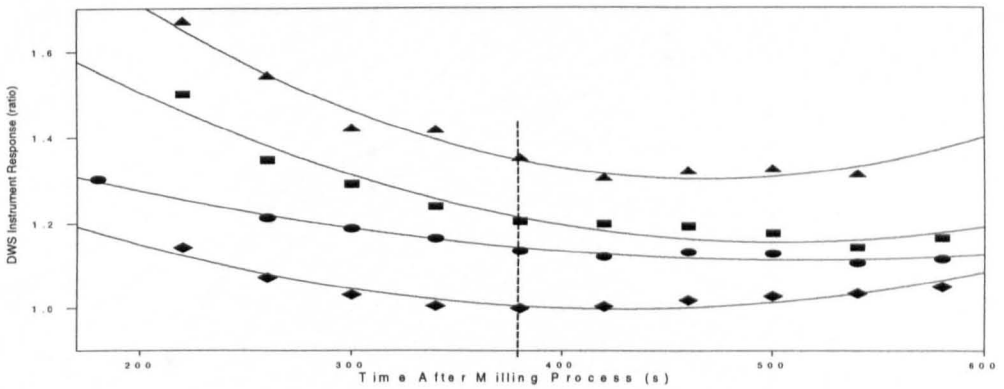

Figure 68 Turning Point Interpolation

As figure 66 except polynomial fits used to define as turning point and thus the plateau region. In addition the instrument response at 380 seconds was analysed

Mill Time	OD	OD Sdev1	OD Sdev2	Value at TP	Value at 400s
5	0.330	1.49	1.51	6.58	6.61
10	0.297	1.46	1.45	7.63	7.78
15	0.285	1.45	1.44	7.91	8.19
30	0.266	1.42	1.40	8.92	9.10
Polynomial Parameters			Turning	S Err in	Corr coeff.
A(0)	A(1)	A(2)	Point	Poly Fit	Polyfit
10.49	-0.017712	2.00E-05	442.43	0.106	0.899
10.59	-0.011558	1.13E-05	512.31	0.067	0.979
14.50	-0.026198	2.60E-05	503.04	0.168	0.946
17.38	-0.036140	3.86E-05	467.76	0.195	0.705

Table 7 Results of 50gpl Milling of Rutile

The table gives the full set of results for DWS and Optical density measurements for samples milled at 50 grams per litre (density ≈ 4), Figure 68.

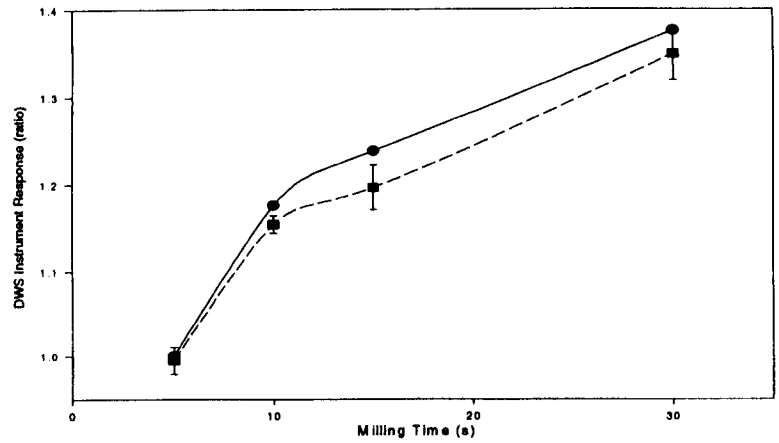

Figure 69 Comparison of Interpolation Techniques A

The value of Γ was selected using 2 interpolation techniques. That at an arbitrary fixed time, selected as 380 seconds as the approximate minima (Figure 68) of the 5minute trace, (circles). The second method considered defining the Γ minima of each trace by curve fitting (square with error bar). The latter has some benefit in allowing the generation of an error estimate of the fit and in suggesting an automatic method. In conjunction the measure may be considered to be at the same 'effective' time for each measurement, in that it was when sedimentation balanced air release. Analysis carried out by second order polynomial fits, Table 5.

Transform for Γ: $\Gamma=\Gamma/\Gamma_{5m}$ where Γ_{5m} is the value at 5 minutes milling.

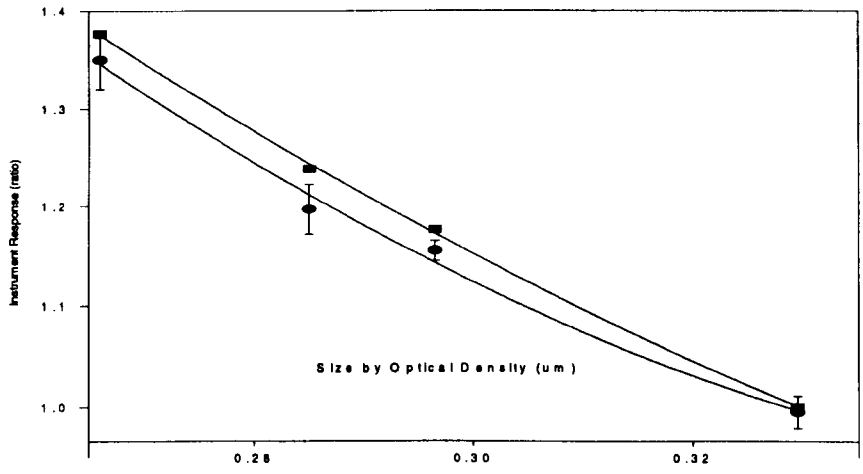

Figure 70 Comparison of Interpolation Techniques B

No significant difference was noted for correlation between optical density measurements and either the turning point Γ value or the fixed time Γ value, key as Figure 62. Transform as Figure 62

Where the fitted curve is known to be of the correct form this also allows a simple method of generating an error measurement. Thus each individual correlation could be a rapid measurement, and have a large statistical error, the curve fit allowing the data points to be effectively averaged thus reducing statistical variance. This is ideal for a process line as the damping of the fit would stop experimental 'glitches' leading to large shifts in the correlation setting parameters, and thus hunting in the reported instrument value. This suggested the method of measuring the change in Γ, with time from measurement, and then using the turning point of a suitable curve to define a single value of Γ.

In this work quadratic fits were used to find the turning point, purely to demonstrate the feasibility. These were shown to be accurate fits provided the measurement duration extended to include the minima (see 5min trace of Figure 68) but may not have been stable if the range of measurements occurred over too short a time-scale such that the minima was extrapolated, as opposed to interpolated. This work suggests that if sample degassing was carried out the slow increase in Γ could be analysed in a period below 10 minutes.

When data was sensibly selected for the Γ versus time fit the error in the fit was useful in giving a real-time measure of the statistical variance of Γ, as opposed to merely the sum of statistical variance and error in model fitting that would normally be possible.

5.4-4/6 Application of the Temporal Variation

In the final stages of milling, analysis of mean size is of limited use as a very small percentage of oversize, which may have an insignificant effect on mean size, can dramatically effect material performance. Off-line single particle detection methods are conventionally the only techniques capable of monitoring oversize, thus milling times may be significantly greater than required.

In the pigment industry the measurement of choice (OD) is known to substantially underweight oversize making it unsuited to analysis of poorly milled samples. Any method of monitoring the oversize on- or in-line allows the possibility of dramatic increases in productivity. PCS results did not show the long term settling behaviour measured by DWS, this may be expected, as dense particles of a few microns would probably settle prior to analysis. Obviously settling of oversize particles in very diluted PCS samples will be very different from their behaviour in dense, slightly gelled materials that are undergoing subsidence.

The lack of stability of oversize is one of the most important factors, thus even if DLS was capable of operating quickly enough the data may not be significant. In addition where the oversize population was small, as was typically the case, standard PCS analysis routines would interpret it as dust and ignore the data, Section 7.5-1/4.

The long term trace shape may also be of significant importance to the DWS technique in all applications as it suggested the possibility of polydispersity analysis that was previously discussed as impractical for conventional DWS analysis, Chapter 2. If the rate of change ($\delta\Gamma/\delta t$) indicated the level of polydispersity , then it would follows that the shape of the trace, ($\delta^2 \Gamma/\delta t^2$), should be indicative of the distribution shape.

A binary suspension should sediment differently to a polydisperse single distribution when related to time. However pigment samples cannot simply be considered as bimodal, they have at least two different populations, each of which has a significant distribution. The primary population is that of the milled pigment and is normally considered approximate to a log-normal distribution with a mean around 200nm. The breadth of this distribution obviously reduces with milling time. The second distribution will typically have a mean size of between 1 and 5 microns. This is the unmilled aggregates. To date no model of this distribution has been found in the literature but there is obviously no reason for an assumption of a log-normal model.

In addition the distribution shape, as well as mean size, is liable to be different for pigments that have undergone different coatings or other processes. Thus settling analysis is liable to be highly complex. The smaller size distribution may have a range of sizes but all particles have been 'wetted' to the continuous phase and thus all should undergo subsidence. Visual inspection of at least the less well wetted samples suggest this occurs. However, the larger size population are both massive and not wetted to the suspending fluid. They are not part of the suspension, and will preferentially settle. Thus, it is suggested that the long term time dependence is primarily due to the oversize population. However, in poorly milled sample the lognormal distribution will be wide and it may be that the 'tail' of the lognormal distribution also settles.

Mixing a monodisperse sample of small latex beads with a small population of much larger beads was thought unlikely to give significant insight into the phenomena. The larger population/s in the TiO_2 samples had a distribution of dispersion as well as size, whereas in polystyrene beads the distribution is of size alone. In addition polystyrene does not have the significant density of TiO_2 and settling of a 5 μm bead in a volume fraction of 0.0125 may take very considerable time.

In some applications the complexity of the DWS index may be limiting. Whereas PCS gives a factor that relates directly to the size distribution/shape in DWS the factor will be a function of concentration, interactions and stability. However, in pigment and other milling processes it may be a significant benefit. Conventionally, pigments are milled long enough that oversize should have been reduced. This may vary for every pigment and process and cannot be analysed on-line by conventional methods.

DWS would appear highly sensitive to it oversize and allow effective real-time control of a pigment's milling cycle. This may save both significant energy and money directly in industrial mills as well as increasing productivity from the high cost plant.

A study of the oversize distribution in TiO_2, and thus modelling the behaviour, is well beyond the scope of this work. To obtain the distribution of such a sparse particles, especially in well milled samples, would require the build-up of many thousands of single particle detection measurements. This would require to be done for different pigments and similar pigments produced by different processes to be of significant industrial usefulness.

5.4-5 Analysis of High Γ Samples

5.4-5/1 Failure of the Step 1 Method

The high concentration, high refractive index samples, such as anatase pigment at volume fractions of 0.2, could not be measured using the Step 1 analysis, Figure 54. Rapid decay rates gave significant biasing, due to both the limited bandwidth of the correlator and the fitting procedure.

The optimum correlator delay (as defined by Step 1, Section 4.3-3.2) was often below 25ns, the correlator bandwidth causing a failure in the method. Altering the correlator delay also gave a large difference in the instrument function when the correlator delay was at, or near, the minimum correlator delay. The temporal region of correlation analysed was varied by order of +/- 100 percent of the first experiment.

5.4-5/2 Dilation and DWS

The range of liquid samples measured suggested that using the correlator at its minimum delay of 25ns and merely varying the number of channels would fail for samples of τ_0 greater than around 6400ns (256 x 25ns). This problem has been overcome in PCS by the use of dilation where the correlator delay is set to increase pseudo-logarithmically and a certain number of points are selected for analysis. This was itself limited, as the majority of the points would lie outside the region of interest for rapidly decaying samples. In addition the implementation in hardware gave a significant bias as the correlator was only capable of introducing a delay that was an integer multiple longer than the base τ, every 16 channels. The pseudo logarithmic spacing could give dramatic differences in measured diffusion coefficient when a few of the increased channels appeared in the fit, Figures 23, 24, Section 3.2-4/4. While, in practice, it is possible to take account of uneven spacing, this relies on an assumption of the correlation line-shape, which cannot be assumed for all concentrations, delay times and materials analysed by DWS.

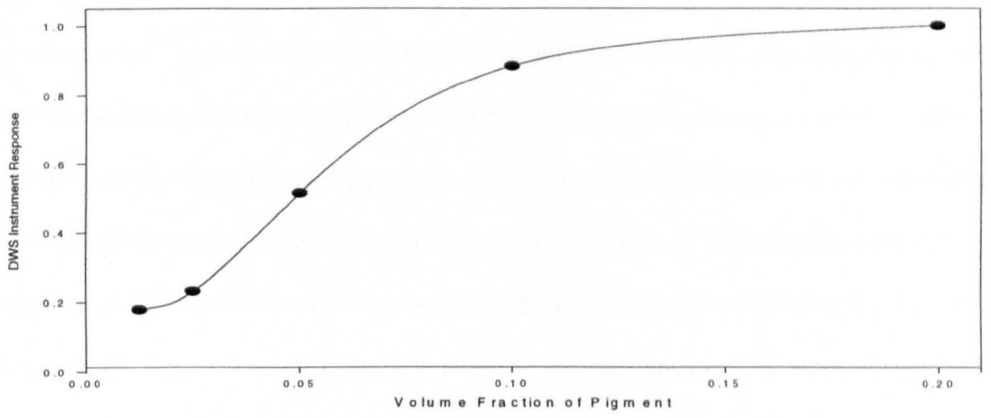

Figure 71 Concentration Dependence Dense Samples

A set of experiments on a milled sample of anatase pigment at concentrations between 50 and 800 grams per litre (volume fractions of 0.0125 and 0.2 respectively) analysed by the Step 2 method.

Transform for Γ: $\Gamma=\Gamma/\Gamma_{20}$ where Γ_{20} is Γ for the volume fraction of 0.2 of RHD-6 pigment

5.4-5/3 Cyclic Correlator Delay Method

The correlator delay resolution, maximum measurable Γ and error were finally improved by manually fitting the cyclic data sets, termed Step 2 analysis, Section 4.3-3/3, the sample being measured at a range (set) of correlator delays a number of times. After collection of many sets the data was analysed. The error in the straight line fit from each experiment (correlation) was plotted against correlator delay time, for each data set. This allowed calculation of the correlator delay that gave the best fit for that set using a cubic spline fit (in Sigmaplot). This correlator delay was interpolated thus any correlator delay could be obtained, as it was not limited to 25ns x 128 channel steps. For each set the instrument response was then fitted against the correlator delay used in its analysis. The value of Γ was found by interpolating to the correlator delay found previously, the one that gave the best fit. Thus this value of Γ was deemed to be the correct one for that set and was plotted versus the time of measurement.

However, the method was not real-time and required operator intervention as the cubic spline could itself find false zeros and occasionally gave erroneous results. In addition the method required vast quantities of data to be collected and analysed off-line, Appendix 3.

5.4-5/4 Step 2 Analysis Results

The Step 2 approach was used to analyse the 180nm polystyrene sample (Figure 54) and the high concentration pigment, Figure 71. Of the latter all concentrations were measured successfully except the undiluted sample where the data using a 25ns delay was used as the instrument was bandwidth limited.

Higher concentration (volume fraction 0.45) samples of pigment were successfully analysed, but the Step 2 method could not be used to select a particular part of the curve. These materials are actually milled at much lower concentrations, and the concentration achieved by a cross flow filtration technique for a specific application. Thus, a range of pigments could not be provided for comparative measurements giving this data only limited value.

5.4-5/5 The Zero Delay Intercept

The Step 2 method increased the resolution and reproducibility of DWS significantly. The measured DWS parameter became a continuous function of the correlator delay selected. However, this method did not allow for proper analysis of samples where the optimum correlator delay (as defined in Step 1 analysis) was below 25ns, for a 128 data point analysis. The method could not be simply changed to allow for the number of correlator channels, as well as the correlator delay, to be varied in a reproducible, efficient and systematic manner. Attempts were made at extrapolating the instrument value to that equivalent to zero correlator delay. This allowed some samples, previously outside the range of DWS (such as those given in Appendix 3) to be successfully analysed.

However, this failed on any measurement where the correlation front end showed significant curvature with extrapolation typically giving $\Gamma=0$. Since interacting samples typically required the extrapolation, and the interaction produced a curved correlation line-shape, the technique was of limited use.

5.5 Summary

Whilst it was not practical to evaluate the accuracy of DWS, the technique was shown to be significantly more reproducible than both the sedimentation and optical density techniques. The work suggested that a reproducibility equivalent to a sub-nanometer size difference was possible. The work also showed that the optical design for the pilot system was successful in generating a signal from the suspension with minimum concentration dependence.

The inability to study the effect of using different fibre NAs and polarisation states, due to physical inaccuracies in the probe blocks suggests that further work could be carried out although theoretical considerations suggest the optimum design was selected for the application.

DWS experiments were carried out at process concentrations where all the existing light based techniques required significant dilution. This led to the problem of calibration of a technique that measured a parameter that is both unobtainable by any other measurement system (a collective diffusion coefficient of high concentration suspensions), and showed variance significantly better than systems operating in dilute suspensions. The problem was exacerbated when dealing with samples that varied with time. The time-dependent behaviour allowed analysis of phenomena that were only present only in concentrated samples, where there was no comparative technique for evaluation. Whilst the exact physics of the variation were not understood the obvious settling of suspensions of a material of 200nm particle diameter, with a relative density of 4, generated a requirement for advances in the model used for measurement. This demonstrated that the analysis of Γ generated from a single correlation was not an absolute number but should be referenced to the time of measurement, and should not be averaged.

Unexpectedly DWS was shown to be only weakly affected by absorption in the continuous phase, for high refractive index particulates. Path-length limitations, due to restricted sample size or laser coherence, are often considered to be the cause of short delay time curvature but this was shown not to be the case in these materials. A novel model of analysis of short-delay time curvature in the correlation line-shape may allow determination of the mean rotational diffusion coefficient of the sample. With significant further work this may allow DWS to measure both mean size and the average aspect ratio, or the type of interactions present. Significant practical problems have been found with sample adhesion although the use of silanised slides was shown to reduce the problem.

CHAPTER 6

Prototype System Development & Evaluation

6.1 Prototype Development

All previous work had been analysed using methods which, whilst not identical, were based on a similar analysis concept. Step 1 analysis introduced the concept of the balance point in the errors between variance and fitting (Section 2.4-2/6). The Step 2 method, whilst allowing finer resolution and analysis of unstable samples, used the same concept in data selection.

However, the analysis of unstable samples had led to two significant limitations:

- The data collection analysis was time consuming, not real time and inefficient in the use of data;
- The method did not allow errors to be estimated in the actual accumulator values, a prerequisite of proper correlation line shape analysis.

These limitations led to a complete re-consideration of the methods and models used in the analysis. For industrial process control the first point was significant: lack of real time analysis made the system unsuited for most process line usage. The second detail was less important for process lines but seen as critical to allow usage of the instrument as a research tool.

Thus, sample instability had led to the existing pilot system that was suited to neither application base. Various iterations of software and methods were attempted to provide a system which would suit either a research or process platform. This section details the final platform produced that was aimed at solution of both limitations and thus, equally suited to either application areas. The limitations of previous methods are summarised, giving the reasons for the dramatic changes in the Step 3 analysis package. This allowed definition of the requirements of the methods and algorithms. The implementation of the algorithms has already been considered in detail (Section 4.3-4, 5) and thus only parts that significantly affected the results of this project are reviewed.

The following section then details the evaluation of this prototype instrument. Size ranking, reproducibility and concentration are considered. The Step 3 method is shown as measuring a similar parameter as Step 0-2, except that a reduced concentration/interaction dependence now appears practical. This is followed by the study of samples that exhibited significant time dependence.

The Step 3 analysis package wass shown capable of following such samples, with the analysis generating meaningful data. Temperature dependence is shown to be similar to previous work.

The final section illustrates the generic nature of DWS applied in two non pigment applications. It is shown that the correlation line-shape contains important information and that in certain cases the instrument factor itself is of secondary importance. The final experiments consider the phenomena of occlusion/localisation, which might allow concentration independent analysis.

6.2 The Step 3 Analysis

6.2-1 Requirement for New Methods and Models

Whilst the pilot system had shown that DWS was a reproducible method of size ranking of similar materials there had been significant inherent limitations in terms of analysis methods and models, namely:

- the correlation line-shapes varied between different types of suspension;
- the concentration dependence varied between different types of suspension;
- the limited resolution of short decay rate (large Γ) samples;
- that large quantities of data required to be stored for off-line analysis (Step 2)
- the samples varied with time;
- the variations of many samples were too rapid to allow evaluation of the sample.

All previous work had utilised variants of the lowest error method from the analysis, Section 4.3-3. This method was robust yet simple but not based on any significant theoretical model, we merely state the straight line part of the correlation should be diffusive and thus always measured this 'portion' of the correlation.

The method balanced curvature in correlation at long delay times versus increased statistical variance at short time scales. Thus when curvature occurred at short decay times, at the front end of the correlation, it was obvious this dramatically affected results and an alternative method was required. The very wide range of decay timescales measurable in DWS (Section 2.2-2/6) had indicated that it would be necessary to alter both the correlator delay and the number of channels used in the analysis, in a manner that was reproducible. In addition, the temporal variations created a significant need for a re-evaluation of both the data collection and analysis methods.

Whilst the Step 2 software had removed the requirement for a pre-measurement, by cycling the correlator delay, this generated vast amounts of data that required off-line analysis. As each 'cycle' contained typically ten measurements the method could only analyse samples which tended to vary over timescales of minutes.

It was obvious that a rapid method was required to allow setting of the correct correlator delay, number of channels and laser intensity. To allow the device to constantly re-set to suit the changing sample, the method required to be automated and to use intelligent feedback.

Previous work (Figure 52,53) had shown the significant difference between fitting errors and statistical variance. The temporal variations made the problem of calculating the statistical variance of the correlation data points more complex, as a simple mean calculation was liable to be a gross overestimate.

6.2-2 Algorithm and Data Analysis Concepts

6.2-2/1 The Correlation Line-shape

The previous chapter had noted that correlation line-shapes varied for different materials. This caused the module that selected the section of the correlation to analyse to be dependent on suspension type. Re-analysis of suspensions that appeared to have been successfully monitored, such as Tioveil, suggested the top 63 percent of the correlation should be used in analysis, to model Step 0-2 methods.

6.2-2/2 Feedback

The temporal variations of the sample required software feedback such that the correct correlator delay could be constantly re-set. This requirement was for near real-time, which was viewed as a significant problem as the actual experiment took a number of seconds, after which analysis and system resetting was required. It was obvious from previous work (Section 5.4-5) that the method required automatically to alter the correlator delay, as well as the number of correlator channels used in the analysis, in a structured reproducible way.

6.2-2/3 Error Analysis

To allow sensible analysis of a function, it is necessary to measure not only the function shape but also the corresponding error and variance in the accumulator values. This would allow both reproducibility and lack of model behaviour to be established, Section 2.4-2/6.

The basic DWS model (Equation 14b) could not be considered a paradigm (Section 2.3-3/4), hence, estimation of statistical variance from the model appeared flawed.

Averaging many correlations, to separate the errors had failed, as the correlation gradient (Γ) was frequently a function of time after mixing/milling/probe insertion. Thus, the error analysis had to allow for the correlator being constantly re-set in near real time. It was know that up to 100 correlations (25,000 data points, each of 32 bit length) may be present in a single analysis. In the Step 2 analysis all data was used in the final analysis but the data collected at delay times furthest from the correct delay, had very little influence on the result, Appendix 3. It was obvious any method that made more efficient use of the collected data would lead to more rapid experiments.

6.2-2/4 Fitting Procedures

Analysis of the correlation line-shape required only conventional two dimensional fitting of the correlation, α versus τ. To allow generation of variance and fitting errors, for correlations changing in time, some type of three dimensional fitting of the correlations was required (α,τ, t).

A three dimensional fit of 25,000 data points is not insignificant and the problem was compounded by the need for near real-time analysis and feedback. It was considered that the method could not utilise conventional file systems or conventional file areas.

6.2-2/5 Measurement Parameters

It was known that the use of two dimensional and later three dimensional fitting would generate a significant amount of data. The increased number of results from different fits led to further complexity that may render it difficult for a user to understand the results.

New measurement parameters were required which allowed definition of the three dimensional surface in a clear and concise manner, whilst ensuring the number of parameters was minimised.

6.2-3 Feedback Implementation

6.2-3/1 Three Stage Feedback Loop

The method and choice of feed back had a significant effect on the fitting procedures. The factor that defined the region of correlation to be analysed was termed f_b and was determined from the baseline so as not to introduce a model error/bias by calculation of the intercept. The user determined which correlator channel, RC, should fall on f_b (default 128 of 256) as well as the value of f_b. The default value of f_b was set at 0.63 (only accumulator values greater than 1.37*baseline used in the analysis), as it gave an equivalent region of the correlation that a Step 2 analysis would select on the water based Tioveil material used as a reference in this work. The ability to modify RC was seen as important in measurement of very rapid decays.

The software required to carry out data collection, data analysis and make a feedback decision prior to the next experiment. This was not seen as viable in real-time, thus initially a three stage loop was designed. After a correlation had been started the previous correlation was analysed and stored. The parameters calculated for the correlation prior to that were used to reset the correlator. This method was considered to reducing down time between experiments. Using this first method the data displayed, and used for feedback, was typically delayed by 15 seconds. This limited its benefits for very rapidly changing samples, Figure 57.

A second problem encountered with the software was actually traced to limitations of the correlator. The high decay rates encountered in DWS would often define an experiment of below 1 second for a 1 percent accuracy. Due to the correlator 'start error' (Section 7.4-3/6), it was necessary to allow a minimum experimental duration to be set, default 1 second. In addition a maximum experiment duration was found to be required to stop data glitches setting very long experiment durations.

6.2-3/2 Two Stage Feedback Loop

It was found that the basic two dimensional analysis and calculation (α,τ) could be carried out in a fraction of a second. Thus, the Step 3 method was actually produced using only a two stage feedback loop. After each correlation the basic analysis, in calculating f_b, was carried out and the correlator reset prior to starting the next correlation.

Provided the measurement duration was over one second duration, the analysis and storage of the previous correlation was complete before the experiment under way was completed. During the correlation the count rate and Γ, of the previous data set, were plotted versus time of measurement, along with all previous measurements. This was fitted with a polynomial (Γ, t) and the parameters displayed. This allowed an 'average Γ' and a measure of statistical variance from the lack of quadratic behaviour in the plot. In addition, the basic correlation fitting errors were displayed.

The actual correlation was not displayed real time. A hardware limitation of the correlator led to display that did not represent the correlation being analysed, Section 7.4-3/5. Different sections of the correlation being output from the correlator at different times leading to a non-continuous displayed function.

6.2-3/3 Feedback loop Complexities, Correlation Delay

The initial software had limitations. One of the most significant problems occurred when starting to measure a new sample. The measurement module would start on a default value of correlator delay time and attempt to modify the correlator settings until the f_b/RC condition was reached, Section 4.3-5/1. Thus, the selected portion of the correlation (f_b) was set to occur at a specific channel number. Where the sample was varying dramatically, typical of milling samples, this led to a significant hunting problem in the first four or five measurements. These measurements required to be removed from the data set prior to analysis to stop bias and unstable fitting. This was overcome by reintroducing a 'start module'. The module contained only the required code from the measurement module to calculate f_b and was coded to run as rapidly as possible. The method took a measurement with the maximum correlator delay and then further measurements at reduced delays until f_b was set at RC. In highly unstable samples, it was known that a statistical error could cause the f_b-RC condition to be met accidentally. This was overcome by requiring the condition to be met a number of times, NT, default value 3.

In unstable samples f_b was not constant for three measurements. This was overcome by ensuring the code required the f_b-RC condition to be met 3 times in sequence.A later addition, to reduce the effects of hunting and glitches, removed the sequence condition such that the f_b-RC only had to be met 3 times in total and that the f_b did not require to be the same value.

The finished method allowed τ to be set typically within 6 measurements, or within one minute, of the measurement start. While testing the module it was discovered that in many instances the decay time would be varied by as little as 25ns when f_b was reset.
Thus the delay would often hunt around the 'correct' correlator delay value. This was limited by the addition of a damping factor, nlim.
The analysis only requiring that the f_b fell on RC+/-nlim to be considered 'correct'. In most instances, a value of +/-1 was found to be sufficient for nlim.

The experiment duration was set to equal a number of decays such that all measurements were carried out with a similar signal to noise. This module automatically started the measurement module when the correlator delay was fixed.

6.2-3/4 Feedback loop Complexities, Channel Number

In samples showing strong temporal variation the channel f_b actually fell on was not RC, as the data was one experiment out of date. In addition, the correlator delay was limited to a minimum length of 25ns x RC, which was a significant sensitivity limitation for rapidly decaying samples.

Both limitations were overcome by using the actual channel that had been closest to f_b when carrying the fit of correlator accumulator channel versus correlator delay time, as opposed to the value defined by RC. This had two secondary beneficial effects in that it reduced the effects of any residual hunting and reduced the effects of any statistical glitches that could otherwise throw the algorithms into an unstable loop.

One of the most significant limits of the DWS package occurred when analysing very complex materials with a small f_b (when only analysing the top few percent of the correlation). If the intercept value was lower than the requested cut-off f_b the sample fell into a loop, as f_b could not be placed on RC. Whilst the value of the first correlator accumulator could be used to set f_b and remove the problem this was not carried out as default as it tended to mask significant sample problems such as adhesion.

6.2-4 Process Control and Research Applications

6.2-4/1 DWS Parameters

The correlation function was plotted as the logarithm of the accumulator value versus the square root of the delay time and then force fitted with both a straight line and a quadratic. This was carried out for the sections of the correlation above and below f_b independently. This itself generated a significant number of parameters to view, which for real-time decisions would not be easy for an operator to follow.

The data was compressed by means of two parameters termed %curvature and %intercept. The curvature compared the gradient from the linear fit with the equivalent polynomial factor, the coefficient of the linear term. Thus, a value of one indicated a straight line.

The %intercept defined the difference in intercepts in a similar manner. In this manner the three terms: linear gradient, %intercept and %curvature defined the instrument response, the straightness of the line and if any non-linear behaviour was at the top or tail of the region of the correlation function analysed.

These parameters were displayed and fitted with a quadratic, versus measurement time, as the measurement module ran. This gave a crude 'mean' value and 'statistical error' continuously, provided the samples were stable or changed in a smooth continuous, single valued manner.

Obviously more complex functions could have been used for the fit but the quadratic was seen as adequate for proof of concept and was robust when noise was present.

Typically 25-100 correlations were analysed as a single measurement. A time delay between measurements could be set, which could be fixed or increased/decreased geometrically. To ensure repetitive background noise, typical of process environments, would not lead to bias part of the delay could be made random.

6.2-4/2 Process Control

The completion of the measurement module effectively gave a practical in-line instrument for process control of samples that were not stable with time. The system allowed a sensible determination of Γ and its variance. The method also allowed highly unstable samples to be analysed, as shown by later milling analysis, Section 6.3-5.

The method was responsive over timescales typically of 2-10 seconds and could output a sensible trace showing variation of a number of simplified parameters within one minute of introduction of the probe, even where samples where unstable.

Output for process control could be generated by the simple addition of a digital input/output card or via a communication/serial port. The anti-hunting algorithms and the method of choice of the correlator delay and number of correlator channels used made the system highly robust to statistical glitches and ensured the system would re-stabilise itself under the most adverse conditions.

6.2-4/3 DWS as a Research Tool

DWS collected 256 accumulator values (α) for each measurement for a set of correlator delays (τ) and at a given time (t), usually set as time from mixing.

Thus, the nature of the data required fits for α versus τ and Γ versus t in real-time. The fit of Γ versus t, as opposed to merely the value of Γ at t, allowed a damped and stable real-time output suitable for process control but did not give the variance in accumulator values, required for a research tool.

The fit of ($\alpha\tau$) versus t for three dimensional analysis was aimed at off-line use for research purposes, when a significant number of points had been collected. Evaluation of three dimensional fitting was carried out with Sigma plot. This took a few minutes to plot a mere 8 correlations in 3D and up to half an hour when 50 or more correlations were analysed (386 computer with maths co-processor). To reduce analysis time the data storage, of the 25,000+ datapoints, was unconventional. Instead of creating a file for each measure of t, which would contain data from a correlation, a file was created for each correlator channel, and analysis parameter. Thus after resetting the correlator and starting a new correlation the measurement module opened, appended and closed 300 files, which could be carried out within 1 second. The files where stored on a high speed RAM 'disk' until the end of each set of experiments when they were copied to the hard disk. The measurements could be stopped early, restarted or reloaded and more data taken as required by the experiment.

Thus at the end of the experiment over half of the analysis had been carried out ($\alpha\tau$ fits) and analysis of the time dependence only required opening and fitting of 300 files. This decreased fitting time to a few seconds even where 100 or more correlations were present.

In addition the parameters from the ($\alpha\tau$ fits) were themselves fitted versus time in the second operation. This gave 16 parameters which crudely defined a 3D surface. Whilst limited by the quadratic assumption, the method indicated a possible method for data compression in storing information on time variant samples in a highly compressed form. It was considered that such methods and data may be ideally suited to neural net or other 'learning' data analysis methods for future use. Data from a complex oil sample analysed later in this work (Section 6.4-3) is given as example, Figure 73

The three dimensional module allowed any stored data or parameter to be plotted versus any other. This was shown to be useful in data selection and analysis of time dependant samples, Figure 74.

6.2-4/4 Module Algorithms

On loading, the final analysis module displayed the same points as the measurement module such that the gradient, %intercept, %curvature and runs in polynomial fit were displayed against measurement time. Each parameter was fitted with a polynomial via time and the value at the centre of each measurement was given. Moving the screen cursor automatically updated the fits such that the values at that time defined by the cursor were displayed.

The operator could select the first and last data point to use in the analysis and remove glitches within the data set before requesting a three dimensional fit. The file management system used in the measurement modules required only 300 files to be opened and 300 second order polynomial fits to be carried out and thus the three dimensional fit was generated in near real-time. The second order polynomial was selected as a stable analytical fit which would allow for variations such as settling.

A three dimensional image was not generated, as this was believed to be difficult to interpret, but a correlation function at a pre-set time was generated. This assumed a 2^{nd} order polynomial variation in the correlator channels and allowed a variance error to be generated for each channel. This correlation could be scrolled in time allowing the correlator line-shape to be studied as a function of time from the experiment start.

6.2-5 The DWS package

The software arrangement and experimental methods were deemed complete, in so far as required by the project. The DWS arrangement, methods and algorithms allowed for real-time in-line monitoring of complex, unstable suspensions, including those with materials added for the purpose of making the material adhesive. In addition, the package appeared to be an adaptable research tool. A set of output traces for a complex oil sample exhibiting temporal changes as well as significant front end curvature have been given as an example. This sample could not be properly analysed by earlier methods as the sample altered too rapidly. Immediately after a collection of correlations, the first correlations, before significant temporal variation were selected (Figure 72) and a three dimensional analysis of the correlation data performed. The raw correlation curve is typically of little use, instead the correlation was normalised to the fitted intercept (Figure 73). The intercept value of almost 1.2 immediately shows that the function being analysed does not fit the basic DWS model used in this work. This is also obvious from the logarithm versus square-root plot shown below, the trace is not linear. The variation in size, with time, may be attributed to a build-up on the probe window, as indicated by the sinusoidal count rate variation and dramatic jump in the correlation decay time, Figure 74. The abnormal tail of the correlation can be observed to occur between blocks of 16 channels. This was found to be due to saturation of these longer time channels of the correlator, these were ignored in the analysis.

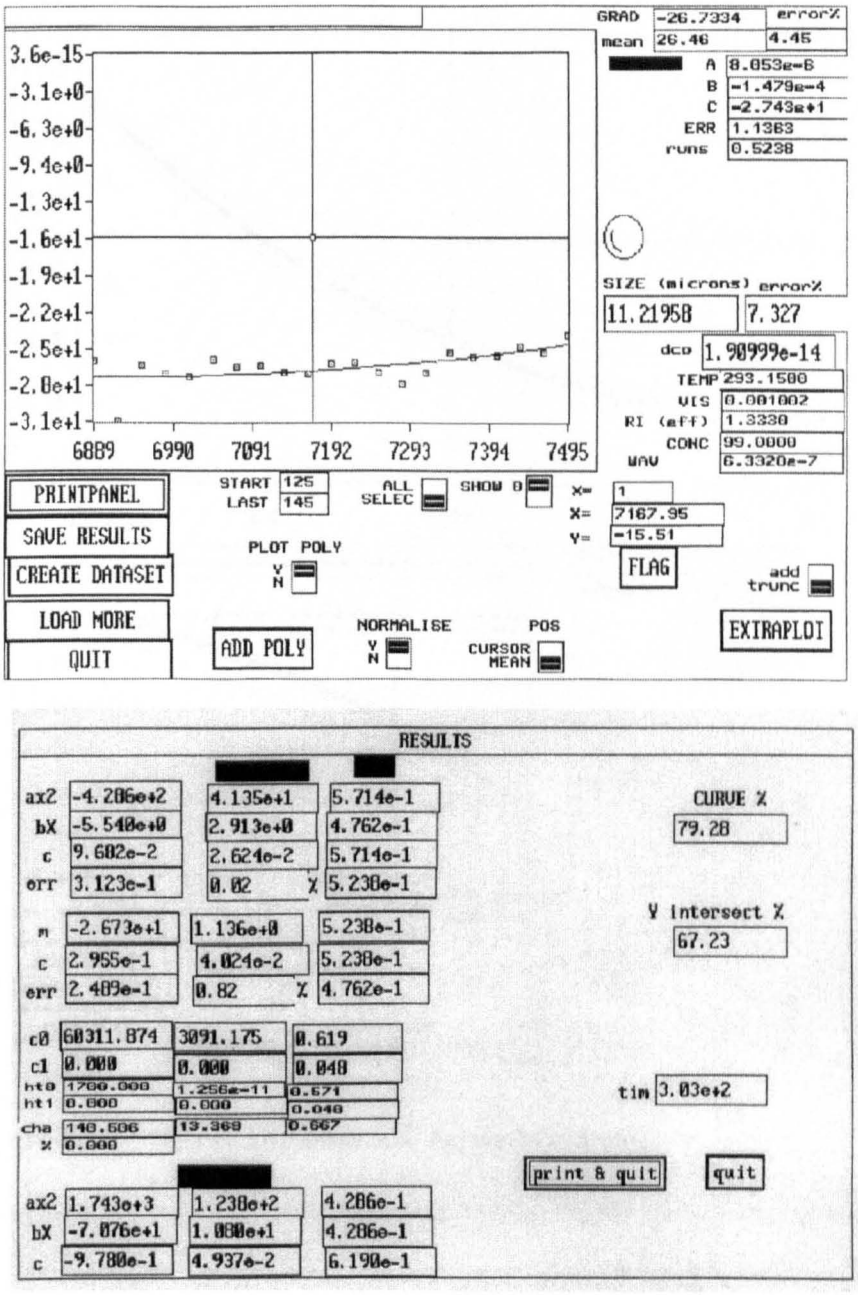

Figure 72 Real Time Instrument Output

The analysis module output, after selection of data points to use in analysis, top plate, showing the variation in instrument response with time and the various fits carried out, analysis is at the centre of the selected point range as default, lower plate. The figures shows a systematic but low decrease in instrument response with time. More detailed analysis output for both the area above and below the selected area f_b was available as a pop up screen, lower plot. The parameters, error from the model used in the fit and variance all being given. Sample contaminated oil sample as Section 6.4-3

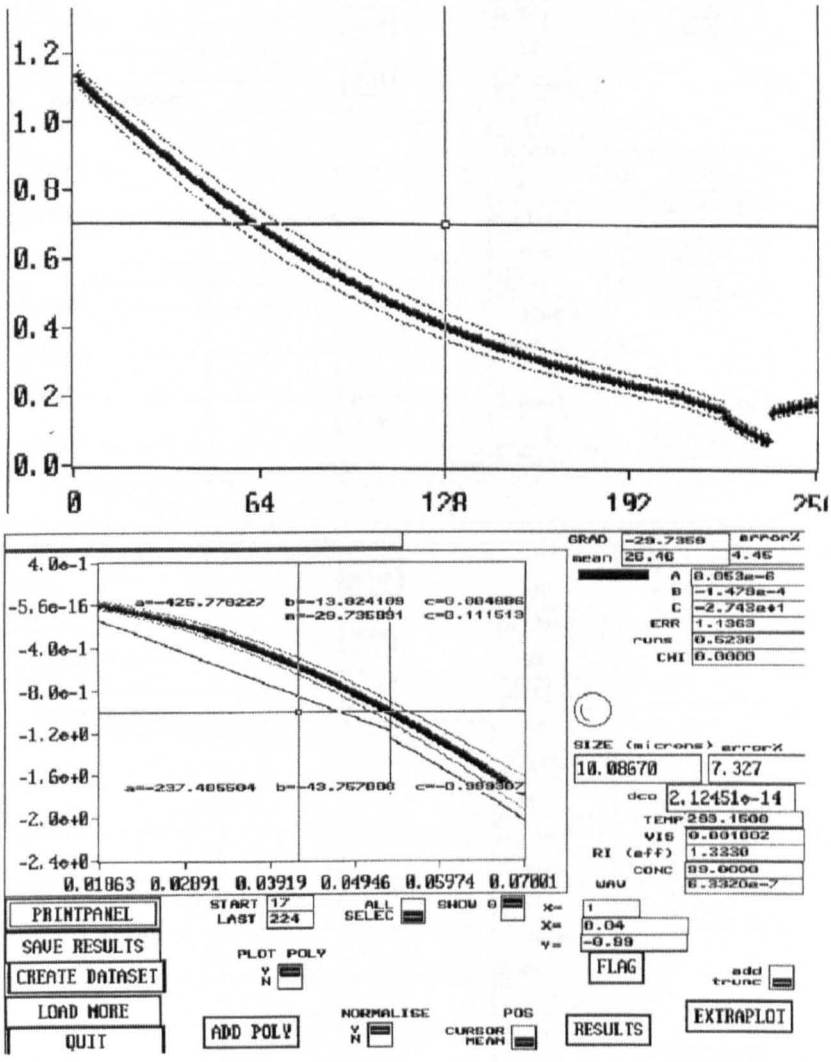

Figure 73 Three Dimensional Analysis Output

Fitting the actual correlation points of the selected data (Figure 72) with respect to time of measurement allowed generation of a correlation function with errors given for each correlator channel at an interpolated time of measurement, top trace. The discontinuity in the correlation at long τ is due to accumulator over-fill, these points were not used in the fit. The display was normalised to the fitted y intercept thereby allowing visualisation of model discrepancies from the raw correlation, upper trace. The correlation and errors were then used to produce a log accumulator versus square root delay time plot, which was re-fitted as if it was a direct data correlation, lower trace. The fitted straight lines being offset from the actual data for clarity and the fitted quadratic (not visible) were plotted in position above the data points in a separate colour on the display, with the error in each channel also being displayed.

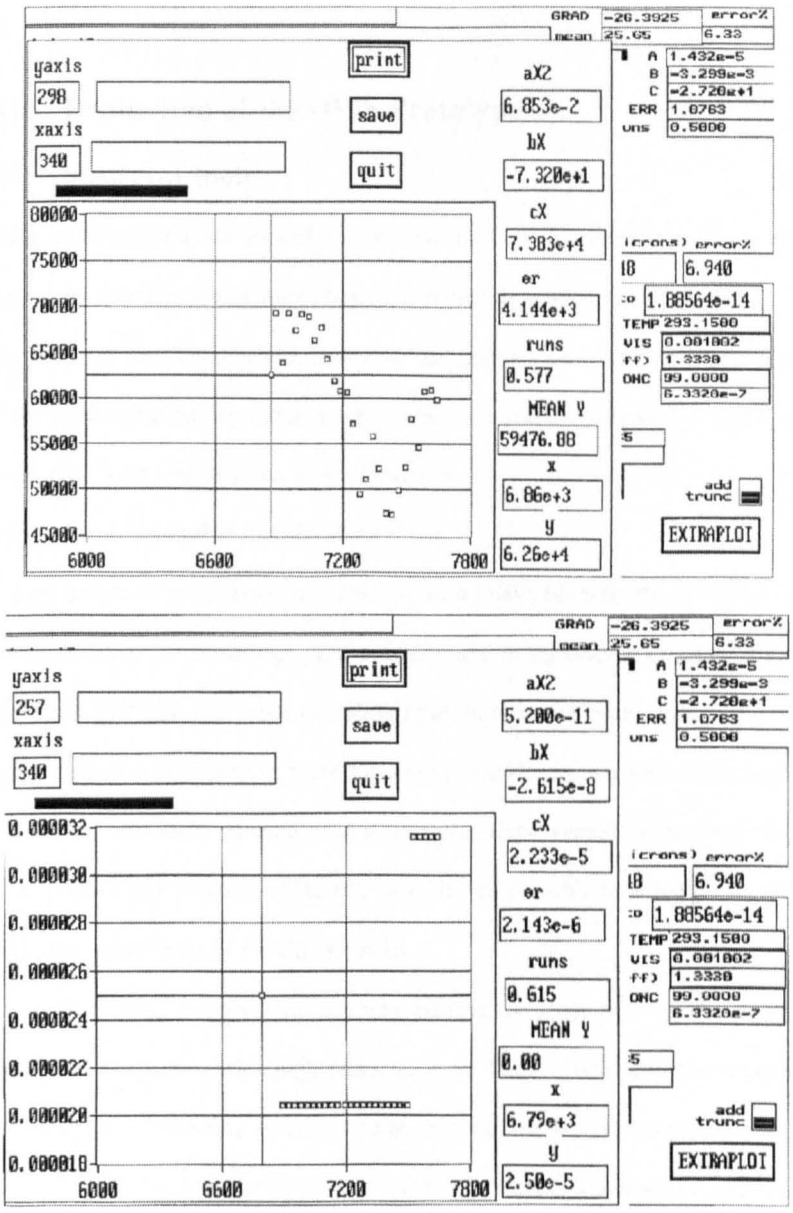

Figure 74 Ancillary 3D Plot Output

The ancillary 3D output allowed any stored data to be plotted versus any other. The top trace shows the count rate alters dramatically from time of measurement in a sinusoidal fashion. This is typical of the build-up of a film on the probe window acting as an etalon. The lower trace shows the correlator delay used in each measurement versus time of measurement and was useful in selection of data for three dimensional fitting. The film build-up eventually leads to a reduction in correlator decay that is probably due to the increase of the lower frequency heterodyne. These auxiliary traces give more information than simply the plot of Γ versus time (Figure 72) that suggests a stable sample. They were also useful selection of sensible data to produce the three dimensional mean correlation, Figure 73.

6.3 Evaluation of the DWS Prototype

6.3-1 Method of Study

Having established a new model for evaluation of DWS parameters, re-calibration was required to ensure Step 3 analysis was valid. Major previous dependencies (temperature, concentration, pigment type) were re-checked, to ensure the analysis was a strong function of particle size, and that the concentration dependence was a smooth continuous function. Additionally more control of the concentration dependence was considered.

6.3-2 Ranking and Reproducibility

The optimum way to analyse size ranking would have been to obtain a large selection of different latex beads all at the same high concentration and in significant volumes. The industrial partner could not supply this and costs prohibited purchase in this work. Samples of high concentration polystyrene, of a similar type, were supplied (Tioxide) in two sizes and diluted to a volume fraction of 0.125, the area least affected by concentration dependence in previous work. By mixing different ratios (by volume) of the two sizes it was possible to generate samples deemed equivalent to different mean sizes of similar material.

The effect of polydispersity was assumed to be minimal on the initial decay of the correlation line-shape at this high concentration. Thus, it was possible to prepare a number of stable samples of differing particle size by mixing two samples of polystyrene beads supplied by Tioxide, Figure 75. The top 63 percent of the correlation was used in analysis, evaluation of earlier Tioveil results suggested typical region selected by earlier software. Straight line and quadratic fits (correlation coefficients of 0.975 and 0.997 respectively) to the trace indicated a linear relationship with theoretical size by volume, within experimental errors. Results were generated from the three dimensional fit. One hundred experiments were gathered on each of the pure 240 and 450nm samples, with experimental durations of around 3 and 5 seconds respectively. The experimental duration was set using a constant 10^5 coherence areas (Equation 65) indicating a theoretical error of the order of 0.33 percent. The average variance was of the order of 1 percent, equating to +/- 3nm for the size range under measurement. The samples were noted to be stable in time. Selection of smaller subsets of data points gave similar errors, indicating this was the minimum practical error of the instrument, independent of the number of the experiments carried out. The actual difference in size between the polystyrene suspensions was of the order of 1.875, independently checked by PCS.

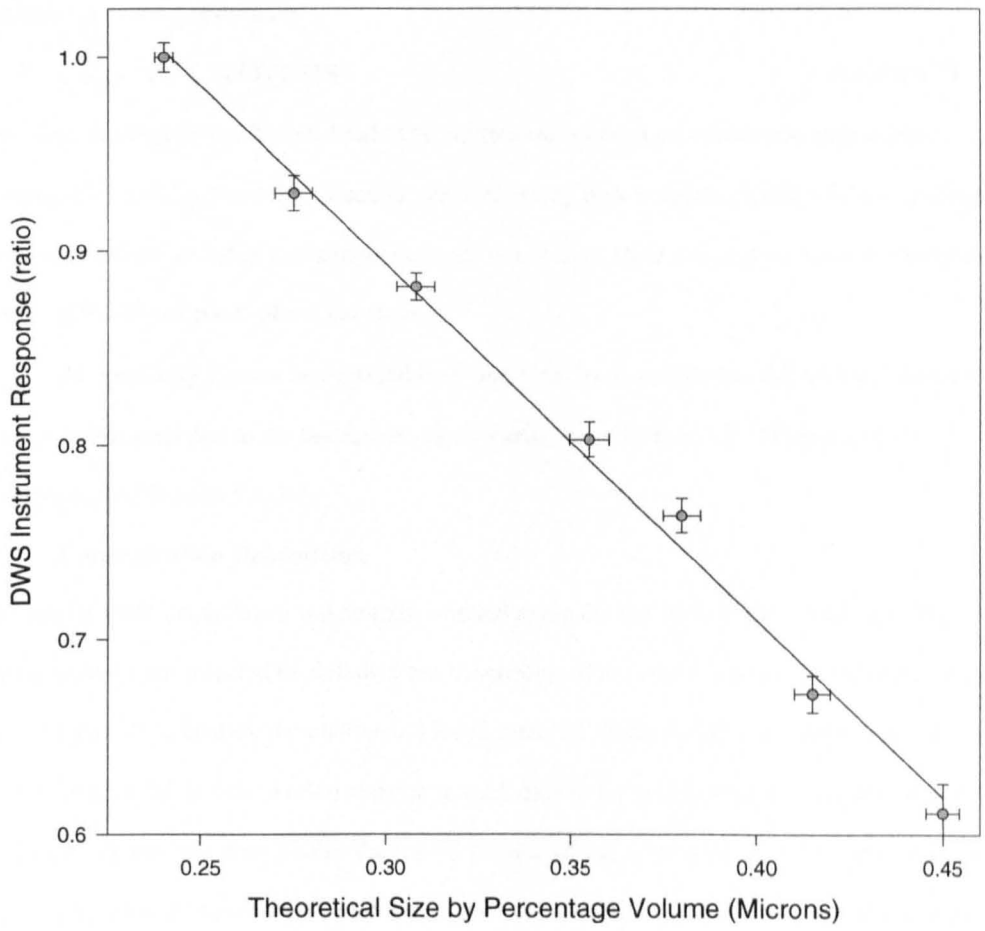

Figure 75 Ranking of DWS Using the New Methodology

Mixtures of 240 and 450nm polystyrene beads at volume fraction (ϕ) of 0.125. Γ is plotted against theoretical size by volume, with errors in volume fractions estimated. The variance (average of all data points on graph) was 1.114 percent, which equates to less than 3nm.

The error bars of all data points appear to intersect the fitted line suggesting the volume weighting is at least correct over the range of sizes measured.

Straight-line fitting gave a $DWS_{240} = -1.3184 size_v + 1.3188$, $r^2 = 0.994$, where $size_v$ is theoretical size by volume, and DWS the size relative to 240 nm polystyrene bead, assuming $\phi = 0.125$.

The graph shows the instrument function normalised to a 240nm bead thus the transform for Γ:

$\Gamma = \Gamma/\Gamma_{240}$, where Γ_{240} is the value for a 240nm bead at a volume fraction of 0.0125

The DWS results indicated the instrument response difference of the order of 1.35. This allowed instrument response calibration

$$size_v = (\Gamma_n - 1.3188)/1.3184 \qquad \text{Equation 74}$$

where $size_v$ is relative to a 240nm bead. The calibration is based on normalised instrument response ($\Gamma_n = \Gamma/\Gamma_{0.125}$) and thus assumptions concerning how to relate mobility factors, diffusion coefficients refractive index and temperature are minimised. However, it does assume a volume fraction of 0.125 and hard sphere interactions.

Alternatively Γ_n may be replaced by Γ and $size_v$ by $size_v/240$, but the measure may vary between instruments due to the instrument factor variations (Section 7.2-1/3) and particle refractive index, Section 5.4-2/1.

6.3-3 Concentration Dependence

The concentration dependence was initially studied using the top 63% of the correlation, Figure 76. This value had been selected by default from the section of the correlation produced from using the Step1, 2 methods to analyse the undiluted Tioveil material. In these earlier methods, the balance between error in the fit due to relative noise in each data point versus error due to curvature in the correlation tail was minimised when the top 63 percent of the correlation was analysed, Section 2.3-2/5. The manner the software selected the portion of data was actually by calculation of the baseline, thus in practice it was the area of 1.37*baseline used in analysis. The beads were supplied at a volume fraction (ϕ) of 0.4 and studied over a relatively wide range of 0.05 to 0.4. Two factors were apparent immediately:

- the concentration dependence was higher than the Step 1, 2 methods;
- the ranking ratio (ratio of Γ for 240/450) was not significantly affected by concentration over a range of ϕ=0.1-0.3.
- the ranking ratio decreased at higher concentrations

The latter point was obviously highly significant as it covers the range of conventional pigment milling where the technique may be applied.

The reduction in ranking, at high concentrations, might have been expected from the hard sphere model, where the effect of interactions are a function of cross-sectional area, via collision frequency.

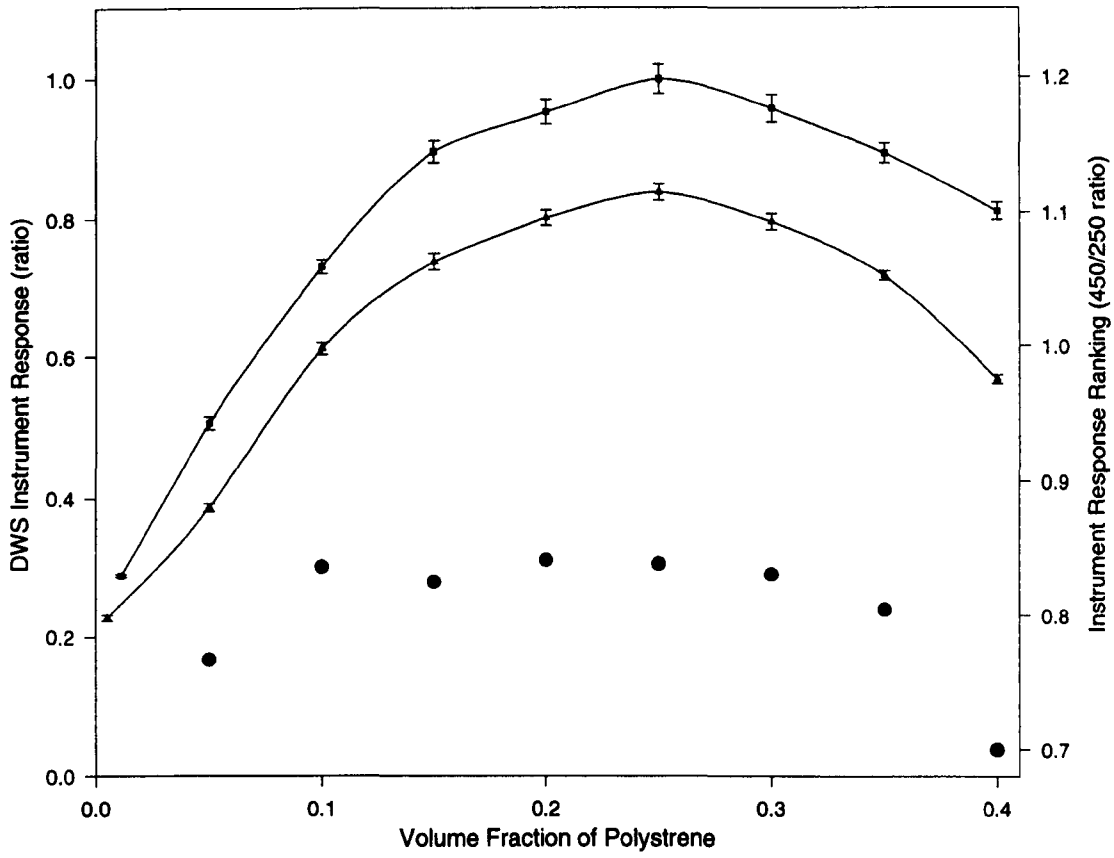

Figure 76 Concentration Dependence, using top 63% of the Correlation

Concentration dependence of the top 63 percent of correlation for 240nm and 450nm polystyrene beads, upper traces left hand axis, squares and triangles respectively. Instrument response normalised to the maxima of the 240nm bead trace, ϕ= 0.25. Ranking of the two beads remains constant to within a few percent between volume fractions of 0.1 and 0.3, circles, right hand axis, solid circles. Statistical variance, RMS errors, shown. Data generated from three dimensional fits at mid experiment time. First and final data points from 100 separate correlations, other data points from 25 separate correlations, statistical variance errors shown.

Transform for Γ: $\Gamma = \Gamma/\Gamma_{25}$, where Γ_{25} is the mean value for a 240nm bead at ϕ=0.25.

Transform for Ranking: Ranking = $\Gamma_{450}/\Gamma_{240}$, where the subscripts define bead size.

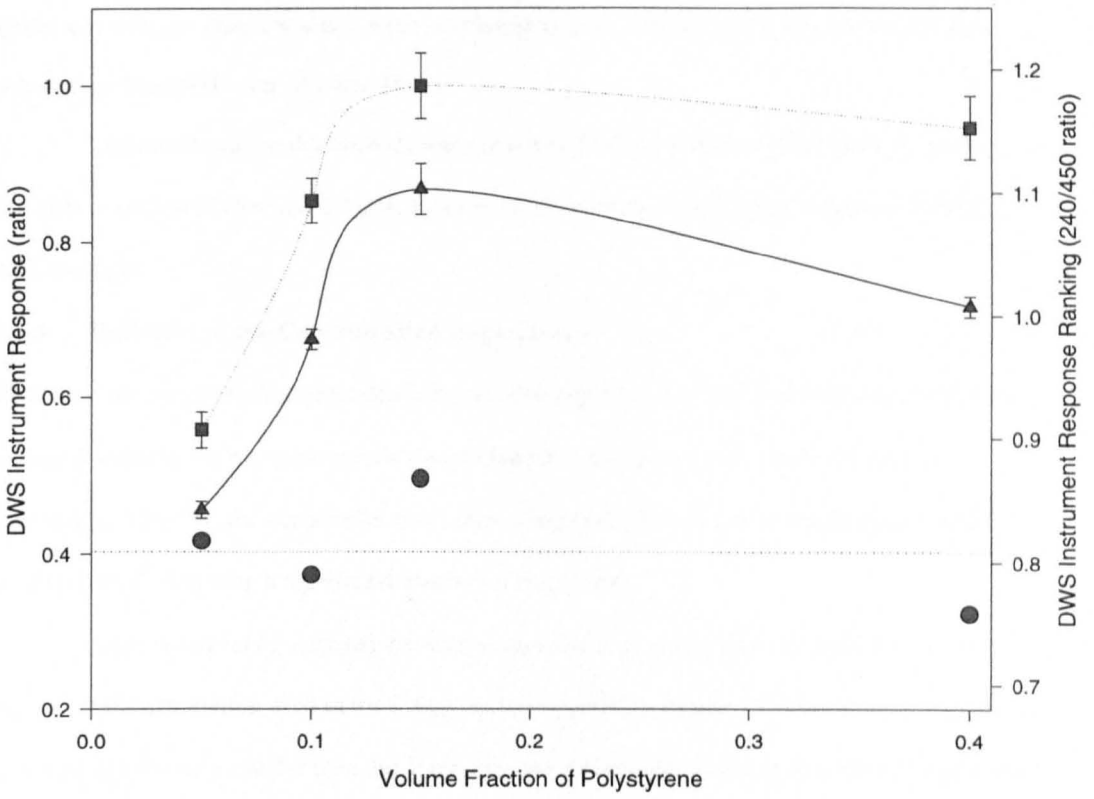

Figure 77 Concentration Dependence using Top 27% of the Correlation

DWS instrument response with concentration on 240nm (squares) and 450nm (triangles) polystyrene beads with the top 27 percent of the correlation used in analysis, left hand axis. Cubic spline of best fit shown. Instrument response normalised to the 240nm bead, $\phi = 0.15$.

The ranking of the instrument stays within +/-8 percent of the mean over the entire concentration range, lower trace and right hand axis, and is thus flat within experimental errors. Each data point generated from a three dimensional fit of 25 separate correlations at a time of mid experiment. Statistical variance errors shown.

Transforms as Figure 76.

The reduction in the diffusion coefficient appears to become significant at ϕ=0.4. This appeared in agreement with the glass transition where diffusion is zero, which is generally around 0.5 for polystyrene beads (Hoover and Ree 1988).

The concentration dependence was considered to be a function of the quantity of the correlation measured (Section 2.4-2/4, Figures 12,13) with the initial decay weighted towards diffusive light.

6.3-4 Variation of the Concentration Dependence

To reduce the concentration dependence it had been argued less of the correlation tail should be analysed. Initially the previous graphs were reanalysed, using a smaller sub-section of the correlation; however, the square root plot of the data points limited the variation that could be obtained, while retaining a significant number of data points.

A restricted set of suspensions were re-measured, as previously but with only the top 27 percent of the correlation used in the fitting analysis (f_b=0.63), Figure 77. This fraction was chosen as it was significantly smaller than the value used previously, whilst being considered large enough to ensure intercept/baseline errors did not effect the correlation, Section 3.2-2/7. The results were also plotted together for comparison (Figure 78) with the ratio of the ranking ratios given.
The results indicated that the ranking ratio was similar at around 0.8. A small but significant decrease in the upper concentration effect was noted along with a significant decrease in the concentration dependence at lower concentrations. The data thus supported the premise that reduction in the portion of correlation analysed reduced the effects of low order scatter.

The results also showed a significant downside to analysis of a reduced section of the correlation, the variance of the data increased significantly. This agreed with the earlier concept of the Step 0 fit, using too little of the correlation curve resulting in amplification of the errors in each correlator channel, Section 6.3-4. Results attempting to use only the top 10 and 15 percent of the correlation failed completely. Whilst using the baseline as the reference ensured bias in measurement of the intercept was not transmitted to the results, it could cause the system to look for data in areas above the actual intercept, where obviously no data existed, making the model non-physical.

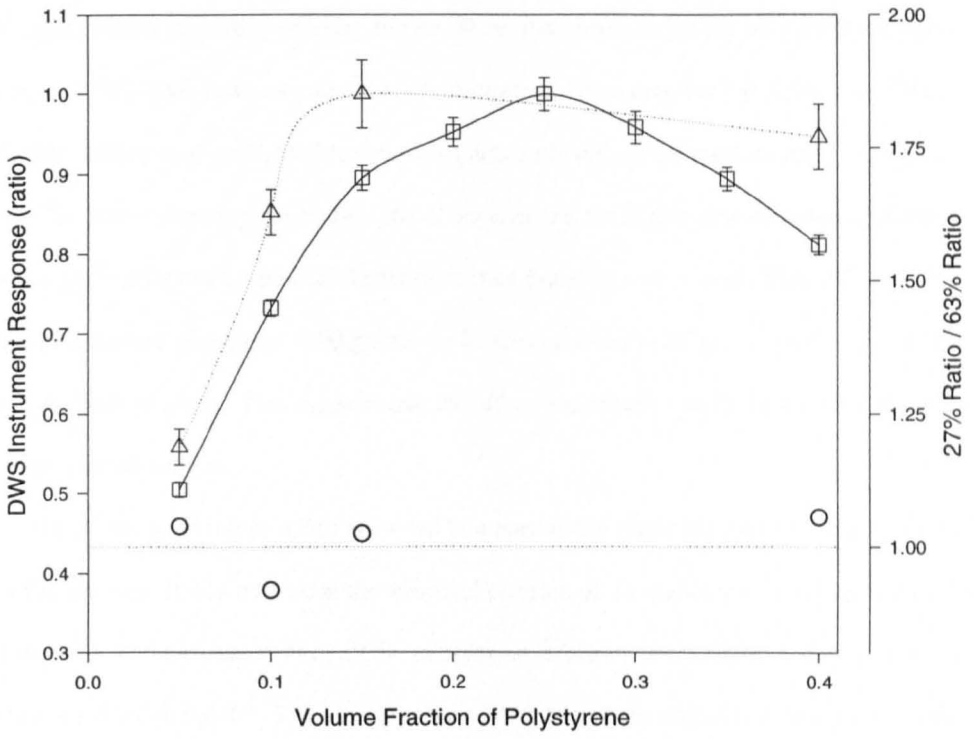

Figure 78 Delay Time Effect on Concentration of Dependence

The upper traces show the DWS diffusion coefficient from both the 27 and 63 percent analysis, of the 240nm polystyrene beads, triangles and squares respectively, Figures 76,77. The maximum instrument response has been normalised to 1, in each case, to allow consideration of the line-shape as opposed to magnitude. Analyses of shorter regions of the correlation reduce concentration dependence, but significantly increase statistical variance.

To ensure the ranking was not weighted to shorter or larger apparent particle sizes, with concentration, for the two analysis methods the relative ranking is given, open circles, right hand trace. This function will magnify differences in ranking of the methods but trace remains constant to within a few percent indicating both traces are measuring similar parameters.

Transform for Γ: $\Gamma = \Gamma / \Gamma_{max}$, where Γ_{max} is the maximum value for that bead size.

Transform for relative ranking: Ranking = $(\Gamma)_{63} / (\Gamma)_{23}$, where 63/23 define fraction of correlation used in the analysis.

6.3-5 Temporal Effects

The ability of the new method to allow for suspensions that varied with time was well illustrated by experimental results of milling of TiO_2, Figure 79. Milling was carried out on samples at volume fractions of 0.025. This is double the usual concentration, when used for the down-scaled milling model, thus milling took considerable time to significantly reduce the particle size.

The traces were typical of this type of experiment, the higher concentration appeared to produce significantly more temporal fluctuations than found in earlier work, Figure 57, 66. The higher concentration of pigment (100 grams per litre as opposed to 50 grams per litre) visibly affected the bulk viscosity. This suggests that the effect was simply due to the air taking longer to escape the viscous sample.

In all cases, an initial erratic trace led to a reasonably stable area, before settling caused further fluctuations. It was noted that the temporal position of the stable area was itself a function of milling time, and measurement of all the samples, at arbitrary common time after milling, would probably fail, Section 5.4-4/5. The sample settled into a two phase suspension, the process termed subsidence, allowing light to escape from the sample. The trace shape was noted as being significantly different to that of earlier work (Figure 57) further supporting the hypothesis that only at low concentrations, where the sample is properly milled, polydispersity information may be available. In these high concentration samples no long term time dependence could be analysed and it appears subsidence predominates. However, it appeared how long the plateau region occurred for (prior to subsidence reducing Γ) may itself be a measure of how well the sample is dispersed.

The initial delay time setting module was shown to be able to select the correct correlator delay within three experiments. In the measurement section, the correlation limits (nlim) were set to vary by the equivalent of a single channel, with no hunting of the correlator delay evident. It was considered this work fully exemplified the ability of the DWS package to follow the rapid fluctuations present in the milling sample, Figure 80. It would obviously have been very time consuming to attempt to find the plateau region (and thus correct correlator delay) using Step 1,2 methods, requiring at least 2 separate samples to be milled, Section 5.2-4/3.

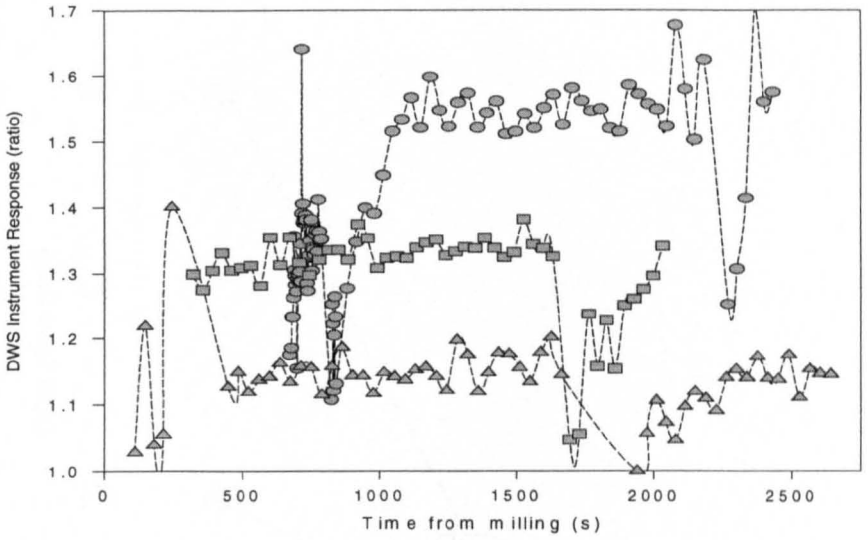

Figure 79 Analysis of Milled TiO_2

The change in instrument response analysed by DWS for both milling and standing time, of a rutile pigment (7089/1) at 100 grams per litre. Key 4 minutes milling (triangles), 11 minutes milling (squares) and 23 minutes milling (circles). Transform for Γ: $\Gamma = \Gamma / \Gamma_4$, where Γ_4 is the lowest value for 4 minutes milling.

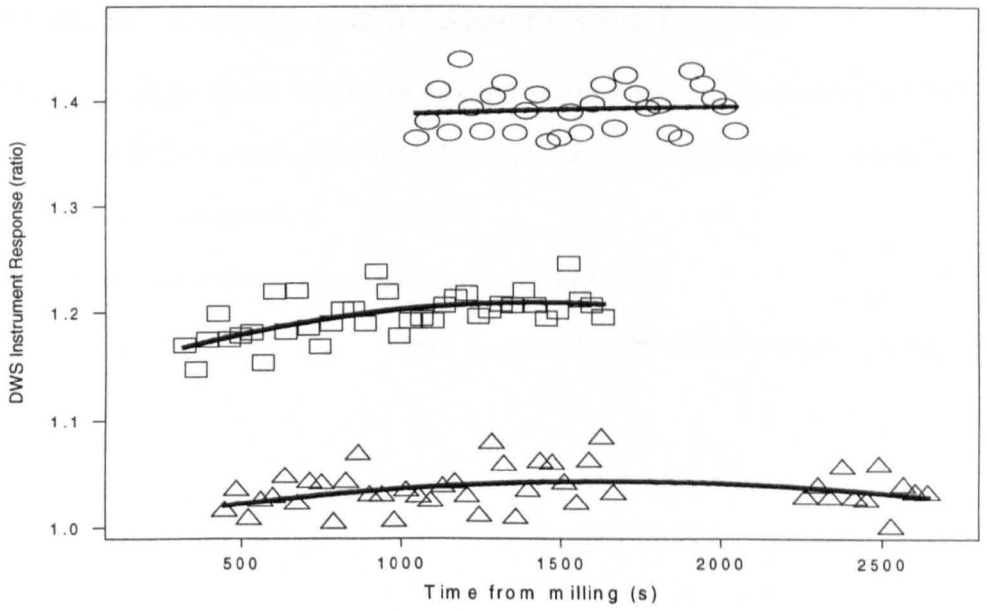

Figure 80 Selected Points of Milled TiO_2 Used in Final Analysis

Selected points (Figure 79) used in the final analysis of the data. Key and Transform as Figure 79, quadratic fits shown.

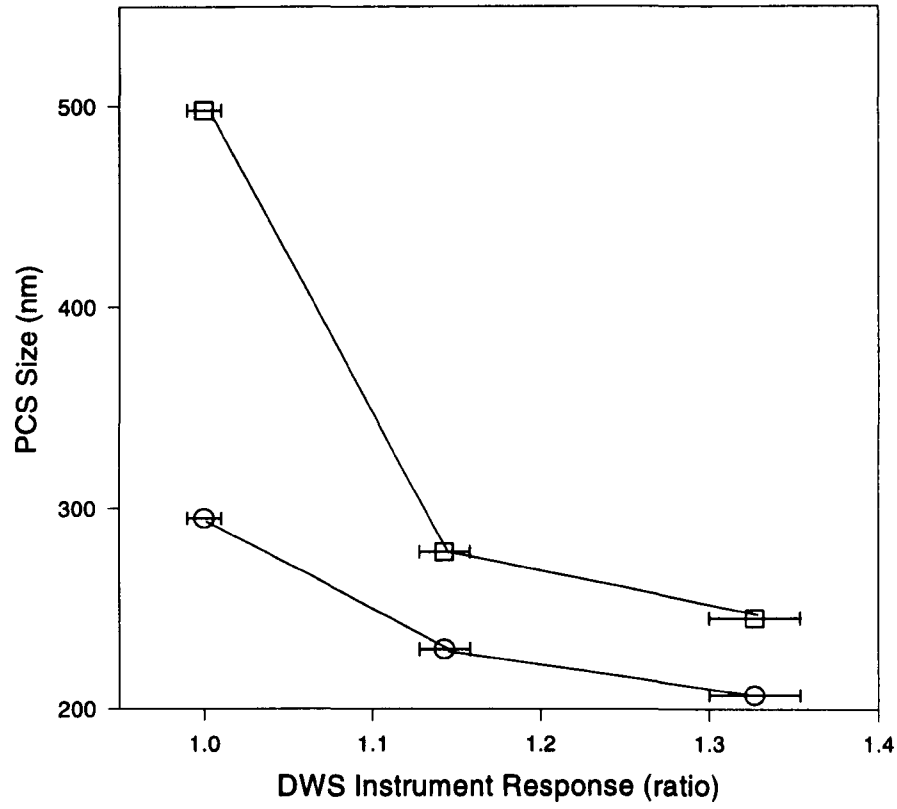

Figure 81 Comparison of DWS and PCS Size Estimates

The plots show the similar function for measured size as a function of milling for PCS and DWS but suggest DWS is better related to the Z average size. DWS is obviously not affected by the same R^6 intensity weighting as PCS

PCS intensity distribution (square) and Z average (circle) sizes

Transform for Γ: $\Gamma = \Gamma / \Gamma_{A4}$ where Γ_{A4} is the average Γ after 4 minutes milling, Figure 79

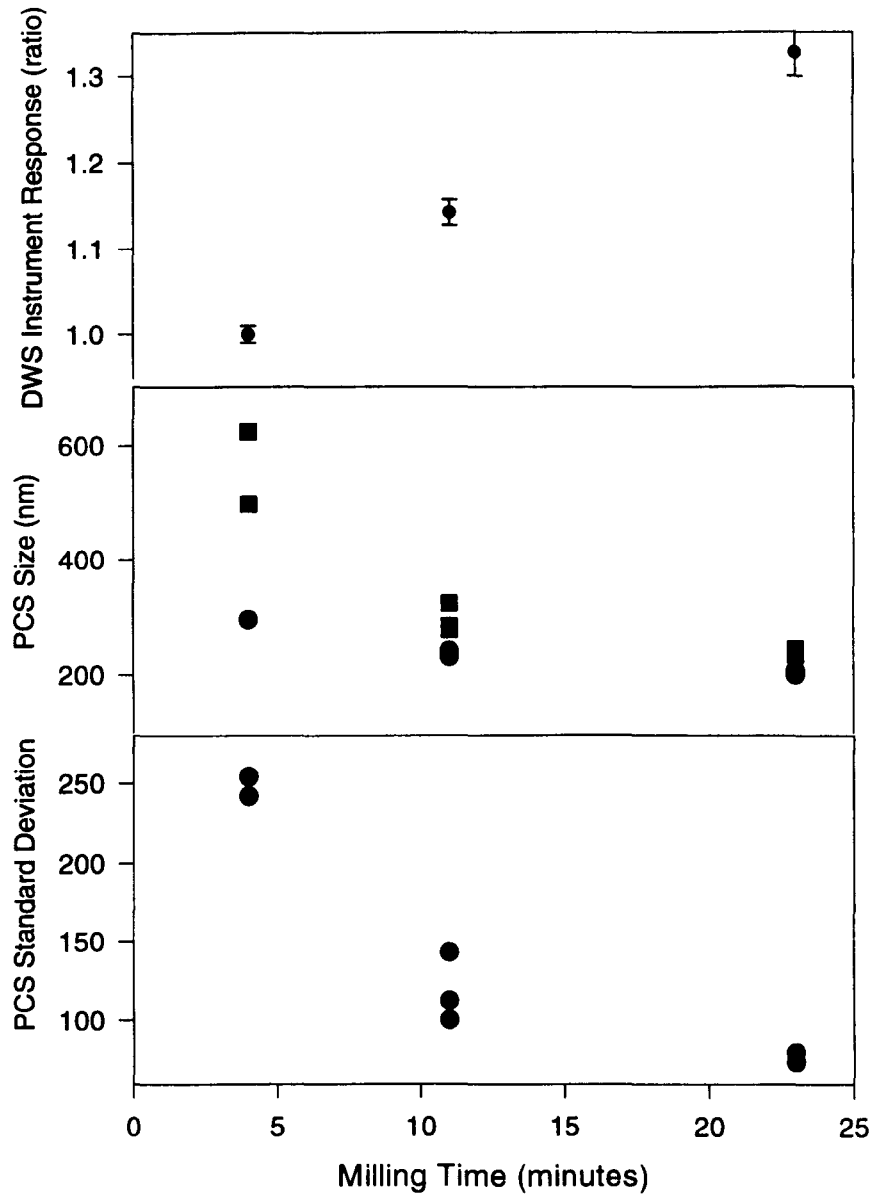

Figure 82 Comparison of Different PCS Size Distributions and DWS

The PCS results also indicate the reduction in the distribution width with increased milling.

Top trace: DWS Γ from 3D to mid point of selected data Figure 79, Middle traces: PCS intensity distribution (square) and Z average (circle) sizes. Lower trace: PCS Standard deviation.

Transform for Γ: $\Gamma = \Gamma / \Gamma_{A4}$ where Γ_{A4} is the average Γ after 4 minutes milling, Figure 79

Whilst a simple polynomial fit to all data points may not have been optimum function for the real-time display, it allowed the plateau region to be clearly visualised. This work gave a clear indication of why the software was written to allow interpolation of results (Figure 68), as opposed to an extrapolation, Figure 67. These results were compared to measurements taken by PCS (by Dr R J G Carr). Increased milling not only reduced the size, but also the standard distribution, as the larger particles were ground down to the base crystal size, Figure 81. DWS showed a stronger relation to the Z average size (Figure 81, 82) than the intensity distribution. Thus, DWS appeared to have a weaker response to small populations of large particles than conventional PCS.

6.3-6 Effect of Temperature & Viscosity

The previous chapter discussed the difficulties encountered in causing major variations in only the viscosity of samples, Section 5.3-5/2. In addition exactly which viscosity should be used, in any size analysis, is ambiguous, Section 5.4-2/3.

For an industrial measurement technique, aimed a at single application, the absolute viscosity dependence is probably of little importance. The viscosities and refractive indices are often unknown in final manufacture, pre-processed OEM materials being used in a product, Section 2.2-1/4. The more important factor is the combined effect of temperature, including its effect on viscosity and refractive index. These may be measured and placed in the look up files used by this DWS software. Results of the temperature dependence of the 240nm suspensions at a volume fraction of 0.125 indicated an identical, within experimental errors, variation in instrument response to that of the Tioveil suspension measured previously, Figures 83, 60 respectively. The measured gradient of the polystyrene dependence was 0.0128, correlation coefficient 0.991, within 3 percent of the Tioveil response. For both materials, the collisional properties are predominantly hard sphere. Experiments were carried out heating the 180nm latex sample, which had exhibited some adhesion, but the sample became unstable coming out of suspension out rapidly.

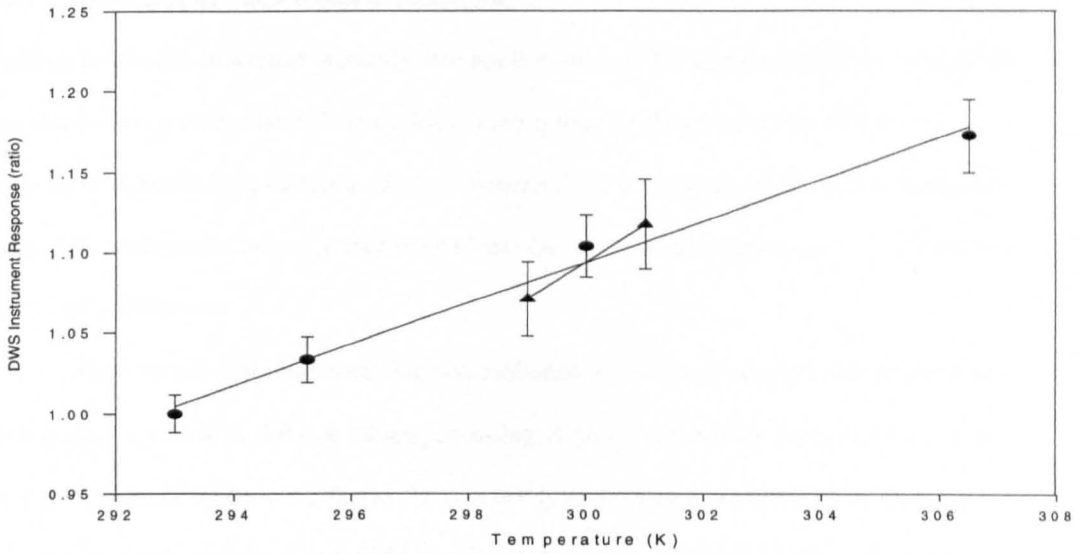

Figure 83 Effect of Temperature

A sample of 240nm polystyrene beads, circles, at a volume fraction of 0.125 at a range of temperatures. Two data points, triangles, taken during cooling not used in the analysis.

Transform for Γ: $\Gamma = \Gamma / \Gamma_{20}$, where Γ_{20} is the average value at 20^0C.

6.4 Applications of DWS to Other Commercial Materials

6.4-1 DWS Applied as a Generic Technique

Previous results are concerned primarily with application of DWS to pigment applications. DWS was also tested on other materials to evaluate if the system produced had more widespread application. A feasibility evaluation of two commercially interesting materials appeared relevant. Both applications were chosen as they were highly dissimilar to the pigments and significant tests of the DWS instrument.

High density cell line processing was evaluated. Unlike pigment applications there was not a gradual decrease in cell size during processing. A cell is either lysed (such that little or no 'particle' exists) or remains unaffected. Thus in cell lysis the major variations are that of concentration and viscosity. The initial viscosity of the sample is usually complex due to the requirement for growth media and because the cell concentration is unknown. The process occurs within a sealed sterile environment where viscosity measurements would lead to wastage of high cost/low volume materials. Initial volume fractions as high as 0.4 may occur and this work increased that to a near gel transition point by sedimentation.

On lysis the cell contents are released which causes a significant change in sample viscosity. Thus, this material appeared a good selection to study media with complex interactions.

The second application studied was cutting fluids. These materials are oil in water dispersions where the oil is brown and was known to absorb of red light. The process to model cutting fluid failure was the addition of tramp oil (heavy black grease). This was believed to affect particle size and was known to decrease the efficiency of the cutting fluid. This second application was selected as earlier data had suggested DWS could operate in systems of absorbing particles (Section 5.4-3/3,4). The application would test if the ensemble averaging and high sensitivity, of DWS, would allow analysis of a change in the absorption properties of small percentage of the particles.

6.4-2 High Density Cell Lines

6.4-2/1 Use of Cell Lines

Microbiological cell lines are grown within industry for a number of commercial activities. CAMR uses the process as a high expression vector in order to grow large amounts of protein products.

The ability to monitor the life-cycle of the product is important in maximising yield, preferably monitoring occurring through a port in a fermentation vessel whilst retaining the vessel's integrity. At present samples need to be removed and diluted for analysis. This reduces yield, reduces the sampling rate and increases risks to both the product and operator. The ability of DWS to operate using a small economic probe, in retroreflection, suggested it might be an ideal choice for the application.

6.4-2/2 Experimental Results

A sample of yeast was made available by the production department. The exact concentration was unknown as the material was too dense for their high concentration optical density techniques. The sample was allowed to stand at room temperature for 48 hours to settle. After which, the supernatant was poured off. Measurement of the viable counts indicating 10^{10} live cells/ml. The suspension behaved more as a plastic, than a liquid, due to the concentration, which suggested a volume fraction of the order of 0.5.

The suspension was measured using the DWS software after various amounts of ultrasonic cell breakage. The sample was packed in ice to stop overheating during the breakage process. The analysis of instrument response versus ultrasound time suggested no sensible data could be extracted as the correlation gradient Γ appeared to vary in a random manner during processing, Figure 84.

However, the newly introduced parameters %intercept and %curvature indicated data could be obtained but not using a standard 'sizing' parameter. These parameters reduced systematically with processing, indicating a straightening of the correlation line-shape. Additionally the measured count rate decreased suggesting a decrease in particle number.

The difference in the correlations was exemplified from the three dimensional fitting of the data sets before and after processing. The change in the correlation line-shape being dramatic, Figure 85. Viable counts indicated that at least 95 percent cell breakage had occurred.

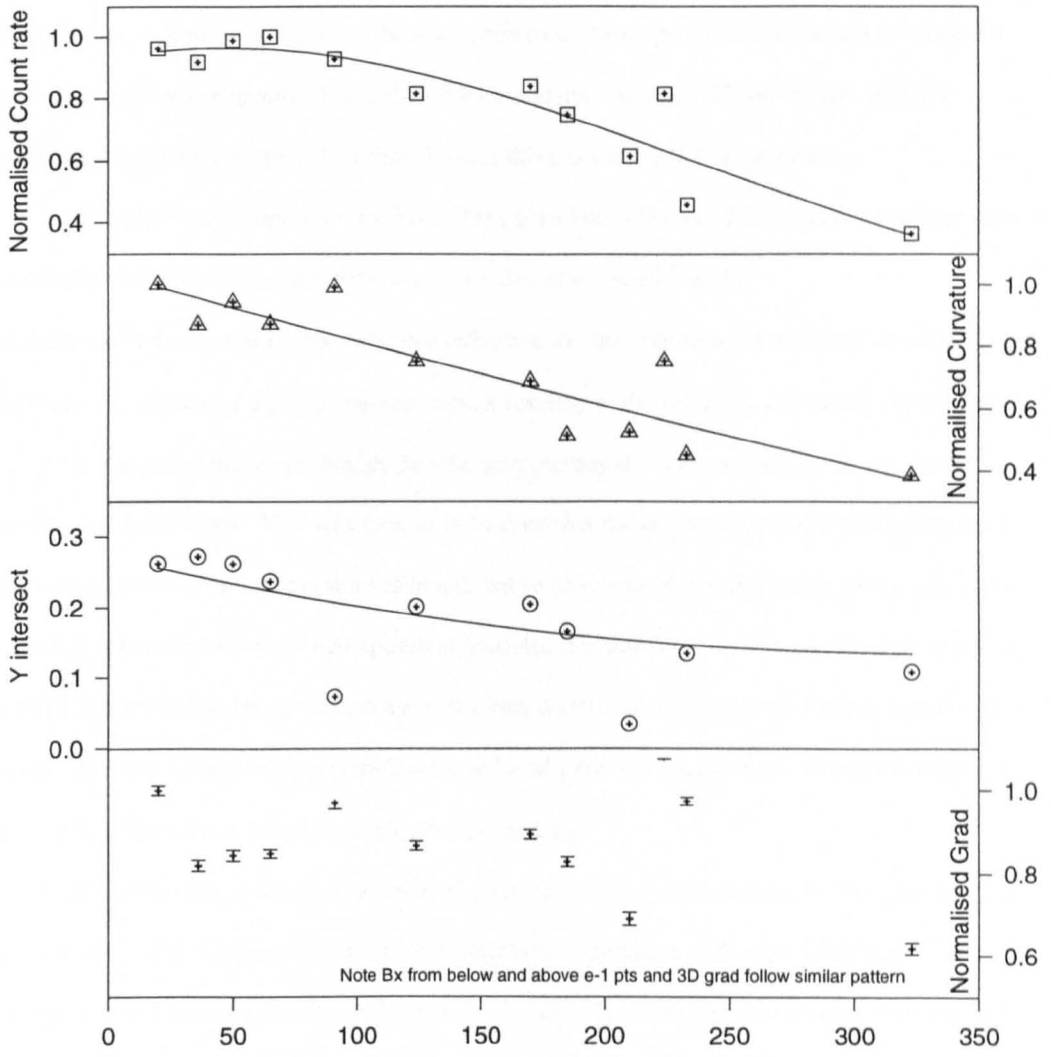

Figure 84 Analysis of Yeast Processing, *Pichia pastaris.*

Parameters measured during the breakage of a yeast sample, each data point was generated from a 3D fit to the top 63% of 20 correlations (squares, count rate; triangles, curvature; circles, Y intercept; points; instrument response). One data point is off scale on the plot of Y intersect.

Transform for Γ: $\Gamma = \Gamma / \Gamma_z$, where Γ_z is the average value for zero processing.

Count rate and curvature parameters normalised by a similar ratio. Viable Counts 22×10^9 per m at t=0 s, 1.3×10^6 per m at t=324 s.

6.4-2/3 The DWS Model and Analysis

The failure of the conventional instrument response measurement, to monitor the four fold change in correlation gradient, was traced to the low correlation intercept. In most materials an intercept value of over 0.9 was expected due to the pure homodyne operation. However, this material unprocessed had an intercept of less than 0.3 and this reduced to 0.1 on processing.

However the curvature in the front of the correlation (Figure 85) can also have been seen to more than halve and the correlation decay has decreased significantly.

The decrease in decay will be due to both a reduction in concentration (of the order of φ=0.5 to 0.025) and the release of the cell contents, which resulted in the viscosity increasing significantly.

It was noted that even though the viscosity increased, with processing, the resulting correlation is more linear. This was seen as indicating that the original curvature was due to hard sphere interactions. Similar curvature although not as pronounced, having being previously noted for moderate concentrations of non-spherical particles, Section 5.4-3/6. The significantly reduced intercept was probably due to an increased baseline, generated by effectively static scatterers. This baseline increase, along with the significantly reduced particle concentration, would also explain the increased variance in the data points after processing.

The count rate trace, as a function of processing, was noted as unusual. The process of cell breakage usually exhibits an exponential decrease in breakage with processing time, similar to a milling curve. However, the data indicated that no significant change in intensity occurred until after 100 seconds of processing, where it would be expected that well over half of the sample had lysd. This suggested that, at high concentrations, the quantity of light scattered by a sample is independent of concentration. This concept would appear to agree with localisation and clouding models of light scattering (Section 2.4-1/3) and leads to significant conclusions, Section 7.2-3.

Further work on *E. coli* was attempted but the bacteria are green and no light (633nm source) was reflected from the sample. It was obvious that the source wavelength must be selected according to the sample being measured.

It was noted that analysis by more conventional DWS methods/models would have only generated the plot of Γ versus processing which suggests that no information can be extracted. The simple intercept and curvature parameters had shown themselves significant tools for visualisation of complex data.

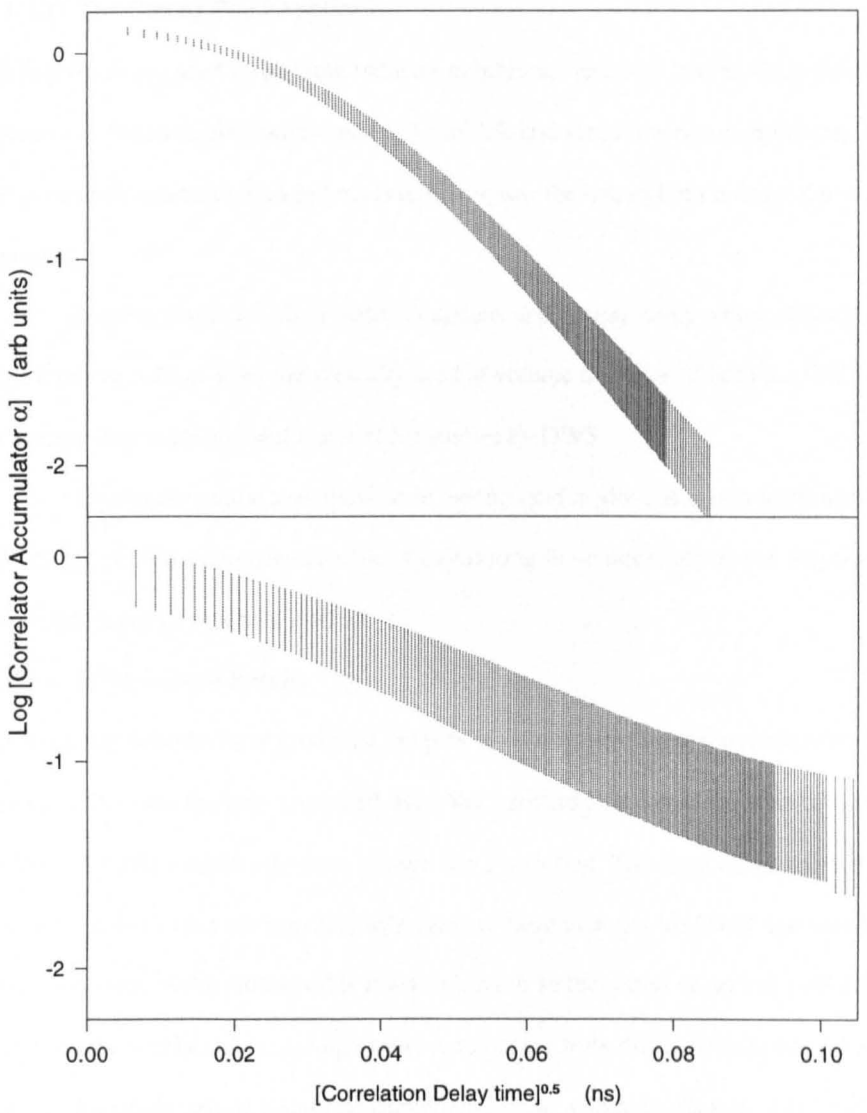

Figure 85 DWS Correlations for Processed and Unprocessed Yeast

The results from the three dimension fitting software giving the 'average' correlation prior to ultrasound treatment, top, and after 95 percent cell breakage, lower (viable counts 2.2 $x10^{10}$ and $1.3x10^{3}$ per ml. The short term correlation curvature appears to reduce with processing.

Each trace is the result of a three dimensional fit of 20 experiments.

(top trace: Log $\alpha = 268.755\ \tau - 0.4392\ \tau^{0.5} + 0.204$, lower: Log $\alpha = 66.097\ \tau - 6.649\ \tau^{0.5} + 0.12$).

Dilation of the correlation was used outside the fitting area of the correlation to generate a display of the long time tail, statistical variance of every other correlator channel shown for clarity.

6.4-3 Analysis of Cutting Fluids

6.4-3/1 The Cutting Fluid Application

Cutting fluids are used throughout industry to lubricate and cool cutting tools used for machining operations. When cutting fluids age, both tool life and scrap rate rise significantly. In addition, close personal contact with aged materials increases the risk of both industrial dermatitis and skin cancers.

Cutting fluids are oil in water emulsions and appear milky white, although pure oil itself is a light brown colour. They are typically used at volume fractions of between 0.03 and 0.06, indicating they were an ideal material for studies by DWS.

One of the major contributions to ageing (and health risks) is contamination with tramp oil[1]. Experimental techniques capable of monitoring these materials on the shopfloor may therefore have significant commercial interest.

6.4-3/2 Experimental Results

An industrial manufacturer produced samples of cutting oil suspensions immediately prior to analysis. The samples were measured using the standard DWS procedure on default settings with f_b=0.63. A contaminated reference sample was also tested. The large droplet size and the low refractive index of the cutting oils made them an ideal material for DWS analysis, Figure 86. The refractive index of the cutting oil is low resulting in an increased mean free path of the photon and increased the number of scattering events required for truly diffusive behaviour. The sample generated a single valued count rate dependence up to a volume fraction of at least 0.15. The average error (variance) in the data points was within 0.3 percent of the mean size. This was noted as exceptional as the low refractive index and large size would normally reduce the measured Γ and thus give increased variance, for a constant experiment duration, Equation 56.

Analyses of the top 63 percent of the curve showed significant concentration dependence, particularly at lower concentrations. However, the function was smooth and well defined. The sample showed a high degree of front end curvature, average %curvature =0.46, Figure 86. In this case the correlation line shape could have been due to both coherence effects (increased l*) and absorption. However the curvature did not increase with dilution (and thus with mean path-length differences between photons) suggesting this was not a laser coherence affect.

1 Tramp oil is the term used for the contamination due to oil leakage from machinery bearings.

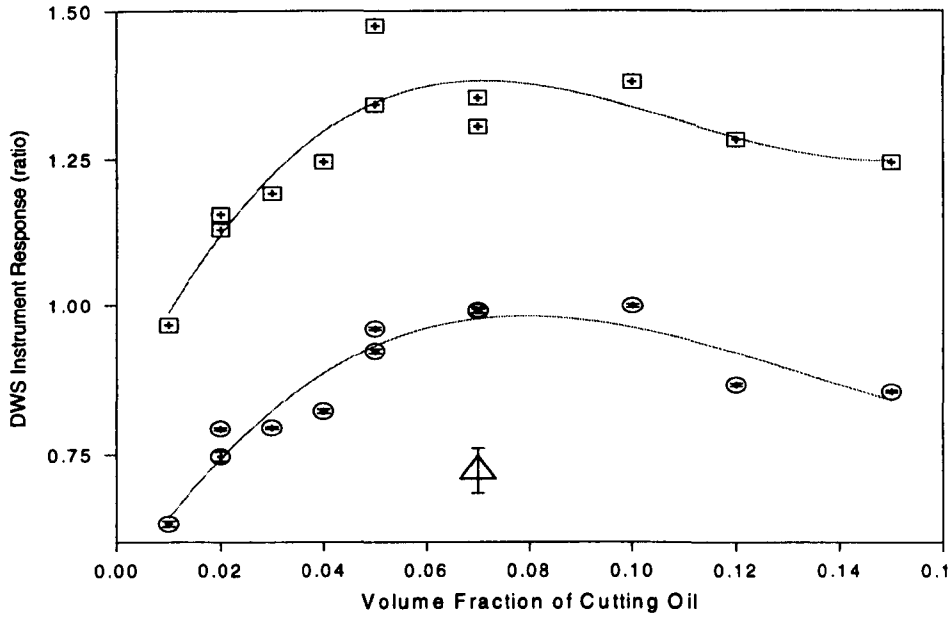

Figure 86 DWS Analysis of Cutting Fluids

Instrument response of DWS to various concentrations of cutting fluid. Both the short time instrument response (circles, normalised to 1 at ϕ= 0.075) and the long time correlation tail (squares, offset by +0.3 for clarity) are shown. The data from the dirty cutting fluid (triangle) is shown for the short time instrument response only, the contamination having a clear effect on the response.

The %curvature values were ϕ=0.01: 53.1, ϕ=0.02: 47.2, 45.0, ϕ=0.03: 45.4, ϕ=0.04: 47.14, ϕ=0.05: 43.0, 47.6, ϕ=0.07: 31.6, 37.6, ϕ=0.1: 31.12, ϕ=0.12: 44.7 ϕ=0.15: 44.1

The data is fitted with third order polynomials, short time response:

Γ/Γ_{75} =305 vf^3-123vf^2+13.7vf^2+0.515, r^2= 0.907.

where Γ is the measured value and Γ_{75} the mean value at a volume fraction of 0.075.

Contaminated sample point not used in fit. Each data point generated from three dimensional fit to 25 correlations, except the contaminated sample, which was formed from 50 correlations.

Transform for Γ: Γ/Γ_{75}. The long time tail data (squares) is offset by 0.3 for clarity

The absorption of the oil, measured as 0.075 at 633nm 1cm path cell, relative to water and the low real refractive index of the sample would require many scattering events for depolarisation of the light source. This is in agreement with the concept of a difference between an absorbing continuous phase and absorbing particles, Section 5.4-3/4. Suspensions of absorbing particle should not show a strong correlation line-shape variation with concentration, as the absorption is not a function of the distance the photon has travelled.

The sample contaminated with tramp oil sample was seen to vary the instrument response by the order of 30 percent (Figure 86) but the correlation line-shape was again similar and the scattered intensity was similar to an uncontaminated sample, Figure 87. The tramp oil was obviously at such a low concentration as not to effect the sample's absorption properties.

The analysis of Γ was carried out using a fixed detected intensity as in all previous work to ensure bias was low and similar for all experiments, Section 5.3-1/2. However, the count rate was then measured using as fixed laser intensity (Figure 87), to allow the calibration detailed later. One significant difference between the measurements on clean and contaminated cutting fluid samples was the oscillation in both the count rate and measured gradient of the sample containing tramp oil. This type of oscillation had been noted previously in samples where the suspension was adhering to the probe window, Figure 74. It is believed that the sinusoidal trace was due to an effective etalon being formed, as an oil film accumulated on the probe. This caused a cyclic variation in intensity as it grew through half-wavelength widths. It is probable that the oil film was due to free oil that was leaving the water phase although it could have been due to contaminated oil particles collapsing on the probe surface.

The results indicate that DWS could be employd as a real-time tool monitoring cutting fluids for contamination and wear. The change in Γ was significant with no other effects noted for correlation line-shape or scattered intensity. The cyclic variation whilst initially being considered an artefact may be a useful parameter in determining the degree of contamination. Increased contamination, and/or contamination not associated with the oil, should affect the 'wavelength' of the oscillation.

One important point was noted in that the increase in particle size should have caused a shift in scattered intensity, as scattering is R^6, however this was not noted. The quantity of scattered light is independent, at least to first order approximation, of particle size.

6.4-3/3 Concentration Independence

Previous work had attempted to minimise the concentration dependence by adaptation of the fitting procedures, Section 6.3-4. However, the scattered intensity was not a strong function of particle size in DWS, unlike conventional DLS. This suggested calibration for concentration could be carried out simply using the scattered intensity magnitude, for a given sample type. The variation of intensity with concentration was found to be crudely modelled by a fourth order polynomial, Figure 87. The trace is indicative of occlusion occurring at $\phi>0.15$, where scattered intensity is not a function of particle size as the scattering cross sections of the particles are overlapping.

This fit was used to recalculate the volume fraction, Figure 88. The third order polynomial, used to fit the instrument response versus concentration was deemed a poor fit, but it was seen as suitable for the initial study of the method. Thus, the intensity scattered by the clean sample was used to calculate sample concentration. This allowed the measured sample to be normalised to a volume fraction of 0.125, Table 7. The calculated 'instrument' response is plotted versus the measured instrument response, Figure 89. The data pertaining to the contaminated sample was not used to produce the model but normalised using the model, Table 8. This trace is highly significant as it shows that the calibration procedure allows the scattered intensity of the sample to be used to calibrate for concentration and that this calibration did not effect the difference between the contaminated and clean samples.

In low order scattering the increase in particle size of the contaminated sample would have led to an increase in scattering and thus the scattered intensity could not be used to calibrate between different samples. However, using the DWS arrangement where only diffuse light is detected the scattered intensity is not a significant function of particle size and the calibration is possible. Thus the concerns raised on a change in refractive index with particle size and concentration in milling samples should not be significant when milling occurs at high volume fractions. The calibration for intensity has been carried out on the most difficult of samples. The material exhibited strong concentration dependence due to the low refractive index and moderate concentration range. This sample gave a correlation with a highly curved front end probably due to absorption by the particles. This suggests that calibration for TiO_2 or other high refractive index or non-absorbing samples might be more accurate. The fixed detected intensity method to reduce bias (Section 5.3-1/2), however disallowed re-analysis of previous data.

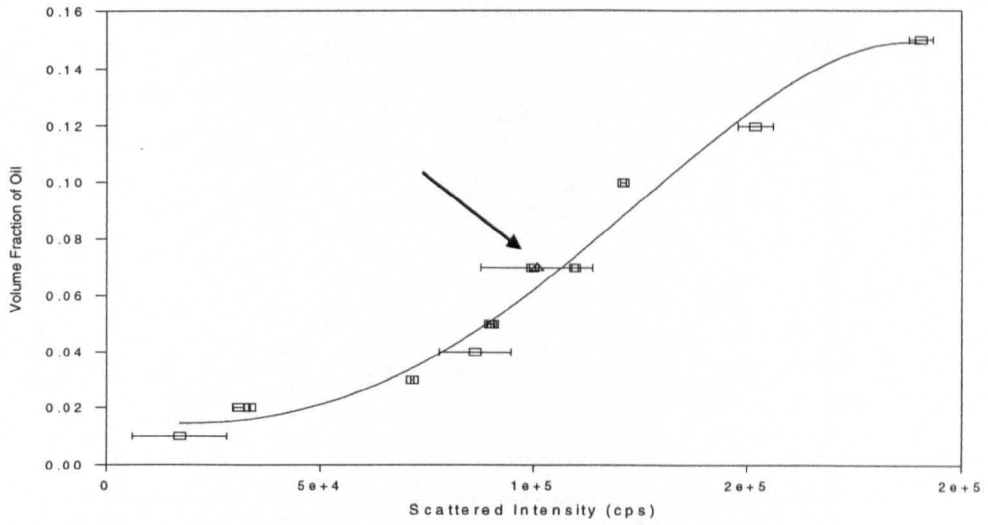

Figure 87 Volume Fraction as a Function of Intensity

The scattered intensity as a function of concentration of cutting fluid (squares). Fit shown:

$\phi = -3.21 \times 10^{-22} I^4 + 7.72 \times 10^{-17} I^3 + 1.14 \times 10^{-12} I^2 - 9.59 \times 10^{-8} I + 0.015$, $r^2 = 0.9809459171$

Contaminated sample shown (triangle) not used in fit. Plot reversed (abscissa not intensity) to allow generation of equation above.

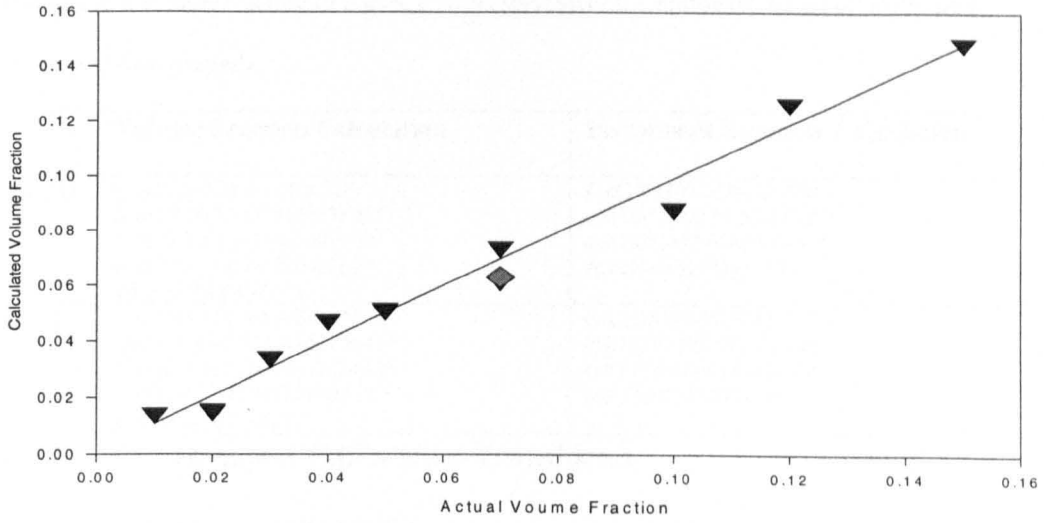

Figure 88 The Concentration Model

Calculated versus actual volume fractions, calculated volume fraction from previous polynomial fit for clean oil (triangles) $vf_c = 0.98vf_a + 1.16 \times 10^{-3}$, $r^2 = 0.981$. The tramp oil sample is also shown (diamond) but not used in the fit

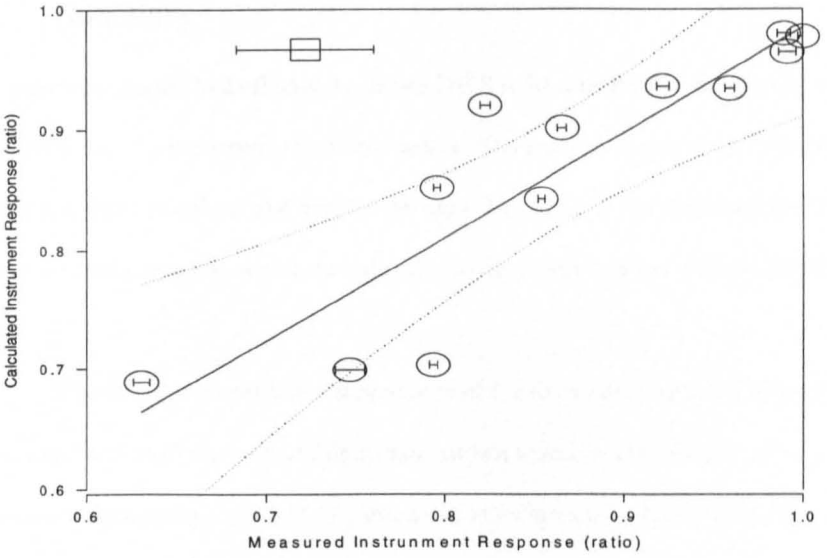

Figure 89 Concentration Independence

Calibrated instrument response versus actual instrument response. The data points for both clean cutting fluid (circles) and the contaminated fluid (square) using calibration data, Figures 87, 88. The concentration normalised and actual instrument functions are shown to correlate whereas the contaminated sample does not. Linear Fit: $\Gamma_C = 0.870\,\Gamma_{75} + 0.115$. Where Γ_c is the calculated instrument response, from the concentration calibration and Γ_{75} the actual instrument response normalised to a volume fraction of 0.075, $r^2 = 0.7964196173$. Confidence limits of ninety nine percent are shown (dotted).

	Volume Fraction Calculation	**Instrument Response Calculation**
Clean Oil	Col(16)=-3.21361982e-22* (col(2)^4)+7.7173516117e-17* (col(2)^3)+1.1419863387e-12* (col(2)^2) -9.5925299402e-8* col(2)+0.0154016574	Col(20)=305.7116063778* col(16)^3-122.5926817085* col(16)^2+13.6740822454* col(16)+0.5153891279
Dirty Oil	Col(17)=-3.21361982e-22* (col(12)^4)+7.7173516117e-17* (col(12)^3)+1.1419863387e-12* (col(12)^2) -9.5925299402e-8 * col(12)+0.0154016574	col(21)=305.7116063778* col(17)^3-122.5926817085* col(17)^2+13.6740822454* col(17)+0.5153891279

Table 8 Sigmaplot Calibration Transforms

Calculations used to normalise the DWS instrument response to intensity and thus ensure a single point measurement, * defines multiplication and col the column number of the spreadsheet.

The data, for an ideal fit, should obviously have been a straight line of gradient 1. Although the calibration was crude, and scatter in the points was high, it was immediately apparent, that the contaminated sample lay well outside the 99 percent confidence levels.

6.5 Summary

The previous chapter had effectively shown DWS to be a method of analysis of samples of known concentration, of a predominately stable nature. The analysis required user intervention and thus skilled operators to collect and analyse the data. This chapter has discussed that the latter three points are rarely possible within an industrial environment and has dealt with each limitation in turn.

Control of concentration dependence of Γ and of dependence of interactions has been considered and analysis methods/algorithms shown based on the quantity of the correlation analysed. Additionally a method of concentration independent measurement has been shown by means of calibration using the scattered intensity. This was only possible because, in this work, the scattered intensity was only a weak function of particle size at high concentrations. This intrinsic property of DWS suggests that, at least with similar suspensions to those measured, 'concentration independent' measurement is possible.

A fully automatic analysis package has been produced and evaluated and the majority of limitations removed. The algorithms have been shown to allow sensitivity below 1 percent/ 3nm, even where dramatic temporal variations were present in the sample and the fitted correlation line-shape was strongly non-linear (when plotted as the logarithm of the correlator accumulator value versus the square root of the correlator delay time). The package was capable of monitoring, resetting and following the changing samples, using intelligent real-time damped feedback loops.

The correlation line-shape was shown to contain important secondary information on sample characteristics which appeared to be correlated with the level of interactions between particles.

The viscosity temperature dependence study was hampered by the lack of suitable samples. Samples provided by the industrial partner not being stable in ethanol where samples of differing viscosity but similar refractive may be produced. However, the temperature dependence was shown to be common for samples as different as polystyrene and titanium dioxide up to volume fractions of 0.125. This suggested complex modelling of interactions may not be of major importance in many applications Two new industrial applications were evaluated, both showing successful monitoring of the required process even at volume fractions at, or approaching, the glass transition.

CHAPTER 7

Conclusions and Further Work

7.1 Overview of DWS

7.1-1 The Project

This project developed a novel measurement technique capable of analysing suspensions at volume fractions over a range from 0.01 to greater than 0.4. The technique was based around the diffusion model of light in dense suspensions, giving a technique that is, theoretically, independent of the photon transport path (Pine *et al.* 1988). This simplifies measurement, as complex background analysis (Garcia *et al.* 1992) is not required.

This work has not considered DWS as a direct extension of PCS, and thus did not rely on the principles or assumptions underlying DLS. Instead, where practical, the work has attempted to follow the theoretical and practical limitations from more basic principles. This has led to a number of conclusions that would not have been considered from the basic DLS/DWS paradigms.

The refractive index that is relevant to the measurement is discussed in terms of both the conventional volume fraction of the particles, and the volume fraction of the particles in terms of their scattering cross section. The latter indicated the scattered intensity to be independent of particle size in the diffusive regime and allowed concentration calibration of the system by analysis of the magnitude of the scattered intensity.

Our utilisation of the most basic DWS model, and design of both the optical system and analysis method to suit, has been shown to have significant advantage. The system acted in pure homodyne mode at all volume fractions analysed (0.01-0.4+), which has been stated as impractical in the literature (Bremer *et al.* 1993). The extinction between scattered light and that of a local oscillator typically is of the order of 1 part in 10^{12}, which is not viable using any true retroreflection arrangement.

The most basic DWS model was used as it tends to be more physical than many of the more complex solutions (Wolf and Maret 1990).

Whilst it may have been obvious that no smaller size limit existed for DWS, as the technique is not photon limited, initially the upper size limit could be considered similar to that of PCS. However, this project has shown its application in gel type materials and this chapter considers implementation in near solids and suspensions of particles too large for conventional DLS analysis.

The main measured parameter of DWS has been discussed as a different to conventional DLS. Whereas in DLS the correlation gradient defines the motion of an individual particle over a distance equivalent to half the wavelength of the incident light, in DWS each particle may only move a short distance in order to de-phase the source. It has been discussed that no practical direct generic relationship may be established to suit any suspension type.

One of the most significant limitations of conventional DLS is that the required dilution not only causes instability but also removes particle-particle interactions. This work has argued that, whilst the DWS parameter cannot be directly related to free diffusion coefficient, it is often a more basic measure of the characteristics of a sample.

The value Γ quoted in this work has, where possible, was normalised to a reference sample reducing the effect of different instrument parameters when comparing this data with that collected by any other DWS system.

The conclusion, that single point DWS measurement cannot establish a polydispersity index, may have been expected at the project onset. The instrument design was intended to lose any ballistic scatter, where information on polydispersity may still be available.

However, this work introduced the concept of a measure of polydispersity due to preferential settling. This work showed that, even at concentrations where subsidence was occurring, preferential settling could still be analysed. It was shown that the variation of the instrument function after milling was related to the dispersion state, and hence polydispersity, of the sample.

This work has shown that all samples that exhibited significant interactions also tended to give curvature in the front end of the correlation line-shape. Interacting spherical particles at volume fraction of the order of 0.5, as well as lower concentration spherical particles which were gelled gave similar responses. This was effect was also noted on non-spherical samples at moderate volume fractions (0.125). It has been suggested that rotational diffusion leads to longer range hydrodynamic interactions.

Further work has been proposed to see if aspect ratio can be measured directly. However, this requires samples of particles differing only in aspect ratio, available at high concentration, which exhibit hard sphere interactions and are stable on dilution. To date these have not been obtainable.

The basic paradigm underlying multiple light scattering would suggest neither particle shape nor distribution may be evaluated. The identification of these novel methods may have significant research and industrial applications, although significantly more analysis will be required.

The concentration dependence has been shown to be minimal over a wide range for many materials and methods of reducing the concentration dependence by control of the optical arrangement and analysis method have been considered and shown experimentally. The DLS scattering vector has been shown to be an incorrect approximation for DWS. This led to the development of a 'corrected' scattering vector based on volume concentrations, Section 5.3-5/4, Equation 68. However, extension of the concept of clouding (Judin 1993), from dried film opacity studies, suggested that suspension refractive index was a more complex function based on volume fraction and particle size itself, Equation 69,70. Fortunately, the same theory suggests that at high volume fractions concentration independence, of the scattering vector, may again be established. Whilst the latter method requires a constant sample type it has been suggested as applicable in many industrial areas.

The Stokes-Einstein relationship is based on free diffusion, which relies on the assumption that particles do not interact. The sample must be approximate to being infinitely dilute, and without charge or cross-linking. Thus, the fact that the temperature and viscosity relationships did not obey this simple model may be expected. The more complex DWS dependencies were described but no simple analytical model has been given. However the temperature dependence was shown to be linear and sample unspecific, for hard-sphere interactions. This chapter discusses how the different nature of the DWS measure may be used to probe non-Newtonian materials fluids without introducing shear.

The limitations of the hardware have been shown to be considerably different between PCS and DWS. In DWS more stringent limits are placed on the laser in terms of coherence (Section 3.3-2) and on the detector and signal processing, in terms of instrument bandwidth, Section 2.5-4/2, 3.3-1/5. This section concludes that the approximations of the digital correlation have more significant consequences than in conventional DLS measurements.

The selection of optics (Section 3.4-2) has been considered for an optimum fibre based instrument (Section 3.4-4) with a thin window of very low cost, low quality, glass shown to be optimum for homodyne arrangements, Sections 5.2-3/6

DLS has previously required experienced and skilled personnel to operate equipment within a controlled environment. It is believed this work has shown significant advances in software, which may be applicable to conventional DLS as well as DWS, for control of such equipment. Algorithms controlling the entire setting up, collection and analysis of data have been generated and implemented. This included intelligent feedback to set the two related variables, correlator delay and number of channels, in a systematic and reproducible way. The software, and intrinsic feedback, has shown DWS may be used to analyse systems exhibiting change over periods of a few seconds, allowing a temporal variation of a sample to act as a fingerprint. Previously DLS has been limited to static and/or slowly changing (and usually triggered) systems. The ability of DWS to respond over time-scales of the order of one second suggested that a number of new applications may be possible.

7.1-2 The Application

The simplicity and robustness of the arrangement have shown themselves to be well suited to the industrial environment with variance as low as 0.1 percent and sizing reproducibility of 0.3 percent, being reported on commercial pigment samples

The industrial process chosen for the DWS evaluation initially appeared a near ideal application, where high concentration, high refractive index, low absorption and mondisperse materials were to be controlled to maximise scattering properties. However, this work has shown that there are significant problems encountered with industrial samples. The pigment industry is not interested in size of the suspension but in producing a stable system that gives maximum scattering when applied, usually as a dried, film.

Given the limitations, this work has shown the measurement of milling curves at concentrations at least an order of magnitude greater than any other established technique.

It should be noted that DWS is the only light scattering method allowing in-line operation at process concentrations. This, in conjunction with the feedback routines that have been produced, may allow for automated control of milling cycles.

This work has suggested DWS need not be limited to a laboratory based research tool, measuring known stable reference samples, but may operate within an industrial setting.

Analysis on real industrial samples with significant unknown parameters was been demonstrated, with significant quantities collected at the industrial site.

7.1-3 Historical Development of DWS

Prior to detailed consideration of what this work aimed to carry out and what it achieved, the historical development of the DWS technique is considered, as this has had significant effects of the type of experiments and modelling that workers in the field have previously attempted.

Whilst this text considers DWS as a method of particle characterisation, the use was in fact a spin-off from localisation studies, where photons are trapped within a crystal, or pseudo-crystal (provided the photons are an exact solution of the crystal spacing).

Particle sizing studies can be traced from the measurement of dense suspensions of polystyrene, with workers experimentally measuring the enhanced backscatter that occurs a few milliradians around retroreflection in localisation studies (Van Albada and Lagendijk 1985, Van Albada *et al.* 1987,1990). This phenomenon was of significant interest, as it was not described by Mie theory. Later work showed that at retroreflection the correlation of densely scattered light could have a solution that is not a function of the mean transport path of the photon, i.e. is concentration independent (Pine *et al.* 1988).

This suggested the possibility of a sizing technique that was fundamentally different to the high concentration analysis (FODA and FODOLS) that had been carried out by earlier workers (Ross *et al.* 1978, Dyott 1978, Thomas and Tjin 1989, Thomas and Dimonie 1987), Auweter and Horn 1985, Floy *et al.* 1988). The most significant difference between these techniques and DWS was that no theoretical model of the light scattering was available for analysis, Section 1.4-9.

Prior to the project, a significant amount of literature existed on diffuse light scattering. However, the majority had been aimed at either the theoretical consideration of scattering and statistics for localisation, or use of DWS as a tool for a particular application. There appeared to be little work carried out on the evaluation and development of DWS as a generic technique suitable for industry and notably process control (Horne 1989,1990).

More recently work has aimed at generation of a new DWS model not based on the diffusion approximation (Durian 1996 Lemieux *et al.* 1998) and DWS arrangement (Kaplan et al. 1993). However, the model is not ideal for industrial application as it has been solved for transmission measurements.

7.1-4 Advances in this Work

This section does not follow the advance in the project historically due to the interdependence of many of the results and conclusions. The first section details the basic DWS model that this project utilised and considers the point source optics and the meaning of the parameters γ and Γ before detailing the wavelength dependence. The refractive index dependence is not considered until the following section, where the failure of the scattering vector and Stoke-Einstein equation are considered as functions of concentration. This section concludes that absolute size is not viable in DWS. This is followed by consideration of the concentration effect of the dependent scattering model, which suggests the scattering vector limitation is not significant at moderate to high volume fractions. The method of concentration independent measurement, based on dependant scattering, is considered in detail. The analysis of the variation of Γ, with time, follows and includes discussion on the effects of sedimentation and subsidence, thus the analysis of the size distribution. The analysis of the amplitude fields generated by multiple light scattering, and thus the effect on the meaning of the measured intensity correlation, defines some of the practical limitations of light scattering. This is followed by evaluation of the equipment required for DWS instrumentation along with the analysis algorithms developed in this work.

7.2 The Diffusive Model of Light

7.2-1 The Basic Paradigm

7.2-1/1 The Delta Model

This section initially considers use of the basic backscattering model proposed by Pine *et al.* (1988) as a method of DWS analysis, as this allowed analysis without the measurement of l^*, as required for transmission measurements. Durian (1995) has discussed how anisotropic scattering, typical of high refractive index materials such as TiO_2, gives more significant complications for transmission measurements. It was known from the onset that the experimental arrangement was flawed for this model. Our arrangement did not correspond to a plane wave for emission or detection and the model ignored concentration effects. This section discusses why the model operated so well and follows this with consideration of γ and thus the choice for the analysis of Γ.

7.2-1/2 The Point Source

This work used the basic retroreflection model (Pine *et al.* 1988), Equation 22. In early work the correctness of the fit was evaluated using a runs test, although this was extended to a comparison between 2nd and 3rd order polynomial fits later, Section 6.2. The linear model appeared a good approximation for the majority of samples, even at high volume fractions. The concentration dependence of the correlation gradient tended to be relatively low, even at volume fractions as low as 0.01 (Figures 52,54, 76,77) and the correlation line-shape was shown to remain constant. The model was only shown to fail catastrophically in near gel systems (Figure 84, 85) or where the sample stuck to the probe window, Figure 54. This failure of the basic model was considered primarily due to be a catastrophic failure of the Siegert relationship, Equation 30. This is known to fail for non-Gaussian fields, Section 7.3-2.

From a theoretical standpoint it was known that the model used in this work was incorrect for the basic arrangement. The model (Equation 14b) assumes plane wave illumination, in direct contradiction to the 3 micron core fibres used. No model existed, in the literature, for point source emission and detection, in retroreflection. Whilst theoretical work may have been undertaken to produce a new model this would not alleviate the problem of low order backscatter, which was considered un-solvable without at least prior knowledge of particle concentration.

The field intensity leaving a probe will decrease as the fourth order of the distance (assuming the light leaves as a hemispherical ball). Such that closer particles are highly illuminated. Furthermore the scattered light that is retro-reflected will decrease in the same manner.

Thus the light entering a conventional near retro-reflection optical probe is highly weighted to scattering near the probe surface, Figure 8. This low order scattering is ballistic which may gives significant variation in correlation gradient and line-shape, with concentration. This is liable to wash out variations due to diffuse scattering, which occurs deeper in the sample[1]. These limitations were solved by the use of low numerical aperture optics spaced to give a far field cross-over, and thus limit single and low order scatter, Figure 11, 33. The NA of the fibres, equating approximately to 1-2 degrees in water, meant that particles had to be a significant distance into the sample for single scatter to be monitored. Furthermore, this allowed for a small spacing (125 micron, defined by the fibre cladding) between fibre emitter and detector such that a retro-reflection model could be assumed for most samples, Figure 11. The quantity of low order scatter was further reduced by only detecting light polarised at ninety degrees to the incident beam. During this work it has been shown that depolarisation for retro-reflected light typically requires many scattering events (Lilge and Horn 1991, Schmitt *et al.* 1992, Bicout and Brosseau 1992, Brugscaglioni *et al.* 1993). Thus measurement of only the depolarised component should reduce effects from the skin layer (Niewenhuizen and Luck 1992). It has been discussed that the scattering angle should approximate to backscatter to ensure the concentration independent model of Equation 14b. It has been shown that use of any angle between 0 and 180 degrees generates an instrument output that varies with concentration (Ansari *et al.* 1993) and it was also argued that this could vary the actual correlation line shape, Figure 10. The NA, fibre spacing and analysis of the depolarised component make this work significantly different from that of Wiese and Horn (1990) who have evaluated a homodyne single mode coupler to preferentially analyse single scattering, where particle interactions with the probe window become more significant.

1 The effect of monitoring deeper within the sample, by using orthogonal polarisation to reduce single scatter has been recently reported (Heckmeier and Maret 1998)

The use of a retro-reflection dip-in probe ensures no sample air interface, which has been shown to be a limitation of many transmission measurements (Kaplan *et al.* 1993). The simple arrangement used in this work allowed the retroreflection approximation to be assumed which obviously could not occur for any other geometry.

This work used the minimum fibre spacing possible as the fibre cladding was touching. The initial cross correlation set-up suggested the fibre spacing was ideal, or too great, for typical pigment samples (ϕ =0.125), Section 5.2-3/2. Thus, analysis with increased fibre spacing did not appear of significant use.

7.2-1/3 The meaning of γ

The retroreflection model has no requirement for a background measurement of the photon mean free path. However, the model has a parameter γ, which is identified as a measure of when the light changes from ballistic to diffusive behaviour. Measurement of the term was only considered useful if it allowed a fundamental measure, such as size, to be found. This text suggested that no generic model exists, Section 5.2-1/2.

This work also suggested that in most applications the term should be replaced by $\gamma\,\chi$ where γ is the theoretical value for a particular arrangement at the diffusion limit. The term χ is an instrument factor that will depend on the difference between the optical arrangement and the theoretical model. In addition, the variation between instruments means that χ will differ even between 'similar' instruments. The fibre spacing of 125 microns and angular alignment of a few degrees means instruments will vary. This work has always given a value of Γ normalised to a reference sample. A benefit of this parameter is that, to at least first order approximation the result is independent of the instrument transfer function, χ, Section 7.2-1/3.

Whilst analysis of absolute size was not considered possible, the factor Γ was shown to be a strong function of size (Figure 55, 56, 76) with a sensitivity of below one percent, Figure 49-51. Additionally it was shown that the ranking of particle size remained constant over a wide range of volume fractions, Figures 76, 77. Later work showed concentration independence for similar sample types, Section 7.2-3/5.

7.2-1/4 The meaning of Γ

In PCS measurements, each photon delay may be considered a measure of the time required for a particle to move the distance of $\lambda/2$. This allows direct analysis, as the particle's movement may be considered diffusive. This situation was shown to be radically different for DWS where each photon delay could be considered a measure of the time taken for the sum of movements, of many particles, to be equivalent of $\lambda/2$. Thus each photon delay could itself be considered an ensemble average. This point had significant implications on the properties of DWS affecting accuracy, concentration dependence, the Siegert relationship and polydispersity. Thus Γ may be considered a measure of the dynamic movement of the system, which may include diffusive particle motion, ballistic particle motion and hindered particle motion, Section 2.2-3, 2.4-2.

7.2-1/5 The Correlation Line-shape

It is known in PCS that the entire correlation line-shape must be used in the analysis, as this is a trace of the particle's movement with time. The requirement to measure the correlation tail and baseline is most stringent when multi-exponential fitting is used to establish a size distribution.

The requirement to measure the correlation tail was considered less important in diffuse scattering, especially by homodyne analysis where baseline errors are less significant, Section3.2-2/3. It has been discussed that the initial decay of the correlation is strongly weighted to the most multiply scattered light, whereas the tail is weighted strongly toward lower order scattering. On average the more multiply scattered photons may be considered to have seen more particles move a shorter distance. The ballistic scattered light may be considered to have seen few particles move a larger distance. This suggested that the initial decay of the correlation should be used for a minimal concentration dependent result, Figures 12, 13, as shown prior to submission of this work (Durian 1996, Lemieux *et al.* 1996). The multiple scattering and ensemble averaging of each photon delay, that occurs in DWS, defines that all polydispersity information is lost.

7.2-1/6 The Limits of Γ

It is known in DLS that there is an upper size limit of measurement, when the particles cease to diffuse, and a lower size limit when scattering intensity falls below measurable values, due to the R^6 dependence of scattering. In DWS it has been shown that neither limit exists.

This work operated at near gels (Figure 84, 85) where particle diffusion does not occur, and where the measurement of ballistic motion has been noted by other workers (Weitz *et al.* 1989, Wang and Miller 1992, Zhu *et al.* 1992, Kao *et al.* 1993). Since this work Menon and Durian (1997) have carried out DWS analysis on particles as large as 200 micron, when undergoing flow.

Whilst minimum size and maximum refractive index limits may be imposed by current correlation speed (Section 3.2-2/4) this may be overcome by using different measurement techniques.

7.2-1/7 Wavelength Dependence

The meaning of Γ has been discussed to be significantly different between DLS and DWS. In conventional DLS the variation in the wavelength rarely has a significant effect on what parameter is measured with the exception of certain specific applications, such as of low angle monitoring of DNA within cells (Thomas and Schurr 1979, Thomas *et al.* 1980). Whilst altering the wavelength alters the value of Γ, the same diffusion coefficient is analysed.

In DWS wavelength will have a more significant effect, especially where only the front end of the correlation is analysed. The use of shorter wavelengths should reduce the effects of particle interactions and allow a more comprehensive measure of free diffusion and ballistic motion. This requires coherent short wave sources. Whilst the argon ion laser can operate in the near UV this is typically a mixture of many lines that are complex to separate (Thomas and Schurr 1979, Thomas *et al.* 1980). However, current progress in diode sources suggests coherent 450nm diode sources may be available in the near future. In addition advances in YAG laser technology suggest that tripled and quadrupled sources (355, 266nm respectively) will soon have suitable coherence. The ballistic measure may be important, as it is a significantly different measure to that of the diffusive particle. Whilst diffusive movement is a function purely of the particle's radius (Equation 12), the ballistic movement is a function of particle mass, Equations 8, 9. Thus a far UV and visible light system should be able to measure particle size and particle weight in unison, giving a much better characterisation of the suspension. Alternatively a visible and near IR system may be able to measure free diffusion and the effect of interactions separately. To monitor shorter time-scales, and the increase in magnitude of Γ with shorter wavelength, requires ultra high-speed digital correlation techniques, Section 7.4-3/8, 9.

7.2-1/8 Viscosity Measurement

DLS has previous been used for viscosity measurement, in samples of known size (Will and Leipertz 1993, Stasiak and Cohen 1993). During this work the analysis of non-Newtonian fluids, under single shear, using multiple scattering has been noted (Bicout 1993). It is believed that the concept of the wavelength dependence may allow DWS to produce a truly non-invasive zero shear viscosity measurement. Measurement of samples with a range of wavelengths and correlator delays would allow analysis of particle movement over different distances.

Whereas conventionally the zero shear viscosity is extrapolated from a series of shear measurements. DWS, operating at a range of wavelengths, would map the particle movement over the entire range of displacements, and thus interactions, without introducing shear. This may be of significant interest in the study of non-Newtonian materials.

7.2-2 Effects of Concentration on the Basic Model

7.2-2/1 The Basic Model

The basic equation underlying this work suggested that the DWS analysis is independent of concentration when the light could be considered diffusive and when particle interactions were negligible. This appeared to place stringent limits on the range of DWS measurements, resulting in the significant study of concentration effects. This section discusses the limits before evaluating the failure in the basic paradigm due to the incorrect scattering vector being used in the analysis. Additionally concentration effects were shown to have consequences on the validity of the Stokes-Einstein relationship, Equation 12.

7.2-2/2 Concentration Limits

In conventional DWS arrangements the concentration required to be significant before the light can be considered diffusive. Measurement below this concentration led to a measurement that was dependent on the mix of scattering orders of the particles. In addition particle-particle interactions are appreciable at concentrations as low as 0.1, which may be below the diffusive limit for many systems. The optical arrangement has already been discussed as reducing low order scatter but in dilute systems higher order scattering is minimal. By fitting to only the initial gradient of the correlation it was considered that the analysis was weighted toward the diffuse light. This also had an effect of the upper concentration limit, where interactions occur. The interactions occur only for particles that have travelled a significant distance and thus may be weighted out, Figure 12.

The methods of fitting and their properties are considered later but data collected in this work supported the concept, Figures 78. The results indicate concentration dependence of the diffusion coefficient that increases rapidly with concentration to a volume fraction of between 0.05 and 0.12 before a slow reduction with increasing concentration. This matches the results of Kaplan *et al.* (1992).

7.2-2/3 Failure of the Paradigm

The scattering vector used in the DWS model is conventionally that of the solvent as is the case for all DLS. This work has discussed, with reference to the original derivation by Pecora (1964), that this is incorrect and that the scattering vector should be that of the suspension, Equation 68. The effect of this has been shown (Figures 61,62) to be significant for high refractive index, high concentration materials, as used in this work. This conclusion originally appeared to show a significant limit in DWS in that the concentration would require to be known, even if Γ appeared concentration independent. However, it was known that the scattered intensity from the sample was not linear with concentration (Figure 87) and for TiO_2 decreased above volume fractions of the order of 0.12 (Fitzwater and Hook 1985). Thus the original correction, Equation 68, would itself fail for high refractive index particles at volume fractions of the order of 0.05. This appears to negate the use of any analysis without prior knowledge of the concentration. However, the following section concludes that the scattering vector may be assumed constant, but not equivalent to its DLS counterpart, at high volume fractions.

7.2-2/4 The Stokes Einstein Equation

The apparent failure of the basic model to take account of the refractive index difference appeared to make the Stokes Einstein equation of no use unless the particle concentration was accurately known. Even then the complex nature of the viscosity dependence, in terms of interactions (Equation 71) suggests limited use. This point is exacerbated as the refractive index, and more particularly the viscosity, become complex functions of temperature and suspension type, Section 5.4-2/3.

However, the work did show that the variation of Γ with temperature was linear for hard sphere type particles and that the magnitude of the variation, over a narrow temperature range, was similar, even for differing material types, Figure 60, 83.

7.2-2/5 Absolute Size

PCS gives a measure of size, which is assumed to be absolute provided the Siegert relationship holds and a hydrodynamic spherical equivalent approximation may be assumed. Furthermore, a polydispersity index may be calculated. Whilst DWS has been considered not to be capable of absolute size, the increased sensitivity (Figures 55,56,75) and reproducibility (Figure 49-51) may compensate for this in many applications. This work has shown that for long experiment durations (typically of the order of 60seconds) a variance of 0.1% may be achieved on industrial samples, Section 5.3-2/2. This is an order of magnitude better than normal with PCS, even when the PCS experimental duration is itself an order of magnitude longer.

Calibration with the Stoke Einstein, or equivalent formula, has been shown to be impractical. However, Γ demonstrated a linear relationship with temperature even at a volume fraction of 0.12, which was similar for polystyrene and TiO_2 when suspended in water. The scattering vector limitation appeared to make DWS measurement of limited use unless the concentration was known, or could be found by diluting and re-measuring the sample or by other background measurements. The next section shows this not to be the case.

7.2-3 Effects of Dependent Scattering

7.2-3/1 Clouding

Techniques of DLS and SLS are both limited by the R^6 dependence of the signal strength due to the effect of the scattering cross-section. This aggravates the effect of dust contamination, which is one the major reason for their limited use in industry. In DWS the dust problem is insignificant, due to both the low effective population of dust and because a photon scattered by a dust particle does not immediately leave the system.

This work also suggests that the usual R^6 weighting of DLS may be incorrect for DWS due to concentration effects. The work on mixed suspensions of 240 and 450nm polystyrene beads supporting this concept, the calibration trace being linear when Γ was plotted versus a volume weighting (R^3), Figure 75. Whilst the larger particles were greater than $\lambda/2$, where the Rayleigh model is limited, the low refractive index would suggest the model is still approximate (Kerker 1969). This effect was studied and considered to be due to the phenomena known as dependent scattering.

It has been know for some time that the optimum backscatter from a material does not linearly increase with concentration but achieves a maximum, which occurs at a volume fraction as low as 0.125 for TiO_2 (Fitzwater and Hook 1985). This maxima, due to the overlapping of scattering vectors makes the quantity of scattered light independent of particle size, above this concentration, to a first order approximation. The gradual reduction in intensity, after the maxima, due to the finite size of the particles effectively blocking returning light.

The prediction of when the pigment will give the most scattering is one of the most important commercial decisions for a paint manufacture, due to the relative high cost of TiO_2. The pigment is reduced to a particle size that will give maximum scattering. As pigment size is reduced the scattering cross section of each particle decreases but the number of particles increases leading to an 'ideal' particle size, for a given material.

A reduction in milling reduces the clouding and thus opacity of the pigment material. However, the milling process is itself costly, in energy and time, as is the alternative of increased pigment loading. An improvement in in-line analysis is obviously of significant commercial interest.

7.2-3/2 Dependent Scattering

Fitzwater and Hook (1985) assumed a model in which the incident plane wave is assumed to be the sum of the scattering of a number of partial waves of quantum number 1. A simpler explanation can be considered from scattering cross section, as the scattering cross section of a particle is significantly greater than its physical size (Equation 2) such that effects of occlusion may occur at very low concentrations, for large high refractive index particles. The concentration that maximum scattering occurs is thus a function of refractive index, however, occlusion will occur in the majority of suspensions prior to a volume fraction of 0.2. The effect was known on TiO_2 before this work but has also been demonstrated on yeast and oil in water emulsions.

Even the very low refractive index oil emulsion used in this work suggested a plateau region above this volume fraction, Figure 87. Thus at low concentration the quantity of scattered light is a function of R^6 but the strength of this dependence decreases dramatically, with concentration, until true occlusion occurs. When all scattering may be considered dependent, termed occlusion in this text, the quantity of light scattered is thus independent of their radius and purely a function of their refractive index.

This has significant effects for DWS in terms of: concentration independent measurement, the effect of absorption of light and on the meaning of the value of Γ.

7.2-3/3 Absorption

Work within the project had attempted to consider why front curvature of the front end of the correlation occurred in certain samples where it was known laser coherence was not the cause, Figure 63. The most probable effect was considered to be absorption (Vankeuren *et al.* 1994). The work attempted to produce samples of complex refractive index particles in a real continuous phase and real refractive index particles in a complex continuous phase, Section 5.4-3/2, 3. The difference between scattering and transport paths in DWS suggested one sample would be concentration dependent and one scattering order dependent. Whilst practical limitations only allowed the complex continuous phase sample to be produced, the effect of the absorbing dye was shown to be low, Figure 63. The stability of the correlation line-shape suggested that dependent scattering may significantly reduce the effect of an absorbing continuous phase.

The sample used was known to be at the clouding point (ϕ= 0.125) such that the scattering cross sections of the particles were overlapping. In this situation the photon would appear rarely to enter the continuous phase but effectively remain in the particle refractive index. This would suggest that the effect of an absorber dissolved in the continuous phase would be minimal.

In addition the concept that an absorbing particle would lead to a low concentration dependence was also supported by the analysis of absorbing oil in water emulsions (Figure 86) where the correlation showed curvature that was constant for all concentrations.

7.2-3/4 Future Absorption Studies

The low refractive index, absorbing, oil emulsion samples supported the concept that the correlation line-shape of a sample containing absorbing particles should not be a function of particle concentration. Samples of an absorbing continuous phase and samples with absorbing particles could be produced at high concentration from small low refractive particles. This would minimise dependent scattering and allow the study of the difference between transport and scattering path effects, as originally required, Section 5.4-3/2. This could be carried out with commercially available dyed and non-dyed latex beads. However obtaining large samples (few mls) at volume fractions of 0.4 or above made it too costly for this work.

Possibly more interesting would be similar work with large high refractive index particles. It is known that a photon senses a dense particle some distance from it, due to the scattering cross section, and that the scattering cross section increases as R^6. In this regime at moderate or high concentrations, typical of the pigment industry, the photons will always be under the influence of a scattering particle. If this is shown to be the case DWS would appear to be effectively independent of the continuous phase absorption, as suggested by Figure (63). This would lead to a further redefinition of the scattering vector.

7.2-3/5 Concentration Independence

From the project outset the concentration dependence of the instrument was known to be one of the most important parameters for industrial usage. The optical arrangement and the analysis/fitting have been designed to reduce the concentration dependence, Section 2.5-1/6, 7

Unfortunately from the study of the scattering vector it appeared the concentration would need to be known, or estimated, at least for high refractive index, high concentration particles. However, the concept of dependent scattering, which made the refractive index correction (Equation 68) invalid, appears to make a concentration independent measurement practical. When samples are at the point of occlusion it has been stated that the amount of scattered light is not a strong function of particle size. Thus at least for common sample types the intensity of the scattered light may be used to calibrate for concentration (Figure 88) and then the concentration used to calibrate the DWS instrument, Figure 89. Thus, the DWS measure is concentration independent, Figure 90. The insensitivity to particle size of the quantity of scattered light can be seen even at relatively low volume fractions (0.06) with low refractive index materials. The difference of 25 percent in Γ due to the size variation (Figure 86) had negligible effect on the quantity of scattered light, Figure 87.

Whilst this requires a known sample type, for industrial usage this is seen as of little consequence in most applications, especially process lines. The method has been illustrated on the oil emulsion sample as this gave a single valued trace of scattered intensity with concentration. On higher refractive index materials the count rate is double valued (as is Γ) such that it must either be assumed to be below, in the region of or above the clouding threshold (ϕ=0.125) for a single point measurement. Whilst exact concentrations are rarely known, the approximate value usually is.

Only a single dilution and extra measurement would be required to show the exact concentration, simply by analysis of whether the count rate increase or decreased.

Obviously for industrial usage this method of removing the effects of concentration is highly important and this study has also suggested significant changes to generic models of DWS may be required for use of the instrument as a research tool. Models not only need to take account of bulk refractive index but also of scattering cross section and if absorption is occurring due to the particles or the continuous phase. It has been suggested that these effects make current generic models of DWS of limited value, Section 7.2-2/5.

7.2-3/6 Further Particle Sizing Studies

The effects of dependent scattering suggest a second measurement technique based on the static light scattering in retroreflection, which would appear complementary to DWS. An absolute measure of size could be obtained provided that the refractive indices and particle concentrations were well defined. The dependent scattering peak (with concentration) previously discussed could be modelled as the percentage overlap of spheres in random positioning, the diameter of the sphere being that of the scattering cross section of the particle. For a given concentration and refractive index the concentration that the peak occurs now relies on one unknown, the sphere size. A complete model may allow analysis with only a small range of dilutions, not necessarily including the turning point, as a model should allow analysis purely on the curve shape.

The method would have significant advantages over conventional turbidity in many applications. The low dilution would make the measurement insensitive to dust, less likely to affect the sample stability and allow measurement of small particles with low power optical sources. Similar advantages to DWS would occur in that the analysis would be insensitive to cell dimensions and multiple scattering, and thus ensemble averaging, would give a highly stable signal. The method described is obviously outside the scope of the present work and will require a range of differently sized monodisperse samples of high refractive index and at high (ϕ=0.5) volume fractions for evaluation.

7.2-3/7 Volume Weighting of Γ

Conventional DLS analysis of pigments, such as PCS, would assume a mean based on an R^6 weighting of particle size distribution, Equation 2. This is obviously in significant error for materials such as TiO_2 for any particle size over 100nm, assuming a wavelength of over 600nm.

Furthermore the high refractive index makes Rayleigh-Gans model only a limited improvement, Section 1.2-3.

This work suggested that this limitation was not only present in DWS but also supports the hypothesis that the situation was more complex, particularly in samples at high volume fractions, large size and/or high refractive indices. The clouding effect has been discussed as removing the strong particle size dependence. At high concentrations/refractive indices it was considered that Γ may vary according to R^3, i.e. purely a function of the volume fraction of each size species.

Data obtained when analysing polystyrene beads (Figure 75) would appear to support this concept. Γ fitted to a straight line against a volume weighting axis. However, it was believed that this data set was too restricted to be considered significant evidence and that a range of mean size varying at least an order in magnitude in size would be needed for this study. This work did not have access to large volumes of such a range of beads. In addition, the work needs to be repeated on a similar range of high refractive index materials for evaluation on TiO_2 and a range of refractive indices for a full model.

7.2-4 Temporal Effects

7.2-4/1 DWS and Multiple Fitting

It was considered that DWS could not provide any measurement on Particle Size Distributions (PSDs) due to the same phenomena of ensemble averaging of each photon interval as previously discussed. Whilst it has been suggested PSD information may be present at dilute regimes in the correlation tail (Ansari *et al.* 1993), the method of light collection and analysis in this work was aimed at losing the ballistic scattering, and thus all PSD, information.

However, it appears that some stability information could be separable from the variation of the instrument function with time, for dense and/or large particulates. The theory is more complex than simple sedimentation and itself is a function of particle concentration and interactions.

7.2-4/2 Subsidence

The traces for many milling curves, of badly processed material, showed a long term time dependence with the instrument function decreasing with time of analysis, Figures 57, 66. However, it was not always possible to plot out the range of milling (processing times) and show a gradual decrease in change with each increment of milling, Figure 79.

In many samples the first milling interval showed significant time dependence, with virtually none present in further samples. The basis of this behaviour appears to be in general agreement with the concept of subsidence, described by Sato (1993).

In concentrated samples sedimentation of a particle is not simply a function of that particle's size and density as the interactions between the particles causes the entire ensemble to settle en-mass. This was clearly visible in many highly processed samples, with settling into two phase mixtures occurring over periods typically of one hour. Dramatic jumps in the measured instrument function often characterised these samples, as the particulate phase fell below the probe, requiring the probe to be inserted deeper, Figure 54. Whilst the technique is of use for industrial pigment research on the model mills, it was shown that at higher concentrations subsidence predominated, Figure 79. However, the time taken for subsidence to occur (for a fixed probe depth) may still allow a simple index of dispersion to be generated.

7.2-4/3 The Dispersion Factor

When samples are highly polydisperse, and more importantly some particles are incorrectly wetted to the continuous phase, this work suggested a size dependent sedimentation effect was still present. In the first stages of milling the particles cannot be simply considered as a dispersion of a range of sizes, as there is also a distribution of the level of wetting of the particles to the continuous phase. The oversize is the sub-population of the pigment that has not yet been milled and cannot be considered dispersed, as they are substantially unwetted. In these conditions the larger, poorly dispersed particles may fall at a significantly different rate to that of the wetted dispersion, Figure 57 (sample 26), Figure 66 (5 minutes milling), Figures 79 (11 minutes milling).

This suggests that a meaningful measure may be possible, at least in terms of a dispersion factor. A dispersion may be considerably more useful, than polydispersity, in processing operations, as it is a direct measure of the material's behaviour. Whilst this is not a true measure of polydispersity it is a measure of the state of the dispersion, which is what the polydispersity index is often used to represent. Bernhardt (1988) has shown that DLS polydispersity measurements often have little, or no, validity in accessing the dispersion state. Thus DWS may have the capacity to analyse a new factor, which no other light scattering method may monitor. The factor is related to polydispersity, to which DWS is usually considered insensitive.

7.2-4/4 Variance in the Dispersion Factor

The previous section discussed a measure, which will be termed the dispersion factor. This is related to the PSD in terms of fluid characteristics as opposed to optical size.

This work suggested that this measure might be a more valid parameter than PSD for characterisation of concentrated samples. The basic dispersion factor could be defined as the normalised rate of change of the instrument response with time d (Γ/Γ_{max}) /dt. This work has shown that in pigment samples this will decrease with milling. This parameter may be of more significance in process industries than of Γ itself. In applications such as pigments milling continues not until an absolute size is reached (the primary particle size may vary batch to batch) but until the size remains stable with further milling, and thus at it's minima. Whilst Γ gives a parameter related to size the parameter d (Γ/Γ_{max}) /dt gives a parameter that shows if further milling is necessary.

Further work may consider if the actual line-shape of Γ with time can give further information on the actual distribution in the oversize itself. This again will be a dispersion distribution as opposed to a size distribution. Obtaining accurate measurements of d (Γ/Γ_{max}) /dt was not simple as within a short period of a significant change in Γ subsidence caused failure of the analysis as the probe was no longer in the particulate sample but above it. The only method of accurate analysis of the function will require many hundreds of milling curves to be analysed, each of which may require a hundred or more correlations to be analysed.

Analysis was carried out on mixtures of the two sizes of latex available to this work, however neither was large or dense enough to show significant settling effects at high concentration. In addition such a model system, even using significantly larger sizes, would be in error as both distributions are equally well dispersed unlike the phenomena described.

7.2-4/5 Short Time Variation in Measured Γ

This work noted short time variation in the samples (Section 5.3-4/3) as well as the long time dependence. It was shown that for samples that were previously milled, and just required mixing to re-suspend, the variation was independent of the milling time of the sample, Figure 57. The behaviour was reproducible on similar mixing. However, for samples that were analysed immediately after milling, the variation was a function of the processing time, Figure 66,79. This is strongly indicative of an effect due purely to the inclusion of air. This suggests that samples (which undergo rigorous mixing) should be degassed, although accurate sizing was shown on samples which all were undergoing this effect, Section 5.3-4/3, Figure55, 70. However, failure to de-gas the sample limits the effective use of the long time dependence, as the extrapolation of this function to time zero introduces significant errors, Figure 67. Milling under vacuum was unsuccessfully attempted but is considered as further work to give more substantive evidence that included air is the cause of this effect.

For on-line industrial usage it may be that addition of antifoam agents, frequently used in the larger industrial mills, allows reduction of this problem. A second method may be to use a small bypass pipe, such that small volumes of sample could be degassed. Samples could be removed, degassed, analysed and reintroduced in minutes, which would be insignificant for the prolonged milling times used by industry which are frequently for many hours. The retroreflection arrangement would make it relatively simple to introduce the probe into a port in a bypass pipe.

7.3 The Amplitude and Intensity Fields

7.3-1 The Scattering Fields of Diffusive Light

7.3-1/1 Types of Scattering Fields

The scattering fields may be considered as two functions. The first relates to the optical arrangement and whether the measured intensity fields are an absolute measure of the amplitude fields. The second is the nature of the amplitude fields themselves, which has a direct effect on which arrangement may be used, and on the effects of the effective optical transfer function of the hardware.

The nature and effect of the scattering fields have been studied in detail for conventional DLS. The heterodyne method has been shown to be the optimum system although the simpler homodyne arrangement is acceptable for most applications. This work suggests that the situation is dramatically different for DWS. Consideration of purely the amplitude fields, with conventional DLS assumptions, suggests that the homodyne arrangement is unsuited to systems of interacting particles, which are typical of DWS. However, this work suggests the intrinsic sensitivity of DWS, along with the significant differences in the scattering fields themselves, make homodyne analysis preferable in many applications.

7.3-1/2 The Amplitude Fields

The nature of the amplitude scattering fields may appear to be an esoteric point, to be considered after many of the other parameters. However, this work showed that the scattering fields have significant effects on the optical arrangement and hardware limitations and they are discussed as a prelude to heterodyne/homodyne operation.

It was obvious that the measured correlation would decay much more rapidly than in PCS ($\tau^{0.5}$ instead of τ) and that this would reduce the maximum intensity that could be used. The standard Malvern commercial PCS arrangement (20MHz resolution) is used as an example. The manufacturer suggests it should be operated with a maximum count rate in the region of 300kcps. This is due to the hardware limitation that no more than one photon should occur in a single time interval of 50ns. In this work even using a high bandwidth correlator (40MHz) and analysing relatively slowly decaying DWS signals, the bias at high count rates was significant, Figure 45. This was considered to be due to the difference in the amplitude fields between DWS and PCS.

The high frequency component in DWS may be a significantly larger ratio of the signal, than is usual in PCS, Equation 26-28. The effect is most pronounced at short intervals (i.e. shorter correlator delay times) and low count rates.. It was thought that this might have significant effects on heterodyne mode, where the reduced signal strength (the scattered light component) is liable to magnify the effect.

7.3-1/3 The Intensity Fields

Section 3.2-1/1 demonstrated that only an intensity measurement of light is possible, as photons are annihilated as they are measured. However, in heterodyne mode (Equation 31) a portion of the laser light is made to interfere with scattered light such that information on the amplitude field results. The measurement can thus be considered an absolute measure of the amplitude fields. In the simpler homodyne measurement scattered light is made to interfere with scattered light, thus the amplitude field is effectively multiplied by its complex conjugate, Figure 15, Equation 29c. Only intensity field information is present and the amplitude correlation must be assumed from the Siegert relationship, Equation 30. This relationship holds only for certain types of scattering field, notably Gaussian. It is known to fail for systems of interacting particles, which become appreciable at volume fractions of the order of 0.1, suggesting the majority of homodyne DWS experiments should fail.

7.3-1/4 Homodyne Operation

This work used a pure homodyne arrangement with a heterodyne component only being visible when material adhered to the probe face. The basic layout has been discussed and allowed a noise component (including the heterodyne component) of below one percent of the signal strength. This subsection considers how homodyne may be operational in areas where particle-particle interactions occur. It had been shown that at very high concentrations around the gel transition and in systems where particles strongly interacted, that the correlation line-shape varied. The best example was that of the yeast, Figure 84, 85. This material changed from the consistency of a near a gel, due to its concentration, to material exhibiting gel like properties, due to bulk viscosity change for the release of cell contents (eg DNA).

It was believed that the reason that the homodyne system did not fail at much lower concentrations could be traced to the analysis methods. This work used only the front end of the correlation to analyse the gradient and thus was more strongly weighted toward heavily scattered photons, which have (on average) seen particles move only a shorter distance. Thus the effects of interactions, which will occur over much longer time-scales, are reduced in significance.

7.3-1/5 Heterodyne Operation

One practical limitation well studied in the literature is the difficulty of providing pure heterodyne measurement (Bremer *et al.* 1993, Van der Meeren *et al.* 1993) with the majority of measurement methods changing from a predominantly homodyne signal, to a predominantly heterodyne signal, with increasing particle concentration and refractive index. No literature has been found showing pure heterodyne analysis, over the range of concentrations measured in this work, leading to complex analysis of heterodyne systems. Van der Meeren *et al.* (1993) has shown that a significant number of measurements at a range of volume fractions are required to take account of the homodyne effect when a heterodyne signal is also present.

Homodyne mode could be argued as superior simply as it is a pure arrangement that does not require bi-exponential fitting. However, further limitations of heterodyne DWS can be traced to the low intercept value of the measurement. This work has shown that a reproducibility of a fraction of one percent, and sensitivity of the order of one percent, can be achieved in a DWS measurement. For a heterodyne measurement to have a similar signal to noise this would require that the intercept is of the order of one percent of the baseline (as opposed to near one hundred percent for a fibre mediated homodyne system). This places very stringent high frequency noise requirements on the source and detector, as minor variations in the baseline will have dramatic effects of the analysis (Oliver 1973). In addition the coherence requirements, of the source, for a heterodyne system are increased due to path length differences. The different optical paths also makes the heterodyne mode much more susceptible to vibration, typical of industrial environments.

This work has suggested that absolute size cannot be analysed by DWS (Section 5.2-1/2, 5.4-2/4), this appears to negate the heterodyne benefit of absolute measurement of the amplitude fields.

7.3-1/6 The Measurement Duration

The optimum count rate for a homodyne DWS arrangement was of the order of 50-75kcps, Figure 46. Increasing the count rate above that would not reduce experimental errors but will increase bias due to hardware limitations, particularly with samples showing more rapid correlation decays, Figure 45.

The high frequency component on the signal had the advantage that even at this low count rate experimental durations were typically only of the order of 3-5 seconds (for 10^5 correlation decays). In a heterodyne signal the measured bandwidth is halved, as the local oscillator signal, which predominates, will not contain the high frequency weighting of diffuse scattering.

This initially suggests an advantage of heterodyne in that detector intensity may be raised to the order of 200kcps and the correlator bandwidth limits are not as severe. However, to achieve 0.5 percent homodyne signal this would require a homodyne signal or the order of 1kcps. For a typical DWS experiment this equates to one photon containing information in each time interval equivalent to 100 correlation decays. The effect of count rate on the reproducibility of the system was analysed and shown to be exponential, Figure 46. Thus this reduction in intensity is liable to require a significant increase in experimental duration.

7.3-1/7 Accuracy, Sensitivity and Reproducibility

Accuracy is a measure of an absolute parameter. This work not only noted that DWS was more reproducible and had better sensitivity than any comparable technique but also that the measurement cannot be simply related to a simple concept like size. The DWS measurement was a complex function of size, refractive index and interactions, suggesting the term accuracy is not relevant.

The very high degree of sensitivity that was possible in DWS was initially surprising. For a common experimental duration the DWS measure would appear to have a noise of $N^{0.5}$ photons as opposed to N in DLS. However, this consideration does not take into account the ensemble averaging of the diffuse scattering. Each measured photon delay is itself an average of the sample as opposed to information from a single scattering event, as is the case in a DLS arrangement.

In DLS the error given for the size analysis is often based on the error in the fit between the PCS model and the data. Thus it is not a measure of statistical variance in the measurement of the parameter, merely if the data obeyed the assumed model.

This method was unsuited for DWS as the model could not be assumed, and was shown not to always follow the correlation line-shape. While it was possible to note a variation of below 1 percent in the gradient, the fitting error was often significantly greater.

It was believed that the suitability, or otherwise, of a model could not be properly considered until a method of generating accurate variance errors for each correlator channel, independently of the DWS model, was established. This led to significant work being carried out in generating average correlations from systems where the correlation line-shape was itself time dependant.

A significant amount of data was collected and analysed within Tioxide factories, which demonstrated the robust nature of the instrument, in allowing it to be both moved to, and operated in, the industrial setting.

7.3-2 Non Gaussian Fields

7.3-2/1 Absorption and the Scattering Fields

It has been noted that certain pigment samples exhibited some front end curvature in the correlation, Figure 63. Previous literatures suggested that this was typically a laser coherence/path-length problem (Wolf and Maret 1990, Bellini *et al.* 1991). However, this work showed a curve in the correlation line-shape in TiO_2 pigments that was not due to absorption. Many of the alcohol coated pigments, at high volume concentrations, showed the effect. Laser coherence could be eliminated, as the effect had not occurred on low refractive index polystyrene beads of similar size/concentration.

This work indicated that for high refractive index materials which give a short l_*, such as TiO_2, analysis in samples containing significant absorbing dyes was possible. In addition this work has proposed that by DWS measurement, as a sample is diluted, it may be possible to analyse if it is the particle or continuous phase that contains the absorber. It has been suggested that only in the latter case will the correlation line-shape will be a function of concentration, Section 5.4-3/2.

This concept was supported by the work on absorbing oil-in-water samples, Section 6.4-3. This demonstrated that when the particles were absorbing the correlation line-shape was constant with concentration, Figure 86.

7.3-2/2 Effect of Non Spherical Particles on DWS

In DLS a measure of particle shape is possible by analysis in a similar manner to that of polydispersity and allows a measurement of aspect ratio (Pecora 1968, Tagami and Pecora 1969, Rarity and Randle 1984, Rarity 1986).

At the start of this work it was assumed that particle shape would have no effect on the DWS correlation line-shape as the information would be washed out in a similar way to that of polydispersity. However, the variation in the correlation line-shape could not be explained as laser coherence limitation, as the mean optical path-length difference for a 0.22micron TiO_2 pigment was obviously less than those of a 0.24 micron polystyrene bead (where no front end curvature was present). In addition the effect had been shown not to be due to absorption, Section 7.2-3/3.

The curvature in the anatase pigments could easily be explained in terms of the coating, as the long chain alcohol coating was intended to cause gelling hence long range interactions even for small particle movements. The Tioveil however was uncoated and after an exhaustive study the major difference between this and all other samples was the strong aspect ratio of the particle, Figure 65. Laser coherence, absorption and size distribution were eliminated as possible causes for the samples behaviour.

7.3-2/3 Measurement of Shape or Interaction

It was known from the literature that the scattering fields are different for linear and rotational diffusion in DLS, thus it may not be a surprising if they also differ for DWS. However, this work was unable to definitively show if the measured variation is due to the effect of shape itself, or long range viscosity interactions. However, all data supports the latter concept. The large aspect ratio of the particles (6:1) suggests that rotational diffusion would be present and gives rise to significant hydrodynamic coupling. The presence of a rotational diffusion coefficient was supported by the long decay time (relative to other pigment samples) of the material.

The same effect on correlation line-shape was noted in high concentration pigment samples with gelling agents and samples of polystyrene that had coalescing agents. Notably the work on yeast showed that at ultra-high concentrations predominantly spherical particles gave a curved correlation line-shape but this line-shape became linear as concentration decreased.

Further work is required in the study of high concentration non-spherical particles compared to spherical particles where both particles exclude the same volume of water and are similar refractive index and can be obtained at a volume fraction of 0.5. By dilution of both samples the shape of the concentration dependence of line-shape should indicate if hydrodynamic coupling is occurring. At very high volume fractions both samples may give rise to a curved correlation line-shape but as dilution occurs the spherical particle correlation should become single exponential much more rapidly. The analysis of the correlator decay Γ with concentration would also indicate if the rotational diffusion coefficient was present and if the rotational diffusion reached an effective glass transition point at a lower concentration the translational diffusion.

This work could be compared with spherical particles that interact; certain polymers exhibit a significant rigidity change on factors such as pH and temperature. Analysis of particles embedded within gels of different bond strengths may give dissimilar results to those particles mentioned previously. In the case of a gel the correlation line-shape should be independent of particle concentration.

Whilst significantly more work is required on the analysis of interactions and particle shape this work suggests that, for simple non-gelled materials, that it may be possible to get a crude analysis of aspect ratio by dilution of the sample. However, this is liable to only be truly valid when the data is normalised to another similar sample where only aspect ratio is altered.

7.4 Hardware Limitations

7.4-1 Source and Detector

7.4-1/1 The Environment

This work aimed at producing a viable system for industrial usage therefore the elements of the arrangement have been considered in conjunction with the technique itself. It has been discussed that the industrial environment is unsuited to free space, high power laser beams and sample cells typical of heterodyne arrangements, Section 2.2-1. The choice of which detector and laser to use have been shown to be interdependent, as well as on what the user wishes to monitor with the equipment. This section also considers limitations of digital correlation prior to evaluation of the optics used in the arrangement.

7.4-1/2 Detectors for DWS

This work has utilised PMTs for detection and has suggested they are the optimum choice for most DWS applications as the gain of a PMT is more deterministic than that of an APD, Equation 42, 43. Additionally APDs operate at high gain only at the red end of the spectrum, where scattering decreases, Equation 1, Figure 90. Whilst APDs may be beneficial in conventional DLS, it is suggested that this is primarily due to their increased quantum efficiency when measuring intensity limited (single scattering) signals. Hybrid detectors improve the short wavelength sensitivity of APDs, but with significant increases in complexity and cost (Fagen 1993). A further disadvantage of APDs is their low bandwidth for repetitive signals (Brown *et al.* 1986,1987, Dautet *et al.* 1993, Grant 1993), although they exhibit excellent timing characteristics for cross-correlation (Cova *et al.* 1981,1982, Antognetti *et al.* 1975).

PMTs are produced with pulse widths as low as 1ns, although jitter is typically in excess of 100ps unless micro-channel plates are used (Louis *et al.* 1988). Whilst significant literature exists on the noise characteristics of PMTs, the majority of this is now out of date and pertains mainly to total detector noise (Foord *et al.* 1975). A more important specification for correlation studies is periodic noise, which is rarely specified. However in the case of PMT's much of the correlatable noise can be removed by the use of a second upper level comparator. No literature has been found where this method has been used for actively quenched APDs. The requirement for feedback would probably make it increase the detector dead time significantly. In addition the less determinate nature of the APD gain would reduce the effectiveness of the technique.

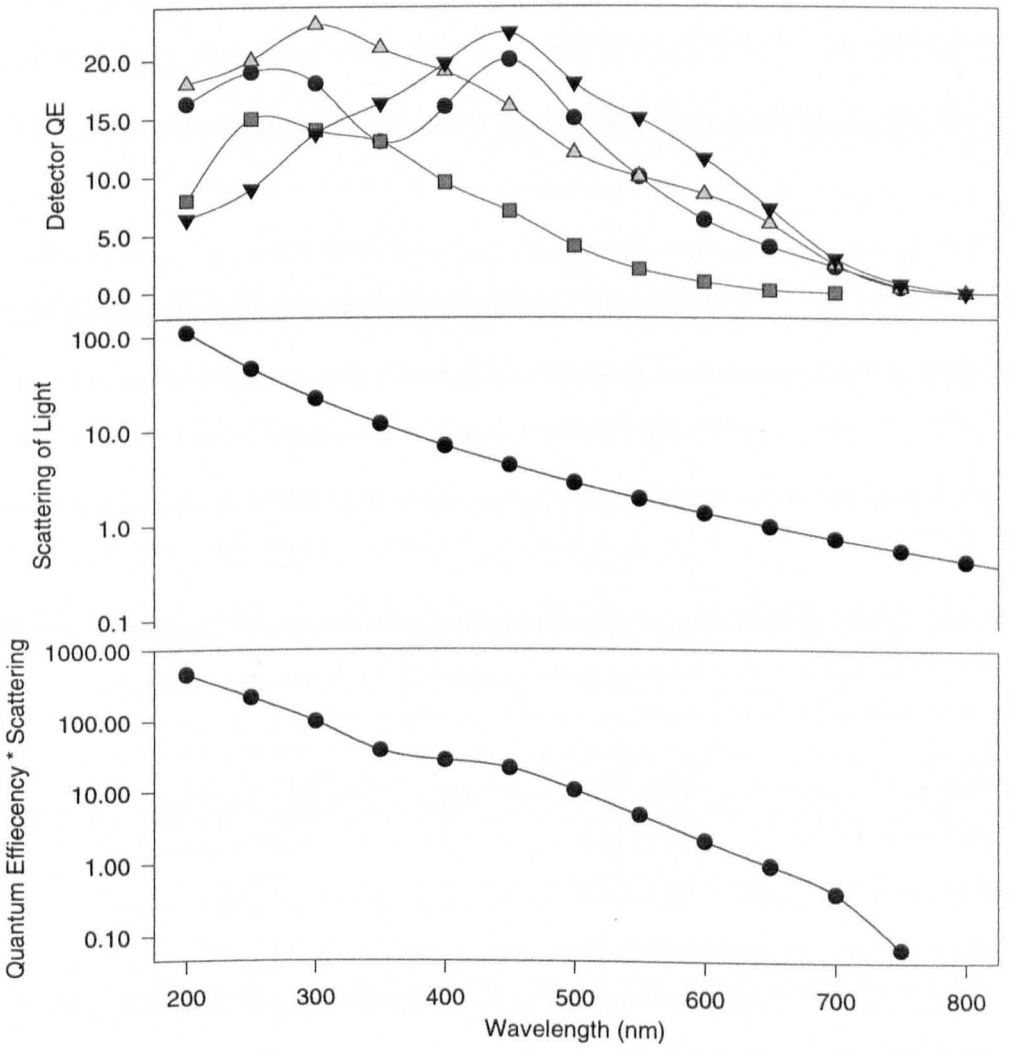

Figure 90 Detection of Scattered Light by Photon Multiplier Tubes

The top trace shows the detection efficiency of various PMTs.

The middle trace shows the effective scattering of light by small particles, normalised to 633nm.

The final trace indicates the detection efficiency versus wavelength when the scattering efficiency has been taken into account (Assuming EMI 98310-Q red sensitive tube).

KEY - Detector Type

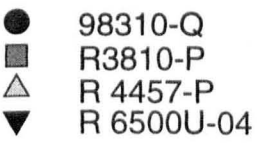

The high frequencies present in DWS may make pulse pile-up a problem when using slow detectors. However, methods of analysis of dead time effects on Lidar (Donovan 1993, Dorshow 1990) may be useful in characterisation of DWS equipment.

7.4-1/3 Source Requirements

DWS has been shown to operate using very low power sources and typically an intensity of the order of 1mW was required, such that it may be made eye-safe for industrial usage. This has a second advantage in that sample heating does not occur and DWS may analyse small particles without the risk of denaturing or other thermal damage.

For DWS the laser requires to be at least single transverse mode and preferably single longitudinal mode (Wolf and Maret 1990, Bellini et al 1991), this requirement being more stringent for low refractive index and/or small particles, as path-length differences increase.

This work utilised a helium neon gas laser, although current advances suggest solid state and/or diode lasers may become advantageous in future work. For measurement of free diffusion coefficient it was been argued that shorter wavelengths should be used, Section 7.2-1/7.

Operation at short wavelengths has a second advantage in terms of detection. Use of short wavelengths significantly increases the quantity of scattering as well as the detection efficiency of PMTs, Figure 90. Conventionally a PMT is defined simply by its quantum efficiency but when the increased scattering of shorter wavelength light is also taken into account it may be shown that 1mW of light at 300nm will generate a similar signal to 100mW at 650nm

Currently single longitudinal mode lasers are available at 532nm and would be commercially viable for low cost equipment. This should extend to 355nm and 255nm in the near future. In the longer term the advent of the blue diode laser should prove advantageous in many light scattering arrangements. The laser should be operated in gain saturated mode, to increase stability and must be plane polarised, Section 3.3-2.

7.4-2 The Optics

7.4-2/1 Physical Limitations of the Arrangement

It was not possible vary the polarisation state and NA of the optical arrangement as was initially planned, due to the lack of stability of the alignment. Each time the fibre was rotated it became misaligned to the laser requiring significant time to realign and giving different polarisation extinction and transmitted power. This made relative measurements time consuming and of limited significance. This work concluded that the measurement of orthogonal polarisation states was the optimum arrangement for this system and as such this arrangement was fixed, Section 2.5-1/6, 7. Similar technical, as opposed to fundamental, problems were encountered with sample adhesion, although this problem was alleviated with non-stick coatings.

7.4-2/2 Fresnel Reflection

This problem was initially encountered due to third order reflections from a polarising beamsplitter that caused laser instability, Section 3.4-1/2. In addition when a window was initially added to the probe a heterodyne component was noted, Section 5.2-3/6. This disallowed the use of high refractive index windows such as sapphire and the possibility of using Grin lenses. Even with a significant angle ground in the plane of the incident polarisation the extinction, in excess of 10^6, cannot be maintained as the grin lens wears. It is envisaged all future work will utilise low refractive index thin windows. These were tested and the hardware is shown, Appendix 1.

This work also suggests that a homodyne instrument is not practical using a monomode fibre coupler. This was also concluded by literature published during the project using a single mode Y coupler (Bremer *et al.* 1993). Homodyne FODA results have been reported using a coupler with slanted optode (Lilge and Horn 1991). However, Wiese and Horn (1991) demonstrated that, even with the angled optode, Fresnel reflection, from the fusion splice in the coupler, was of the order of 3Kcps. The lowest intensity used in their work was 300kcps to ensure a homodyne operation. This would indicate significant bias may have been present, Figure 45, 46, Section 5.3-1/2. In their work each measurement was carried out at a different scattering intensity and it is suggested that this would increase the error in terms of both size ranking and reproducibility, compared to analysis using a constant scattered intensity.

7.4-2/3 Fibres

This project utilised monomode fibres thus ensuring a near ideal correlation intercept (Section 3.4-2/3) and ensuring environmental perturbations did not scramble the signal, Section 3.4-2/2. The Bow tie birefringent fibre utilised, whilst showing the highest loss of any birefringent type, allows the highest birefringence and thus vibration stability, Section 3.4-3/4. The narrow NA in a single dimension allows for a distant ballistic crossover and negligible heterodyne signal from multiple reflections in the probe window.

The theory of monomode fibres is often related to that of the TEM_{00} laser mode. This may be misleading as it does not take account of the length of fibre required for the LP_{11} mode to stabilise, which may cause noise in the short lengths of fibre typical of optical probes. This work used a fibre length of 5m to ensure mode stability, as mode scrambling cannot be used with birefringent fibres, Section 3.4-2/5.

To ensure stability this work has suggested that the fibre launch should tend toward over-fill and that mode stripping should occur on launch, Section 3.4-2/4. The work of Vankeuren *et al.* (1993b) supports the concept of near-retroreflection for diffuse scattering.

Dhadwal *et al.* (1993) suggested a novel lens based on fusing a length of gradient index fibre to a single core fibre. This may improve collection efficiency but the grin fibre is liable to suffer modal noise, particularly in the short lengths proposed. Any change in the environmental or the fibre fill condition will lead to variation in the detected intensity, Section 3.4-2/4. Polarisation noise may also occur, as the fibres will not maintain the polarisation states in a stable manner. The limitation of fusion splices has also been discussed as creating a significant local oscillator (Wiese and Horn 1991).

7.4-2/4 Optical Components

Achromatic lenses have the smallest blur surface possible and are the optimum choice for fibre launch. On detection grin lenses may be used which are economical and simpler to align, as well as having a larger blur circle radius than plano-convex lenses (Brown and Jackson 1987). For collimation the SLS 2 variety appeared to be the optimum lens (Sakamoto 1992). Achromatic and plano-grin lenses, as discussed, were used for this work. This work has stated for maximum signal to noise a neutral density filter should be used at detection as opposed to launch.

The use of narrow-band polarising beamsplitting cubes gave in excess of the 500:1 extinction, which was the limit maintained by the fibre. Where lasers are operated at full power it may not be necessary to utilise a polarising filter on launch. Whilst a fibre may be made to be intrinsically polarising they are not beneficial for DWS as large lengths are required for a reasonable extinction and they are susceptible to noise if their environment varies (Okoshi 1981, Varhnam *et al.* 1983B).

7.4-3 Limitations of The Sensor Dynamics Correlator

7.4-3/1 Hardwired Correlation

A significant amount of work has been carried out on both the theoretical methods of signal processing and on the implementation of the single clipping, digital correlation approximation, Section 3.2-3. The project used post detection autocorrelation carried out by hardwired digital correlators, as the technique has been shown to be highly successful in PCS. However, the limitations of the technique for DWS, due to the limited correlation speed, suggested other methods should be considered. This section also considers some of the limitations of the Sensor dynamics correlator, which were found in this work.

7.4-3/2 Correlator Bandwidth

The theoretical optimum layout for DWS would appear to be (log (channel number))^2 such that the final output trace was log spaced as is the case in most DLS experiments. However, there are two limitations of digital correlation that suggest this is not viable using conventional hardware. The major limit is the minimum delay time of digital correlators, which is typically 25-50nanoseconds. Correlators have been produced with higher bandwidths but usually with a very limited number of channels. Thus it is not practical to have a significant number of points on the front end of the correlation with this technology. A second problem with this technology is that the channel spacing does not increase as a continuous function, causing fitting problems when dealing with complex line-shapes, Figures 21-24.

7.4-3/3 Correlator Feedback

The Sensor Dynamics correlator had various problems, some of which were corrected during the course of the project. One concern is the lack of feedback from the correlator when the various parameters were set. The SensorDynamics module reported back requested settings, as opposed to those actually used by the hardware. Unless the correlator operator was aware of its functionality, ludicrous parameters could be used in analysis. One of the more serious incorrect feedback problems related to the correlator flagging a measurement finished prior to the accumulator readout being stable.

7.4-3/4 Measurement Finished Flag

The correlator had a measurement finished flag that could be accessed by the software driver. However it was found that this flag indicated only that the measurement and not the calculations had ceased. This was overcome by downloading the correlation repeatedly, after the measurement finished flag had gone high. The value of all the accumulators was summed and the experiment deemed finished when the sum stabilised.

7.4-3/5 Real Time Display

The real time display was found to be of limited use. The requirement for long integer numbers in the accumulators had led to data transfer being carried out cyclically. When operating at short correlator delays the correlator often performed a calculation during readout, leading to a stepped correlation function. This suggests that useful real-time display could be generated by the output of one (of 16) correlator channels per chip, at the same time.

7.4-3/6 The Start Error

In principle, the experimental duration for a single correlation may be quite short. A sample with a coherence time of 0.1μs may be measured to a 1 percent accuracy in 0.1 second, Equation 33.

However, the correlator was shown to have a start bias that significantly affected the results, on short measurements.

This situation is rarely a concern in PCS, due to the low frequencies of single scattering where experimental durations of 30-300s are typical, which may explain why the error was unreported.

However, DWS operates over rapid time-scales and short experiments are practical provided background noise has been correlated out (which is rarely a problem for experimental durations in excess of 1s).

Bias was shown to be a problem since the electronic circuits carry out only an approximation to a digital correlation. If the correlation registers are set to zero at the start of an experiment, then as they begin to fill the input data is correlated with zero. While the first channel has had 256 numbers to correlate, the last channel has just received its first. This error will be weighted out within a few seconds, but the high level of reproducibility of DWS and practicality of 1-2 second experiments has shown that the error must be removed or at least taken into account.

7.4-3/7 Modelling or Removing the Start Error

The error could be reduced to an average of 50% of its usual value simply by filling the registers with random numbers prior to the start of the experiment. The correlation of the first 256 numbers is with a random signal as opposed to a null one. However, more accurately, for constant illumination intensity, the error will be estimated by:

$$N_{correlator\ runs} = Duration / (\tau \times N_{channels}) \qquad \text{Equation 75}$$

$$Error = \alpha(0) / N_{correlator\ runs} \qquad \text{Equation 76}$$

$$\alpha (n) = \alpha (n) - (n\ Error / N_{channels}) \qquad \text{Equation 77}$$

In practice α (1) was used for efficiency in this work.

The optimum option would be to remove the error completely by resetting the accumulators (delay x $N_{channels}$) into the experiment, or holding ADD ENABLE low until a similar period. The latter should be trivial to carry out in hardware, a counter and flip-flop releasing ADD ENABLE after $N_{channels}$ clock periods.

7.4-3/8 New Signal Processing Techniques

The major reasons for developing a new analysis technique over conventional correlation would be to enable higher speed operation and to allow short unbiased measurements. Whilst real time electronic correlators could be produced that operated more rapidly, it appears likely that there is an inherent limitation around 100 MHz, due the speed of electronic switching. There is also unlikely to be a market ready to support this type of development.

Whilst true optical correlators do not yet exist, work has been carried out producing the correlator delay lines from optical fibres operating at 1GHz (Sampson *et al.* 1993).

7.4-3/9 Timing Circuits

Phase measurements of DLS signals have been considered by Rebolledo *et al.* (1984), Lopez *et al.* (1986) and Moreno et al. (1988). Szajnowski (1993) discussed the use of measurement of the correlation from a set of independent measurements in time but this assumed a Gaussian process. This is not suitable for multiple light scattering where the statistics may differ with concentration due to interactions.

A continuous method of timing was proposed by Basano *et al.* (1993) following methods similar to earlier workers (Hallet *et al.*1972, Subrahmanyam 1986, Bruge *et al.* 1989). The device operated by storing the time between pulses to a FIFO memory, as opposed to the actual data stream, but was still limited by the time required to reset the device after a single event (100 us) and the maximum number of the counter (32)[1].

Provided the detected count rate is low (less than one photon per τ_0) continuous timing circuits may be used to generate an unbiased pulse arrival distribution, which may be analysed by Fourier Transform methods. These have not been significantly commercially exploited, probably because of noise in DLS experiments (Gardner *et al.* 1959, Finsy *et al.* 1992).

However, the reproducibility of the DWS signal suggest that timing methods may be well suited for analysis allowing a significant bandwidth increase in electronically analysed DWS measurements.

1 Recent work has suggested that continuous timing with a two photon bandwidth of the order of 1GHz, and a repetitive frequency limit of the order of 200MHz, could be achieved using parallel timing circuits. The concept is only made practical by the use of real-time data compression, equivalent to the typical logarithmic correlation spacing (Lloyd and Clarke 1999)

7.5 Analysis Methods

7.5-1 Analysis of the Correlation

7.5-1/1 Normalisation and Data Selection

In DLS studies it is necessary to measure the baseline accurately in order to normalise the data. While all data presented in this work is normalised to the baseline it was found to be less critical than most DLS and DWS work. This can be traced to the very low noise of the system (typically 100cps) and the high intercept. Whilst the majority of PCS instrumentation is based on a pinhole approach, the use of monomode fibres and the use of homodyne operation ensured the correlation intercept was typically above 0.9 and the system operated successfully with all Step 0, 1, 2 measurements.

In later work only a restricted portion of the correlation was analysed to reduce the variation of Γ with concentration. Problems were encountered when the analysis area was restricted to the area around the correlation intercept, Section 6.3-4. As less of the correlation is measured the relative error in Γ increases, as shown on Figure 78, exemplifying the differences in variance when analysing 63 and 27 percent of the correlation. When analysis was restricted to only the top 15 percent of the correlation function the measurement crashed. The software required the user to give a percentage (%) of the correlation to be used in analysis and only correlation channels with accumulator values given by Equation 65 were used in the analysis. Thus if the normalised intercept value was lower than the percentage requested then no data was within the selected window.

The data area could be selected from a percentage below the actual intercept value as opposed to the theoretical one of twice the baseline. However, the variation in the correlation line-shape at short delay times exhibited by complex samples would significantly alter what was being monitored. This problem is re-addressed later, Section 7.5-1/3.

7.5-1/2 Straight Line Fitting

The original Step 0,1 methods were very crude techniques for obtaining the straight line portion of the correlation. However, they operated very successfully giving a good sensitivity (Figure 54) and reproducibility (Figure 49). The stability of the method can be traced to the beneficial effect of the correlator channel spacing, Figure 21.

The square root spacing of the data points weighted the analysis making the instrument more sensitive to short decay effects, as opposed to shifts in the curvature of the long delay tail. Only a small linear portion of correlation was required to stabilise the fit.

The major reason for moving away from the original method was that of correlator temporal resolution. It was apparent even when setting the correlator at its shortest decay that the number of channels used in the analysis also had to be varied.

The Step 2 method reduced the effect of the number of channels and correlator delay on the measurement and analysis but only with significantly increased data and complexity. The method involved interpolation of data sets after analysis, Appendix 3. The final Step 3 approach allowed the correlator channels and delay to be varied in a stable and reproducible way that could be automatically controlled. The parameters %curvature and % intercept (Section 6.2-3) were found to be useful in allowing a simple and robust method of describing variation between the actual correlation line-shape and the theoretical model.

7.5-1/3 Future Fitting Methods

The final Step 3 method operated successfully in most samples and allowed the correlation to be analysed in a stable and reproducible manner. However in gel systems where the correlation intercept was reduced the method was limited. It is proposed that any next generation analysis method should incorporate the Step 3 method of making a certain sub-section of the correlation (f_b) occur on a given channel (RC) and thus allow the full automation that has been described, Section 6.2-3.

However, the linear fit should not be forced to analyse a specific section of the correlation but follow the floating method of Step 0, 1. To overcome the effect of the short time curvature the correlation should be fitted with a quadratic. If this fit occurred without further restriction the portion of correlation used in analysis would vary significantly between sample types. Where the sample generated a short term curve in the correlation the method would analyse only the rapid decaying section as required. However, in samples where short term curvature did not exist or was more pronounced then the quadratic would allow a significant portion of the long time delaying tail to be analysed.

Thus, the fit requires to be restricted such that curvature gives a negative or null parameter in the quadratic so that this parameter is a direct measure of front end curvature alone.

The use of a cubic spline, allowing both short and long time curvature to be analysed, has been considered but this may over-resolve the actual data. Consideration has also been given to analysis of the curve shape by neural net type approaches to obtain more information than is conventionally apparent. Methods of compression that would allow analysis of three dimensional correlation line shapes with a reduced number of parameters have been discussed, Section 6.2-4/4.

DWS data is more reproducible than DLS data and should not exhibit the same noise limitations of previous DLS studies (Gardner *et al.* 1959).

7.5-1/4 Noise Rejection

In commercial DLS equipment it is common to reject a percentage of the raw data to increase the accuracy of the analysis. Two separate arguments have been used to support this but this work suggests that they are contradictory. The first argument is that DLS is a purely statistical process and it is allowable to disregard random errors. The second argument suggests the probability of dust within the measured volume is statistical and that measurements affected by dust may be disregarded.

In the first case experiments furthest from the mean are disregarded, the decision based purely on the magnitude of their error. However, in the second case it is only measurements of long decay times that are disregarded, a decision based on measurements giving a large mean size, or high count rate. It follows that in the latter case, in highly disperse samples especially those with a small population of larger particles, the rejection principles may bias the results.

This would appear to be true of pigment samples containing oversize, a conventional PCS analysis may report the sample as monodisperse but dirty. The rejection criteria are usually fixed percentage, i.e. a given percentage of experiments are excluded or data is excluded until a certain standard deviation is reached. This work suggests that neither is optimum and that data should be disregarded until the variance in the measured parameter ceases to decrease significantly, Figure 50. This may not be practical for DLS, as experiment durations may become excessive to allow the variance to approximate that of infinite experiments.

In DWS the statistical variance has been shown to be significantly smaller than in DLS, due to both the rapid decay and the effective ensemble average contained in each photon delay. Thus results obtained from measurement durations of as little as two seconds will rapidly sum to give an error that is as low as is possible for that arrangement, equivalent to that of an infinite experiment duration.

The averaging of each photon delay in DWS has a secondary benefit in that it makes the error in the DWS signal purely statistical. Whereas in DLS the presence of a small percentage of large particles leads to a few experiments that are significantly biased, in DWS the multiple scattering ensures each photon delay is a function of all particle sizes. This suggests a significant benefit of DWS, especially in milling applications, as oversize particles are not ignored as dust and affect all measurements equally, regardless of how small the population is.

7.5-2 The Time Dependent Correlation

7.5-2/1 Pigment and Related Materials

A significant amount of work in published literature uses only polystyrene reference beads as an example. Whilst some measurements on industrial samples have been carried out (Horne 1989,1992), these are typically of highly stable media, or during a known processing cycle. This work operated on very dense industrial samples. The difference was highlighted by the industries use of the term 'stable' to mean a sample that could be re-suspended after it had settled (flocculation was weak). The nature of the settling pigment gave a correlation that was a function of t as well as τ, Figure 57

7.5-2/2 Early Temporal Analysis

Originally the time analysis was carried out by re-running measurement routines meant for stable materials and selection of the best-suited data after collection, Appendix 2. This was time consuming, required vast quantities of data and was inefficient in that it made minimal use of most of that data, Section 5.4-5/3. A significant amount of work was carried out in design and evaluation of a system, which could realistically monitor rapidly changing samples and deliver stable real-time output.

7.5-2/3 Automatic Delay and Channel Number Setting.

The algorithms for setting the correlator delay time, calculated from the previous experiment, and then selecting the correct channel for the data being analysed showed themselves to be highly stable. Even where the sample underwent dramatic variations the methods were self stabilising and did not hunt, Figure 75, 90. The rapid stabilisation time of the method allowed the system to follow samples could not be analysed by other light scattering methods, even assuming dilution was possible.

7.5-2/4 Three Dimensional Fitting

The original work was aimed at using a three dimensional fit for each correlator channel purely to produce variance errors in each correlator channel, such that correct fitting could be carried out. However, the method allowed for the production of a 'mean' correlation interpolated to any time of the measurement and thus allowed visualisation of changes in the correlator line-shape at any measurement time, Figure 72, 73, Section 6.2-5. It also allowed for comparison between different variables, i.e. Γ could be plotted as a function of intensity or refractive index etc, Figure 74. The model assumed the variation, in the value of each normalised correlation channel, could be considered quadratic over a selected time period. This proved to be suitable for the majority of samples, provided the time range was sensibly selected. Whilst more complex models could be used, this method was seen as acceptable for a feasibility evaluation, and ensured no limitation due to over-resolving data.

7.6 Summary

This work has investigated the technique known as diffusing wave spectroscopy as a method of real-time in-line characterisation of industrial materials. It has been shown that the technique cannot be related to absolute size but allows a ranking ability of better than 1 percent and variance of 0.1 percent to be achieved in industrial samples. A range of suspensions and emulsions have been analysed, including TiO_2 pigments, which were the major project application.

The concentration dependence of the instrument function, for TiO_2, has been shown to be minimal over volume fractions between 0.075 and 0.35 and methods of calibration of the measurement by analysis of the intensity of the scattered signal have been shown to be practical.

Most techniques to analyse dense suspensions require a dilution or other pre-processing stage. DWS has shown to have sensitivity that is comparable to, or better than, conventional measurements without the need for any dilution or pre-processing. The technique used a dip-in probe, which could be mounted, within a pipeline port. The technique requires low laser powers allowing for simple implementation in an industrial environment.

Homodyne operation has been shown to operate successfully with no significant heterodyne component present, even at low volume fractions. An extinction of the heterodyne signal of 1 part in 10^{12} was achieved at all volume fractions analysed.

A significant quantity of software and algorithms were produced to allow an automated measurement, even in samples that exhibit rapid variation. Conventional DLS techniques of merely altering the correlator length by an integer number of the minimum correlator delay did not allow for the high frequency signals that were analysed. The algorithms used feedback to dynamically set both the correlator delay and the number of channels used in analysis, in a manner that was stable and did not introduce hunting.

Many of these algorithms are equally applicable to conventional DLS instrumentation, which conventionally requires a skilled operator.

The algorithms and methods were capable of analysing vast data sets of 100 separate correlations and their fits whilst also producing a sensible data restricted output. Various new parameters were defined to describe the correlation line-shape in concise and simple to evaluate factors.

The instrument function has been shown to be able to analyse different parameters to conventional DLS and the wavelength dependence of the instrument function has been discussed as being significantly different. The work has also led to consideration of analysis of a dispersion factor, by means of the time dependent nature of the samples. This has been discussed as being more valid for the evaluation of dense sample characteristics and behaviour than the of the particle size distribution. In addition the dilution required for PSD analysis has been discussed as further reducing its validity.

The methods used in conventional DLS noise reduction have been discussed as producing significant bias in samples that include a very small population of particles significantly greater than the mean. Thus in samples from milling operations, where oversize is present, results may be misleading. This work has also considered that the intrinsic ensemble averaging that occurs within DWS allows similar noise reduction methods to be used without introducing the bias.

Particle shape and interactions have been shown to strongly affect the correlation line-shape. It has been suggested that further work may allow new characterisation methods of aspect ratio in dense suspensions. Complementary methods of static light scattering analysis of the diffuse signal have been described.

The theory of dependant scattering has been reviewed and methods of concentration independent analysis, of particles of similar refractive index, have been described.

The optical arrangement and analysis methods have been shown as suitable to operate within an industrial setting.

References

Anderson P. W., 1958, Absence of diffusion in certain random lattices, Phys. Rev., Vol. 109, No. 5 pages 1492-1505

Ansari R., Dhadwal H. S., Cheung H. M., Meyer V. W., 1993, Microemulsion characterisation by the use of a noninvasive backscatter fibre optic probe, Appl. Optics, Vol. 32, No. 21, pages 3822-3827

Antognetti A., Cova S., Longoni A., 1975, Proc 2nd ISPRA Nuc. Elect. Synops., Euratom Pubs, page 453

Auweter G., Horn D., 1985, Fibre optic quasielastic light scattering of concentrated solutions, J. Colloid and Interface Sci, Vol. 105, No. 2, pages 399-405

Barlow A. J., Payne D. N., Hadley M. R., Mansfield R. J., 1981, Production of single mode fibres with negligible intrinsic birefringence and polarisation mode dispersion, Elect. Lett., Vol. 17, No. 20, pages 725-726

Basano L., Ottonello P., Schiavi E., 1993, Multipurpose analysers for photoelectron statistics implementation and use, Appl. Optics, Vol. 32, No. 23, pages 4430-4436

Bellini T., Glaser M. A., Clark N. A., Degiorgio V., 1991, Effects of finite laser source coherence in quasielastic multiple scattering, Phys. Rev. A, Vol. 44, No. 8, pages 5125-5223

Bernhardt C., 1988, Preparation of suspensions for particle size analysis methodical recommendations liquids and dispersing agents, Advances in Colloid and Interface Sci., Vol. 29, pages 79-139

Bertolotti M., 1973, Photon statistics, Photon Correlation and Light Beating Spectroscopy, pages 41-74, Ed. Cummins H. Z., Pike E. R., Plenium Press NY, ISBN 0-306-35703-8

Bicout D., 1993, Non Newtonian behaviour of colloidal suspensions from multiple light scattering, Phys. Lett. A, Vol. 180, pages 375-378,

Bicout D., Brosseau C., 1992, Multiply scattered light through a spatially random media entropy production and depolarisation, J. Phys. I, France, No. 2, pages 2047-2063

Birch R. Payne D. N. Varnham M. P., 1982, Fabrication of polarisation maintaining fibres using gas phase etching, Elect. Lett., Vol. 18, pages 1036-1038

Bremer L. G., Deriemaeker B. L., Finsey R., Gelade E., Joosten J. G.H., 1993, Fibre optic light scattering, neither homodyne nor heterodyne, Am. Chem. Soc, Langmuir, No. 9, pages 2008-2014

Brown G. W., 1987, Dynamic light scattering using monomode fibres, Appl. Optics, Vol. 26, pages 4846-4851.

Brown G. W., Grant R. S., 1987, Photon statistical properties of visible laser diodes, Rev. Sci. Instrum., Vol. 58, No. 6, pages 928-931

Brown G. W., Jackson A. P., 1987, Monomode fibre components for optical light scattering, J. Phys. E, Sci. Instrum., Vol. 20, pages 1503-1507

Brown G. W., Jones R., Rarity J. G., Ridley K. D., 1987, Characterisation of silicon avalanche photodiodes for photon correlation measurements 1: active quenching, App. Optics, Vol. 26, No. 12, pages 2383-2389

Brown G. W., Rarity J. G., Ridley K. D., 1986, Characterization of silicon avalanche photodiodes for photon correlation measurements 2: passive quenching, App. Optics, Vol. 25, No. 22, pages 4122-4126

Bruge F., Biagio P. L. S., Fornili S. L., 1989, New photon correlator design based on transputer array concurrency, Rev. Sci. Instrum., Vol. 60, No. 11, pages 3425-3249

Bruscaglioni P., Zaccanti G., Wei Q., 1993, Transmission of a pulsed polarised light beam through thick turbid media numerical results, Appl. Optics, Vol. 32, No. 30 pages 6142-6150

Carr R. J. G., Rarity J. G., Stansfield A. G., Brown R. G. W., Clarke D. J., Atkinson T., 1988, Determination of protein size in chromatography column eluants by online photon correlation spectroscopy, Analytic Biochem., Vol. 175, pages 492-499

Cherin A. H., 1983, An Introduction to optical fibres, Pub. McGraw-Hill, ISBN 0-07-010703-3

Chow K. M., Stansfield A. G., Carr R. J. G., Rarity J. G., Brown R. G. W., 1988, Online photon correlation spectroscopy using fibre optic probes, J. Phys. E, Sci. Instrum., Vol. 21, pages 1186-1190

Chowdhury D. P., Sorensen C. M., Taylor T. W., Merklin J. F., Lester T. W., 1984, Application of Photon Correlation Spectroscopy to flowing Brownian motion systems, App. Optic Vol. 23, No. 22 pages 4149-4153

Chu B., 1970, Laser light scattering, Ann. Rev. Phys. Chem., No.21, pages 145-174

Coates P. B., 1973, The origins of afterpulses in photon multipliers, J. Phys. D, No. 6, pages 1159-1165

Cova S., Longoni A., Andreoni A., 1981, Towards picosecond resolution with single photon avalanche diodes, Rev. Sci. Instrum., Vol. 52, pages 408-412

Cova S., Longoni A., Ripamonti G., 1982, Active quenching for single photon avalanche diodes spads, IEEE Trans. on Nuc. Sci., Vol. 29, No. 1, pages599-601

Cummins H. Z., Carlson F. D., Herbet T. J., Woods G., 1969, Translational and rotational diffusion coefficients of tobacco mosaic virus from Rayleigh linewidths, Biophysical J. Vol. 9, pages 519-546

Cummins H. Z., Knable N.,Yeh Y., 1964, Observation of diffusion broadening of Rayleigh scattered light, Phys. Rev. Lett., Vol. 12, No.6, pages 150-153

Cummins H. Z., Pike E.R., 1974, Photon correlation and light beating spectroscopy, Plenum Press, ISBN 0-306-35703-8

Cummins P. G., Staples E. J., 1981, Particle size measurements on turbid latex systems using heterodyne intensity autocorrelation spectroscopy, J. Phys. E: Sci. Instrum., Vol. 14, pages 1171-1177

Cummins H. Z., Swimney H. L., 1970, Light beating spectroscopy, Prog. in Optics, Ed. Wolf E., Vol. 8, Chap. 3, pages 133-200

Dautet H., Deschamps P., Dion B., Macgregor A. D., Macsween D., Mcintyre R. J., Trotter C., Webb P. P., 1993, Photon counting with silicon avalanche photodiodes, Appl. Optics, Vol. 31, No. 21, pages 3894-3900

De Wolf D. A., 1971, Electromagnetic reflection from an extended turbulant medium cumulative forward-scatter single back-scatter approach, IEEE. Trans. Attennas Propag., Vol. AP-19, No. 2, pages 254-262

Dhadwal H. S., Khan R. R., Suh K., 1993, Integrated fibre optic probe for light scattering, App. Optics, Vol. 32, No. 21, pages 3901-3904

Dhadwal H. S., Ross D. A., 1980, Size and concentration of particles in syton using the fibre optic doppler anemometer, FODA, J of Coll. and Inter. Sci., Vol. 76, No. 2, pages 478-489

DonoVan D. P., Whiteway J. A., Carswell A. I., 1993, Correction for nonlinear photon counting effects in lidar systems, Appl. Optics. Vol. 32, No. 33, pages 6742-6753

Dorshow R. B., Photon counting dead time measurement in commercial laser light scattering instrumentation, 1990 Rev. Sci. Instrum. Vol. 61, No. 1, pages 186-188

Durian D. J., 1995, Accuracy of diffusing-wave spectrocsopy theories, Phys. Rev. E, Vol. 51, No. 4, pages 3350-3358

Durian D. J., 1996, Two stream theory of diffusing light spectroscopies, Physica A, Vol. 229, Iss. 2 pages 218-235

Dyott R. B., 1978, The fibre optic Doppler anemometer, Microwaves Opt. Acoust., Vol. 2, No.1, pages 13-27

Fagen S. J., 1993, Vacuum avalanche photodiodes can count single photons, Laser Focus World Nov., pages 125-132

Finsy R., Deriemaeker L., Gelade E., Joosten J., 1992, Inversion of static light scattering measurements for particle size distributions, J. of Colloid and Interface Sci., Vol. 153, No. 2, pages 337-354

Fitzwater S., Hook III J. W., 1985, Dependent scattering theory a new approach to predicting scattering in paints, J. of Coatings Tech., Vol. 57, No.721, pages 39-50

Floy B. J., White J. L., Hem S. L., 1988, Fibre optic doppler anemometry FODA as a tool in formulating emusions, J. of Coll. and Inter. Sci., Vol. 125, No. 1, pages 1020-1031

Foord R., Jones R., Oliver C. J., Pike E. R., 1975, The use of photonmultiplier tubes for photon counting, App. Opt., Vol. 8, No. 10, pages 1975

Ford Jnr. N. C., 1972, Biochemical applications of laser Rayleigh scattering, Chem. Scripta., No. 2, pages 193-206

Forrester A. T., 1961, Photoelectric mixing as a spectroscopic tool, Opt. Soc. Am., Vol. 51, No. 3, pages 253-259

Forrester A. T., Gudmudsen R. A., Johnson P. O., 1955, Photoelectric mixing of incoherent light, Phys. Rev. Vol. 99, No.6, pages 1691-1700

Garcia N., Genack A. Z., Lisyansky A., 1992, Measurement of the transport mean free path of diffusing photons, Phys. Rev. B, Vol. 46, No. 22, pages 14-475

Gardner D. G., Gardner J. C., Laursh G., Meinke W. W., 1978, Method for the analysis of multicomponent exponetial decay curves, J. Chem. Phys., Vol. 31, pages 978-986

Goddard A., 1995, Freshness Test gets to the thick of it, New Scientist page 6, May

Grant A., 1993, Avalnache Photodiode Quenching Circuit, MSc Thesis, University of Northumbria

Hallet F. R., Gray A. L., Rybakowski A., Hunt J. L., Stevens J. R., 1972, Photon correlation spectroscopy using a digital PDP-9 computer, Canada J. of Phys., Vol. 50 pages 2368-2372

Hanbury Brown R., Twiss R. Q., 1956, Correlation between photons in two coherent beams of light, Nature, Vol 177, pages 27-29,

Heckmeier M., Maret G., 1998, Static imaging of dynamic fluctuations in multiple light scattering media, Optics Comms., No. 148, pages 1-5

Hoover W. G., Ree F. H., 1988, J. Chem. Phys.,Vol. . 49, pages 3609-3617

Horne D. S., 1989, Particle size measurement in concentrated latex suspensions using fibre optic photon correlation spectroscopy, J. Phys., Appl. Phys., No. 22, pages 1257-1264

Horne D. S., 1990, Influence of polydispersity on dynamic light scattering measurements in concentrated suspensions, J. Chem. Soc., Faraday Trans, Vol. 86, No. 7, page 1149

Horne D.S., Davidson C. M., 1993, Application of diffusing wave spectroscopy to particle sizing in concentrated dispersions, Coll. and Sur. A., Vol. 77, No. 1, pages 1-8

Jakeman E., 1973, Photon correlation, Photon Correlation and Light Beating Spectroscopy, pages 75-150, Ed. Cummins H. Z., Pike E. R., Plenium Press NY, ISBN 0-306-35703-8

Javan A., Bennet Jnr. W. R., Herriott D. R., 1961, Population inversion and continuous optical maser oscillation in a gas discharge containing a He-Ne mixture, Phys. Rev. Lett., Vol. 6, No. 3, pages 106-110

Judin V. P., 1993, The lighter side of TiO_2, Chem. in Brit. June, Pages 503-505

Kao M. H., Yodh A. G., Pine D. J., 1993, Observation of Brownian motion on the time scale of hydrodynamic interactions, Phys. Rev. Lett., Vol. 70, No. 2, pages 242-245

Kaplan P. D., Ming H. K., Yodh A. G., Pine D. J., 1993, Geometric constraints for the design of diffusing wave experiments, Appl. Optics, Vol. 32 Iss. 21 pages 3828-3826

Kaplan P. D., Yodh A. G., Pine D. J., 1992, Diffusion and Structure in Dense Binary Suspensions, Phys. Rev. Lett., Vol. 68, pages 393-396

Kerker M., 1969, The scattering of light and other electromagnetic radiation, Ed. Lobel E., Academic Press, LCCN 69-26644

Koppel D. E., 1972, Analysis of macromolecular polydispersity in intensity correlation spectroscopy: The method of cumulants, J. Chem. Phys., Vol. 57, No.11, pages 4814-4820.

Lawson J., 1992, Tioxide plc, in-house prepublication text

Lemieux P. A., Ver M.U., Durian D.J., 1996, Diffusing light spectroscopies beyond the diffusion limit: the role of ballistic scattering, Phys. Rev. E, Vol. 57, No. 4, pages 4498-4515

Levine B. F., Bethea C. G., 1984, Detection of single 1.3 micron photons at 45 mbit/s, Elect. Lett., Vol. 20, No. 6 pages 269-271

Lightstone A. W., Mcintyre R. J., 1988, Photon counting silicon avalanche photodiodes for correlation spectroscopy, Proc. Photon Correlation Tech. and App., OSA, Washington, pages 183-191

Lilge D., Horn D., 1991, Diffusion in concentrated suspensions: a study with fibre-optic quasielastic light scattering FOQELS, Colloid and Polymer Sci., Vol. 269, pages 704-712

Lloyd C. J., Perkins E. A., Atkinson T., Carr R. J. G., 1993, Diffusing wave spectroscopy, Proc. Biomedical Optics Europe, Budapest. SPIE, Vol. 2082, pages 279-287

Lloyd C. J., Perkins E.A., Carr R. J. G., 1997, Dynamic light scattering and its application in concentrated dispersions, Advances in Fibre Sensors, Editors Culshaw B. and Dakin J., Artech Books pages 109-127

Lloyd C. J., Carr R. J. G., Diffusing wave spectroscopy - invited presentation at the Ann. Chem. Conf., Heriot Watt University April 1995

Lloyd C. J., Diffusing wave spectroscopy - invited presentation, Rank Prize Funds Mini Symposium on Optical Localisation and Slow Waves, Grasmere, September 93,

Lloyd C.J., 1991, Diffusing wave spectroscopy, MSc Optoelectronics Thesis Newcastle Polytechnic

Lloyd, Clarke, 1999, Non-stop non-linear timing, UK Patent Application, GB 98/03093

Lopez R. J., Moreno F., Robelledo M. A., 1986, Determination of the period of a low-intensity square-wave-modulated beam by measuring a square-wave transform of the time interval probability, M. A., Opt. Soc. Am. Vol. 3, No. 3, pages 365-368

Louis T., Schatz G. H., Klein-Bolting P., Hozwarth A. R., Ripamonti G., Cova S., 1988, Performance comparison of single photon avalanche diode with a micro channel plate photon multiplier in time correlated single photon counting, Rev. Sci. Instrum., Vol. 56, No. 7, pages 1148-1152

Macfayden A. J., Jennings B. R., 1990, Fibre optic systems for dynamic light scattering, Optics and Laser Tech., Vol. 22, No. 3, pages 175-187

Mackintosh F. C., John S., 1989, Diffusing wave spectroscopy and multiple light scattering in concentrated dispersions, Phys. Rev. B, Vol. 40 No. 4, pages 2383-2406

Mandel L., 1963, Fluctuations of light beams, Prog. in Optics, Ed. Wolf E, Pub. N. Holland Amsterdam, Vol. 2, Chapter 5, pages 183-248

Maret G., Wolf P. E., 1987, Multiple light scattering from disordered media. The effect of Brownian motion on scatterers, Z. Phys. B, Con. Matter, Vol. 65, pages 409-413

Martiensen W., Spiller E., 1964, Coherence and Fluctuations in Light Beams, Am. J. Phys., Vol. 32, pages 919-926

Menon N., Durian D. J., 1997, Diffusing Wave Spectroscopy of dynamics in three-dimensional granular flow, Science., Vol. 275, pages 1920-1922

Moreno. F., Gonzalez F., Lopez R. J., Lavin A., 1988, Time-interval statistics through a lapace transform method in quasi-elastic light-scattering experiments for low-intensity levels, J. Opt. Soc. Am. Vol. 13, pages 637-639

Muller P., Muller J.,, 1984, Particle size analysis of latex suspensions and micro emulsions by photon correlation spectroscopy, J. Pharm Sci, Vol. 73, No. 7, pages 915

Nieuwenhuizen T. M., Luck J. M., 1992, Skin layer of diffusive media, Phys. Rev. E, Vol 48,No. 1, pages 569-588

Okashi T., 1981, Single polarisation single mode optical fibres, IEEE J. Quantum Elect, Vol. 17, pages 879-884

Oliver C. J., 1973, Correlation Techniques, Photon Correlation and Light Beating Spectroscopy, pages 41-74, Ed. Cummins H. Z., Pike E. R., Plenium Press NY, ISBN 0-306-35703-8

Owens P. C. M., Rarity J. G., Tapster P. R., Knight B., Townsend P. D., 1994, Photon counting with passively quenched germanium avalanche photodiodes, App. Optics, Vol. 33, No. 30, pages 6895-6901

Pecora R., 1964, Doppler shifts in light scattering from pure liquids and polymer solutions, J. Chem. Phys., Vol. 40, pages 1604-1614

Pecora R., 1968, Spectral distribution of light scattered by monodisperse rigid rods, J. Chem. Phys., Vol. 48, No. 9, pages 4126-4128

Pecora R. J., 1985, Dynamic light scattering, Pleneum Press, ISBN 0-306-41790-1

Perkins E. A., 1990, CAMR (now DERA) unpublished work

Peters R., Georgalis Y., Saenger W., Accessing liposome nucleation with a novel dynamic light scattering detector, 1988, Acta Cryst, No. D54 pages 873-877

Phillies G. J. D., 1990, Quasi-elastic light scattering, Analyt. Chem., Vol. 62, No. 20 pages 1049-1047

Pine D. J., Weitz D. A., Chaikin P. M., Herbolzheimer E., 1988, Diffusing wave spectroscopy, Phys. Rev. Lett., Vol. 60, No.12, pages 1134-1137

Pusey P. N., 1975, The dynamics of interacting Brownian particles, J. Phys. A: Math Gen, Vol. 8, No. 9 pages 1433-1440

Pusey P. N., Van Megen W., 1984, Detection of small polydispersities by photon correlation spectroscopy, J. Chem. Phys., Vol. 80, No.8, pages 3513-3519

Pusey P. N., Van Megen W. 1992, The glass transition of hard sphere colloids, Physica Scripta., Vol. T45, pages 261-264

Pusey P. N., Tough R. J. A., 1983, Hydrodynamic interactions and diffusions in concentrated particle suspensions, Faraday Discuss. Chem. Soc., Vol. 76, pages 123-136

Pusey P. N., Vaughan J. M., 1975, Light scattering and intensity fluctuation spectroscopy, Dielectric and Related Processes, Chap. 2, Chem. Soc. pages 48-105

Qiu X., Wu X. L., Xue J. Z., Pine D. J., Weitz D. A., Chaikin P.M., Hydrodynamic interactions in concentrated dispersions, 1990, Phys. Rev. Lett. Vol. 65, No. 4, pages 516-519

Rashleigh S. C., Marrone M. J., 1982, Polarisation holding in randomly perturbed fibres, Opt. Fibre Conf., pages 56-57

Rebolledo M. A., Lopez R. J., Moreno F., 1984, Analysis of low intensity square wave modulated light beams by measuring the laplace or squared cosine transform on time-interval probability, Optics Comms. Vol. 52 , No.2, pages 81-86

Ricka J., 1993, Dynamic light scattering with single mode and multimode receivers, Appl. Opt., Vol. 32, No. 15. pages 2860-2874

Ross D. A., Dhadwal, H. S., Dyott R. B., 1978, The determination of the mean standard deviation of the size distribution of a colloidal suspension of submicron particles using the fibre optic Doppler Anemometer FODA, J. Colloid Interface Sci., Vol. 64, No. 3, pages 533-543

Russel W. B., 1981, Brownian motion of small particles suspended in liquids, Ann. Rev. Fluid Mech, Vol. 13, pages 425-455

Sakamoto T, 1992, Coupling characteristics and analysis of single mode and multimode optical fibre connectors using gradient index rod lenses, Appl. Optics, Vol. 31, No. 25, pages 5184-5191

Sampson D. S., Dove W. T., Jackson D. A., 1993, High bandwidth optical fibre delay line multichannel digital correlator, Appl. Optics, Vol. 32, No. 21, pages 3905-3916

Sasaki Y., Okamoto K., Hosaka T., 1982, Polarisation maintaining and absorption reducing fibres, Opt. Fibre Conf., pages 54-56,

Sato T., 1979, Assessment of dispersion, J. Coatings Tech, Vol. 51, No.657, pages 79-85

Schatzel K., J., 1991, Suppression of multiple scattering by photon cross correlation techniques, Modern Optics, Vol. 38, No.9, pages 1849-1865

Schmitt J. M., Gandjbakhche A. H., Bonner R. F., 1992, Use of polarised light to discriminate short path photons in multiply scattering media, Appl. Optics, Vol. 31, No. 30, pages 6535

Sorensen C. M., Mockler R. C., O'Sullivan W. J., 1976, Depolarised correlation function of light double scattered from a system of Brownian particles, Phys. Rev. A, Vol. 14, No. 4, pages 1520-1532

Sorensen C. M., Mockler R. C., O'Sullivan W., 1978, Multiple light scattering from a system of Brownian particles, J Phys. Rev. A, Vol 17, pages 2030-2035

Stasiak W., Cohen C., 1993, Concentration fluctuations of Brownian particles in a viscoelastic solvent, J. Chem. Phys., Vol. 98, No. 8, pages 6510-6515

Streetman B. G., 1990, Solid state electronic devices, Pub. Prentice Hall, ISBN 0-13-824749-8

Subrahmanyam V. R., Devraj B., Chopra S., 1987, Microprocessor based photon correlator for intensity fluctuation studies, J. Phys. E, Sci. Instrum, Vol. 20 pages 340-343

Szajnowski W. J., 1993, Efficient Estimation of a normalised correlation function from descrete-time samples, Electronics Lett. Vol. 29, No. 16, pages 1398-1400

Tagami Y., Pecora R., 1969, Light scattering from polydisperse rods and gaussian coils. I. integrated intensities, J. Chem. Phys., Vol. 51, No. 8, pages 3293-3298

Tanaka T., Benedek G. B., 1975, Measurement of the velocity of blood flow (in vivo) using a fibre optic catheter and optical mixing spectroscopy, Appl. Optics Vol. 14, No.1, pages 189-196

Tinsley-Bown A., 1991, CAMR, Phd thesis submitted to the Open University.

Thomas J. C., Allison S. A., Schurr J. M., Holder R. D., 1980, Dynamic light scattering studies of internal motions in DNA 2 clean viral dnas, Biopolymers, Vol. 19, pages 1451-1474

Thomas J. C., Dimonie V., 1990, Fibre optic dynamic light scattering from concentrated dispersions. 3: particle sizing in concentrates, App. Optics, Vol. 29, No.36, pages 5332-5335

Thomas J. C., Tjin S. C., 1989, Fiber optic dynamic light scattering (FODLS) from moderately concentrated solutions, J. Colloid and Interface Sci, Vol. 129, No.1, pages 15-31

Thomas J. C., Schurr M. J., 1979, Photon correlation spectroscopy in the near ultraviolet, Optic. Lett., Vol. 4, pages 222-223

Turnstall D. F., 1980, Method of measurement of particles, UK Patent Application GB 2046898A

Urban C., Schurtenberger P., 1988, Characterisation of turbid colloidal suspensions using light scattering techniques combined with cross correlation methods, J. Coll. Inter. Sci., No. 207, pages 150-158

Van Albada M. P., Lagendijk A., 1985, Observation of weak localisation in random media, Phys. Rev. Lett., Vol. 55, No. 24, pages 2962-2695

Van Albada M. P., Lagendijk A., Van der Mark M. B., 1990, Towards observation of Anderson localisation of light, Analogies in Optics and Microelectronics, Ed. Van Haeringen W, Lenstra D., Pub. Kuwer Academic, pages 85 -103

Van Albada M. P., Van der Mark M. B., Lagendijk A., 1987, Observation of weak localisation in a finite slab: anisotropy effects and light path classification, Phys. Rev. Lett. Vol. 58, No. 4 , pages 361-364

Van Der Meeren P., Bogaert H., Stastny M., Vanderdeelen J, Baert L., 1993, Accurate Determination of the short time self diffusion coefficient by fibre optic quasielastic light scattering new methods for correcting the homodyne effect, J. Coll. and Inter. Sci., Vol. 160, pages 117-126,

Van Megen W., Ottewill R. H., Owens S. M., Pusey P. N., 1985, Measurement of wave vector dependant diffusion coefficient in concentrated particle dispersions, J. Chem. Phys., Vol. 82, No. 1 pages 508-515

Varnham M. P., Payne D. N., Birch R. D., Tarbox E. J., 1983a, Single polarisation operation of highly birefingent bow tie optical fibres, Elect. Lett., Vol. 19, No. 7, pages 246-247

Varnham M. P., Payne D. N., Birch R. D., Tarbox E. J., 1983b, Bend behaviour of polarising optical fibres, Elect. Lett., Vol. 19, No. 17, pages 679-680

Vankeuren E. R., Wiese H., 1993a, Horn D., Diffusing wave spectroscopy in concentrated latex dispersions an investigation using single mode fibres, Coll. Surf. A, Vol. 77, No. 1, pages 29-27

Vankeuren E. R., Wiese H., Horn D., 1993b, Fibre optic quasielastic light scattering in concentrated latex dispersions- angular dependant measurements of singly scattered light, Langmuir, Vol. 9, No. 11, pages 2883-2887

Vankeuren E. R., Wiese H., Horn D., 1994, Fibre optic diffusing wave spectroscopy on concentrated dispersions of large polymer latex samples, J. Physical Chem., Vol. 98, No. 2, pages 269-271

Verdeyen J. T., 1981, Laser Electronics, Pub. Prentice Hall, ISBN 0-13-523655-X

Wang L., Miller W. G., 1992, Short time mobility of spherical particles in concentrated aqueous dispersions determined by DWS, Theor. Chim. Acta., Vol. 82, pages 419-423

Weast., 1979, Handbook of Chemistry and Physics, 1979, CRC Press Inc., ISBN 0-8493-0459-8

Weitz D. A., Pine D. J., Pusey P. N., Tough R. J. A., 1989, Nondiffusive Brownian motion studied by diffusing wave spectroscopy, Phys. Rev. Lett., Vol. 63, No. 16, pages 1747-1751

Wiese H., Horn D., 1991, Single mode fibres in fibre optic quasi-elastic light scattering: a study of the dynamics of concentrated dispersions, J. Chem. Phys., No. 94, Vol. 10, pages 6429-6443

Will S., Leipertz A ., 1993, Determination of the dynamic viscosity of transparent fluids by using dynamic light scattering techniques,., Appl. Optics, Vol. 32, No. 21, pages 3813-3821

Wolf P. E., Maret G., 1990, Dynamics of Brownian particles from strongly multiple light scattering, Scattering in Volumes and Surfaces, Elsevier Sc. Pub. b. v. pages 37-52

Yang S., Mickelson A. R., 1992, Coupling mechanisms and transfer functions of optical fibre devices, , Appl. Optics, Vol. 31, No. 36, pages 7587-7589

Zaccanti, 1991, Monte carlo study of light propagation in optically thick media point source case, App. Optics, Vol. 30, No. 15, pages 2031

Zhu J. X., Durian D. J., Muller J., Weitz D. A., Pine D. J., 1992, Scaling of transient hydrodynamic interactions in concentrated suspensions, Phys. Rev. Lett., Vol. 68, No. 16, pages 2559-2563

APPENDIX 1

Engineering Drawings of the Arrangement

This appendix gives the engineering diagrams used in the final arrangement. The Step 0 hardware has not been included for brevity. The optical probe designs are shown first, followed by that of the detectors/optic block, with the laser mount last. The probe was constructed by Dr T Withers (Sensor Dynamics) and modified in house to suit. The mechanical parts were produced by Tioxide to these designs and the assembled and tested in-house.

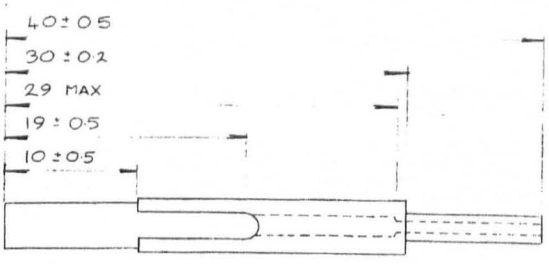

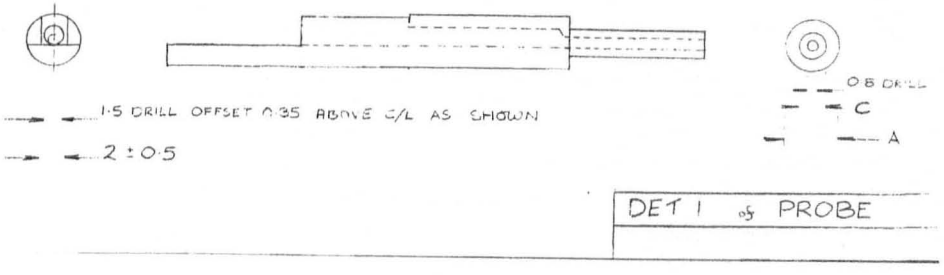

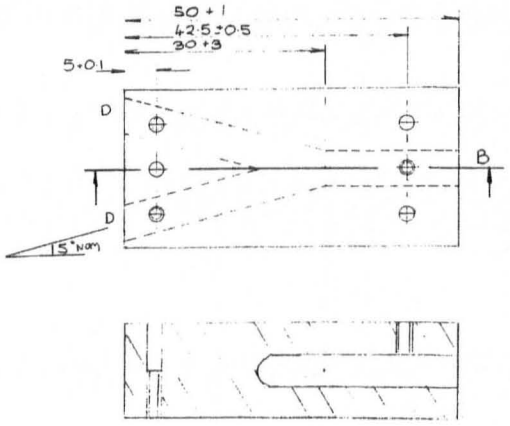

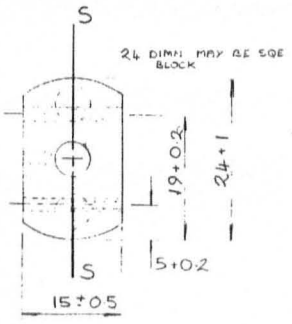

FITS TO BE BEST DRILL OR REAMER SIZE.

3 HOLES M2 TAP, TO LOCK TUBES INTO BORES
3 HOLES DRILL 2·1 × 8 Dp THEN TAP M2 THRO', TO LOCK 2 HALVES

THIS COMPONENT TO BE SPLIT ALONG SS, MAY BE MADE FROM 2 PIECES OR SPLIT AFTER, MAX GAP 1mm

DET 2 OF PROBE

* IMPORTANT NOTE
BORES E + F MUST BE CENTERAL IN BLOCK AND SQUARE TO SIDES, MACHINE 4 SIDES 13·0 ROUGH BORE E, DRILL BORE F, FINISH E AND FACE TOP FACE 13·0 × 13·0 IN ONE OPERATION V/MILL POSN AND ⊥ OF 5·1 BORE NOT IMPORTANT.

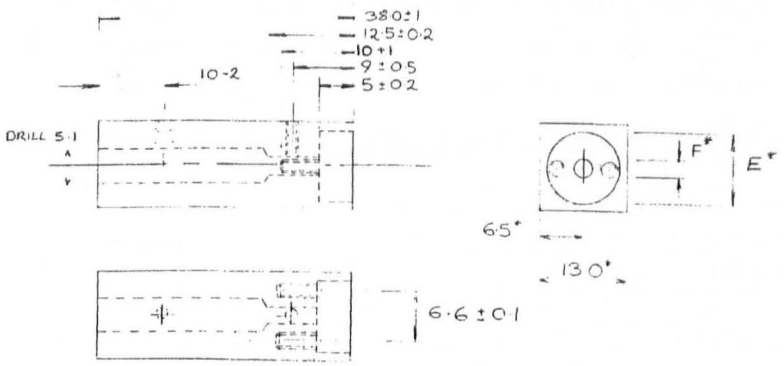

4 HOLES TAP M2, 2 OFF THRO INTO BORES

3 OFF

DET 3 OF PROBE

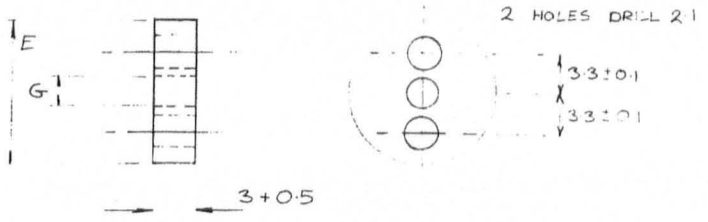

BORE G ⊥ 2 SIDES 3+0·5 DIMN

5 OFF

DET 7 OF PROBE

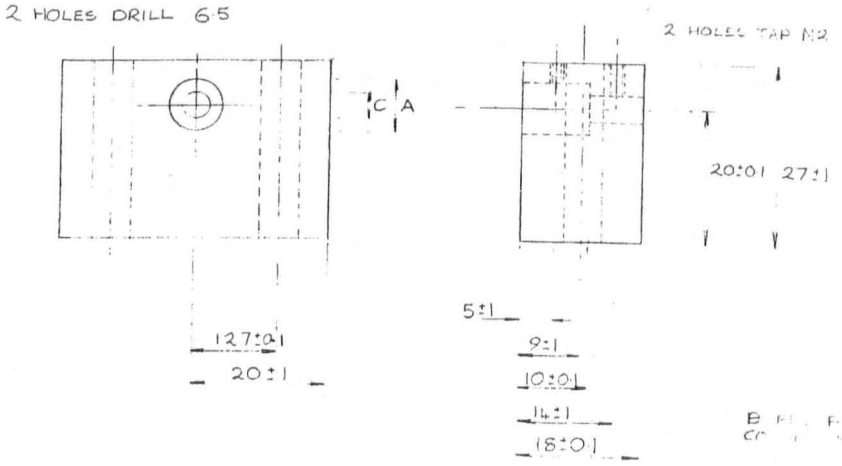

DET 4 OF PROBE

WINDOW HOLDER

Dear Rod

Disk 32 probe.gal

Very similar to last window holder except slightly smaller diameters. Steel shaft with two concentric holes drilled 2." and 5mm (to clear (2." and 5 diameters) Two tapped holes to lightly grip probe inside

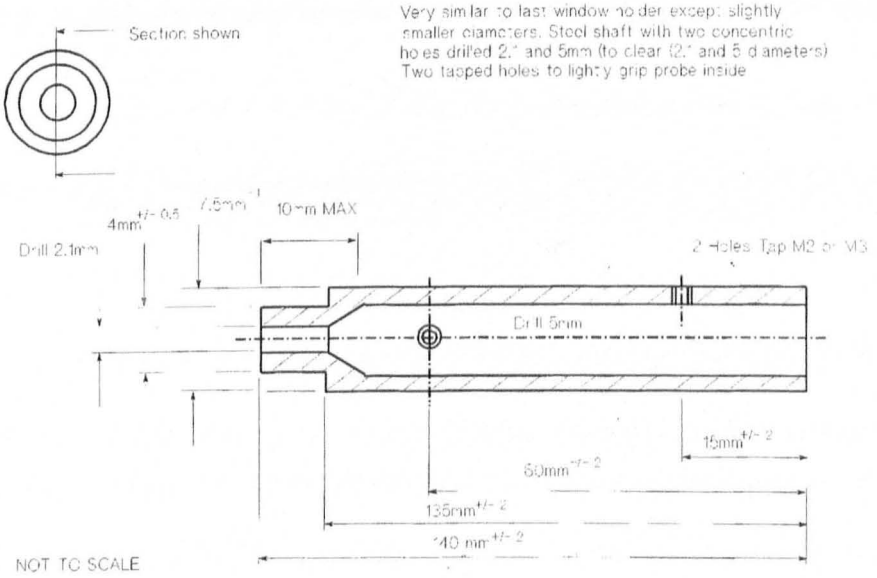

WINDOW FOR DWS PROBE

See drawing 1 of probe, all sizes may be altered to suit

4 Holes at 60 degrees to lock to probe

tapped for suitable nylon screw

This face to be perpendicular to bore

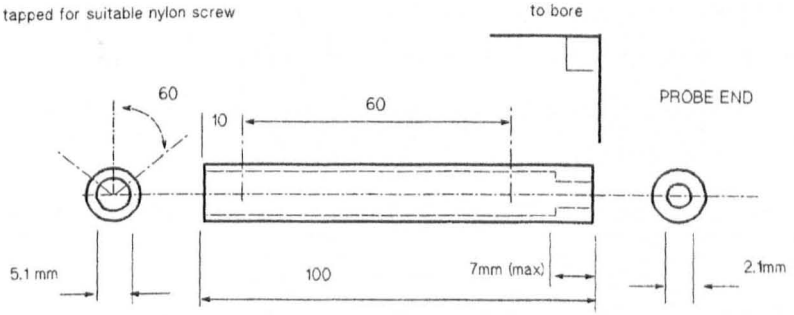

LENS HOLDER FOR DWS PROBE SHT 1/2

See drawing 1 of probe, all sizes may be altered to suit

AS DRAWING FOR WINDOW BUT WITH EXTRA TAPPED HOLES

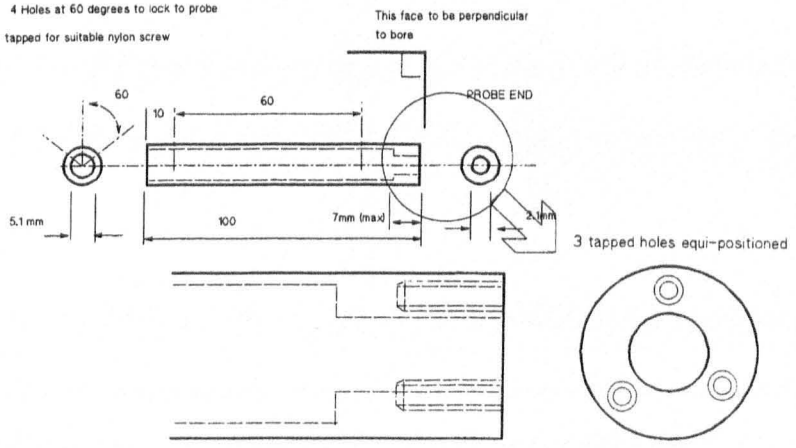

LENS HOLDER FOR DWS PROBE SHT 2/2

See drawing 1 of probe, all sizes may be altered to suit

3 Holes to suit sheet 1, clearenec on screws to allow +/- 0.25mm
Holes must not be countersunk

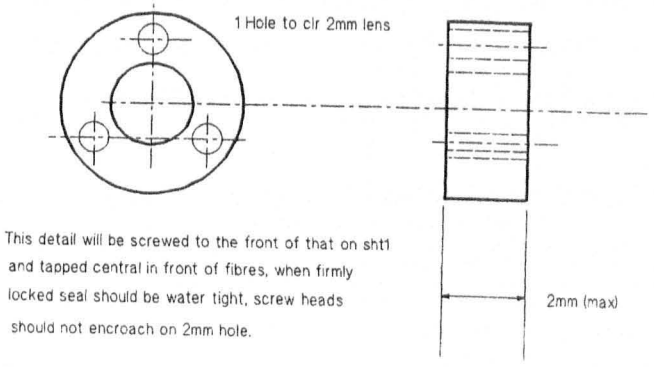

This detail will be screwed to the front of that on sht1 and tapped central in front of fibres, when firmly locked seal should be water tight, screw heads should not encroach on 2mm hole.

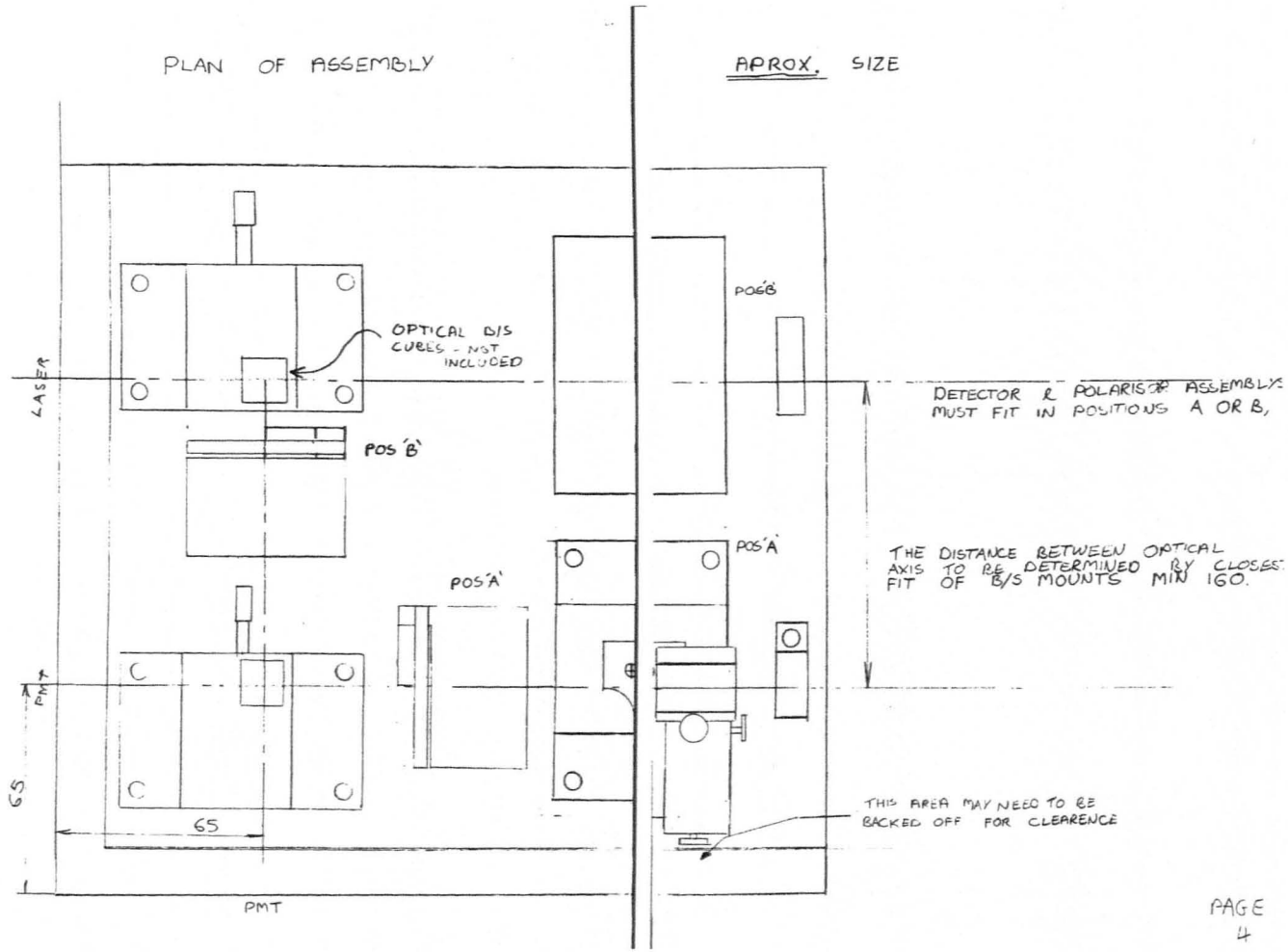
PLAN OF ASSEMBLY
APROX. SIZE
OPTICAL B/S CUBES - NOT INCLUDED
POS 'B'
POS 'A'
POS'B
POS'A
LASER
PMT
65
65
PMT
DETECTOR & POLARISER ASSEMBLYS MUST FIT IN POSITIONS A OR B,
THE DISTANCE BETWEEN OPTICAL AXIS TO BE DETERMINED BY CLOSEST FIT OF B/S MOUNTS MIN 160.
THIS AREA MAY NEED TO BE BACKED OFF FOR CLEARENCE

ANGLE BRACKET

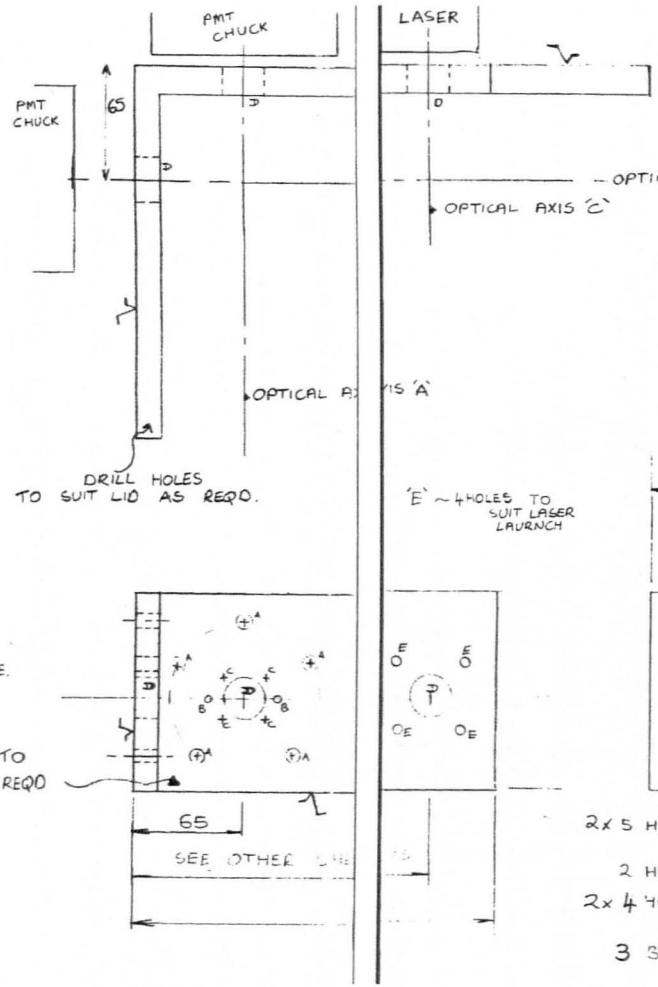

ALL AXIS AT HEIGHT TO BE AS 11^{thou} AND $\perp^{r}$ AS POSSIBLE

MAIN ANGLE BRACKET HEIGHT = (PMT + 2)$^{+1}$

SURFACES MARKED √ TO BE M/C ALL OTHERS ROUGH CUT/AS STOCK

(E) INTERNAL FACES AND TOP, SIDE FACES MAY BE COURSE.

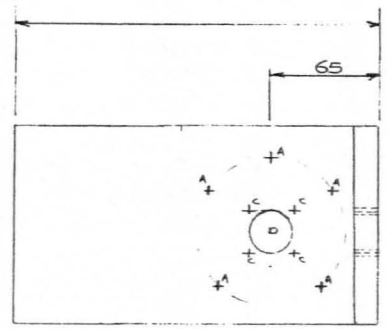

2x 5 HOLES 'A' TO SUIT HOLES ON PMT CHUCK, NO C/BORE

2 HOLES 'B' TO SUIT DOWELS ON CHUCK

2x 4 HOLES 'C' TO FORM 1 INCH SQE TAP M3 THRO'

3 BORES 'D' 25.5 + 0.1 (TO SUIT 1")

SKETCH 2

POLAROID HOUSING & ROTATOR
-ALLOWS THE BRASS CYLINDER TO BE ROTATED THRO' 90° AND BACK

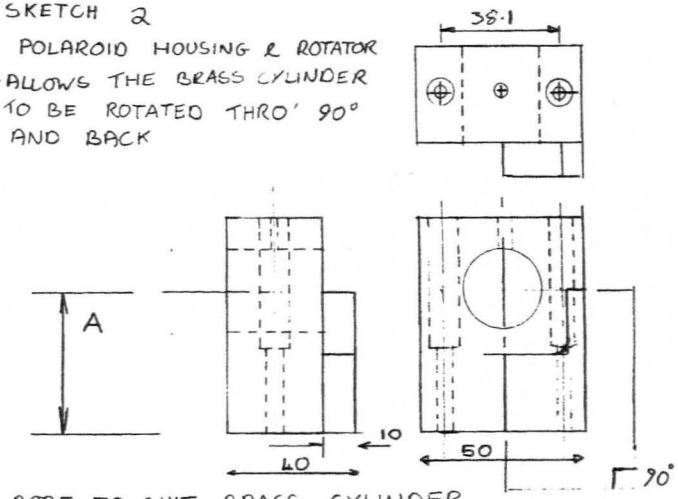

1 BORE TO SUIT BRASS CYLINDER
1 HOLE TAPPED INTO BORE TO GRIP
2 C/BORED HOLES TO ALLOW LOCKING TO BASE PLATE, CLAMPING MUST BE FROM TOP FACE

THRO' C/L

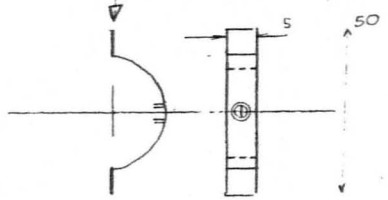

DISK, BORE TO SUIT BRASS CYLINDER
50% OF DISK BACKED OFF, 1 GRUB SCREW

SKETCH 1 MOD OF PMT CHUCK - TURNING SNOUTED CHUCK INTO UNSNOUTED CHUCK

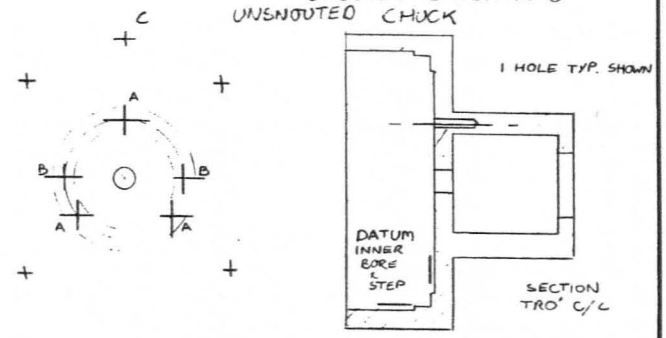

DRILL 3 EQUISPACED HOLES MARKED 'A', C/SUNK
DRILL 2 HOLES MARKED 'B' HOROZONTAL

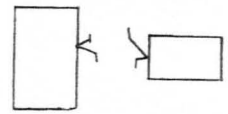

SEPERATE AND M/C 2 SURFACES TO FINISH

LHS RHS

TAP 3 HOLES A

DRILL OUT 3 HOLES 'A' TO CLR TAP

FIT 2 DOWLS, HOLES 'B'
1 FISHBACK.

PLEASE PRODUCE 1 SPACER WITH 5 CLEARENCE HOLES SO PART MAY BE REASSEMBLED

DRILL 5 HOLES C AS PER UNSNOUTED PMT CHUCK (SIZE OF THREADS MAY BE DIFFERENT

B/S SPRING SKETCH 5 2 OFF

1) HOLE TO FIT DOWL, INTFERENCE FIT OR TAP
2) HOLES 'B' TAP WITH A FINE THREAD
3) 1 HOLE 'C' TO CLEAR THREAD 'B'
4) 4 HOLES 'D' ON 1 INCH SPACING TO CLAMP 1 AXIS POSITIONER.

THE SPRING IS HELD TO THE BASEPLATE BY ONE DOWEL, HOLES 'B' USED TO EXERT PRESSURE HENCE LIFT THE PLATE, HOLE C HAS A CAP SCREW PASSING THROUGH INTO THE BASEPLATE TO EXERT -VE PRESSURE.

BY SETTING SCREWS IN HOLES 'B' & 'C' IT WILL THEREFORE BE POSSIBE TO ENSURE COMPONENT IS ALIGNED IN 2 AXIS, ANGULAR.

THE 4 HOLES 'D' LOCK THE 1 AXIS POSITIONER TO THE PLATE

THE THICKNESS OF PLATE & THE DOWEL LENGTH MAY BE VARIED TO ENSURE B/S CLAMP IS AT DIMN A, ON 2 AXIS.

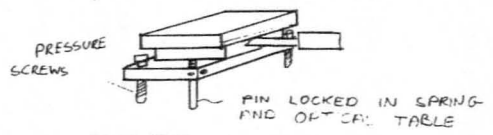

S/S SKETCH 3

THIS ONE AXIS STAGE WILL REQUIRE A SLIGHT MOD. TWO CLEARENCE HOLES TO BE TAPPED TO ALLOW CLAMP STAGE TO BE BOLTED DOWN, AS SHOWN

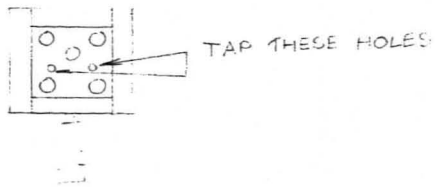

DUE TO AN ERROR IN EARLIER DRAWINGS I HAVE NOT BEEN ABLE TO CALC POSITION IN AXES. PLEASE FIT AS SKETCH " PLAN OF ASSEMBLY

2 SEPARATE MOUNTS ARE REQUIRED

B/S SPRING SKETCH 3

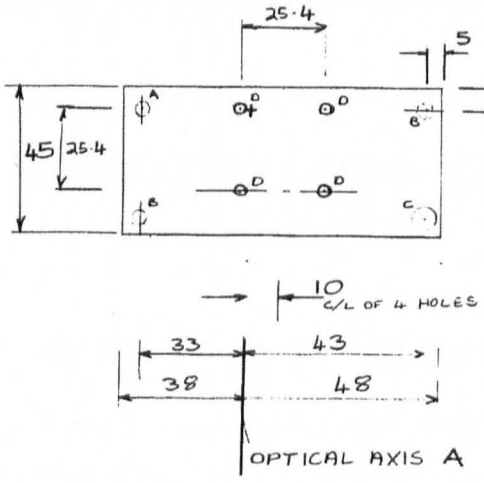

A - 1 HOLE TO SUIT DOWEL

B - 2 HOLES M6 TO EXERT PRESSURE ON BASE PLATE

C - 1 HOLE CLR M6 TO ALLOW SPRING TO BE DRAWN TO BASEPLATE

PAG 10

B/S CLAMP SKETCH 3

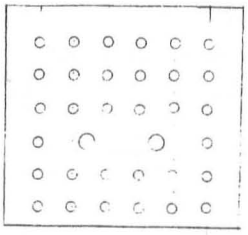

2 HOLES C/SINK OR C/BORE TO LOCK TO TAPPED HOLES ON 1 AXIS STAGE

WHEN THIS DETAIL IS FITTED TO 1 AXIS POSITIONER ON CLAMP THE DISTANCE FROM BASE TO TOP FACE TO BE (DIM A -5mm)±1
IE THE PLATE SITS 5mm BELOW THE OPTICAL AXIS

VARIOUS TYPES OF B/S WILL BE USED SO THE MOST USEFULL 'FACE' WOULD BE AN ARRAY OF M3 TAPPED HOLES.

THE PLATE SHOULD OVERHANG THE 1 AXIS POSITIONER BY 5 ~ 10 mm.

PAGE 11

ASSEMBLY OF DETECTOR

SKETCH 4

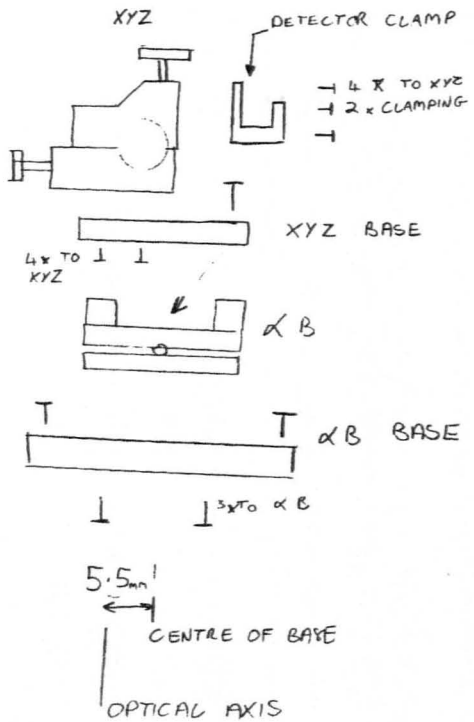

THE αB BASE IS SOLELY TO ALLOW CLAMPING VIA TOP FACE, HENCE EASY REPOSITIONING.

A 13mm BLOCK MUST BE CENTERED, AND SQE ON THE OPTICAL AXIS A FOR THE FINAL SETUP.

THE BLOCK IS HELD IN THE DETECTOR CLAMP LOCKED IN BY TWO CLAMPING SCREWS 'B'. 4 HOLES 'A' LOCK THIS TO THE XYZ STAGE.

THE XYZ STAGE IS CLAMPED ONTO XYZ BASE VIA 4 HOLES C/SUNK FROM BACK FACE

THIS IN TURN IS LOCKED TO AN αB STAGE VIA ONE CENTERAL SCREW.

THE αB IS MOUNTED ONTO THE BASE PLATE VIA THE αB BASE. 4 HOLES 'B' TO THE BASEPLATE, 3 HOLES 'A' TO THE αB.

THE 13mm BLOCK WILL BE 5·5mm OUT OF LINE WITH THE CENTRE OF THE αB BASE. THE BASE TO BE OFFSET.

THIS MAY BE ALTERED PROVIDING THE BLOCK BECOMES CENTERED IN THE FINAL PIECE

THE DETECTION MOUNT WILL BE USED IN A POSITION ON THE αB

α B BASE SKETCH 4

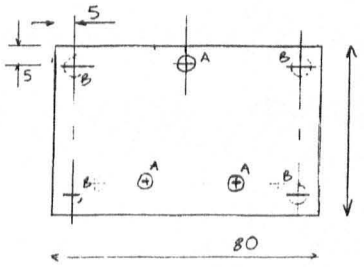

c/BORE

3 HOLES 'A' TO SUIT α, B, STAGE ✓

4 HOLES 'B' TO LOCK TO BASEPLATE

THICKNESS TO BE VARIED TO PRODUCE DIMN A FOR DEFECTION CLAMP

XYZ POSITIONER BASE SKETCH 4

1 HOLE TO SUIT α,B POSITIONER CENTER HOLE

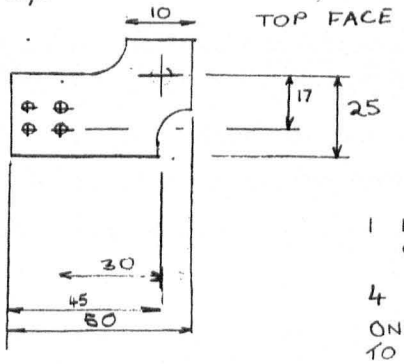

1 HOLE TO LOCK TO α B STAGE

4 HOLES

ONE POSITION SHOWN TO SUIT X,YZ STAGE

C/SINK BACK FACE

AS THIN SECTION AS POSSIBLE

DETECTOR CLAMP

SKETCH 4

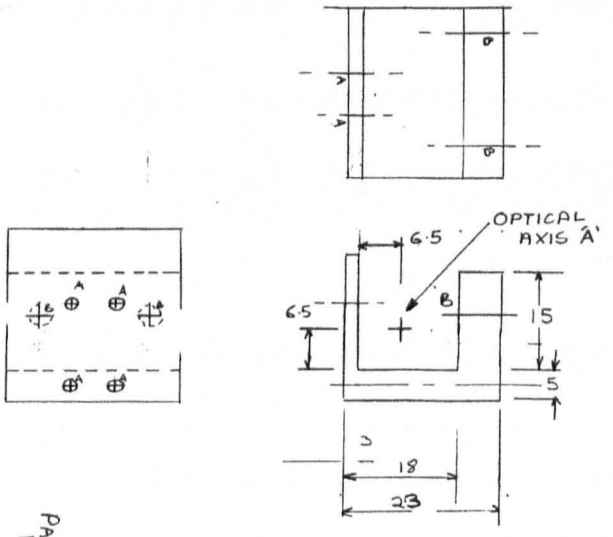

'A' 4 HOLES TO MOUNT ON X,Y,Z POSITIONER

'B' 2 CLAMPING SCREWS TAPPED

CABLE CLAMP

SKETCH 4

SIMPLE 'V' CLAMP TO LOCK A 5mm STEEL CLAD FLEXIBLE CABLE ON OPTICAL AXIS ± 2mm.

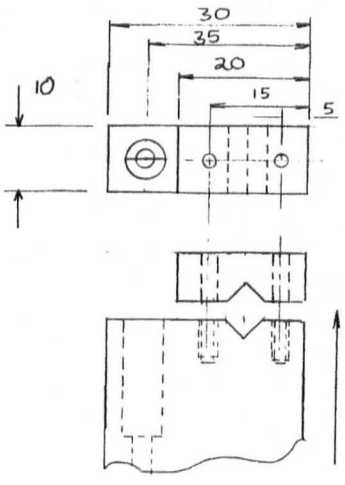

1 HOLE TO LOCK TO BASE

2 HOLES TO LOCK V TO CABLE

LASER ASSEMBY SKETCH 5

VERY FEW DIMN's GIVEN

MOST IMPORTANT DETAIL IS THAT END FACE OF LAURNCH BLOCK IS SQUARE TO OPTICAL AXIS. THIS FACE WILL BE USED, WHEN POINT SOURCE IS REMOVED TO LOCK TO ANGLE BRACKET, OPTICAL AXIS 'C'

THE ROTATOR BLOCK MAY HAVE TO BE TWISTED 2-5° SO ALLOW CLEARENCE ON LOCKING BOLTS.

THE HEIGHT OF THE BLOCKS TO BE DEFINED BY SIZE OF LASER MOUNTS

PLEASE TAP PLATE IN 6 PLACES M6 TO PROVIDE FEET, SPACING OF FEET MUST NOT BE A WHOLE NUMBER OF INCHES (THEY WILL FOUL OPTICAL TABLE DRILLED WITH 1" ARRAY.

THE DIMN B FROM SKETCH

SKETCH 5

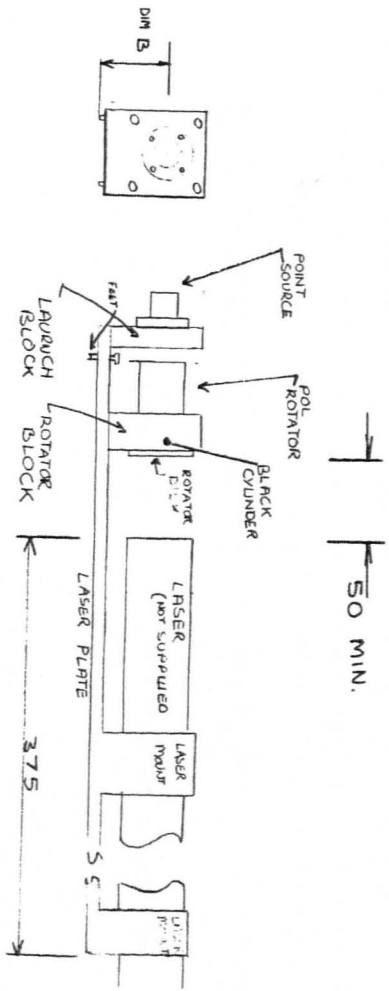

DIAGRAM
LASER PLATE ASSEMBLED

ALL BLOCKS & BASE
60mm WIDE

LASER Ø 44mm
LASER LENGTH 486mm

SKETCH 5

A - 5 HOLES LAUNCH BLOCK
B - 2 HOLES LASER RAIL, MAY BE SLOTS
C - 2 HOLES POL ROTATOR
D - 4 HOLES LASER MOUNT

SIZES, POSITIONS MAY BE ALTERED.

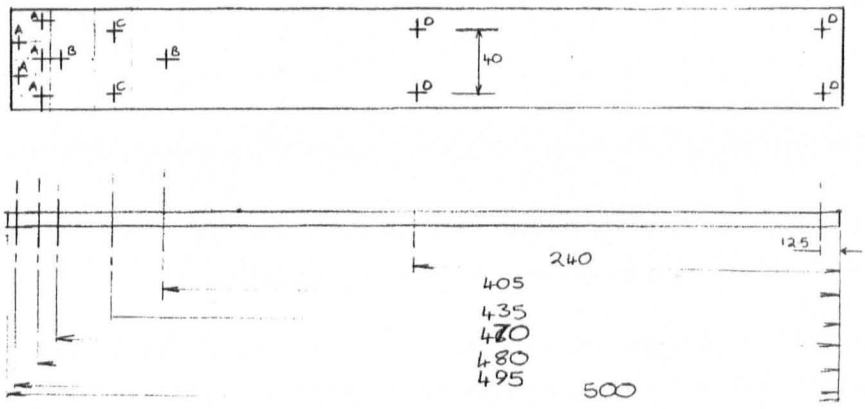

SKETCH 5 LAUNCH BLOCK

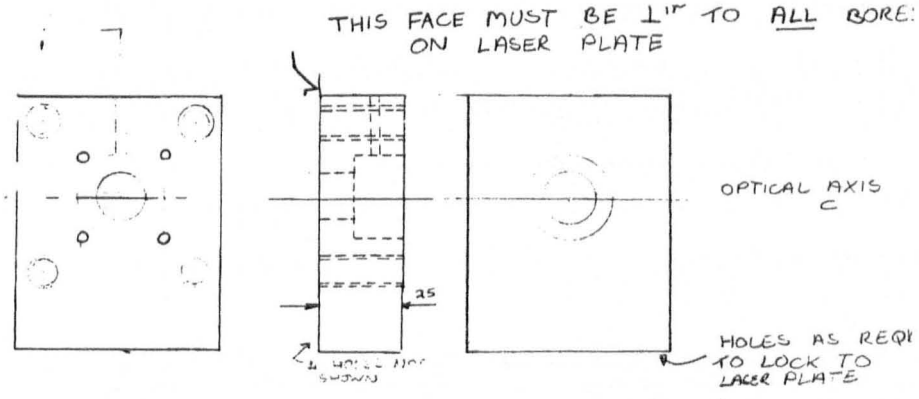

4 LARGE HOLES TO CLAMP TO ANGLE BRACKET TAPPED.
4 SMALL HOLES TO GRIP POINT SOURCE, ⌀ Dp.
1 BORE TO CLEAR 0.5 INCH
1 BORE TO CLEAR 1 INCH
1 TAPPED HOLE INTO 1 INCH BORE.

SKETCHES

LASER MOUNTS ×2

MUST GRIP LASER WITHOUT PINCHING EITHER BORE AS BELOW OR 3× SCREWS TO CLAMP

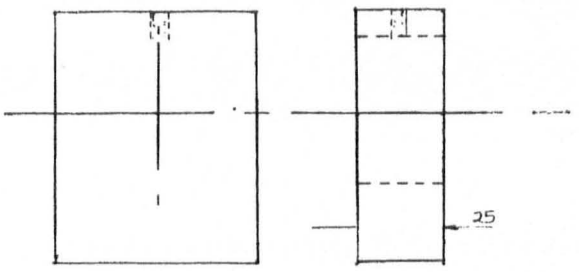

1 BORE TO SUIT LASER

1 × GRUB SCREW TO LOCK.

ANY METHOD THAT PROVIDES STABILITY IS ACCEPTABLE

SKETCHES

ROTATOR DISK

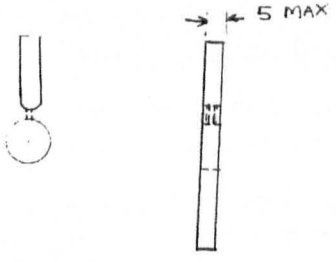

DISK Ø 55 ± 4, BORE TO SUIT BLACK CYLINDER
& GRUB SCREW TO LOCK, SECTION OR SEGMENT MAY BE CUT AWAY FOR ACCESS.

SKETCH 5

ROTATOR BLOCK

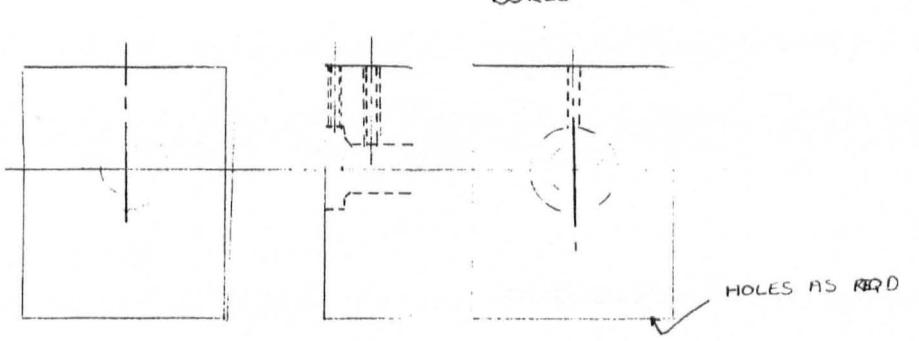

1 BORE TO SUIT BLACK CYLINDER
1 BORE TO SUIT POLARISATION ROTATOR
(THIS NEED NOT BE THREADED, CLOSE FIT & GRUB SCREW)

COVER

SKETCH 6

THE ASSEMBLY IS 3 SIDES OF A CUBE, A COVER IS REQUIRED TO FORM THE OTHER 3 SIDES, 2 SLOTS OVER 5mm ARE REQUIRED TO ALLOW EXIT OF CABLES. A 5~10mm OVERHANG WOULD HELP LIMIT STRAY LIGHT, AS SHOWN

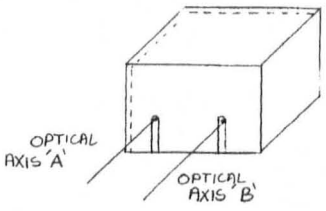

Fig 1A

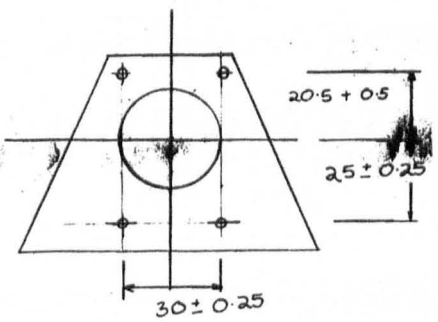

BORE 30 ±1

4 HOLES MS

FIG 1B

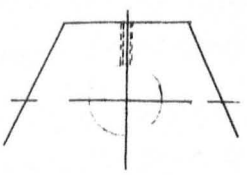

BORE TO SUIT POL. ROTATOR (STEEL DRUM WITH THRU 1 SCREW TO LOCK ON BORE

SHT 1 2 OFF FACES AS FIGS 1A & 1B

C/L INSIDE BOX

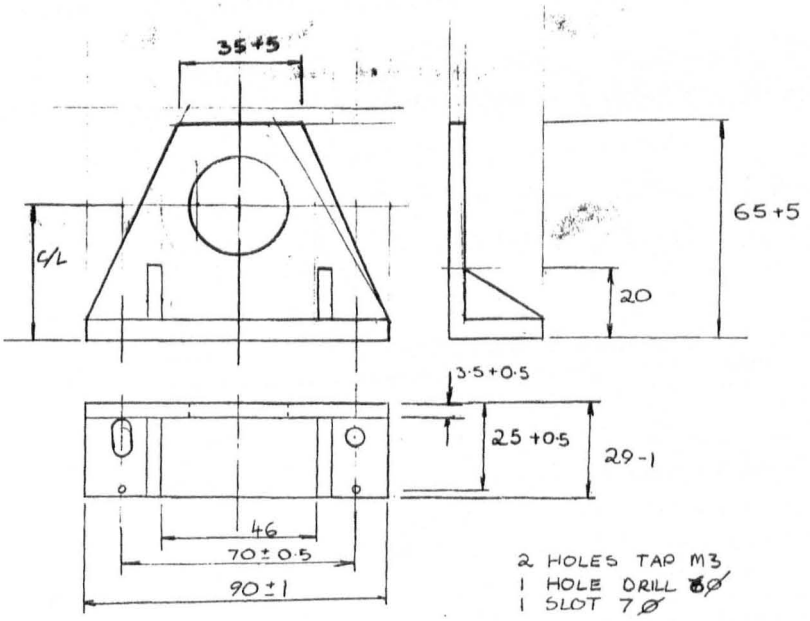

2 HOLES TAP M3
1 HOLE DRILL 8Ø
1 SLOT 7Ø

SHT 2 CLAMPING DETAILS

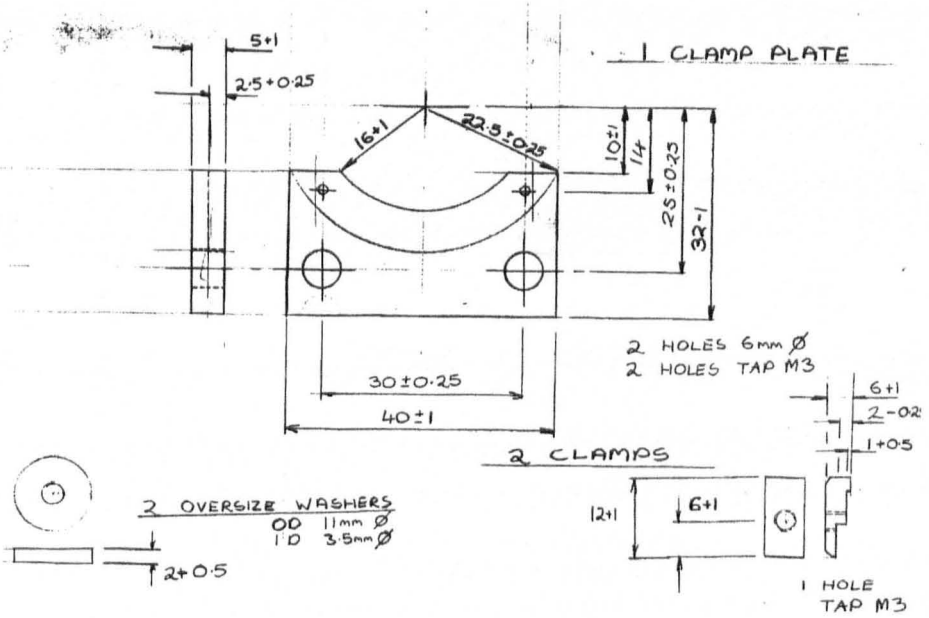

SHT 3

PROBLEM - BOWING OF LASER MOUNT, NOT ENOUGH RIGIDITY

- PRODUCE 2 SIDE WALLS - AS SHOWN. 'U' SECTION SHOULD INCREASE RIGIDITY WITHOUT LARGE WEIGHT INCREASE.

DESIGN AS SHOWN WILL ALSO ALLOW OPTICAL COMPONENTS TO BE 'BOXED IN' REDUCING DUST PROBLEMS

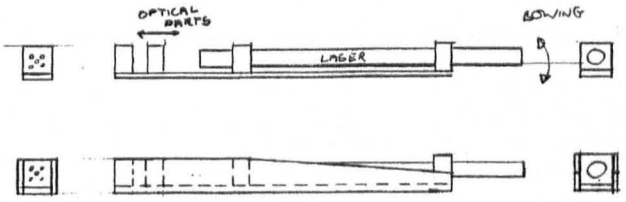

UNSCALED 3RD ANG "BEFORE & AFTER" SKETCHES

OVERALL DIMNS

SHT 4

Dear Rod
I have zero knowledge of actual sheet metal work, hence, I leave the thickness and material for your best 'guess-timate'.

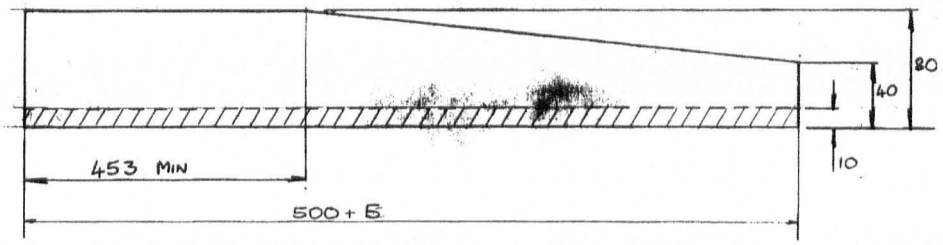

HATCHED AREA TO BE BONDED TO BASEPLATE

TOLERANCES - PLEASE WORK TO MIN MATL CONDITION
ie BOTTOM SIZE IS IDEAL SIZE

UNSCALED

HOLE POSITIONS

SHT 5

Dear Rod, Positions may vary ±1mm, I will use the side as a template to mark positions on Laser Plate.

24 HOLES CLR M3 C/SINK

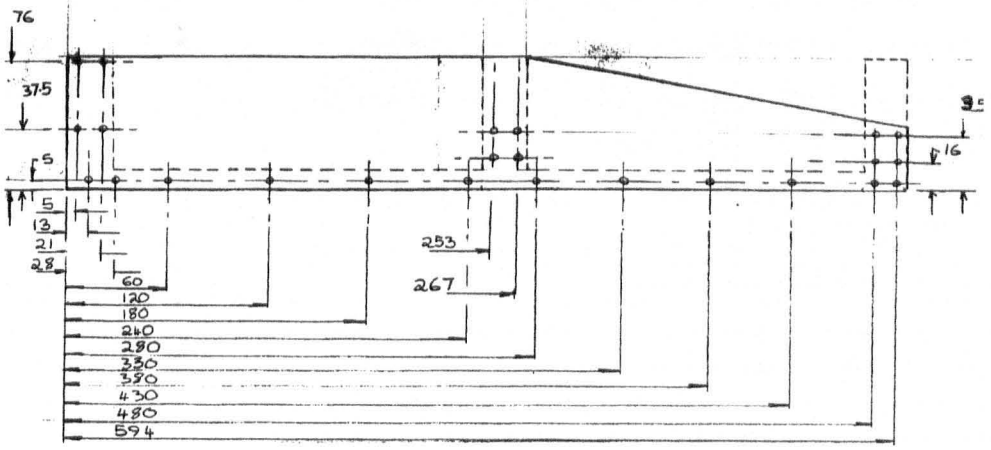

LASER LID 2

BEAMSTOP

DISK 32 LASLID2.gal

Dear Rod

This is a bent piece of metal that may be dropped in place to block the laser.
The notches are to ensure it can lock in the open and closed positions

DIM A CLEARENCE ON LID THICKNESS

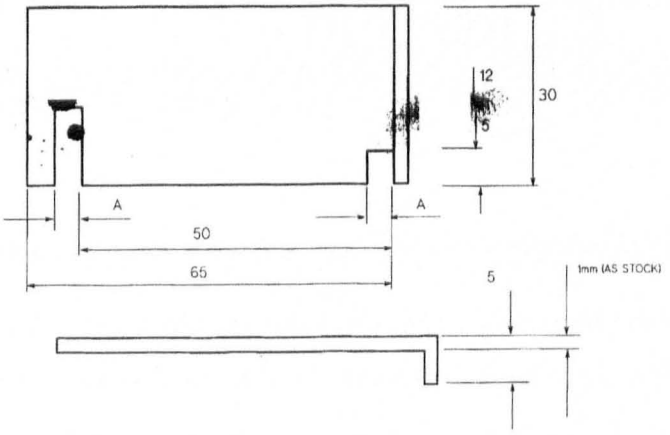

LASER LID

DISK 32 LASLID.GAL

Dear Rod

CENTER SET AT 5 DEGREES TO ACCEPT BEAM STOP

2 SLOTS 5MM DIA

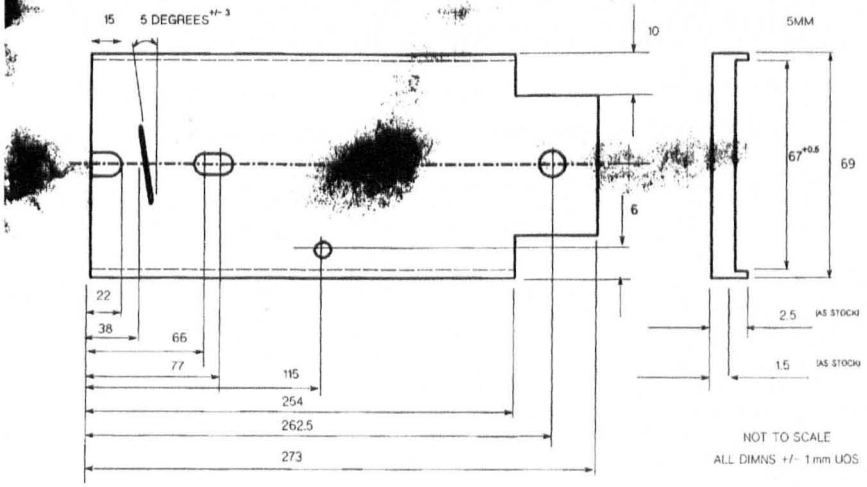

NOT TO SCALE

ALL DIMNS +/- 1 mm UOS

APPENDIX 2

Software Schematics

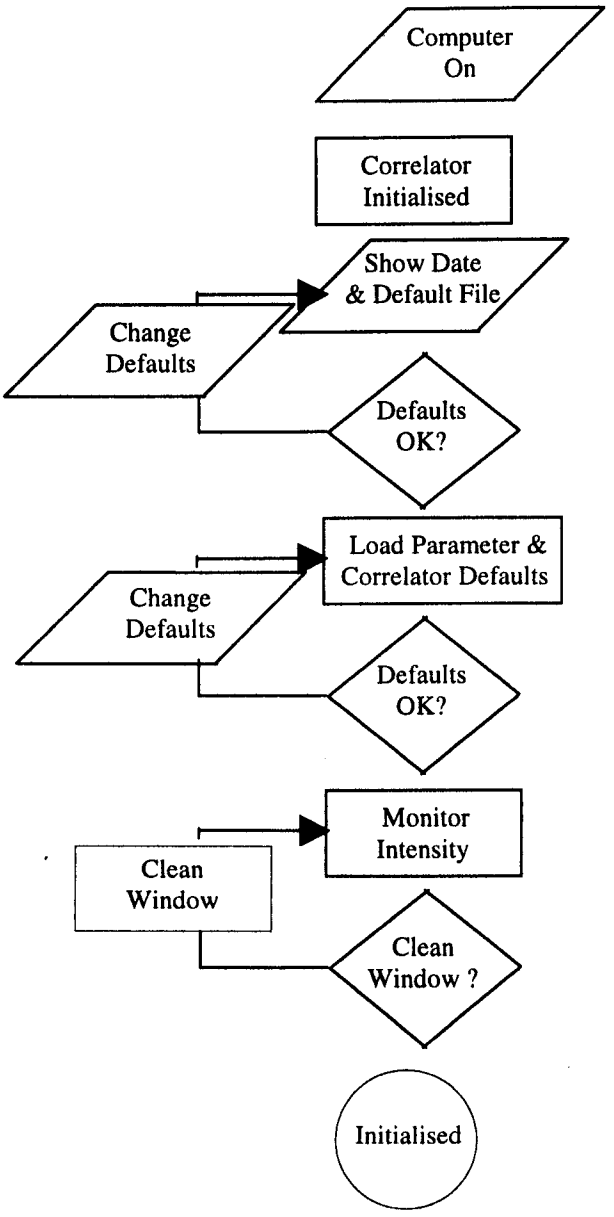

Simplified initialisation procedure of final software developed in this work.

After initialisation the modules could be operated in any order. The schematics are significantly simplified, assuming all default parameter values are used. The software listing runs to many thousands of lines, it will be supplied on suitable media on request, Chapter (4)

Flow chart symbols have the standard meanings, except a box with a dotted line has been used to denote operations not carried out by the software.

Key: Diamond is decision, box is operation; rhomboid is input/output; circle is start or stop.

Yes is straight down

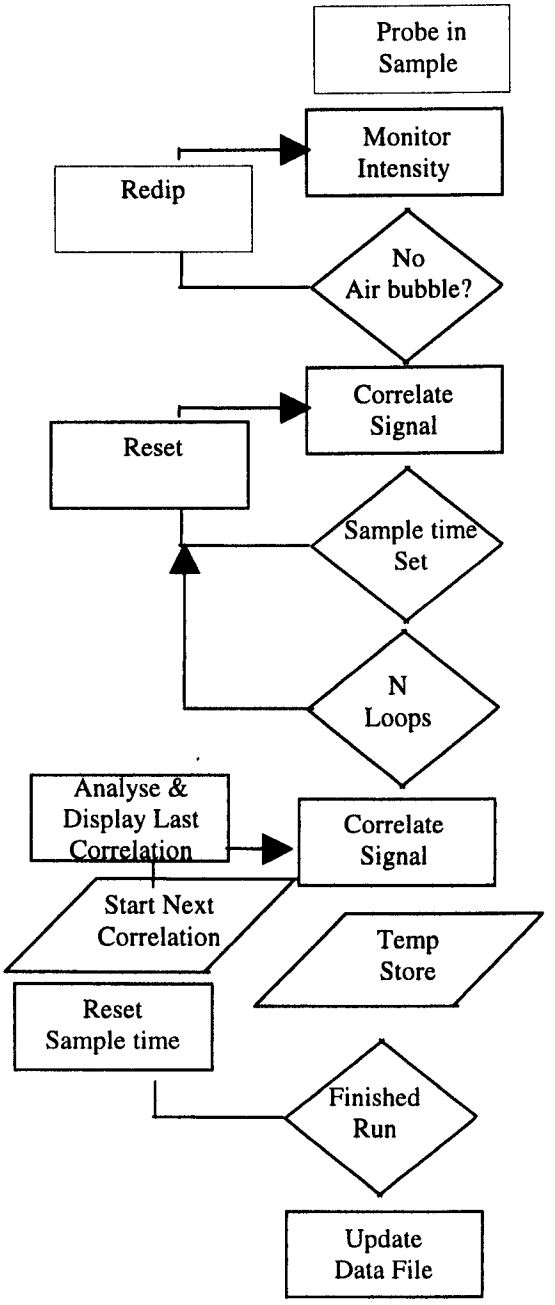

70kcps<Counts<80kcps

Sine wave, adhesion sine wave superimposed on reducing intensity

Does NQ+/-lim lie on f_b ?

Straight line and polynomial fits on channels 0 to f_b and f_b to end.

Correlation, curvature, runs and errors to 340 files on Ram Disk

From this point control can go to any module

Correlator Delay Setting and Measurement Module

The concepts, definitions, algorithms and their implementation are discussed Chapter (6)

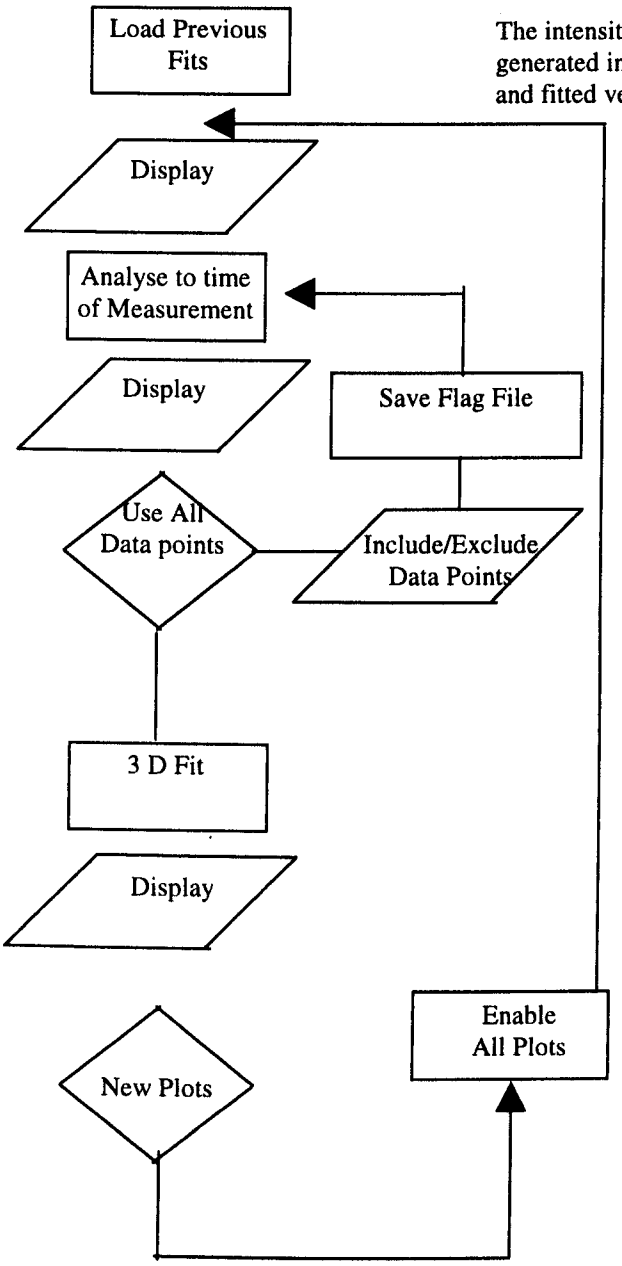

The intensities, gradients and all fitting parameters generated in the measurement module were loaded and fitted versus time of experiment.

Correlations could be removed, all parameters were refitted automatically, this information stored in the flags file

A 3 D fit with error bas on the data points and reproducibility and model errors were displayed.

After the fit any stored variable could be plotted versus any other i.e. temperature versus count rate.

3 Dimensional Fitting Module

The fitting concepts, definitions and algorithms are given in Chapter (6)

APPENDIX 3

Step 2 Data

This data is presented as an example of a sample which adhered to the probe due to the cross-linking coating of the pigment. This was significant problem in samples where the continuous phase was propylene glycol.

The trace that is the sum of 72 correlations for samples of anatase pigment at 50 and 100 grams per litre (gpl). The underlying Step 2 analysis is shown for the 50gpl samples only.

Correlation delay (for a set correlation) was plotted versus goodness of fit (sum of variance and fitting error), the optimum correlator delay was assumed to be the one with the lowest error. The instrument function (correlation gradient) was then plotted versus correlator delay and the value interpolated to that at the correlation delay previous selected. This gave a gradient value for that data set, along with the time it was measured at. This gradient was then plotted versus 'time since probe' introduction to allow a zero time extrapolation.

This allowed data analysis of a single sample and had to be repeated for each sample with a new probe window attached.

These samples were also found to be physically unstable with time, irreversible flocculation occurring over a 24 hour period.

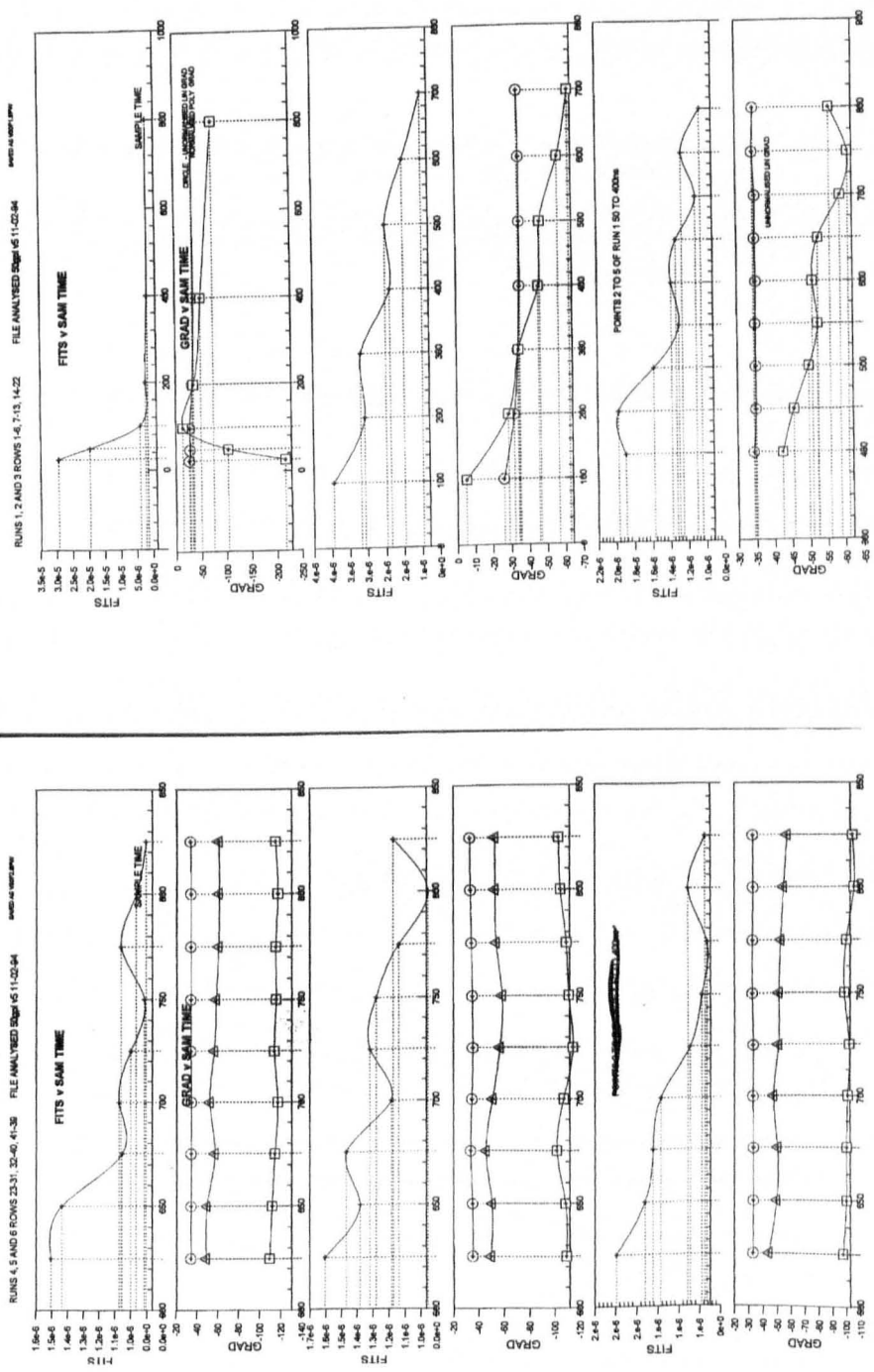

Data analysis for a single sample of pigment material at 50 grams per litre (density ≈ 4)

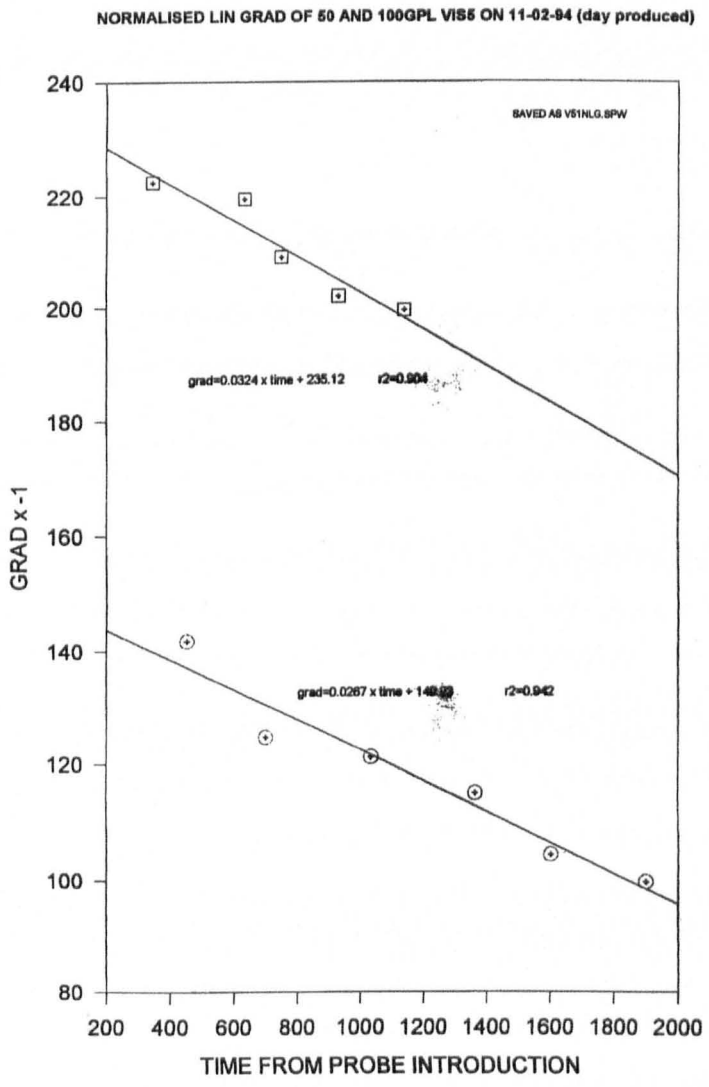

The previous data set produced the upper trace, which allowed extrapolation of Γ at t=0 for unstable suspensions.